UNIVERSIDADE DE LISBOA
INSTITUTO SUPERIOR TÉCNICO

Novel bioengineering strategies for modeling cerebellar ataxias

Teresa Maria Pereira da Silva

Supervisor: Doctor Maria do Carmo Salazar Velez Roque da Fonseca
Co-supervisors: Doctor Evguenia Pavlovna Bekman
Doctor Tiago Paulo Gonçalves Fernandes

Thesis approved in public session to obtain the PhD Degree in

Bioengineering

Jury final classification: **Pass with Distinction**

2018

TÉCNICO LISBOA

UNIVERSIDADE DE LISBOA

INSTITUTO SUPERIOR TÉCNICO

Novel bioengineering strategies for modeling cerebellar ataxias

Teresa Maria Pereira da Silva

Supervisor: Doctor Maria do Carmo Salazar Velez Roque da Fonseca
Co-supervisors: Doctor Evguenia Pavlovna Bekman
Doctor Tiago Paulo Gonçalves Fernandes

Thesis approved in public session to obtain the PhD Degree in
Bioengineering

Jury final classification: **Pass with Distinction**

Jury:

Chairperson: Doctor Joaquim Manuel Sampaio Cabral, Instituto Superior Técnico, Universidade de Lisboa

Members of the Committee:

Doctor Maria do Carmo Salazar Velez Roque da Fonseca, Faculdade de Medicina, Universidade de Lisboa;
Doctor Joaquim Manuel Sampaio Cabral, Instituto Superior Técnico, Universidade de Lisboa;
Doctor João Ramalho de Sousa Santos, Faculdade de Ciências e Tecnologia, Universidade de Coimbra;
Doctor Luís Fernando Morgado Pereira de Almeida, Faculdade de Farmácia, Universidade de Coimbra
Doctor Maria Margarida Fonseca Rodrigues Diogo, Instituto Superior Técnico, Universidade de Lisboa.

2018

RESUMO

O cerebelo humano apresenta diversas funções em todos os organismos vertebrados, estando envolvido sobretudo na coordenação motora. Muitas doenças neurodegenerativas apresentam uma disfunção do cerebelo como marca neuropatológica e perda de coordenação motora como um dos principais sintomas, como é o caso das ataxias cerebelosas. Tudo o que se sabe atualmente sobre ataxias é baseado em estudos com modelos animais ou realizados em tecidos humanos recolhidos pós-morte, os quais não refletem as características de uma doença humana. Desta forma, é extremamente necessário o desenvolvimento de novos modelos de doença que consigam mimetizar o seu fenótipo. As células estaminais pluripotentes induzidas representam uma ferramenta valiosa para modelar diferentes doenças humanas *in vitro*. Neste trabalho, o principal objetivo foi gerar novas condições para diferenciar neurónios cerebelares a partir de células estaminais pluripotentes induzidas, que possam ser usados como modelos para as ataxias. Na primeira abordagem, estabelecemos um novo método para gerar neurónios cerebelares usando condições definidas, sem recorrer a co-culturas com outros tipos celulares. Adicionalmente, a manipulação de diferentes vias de sinalização foi estudada de forma a aumentar a eficiência do protocolo para gerar um maior número de progenitores cerebelares GABAérgicos bem como maior número de células de Purkinje funcionais. Despois da criação de uma nova metodologia para gerar neurónios cerebelares em condições definidas, foi feita uma translação do protocolo de forma a produzir grandes quantidades de células necessárias para investigação de novos possíveis fármacos bem como testes toxicológicos. Neste novo sistema dinâmico, conseguimos gerar agregados homogéneos de células estaminais pluripotentes que diferenciaram eficientemente em progenitores cerebelares e mais tarde maturaram em neurónios cerebelares funcionais.

É esperado que o presente trabalho possa contribuir para o desenvolvimento de novos modelos para as ataxias, de forma a facilitar o desenvolvimento de novas terapias bem como o estudo de mecanismos que possam estar especificamente envolvidos na manifestação do fenótipo, associados com o aparecimento e progresso da neuropatologia.

Palavras-chave: Cerebelo, ataxia, células estaminais pluripotentes induzidas, diferenciação cerebelar, células de Purkinje.

ABSTRACT

The cerebellum plays a critical role in all vertebrates, and many neurological disorders such as ataxias are associated with cerebellar dysfunction. A major limitation in cerebellar research has been the lack of adequate disease models. Human induced pluripotent stem cells (iPSCs) have great potential for disease modeling and provide a valuable source for regenerative approaches. Therefore, the main objective of this thesis was to create new approaches for modeling cerebellar ataxias using iPSC technology. Firstly, a highly reproducible methodology for generating cerebellar neurons under chemically defined and feeder-free culture conditions was established. Besides that, the manipulation of different signaling pathways was performed in order to achieve a higher number of GABAergic progenitors and functional Purkinje cells, which are important cerebellar neurons involved in cerebellar dysfunction. After the establishment of a new protocol for cerebellar differentiation, scalable generation of human iPSC-derived organoids using the novel PBS 0.1 (100 mL) Vertical-Wheel single-use bioreactors was implemented. In this system, human iPSC-derived organoids were able to adopt cerebellar identity and mature into different cerebellar neurons and to survive for up to 3 months, without feeder layers.

The presented work sets the foundation for developing new models for cerebellar ataxias, facilitating drug screening and the study of specific pathways involved in disease development and progression.

Keywords: Cerebellum, ataxias, human induced pluripotent stem cells, cerebellar differentiation, Purkinje cells

ACKNOWLEDGMENTS

Durante estes últimos anos, várias foram as pessoas que passaram e deixaram um pedacinho de si! É a vocês que devo o facto de ter alcançado a recta final e é sem dúvida graças a vocês que termino esta fase da minha vida de coração cheio! A todos, um profundo obrigado!

Em primeiro lugar, agradeço à Professora Carmo Fonseca e ao Professor Joaquim Cabral pela oportunidade de integrar os respetivos grupos de investigação e me darem a oportunidade de explorar este ambicioso projeto. À Professora Carmo agradeço todos os ensinamentos vindos de uma excelente cientista. Por ter acompanhado de perto todo o trabalho de forma tão entusiasta e me ter feito ver mais além. Ao Professor Joaquim, agradeço por toda a amabilidade, por estar sempre disponível a ajudar. E sobretudo pelas palavras amigas nos momentos de maior desespero.

À Geni e ao Tiago, a quem tenho a sorte de chamar de orientadores, mas acima de tudo de amigos! Geni, um grande obrigado, por me teres recebido tão amavelmente desde o meu primeiro dia de laboratório. Por me teres acompanhado de perto na bancada e por teres sempre uma explicação científica para me dar. Além disso, um obrigado pela excelente pessoa que és, por estares sempre disponível para mim. Foi um enorme prazer trabalhar contigo, com alguém tão modesto e com tantos ensinamentos para transmitir. Tiago, “Life is like music, it must be composed by ear, feeling and instinct, not by rule”, Samuel Butler. Um obrigado por teres acreditado em mim e teres depositado uma profunda confiança nas minhas capacidades e instintos. Foste um dos grandes pilares nesta fase da minha vida. Um profundo obrigado por me teres acompanhado de perto e me teres ajudado a ser uma melhor cientista.

Agradeço também a todos os meus amigos e colegas do SCERG e do IMM, que me deram suporte nesta importante fase da minha vida e tornaram esta caminhada bem mais fácil.

À Sandra Vaz agradeço todo o tempo que disponibilizou neste trabalho para apoiar nas análises funcionais. Todas as conversas e conselhos que tão amigavelmente me deste.

À team PBS, Carlos Rodrigues e Diogo Nogueira. Carlos, obrigada por me teres acompanhado no laboratório durante todos os meses de aprendizagem e por toda a disponibilidade. Diogo Nogueira, obrigada pelos conselhos e dicas, mas também pelas brincadeiras proporcionadas no laboratório.

Ana Rita Gomes e Mariana Branco, minhas princesas, o meu maior agradecimento é para vocês. Obrigado por estarem sempre presentes nos momentos de maior desânimo. Por estarem disponíveis a qualquer hora e momento para me ouvir e ajudar. Primeiro lugar, por todas as discussões de trabalho, todos os conselhos e dicas. Mas sobretudo, por serem o meu apoio incondicional! Obrigado pela partilha de risos, brincadeiras e bons momentos, mas também pela partilha de choros e abraços. Tenho a certeza que vos levarei comigo para o resto da vida independentemente do que o futuro nos reserve. Desejo-vos o melhor do mundo!

Joãozinho Cotovio, meu “filhote”, espero que depois destes anos todos consigas finalmente fazer ciência “a olho”. Foi um prazer enorme ver-te crescer. Obrigado pela partilha de bons momentos, por estares sempre disponível para me ouvir. És um orgulho para mim!

Aos primos, André Rodrigues e Diogo Pinto, obrigada pela partilha de momentos inesquecíveis. Foi bom poder rir ao vosso lado. Tornaram esta caminhada bem mais fácil. Aos meus companheiros de viagem, André Branco, Sara Bucar, Margarida Alves, Carina Manjua, Marília Silva e Sara Morini. Obrigado pela partilha de momentos tão especiais. Carina Maranga, minha pupila, obrigada pela ajuda nesta recta final.

Ao Jorge Pascoal, por me ter recebido tão bem no laboratório, me ter ensinado e apoiado durante o meu processo de aprendizagem, e por todas as discussões pertinentes. Ao Tiago Dias, por ter sempre a palavra certa, por me chamar à razão e fazer ver qual o caminho mais correto a seguir. À Cláudia Miranda, obrigada pelo companheirismo e ajuda no laboratório, a sénior mais querida de sempre! Ao Gonçalo Rodrigues, pelas valiosas conversas, por levantar as questões mais pertinentes e me "obrigar" a pensar seriamente em alcançar objetivos.

À Teresa Carvalho, Sandra Martins, Noélia Custódio, Simão Rocha e Bruno Jesus, por todas as dicas no laboratório e por estarem sempre disponíveis a ajudar. À Dinora Levy, agradeço todo o apoio técnico, mas também todas as nossas conversas. Aos meus meninos, Ana, Maria, Inês, Kenny, Rui, Pedro Prudêncio, Pedro Barbosa e Marta, obrigado pelo companheirismo e pela boa disposição. À Ritinha Drago, agradeço toda a amizade, por ter sempre uma palavra amiga. Um obrigado por todo o carinho e apoio. És sem dúvida uma pessoa muito especial!

Às minhas meninas do CNC, que apesar de estarem longe continuam sempre pertinho. Um especial obrigado à piolha Patrícia Rosado, que sempre acreditou em mim e que muito me ensinou.

Às minhas companheiras de sempre, Sarita, Magui, Raquel e Amandine, obrigado por estarem sempre presentes e acompanharem todo o meu percurso desde o início. Obrigada por todo o conforto e felicidade que me têm proporcionado durante estes longos anos.

Ao João Pedro, pelo apoio incondicional. Obrigado por sempre acreditares na minha genialidade, por toda a paciência e por tornares os meus problemas em tarefas simples de resolver. Muito obrigado!

A toda a minha família e amigos, o verdadeiro suporte que tornou tudo isto possível! Aos companheiros de uma vida, os meus irmãos, por estarem sempre presentes! Por sempre acreditarem incondicionalmente em mim e me apoiarem em tudo. Aos meus pais,

sem os quais isto não seria possível, agradeço por todo o esforço e dedicação para me verem chegar até aqui, por estarem ao meu lado de forma incondicional e apoiarem todas as minhas escolhas. É a vocês que devo aquilo que hoje sou! Um enorme obrigado!

Por fim, agradeço ao pequeno Rodrigo, a minha maior razão de sorrir!

“Recomeça…

Se puderes,

Sem angústia e sem pressa.

E os passos que deres,

Nesse caminho duro

Do futuro,

Dá-os em liberdade.

Enquanto não alcances

Não descanses.

De nenhum fruto queiras só metade.”

- Miguel Torga

INDEX

LIST OF FIGURES

LIST OF TABLES

LIST OF ABBREVIATIONS

2D - Two-dimensional

3D - Three-dimensional

5-HT - 5-hydroxytryptoamine, serotonin

AFALIFT - Absorbing film-assisted laser-induced forward transfer

A-T - Ataxia-telangiectasia

ATM - Ataxia-telangiectasia mutated

ATOH1 - Atonal homolog 1, also known as MATH1

BARLH1 - BarH Like Homeobox 1

BDNF - Brain Derived Neurotrophic Factor

BioLP - Biological laser processing

BMP - Bone morphogenetic protein

BSA - Bovine serum albumin

CALB - Calbindin

c-MYC - v-myc avian myeolocytomatosis viral oncogene homolog

CNQX - 6-cano-7-nitroquinoxaline-2, 3-dione

CNS - central nervous system

CV - coefficient of variation

DAPI - 4',6-diamidino-2-phenylindole

DCN - Deep cerebellar nuclei

DL-APV - DL-(−)-2-amino-5-phosphonopentanoic acid

DPAC - DNA-programmed assembly of cells

D-V - Dorsal-ventral

EBs - Embryoid bodies

ECM - Extracellular matrix

EGL - External germinal layer

EMT - Epithelial–mesenchymal transition

EN - Homeobox protein engrailed

ESCs - Embryonic stem cells

FGF - Fibroblast growth factor

FGS - Fetal goat serum

FLK-1 - Fetal Liver Kinase 1

FOXA2 - Forkhead box protein A2

FRDA - Friedreich ataxia

FRESH - Freeform reversible embedding of suspended hydrogels

GABA - Gamma-AminoButyric Acid

GAD - Glutamic acid decarboxylase

GAPDH - Glyceraldehyde-3-Phosphate Dehydrogenase

GBX2 - Gastrulation Brain Homeobox 2

GDNF - Glial-Derived Neurotrophic Factor

gfCDM - Growth-factor-free chemically defined medium

GMP - Good manufacturing practices

GRID2 - Glutamate Ionotropic Receptor Delta Type Subunit 2

HOXA2 - Homeobox protein Hox-A2

ICM - Inner cell mass

IP3R - Inositol trisphosphate receptor

iPSC - Induced pluripotent stem cell

IsO - Isthmic organizer

JAG1 - Jagged1

KIRREL2 - Kin of IRRE-like protein 2, also known as NEPH3

KLF4 - Krüppel-like factor 4

LG-DW - Laser-guided direct writing

LHX - LIM homeobox

LIFT - Laser-induced forward transfer

LIN28 - Lin-28 homolog A

LMX1b - Lim homeobox 1b

MAP2 - Microtubule-associated protein 2

MAPLE-DW - Matrix-assisted pulsed laser evaporation direct writing

MEIS2 - Meis Homeobox 2

MHB - Mid-hindbrain boundary

MIXL1 - Mix Paired-Like Homeobox 1

NGS - normal goat serum

NRGN - Neurogranin

NSCs - Neural stem cells

OCT4 - Octamer-binding transcription factor 4

OLIG2 - Oligodendrocyte transcription factor 2

OTX2 - Orthodenticle Homeobox 2

PAX - Paired box protein

PBS - Phosphate buffered saline

PCP2 - Purkinje Cell Protein 2, also known as L7

PDPA - Poly(2-(diisopropylamino)ethyl methacrylate)

PFA - Paraformaldehyde

PGD - Pre-implantation genetic diagnosis

PLGA - Poly(lactic-co-glycolic acid)

PMPC - Poly(2 (methacryloyloxy)ethyl phosphorylcholine)

PS - Penicillin/streptomycin

PSCs - Pluripotent stem cells

PTF1a - Pancreas specific transcription factor 1a

PVALB - Parvalbumin

PVOH - Poly-vinyl alcohol

PWM - Prospective white matter

r1 - Rhombomere 1

RA - Retinoic acid

R-C - Rostral-caudal

RL - Rhombic lip

ROCKi - Rho-associated coiled protein kinase inhibitor

RT - Room temperature

SB - SB431542

SCA - Spinocerebellar ataxias

SDF1 - Stromal cell-derived factor 1

SHH - Sonic hedgehog

SKOR2 - Ski family transcriptional corepressor 2, also known as CORL2

SOX - Sex determining region Y-box

TBR - T-box brain protein

TGFβ - Transforming growth factor β

TTX - Tetrodotoxin

TUJ1 - Neuron-specific class III beta-tubulin

VGAT - Vesicular GABA Transporter

VGLUT - vesicular glutamate transporter

VZ - ventricular zone

I. GENERAL INTRODUCTION

I.1 RESEARCH SUBJECT AND AIM

The cerebellum plays a critical role in the maintenance of balance and posture, coordination of voluntary movements and motor learning (Glickstein, 1993; McLachlan and Wilson, 2017; Schmahmann, 1997; Wassarman et al., 1997). Thus, a dysfunction of the cerebellum leads to cerebellar ataxia, a disorder characterized by severe impairment in motor coordination, for which no effective treatment is available (Klockgether, 2011). Most of the current knowledge about ataxias is based on postmortem studies and animal models that do not fully recapitulate the features of human disease (Manto and Marmolino, 2009a; Tiscornia et al., 2011). The development of new disease models is therefore an important unmet medical need.

The emergence of human induced pluripotent stem cells (iPSCs) holds great promise for regenerative medicine and disease modeling, since they can be differentiated into most cell lineages of the human body (Takahashi et al., 2007). Recently, the differentiation of human iPSCs into cerebellar organoids was reported, in which spatial patterning and morphogenesis of cerebellar development was recapitulated, generating polarized structures reminiscent of the first trimester cerebellum (Muguruma et al., 2015). Further maturation to functional cerebellar neurons, including Purkinje cells and Granule cells, was achieved by co-culture with human fetal cerebellar slices (Wang et al., 2015b) or mouse granule cells (Muguruma et al., 2015). As reported protocols for cerebellar differentiation involve the co-culturing systems and some variability associated with feeder cell source was reported (Wang et al., 2015b), the first aim of this thesis is to create a highly reproductive approach for generating cerebellar neurons under chemically defined and feeder-free culture conditions. Besides that, the described efficiency of Purkinje cell differentiation and further maturation is still very low. Thus, by manipulating different signaling pathways that

are be involved in Purkinje cell generation and functionalization, a higher number of GABAergic progenitors and further functional Purkinje cells can be reached.

In fact, the ability to produce cerebellar organoids opens up new avenues for regenerative medicine for disorders of the cerebellum. It can be used as model to study disease mechanisms, leading to the discovery of novel therapeutic targets, and patient-derived cerebellar organoids could be used to predict personalized response to drug treatment. Thus, our last aim is to develop the culture conditions to scale-up the production of size-controlled cerebellar organoids in bioreactors. Not only a greater number of organoids can be generated, but also the 3D maturation of the cerebellar neurons can be explored. Thus, this project aims to generate innovative *in vitro* models for studying and potentially reversing cerebellar dysfunction.

I.2 CEREBELLUM

Cerebellum is one of the most structurally conserved and elaborated region of the central nervous system (CNS), located in the posterior cranial fossa (Weaver, 2005). The involvement of this brain structure in motor functions is already well established, comprising the maintenance of balance and posture and the coordination of voluntary movements (Glickstein, 1993; Ito, 1984; Schmahmann, 1997). More recently, cerebellum has been also associated to non-motor functions, including auditory processing tasks (McLachlan and Wilson, 2017), reward expectation (Wagner et al., 2017) and other forms of emotional processing (Adamaszek et al., 2017). It contains significantly higher number of neurons than the cerebral cortex, even when cortical mass is larger and cerebellum only represents approximately 10% of the brain volume (Herculano-Houzel, 2010). Cerebellum is characterized by a well-defined structure, divided into two hemispheres with a midline vermis and it is organized into 3 different lobes that are divided into 10 lobules (Figure 1.1-A) (Marzban et al., 2015).

Cerebellum is formed by different sets of neurons, including inhibitory gamma-butyric acid (GABAergic) and excitatory Glutamatergic neurons, anatomically arranged into the cerebellar cortex that surrounds the white matter and the cerebellar nuclei. The cerebellar cortex is composed by different cell layers containing several types of neurons with an organized arrangement. This includes the Purkinje cell layer, containing a monolayer of the Purkinje cell bodies, Bergmann glial cells and a lower number of Candelabrum cells; between the innermost dense layer of Granule cells and Interneurons (Golgi cells, Unipolar Brush cells, and Lugaro cells), constituting the Granular layer; and the outermost layer with the inhibitory Interneurons (Stellate cells and Basket cells), which is the Molecular layer (**Figure I.1-B**). On the other hand, cerebellar nuclei are constituted by three major different neuronal types: large glutamatergic projection neurons, mid-sized GABAergic inhibitory

projection neurons and small GABAergic interneurons (Hoshino, 2012; Marzban et al., 2015; White and Sillitoe, 2013).

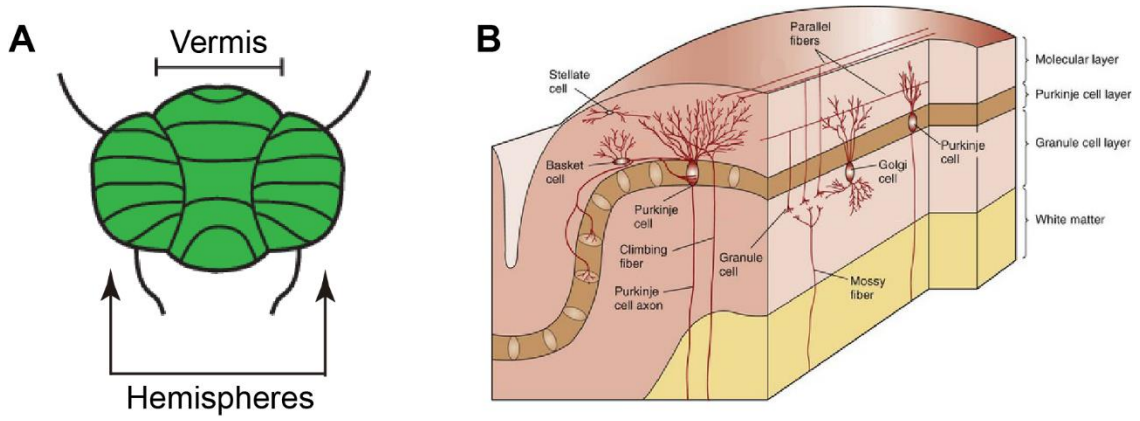

Figure I.1. Cerebellar structure. A) Superficial view of the cerebellum. The structure of mammalian cerebellum is characterized by the presence of two hemispheres with a midline vermis (Adapted from Butts et al., 2014). **B)** Structure of the cerebellar cortex. Sagittal and transversal view of the organization of the cerebellar cortex, with three different layers: Molecular, Purkinje cell and Granular layer (Adapted from Kandel et al., 2000).

Cerebellar development

During human embryogenesis, the generation of the CNS involves several crucial steps. It starts at an early embryonic stage, the third gestational week, and its development continues in the post-natal stage, up to and beyond late adolescence (Stiles and Jernigan, 2010). The neural induction, which is the earliest step of the neural development, occurs mainly by the inhibition of BMP (bone morphogenetic protein)/Nodal signaling and gives rise to the division of the ectoderm (Harland, 2000; Weinstein and Hemmati-Brivanlou, 1999). As a consequence, three different regions are formed: neural ectoderm or neural plate that originates the CNS; non-neuronal ectoderm, which will form the epidermis; and a region between neural and non-neural ectoderm, where the most part will convert to the neural crest (Gammill and Bronner-Fraser, 2003; Sadler, 2005). Once formed, the neural plate

borders elevate, neural tissue folds and forms the neural tube. When the formation of the neural tube is completed, a single layer of neural progenitor cells is exhibited that delineates the hollow center of the neural tube (Colas and Schoenwolf, 2001; Gammill and Bronner-Fraser, 2003; Martínez et al., 2012). The regional patterning of neural progenitor cells starts in the most rostral identity, the “primitive identity” (Levine and Brivanlou, 2007; Stern, 2001; Suzuki and Vanderhaeghen, 2015; Wilson and Houart, 2004). Later, this primitive identity can be converted to more caudal fates by the action of some morphogens, including retinoic acid (RA), WNT (protein wingless) and FGF (fibroblast growth factor) (Imaizumi et al., 2015; Irioka et al., 2005; Kirkeby et al., 2012). Consequently, four different regions are created along the rostral-caudal (R-C) axis of the neural tube: forebrain (prosencephalon), midbrain (mesencephalon), hindbrain (rhombencephalon) and spinal cord (**Figure I.2**). In addition to R-C axis, dorsal-ventral (D-V) direction is also determined by different concentration of morphogens provided by different organizing centers. For instance, while sonic hedgehog (SHH) is produced at the ventral side of the neural tube (Chiang et al., 1996; Martínez et al., 2012), at the opposite side BMPs and WNTs constitute dorsal signals (Basler et al., 1993; Dickinson et al., 1995; Ulloa and Martí, 2010) (**Figure I.2**). Thus, neural tube can be organized into different zones along the D-V axis: roof plate (dorsal-most), alar plate (dorsal), basal plate (ventral) and floor plate (ventral-most) (Eiraku and Sasai, 2012; **Figure I.2**). Subsequently, different types of neural progenitors are formed with capacity to originate specific types of neurons and glial cells.

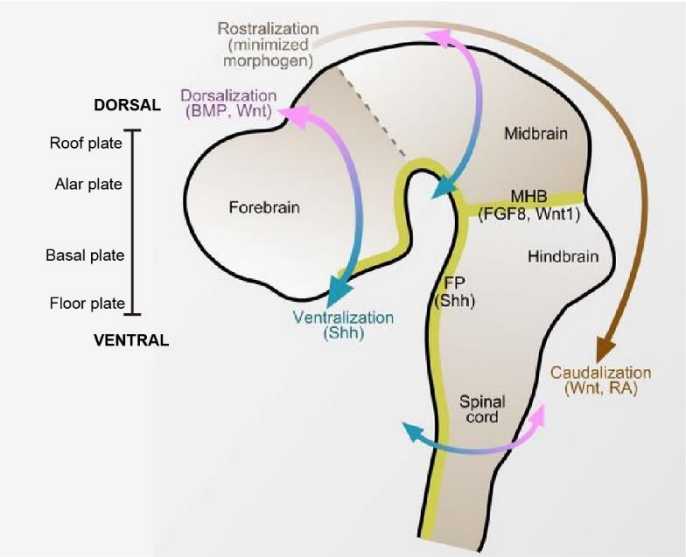

Figure I.2. Regional patterning of neural tube. Rostral-caudal (R-C) and dorsal-ventral (D-V) axis are determined by the action of various morphogens from different organizing centers. FP, floor plate; MHB, midbrain-hindbrain boundary (Adapted from Suzuki and Vanderhaeghen, 2015).

During early development, when the neural tube is being regionalized, the hindbrain or rhombencephalon is presented as a segmental structure, containing eleven different rhombomeres (Andreu et al., 2014; Morales and Hatten, 2006). The cerebellum primordium, called “cerebellar anlage”, is originated from one of the hindbrain segments, the rhombomere 1 – r1 (Zervas et al., 2004), which comprises the most anterior zone of the hindbrain caudally to the mid-hindbrain boundary (MHB), the isthmic organizer (IsO) (Butts et al., 2014). This boundary appears to be maintained by the differential expression of transcription factors OTX2 and GBX2, which are important for the development of forebrain/midbrain and anterior hindbrain respectively (Broccoli et al., 1999; Millet et al., 1999; Wassarman et al., 1997; Wurst et al., 2001). Therefore, the molecular limits of the IsO are delineating the rostral expression of OTX2 and caudal expression of GBX2 (Figure 1.3-A). The organizing activity of the IsO is essentially mediated by the secretion of FGF8, which is strongly expressed in the MHB and its confined localization is induced by the interaction of different transcription factors (Chizhikov and Millen, 2013; Crossley and Martin, 1995;

Heikinheimo et al., 1994; Joyner et al., 2000; Wurst et al., 2001) (**Figure I.3-A**). For instance, Lim homeobox 1b (LMX1b) appears to be important for FGF8 expression, while OTX2 induces the expression of LMX1b and consequently the repression of FGF8, LMX1b will trigger the expression of WNT1, which is able to stimulate neighboring cells to produce FGF8 (Adams et al., 2000; Guo et al., 2007; Matsunaga et al., 2002; **Figure I.3-B**). In contrast, GBX2 represses LMX1b (Chizhikov and Millen, 2013). As FGF8 also triggers the expression of WNT1, its maximum expression is present in $FGF8^{+}$ zone and decreases towards midbrain neuroepithelium, defining the rostral domain of MHB. In addition to WNT1, FGF8 also mediates the expression of the homeodomain transcription factors of engrailed family EN1/2 that, like WNT1, have the maximum expression levels near to $FGF8^{+}$ domain showing decreasing gradients towards hindbrain neuroepithelium (Andreu et al., 2014; Danielian and McMahon, 1996; Garda et al., 2001; Joyner, 1996; Martinez et al., 2013; **Figure I.3-B**). The organizing action of IsO plays an important role in the formation of the cerebellum, because it regulates expression of different transcription factors involved in r1 patterning (Irving and Mason, 2000). While OTX2 defines the rostral limit of the cerebellar territory, the caudal limit of the cerebellum is determined by the expression of HOX genes, particularly HOXA2, in the hindbrain region, also in response to FGF8 signaling from MHB (Gavalas et al., 1997; Irving and Mason, 2000).

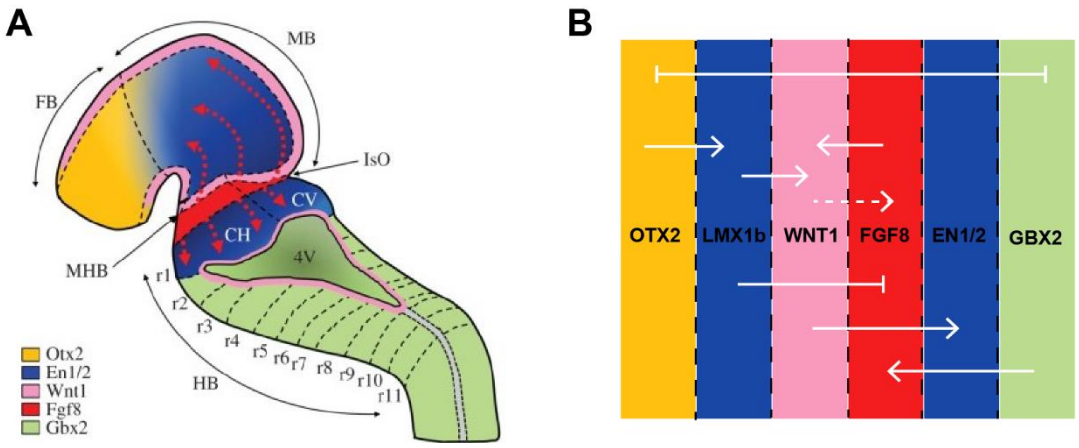

Figure I.3. Specification of cerebellar territory. A) Distribution of the gene expression gradients within mouse neural tube at E11.5. Interactions between the expression gradients define the boundaries between the forebrain (FB), midbrain (MB) and hindbrain (HB). Red dotted arrows indicate the FGF8 expression gradients. CH, cerebellar hemisphere; CV, cerebellar vermis (Watson et al., 2015). **B)** Molecular interactions of the major genes that coordinate the patterning of the midbrain/hindbrain region and cerebellar anlage specification.

After cerebellar territory formation, the cerebellar anlage is divided into two germinal centers that originate all cerebellar neurons, the ventricular zone (VZ) and the rhombic lip (RL) (Marzban et al., 2015; White and Sillitoe, 2013). The VZ is characterized by the expression of pancreas specific transcription factor 1a (PTF1a) and gives rise to all GABAergic neurons seen in the adult cerebellum (Hoshino et al., 2005). In contrast, the RL is a source of all cerebellar glutamatergic neurons and is essentially composed by atonal homolog 1 (ATOH1, also known as MATH1)-expressing progenitors (MacHold and Fishell, 2005; Wang et al., 2005). During development, cerebellar regionalization is achieved by the radial and tangential migration of post-mitotic neurons from the different germinal zones that will contribute to the final shape and size of the cerebellum (Andreu et al., 2014; Butts et al., 2014). The appearance of a temporary layer containing ATOH1^{+} proliferative progenitors derived from RL, at the surface of the developing cerebellum (Ben-Arie et al., 1996, 1997), the external germinal layer (EGL), is a key feature in the cerebellar development (White and Sillitoe, 2013). Already at a postnatal stage, the EGL-derived granule cells differentiate and

migrate radially from the molecular layer across Purkinje cell layer to the final destination, the granular cell layer. When granule cell migration is completed the final stage of cerebellum foliation is observed (Marzban et al., 2015; White and Sillitoe, 2013). Thus, the cerebellar specification starts early in the human embryonic development, at 6 weeks with the emergence of cerebellar anlage, and its final cytoarchitecture is only achieved in a postnatal stage (Cho et al., 2011; Millen et al., 1994).

GABAergic and Glutamatergic neurons of cerebellum

In the CNS, the neurotransmission is essentially based on excitatory and inhibitory outputs from Glutamate-releasing neurons (Glutamatergic neurons) and gamma-aminobutyric acid (GABA)-releasing neurons (GABAergic neurons), respectively. Both neurotransmitters are released from the synaptic terminals to activate postsynaptic ionotropic receptors, generating excitatory or inhibitory postsynaptic potentials. While GABA is synthesized in the GABAergic nerve terminal by the enzyme glutamate decarboxylase (GAD) and is accumulated into synaptic vesicles by the vesicular inhibitory amino acid transporter (VGAT) in the GABAergic neurons, for the glutamate there are no unique synthetic enzyme and it is accumulated into the synaptic vesicles of glutamatergic neurons by different specialized transporters (VGLUT1, 2 and 3) (Foster and Kemp, 2006).

As already mentioned above, the cerebellum is composed by two major subtypes of neurons, GABAergic and glutamatergic. While cerebellar cortex is mostly composed by GABAergic neuronal subtypes, containing six GABAergic (Purkinje cells, Golgi, Lugaro, Stellate, Basket and Candelabrum) and only two glutamatergic subtypes (Granule cells and unipolar brush cells), the deep cerebellar nuclei (DCN) contain GABAergic interneurons and both GABAergic and glutamatergic projection neurons (Andreu et al., 2014; Wang and Zoghbi, 2001).

GABAergic neurons can be divided into two different subtypes: GABAergic projection neurons (Purkinje cells and nuclei-olivary neurons) and interneurons (Leto and Rossi, 2012). Both cell types arise from $PTF1^+$ VZ, however the projection GABAergic neurons are originated from progenitors that are specified within the ventricular germinal layer, while the interneurons arise from a single $PAX2^+$ proliferative progenitor population that is generated in the VZ but later populates the prospective white matter (PWM) (Carletti and Rossi, 2007; Leto and Rossi, 2012; Maricich and Herrup, 1999; Zhang and Goldman, 1996; **Figure I.4**). Purkinje cells are the first to be specified, acquiring their positional information at or shortly after their differentiation in the VZ (Dastjerdi et al., 2012; Hoshino, 2012). Afterward, post-mitotic Purkinje cells migrate from VZ to a sub-ventricular zone, characterized by the stronger expression of LHX1/LHX5 and CORL2 (Leto et al., 2016). On the other hand, within the PWM, $PAX2^+$ progenitors continue to divide and mature acquiring their final phenotypic choice, before migrating from the white matter to reach their final location (Leto et al., 2012). In this manner different cerebellar interneurons are generated including Golgi, Lugaro, Basket and stellate cells and DCN interneurons. The phenotype of distinct GABAergic interneurons is defined by their expression of different specific markers: PAX2 and neurogranin for Golgi neurons, parvalbumin for the molecular layer interneurons (Stellate cells and Basket cells), and NeuN and calretinin for DCN interneurons (Bastianelli, 2003; Leto et al., 2012; Singec et al., 2003). The GABAergic Purkinje cells are the most salient cells of the cerebellar cortex and constitute the sole output of cerebellar cortical processing (Ruigrok et al., 2014). Their characteristic morphology is exhibited by a very large cell body and an elaborated dendritic tree (Goodlett and Mittleman, 2016). The expression of Purkinje cell markers is temporally dynamic, while some are selectively expressed in the embryonic stage, some expressed by Purkinje cells in adult, and in all cells or selectively expressed by Purkinje cell subsets (Dastjerdi et al., 2012; White and Sillitoe, 2013). Noteworthy, Calbindin is uniformly expressed by all Purkinje cells in adult (Whitney et al., 2008), as well as L7/PCP2

(Oberdick et al., 1990; Ozol et al., 1999), which is widely expressed in the stripes of Purkinje cells. In addition, IP3R and GRID2 are also specific markers for the stripes of adult Purkinje cells (Furutama et al., 2010; Yawata et al., 2006). On the other hand, neurogranin is expressed in a Purkinje cell cluster during embryogenesis but disappears in the adult (Larouche et al., 2006). Other marker that is expressed during cerebellar development is KIRREL2, also known as NEPH3, which is a GABAergic progenitor marker, being a direct downstream target of PTF1a that is involved in Purkinje cell fate specification (Mizuhara et al., 2010).

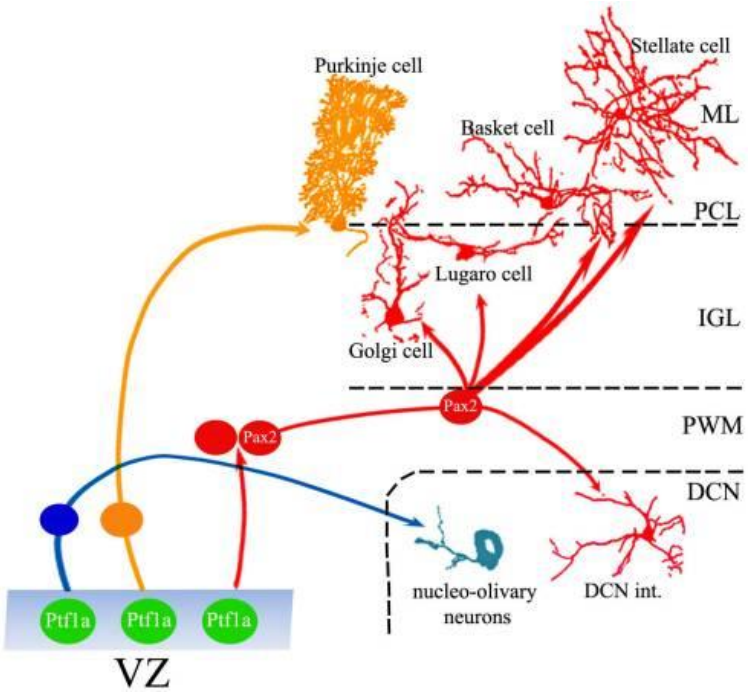

Figure I.4. Specification of cerebellar GABAergic neurons. All GABAergic neurons are originated from PTF1-a-positive progenitors in the VZ. Projection neurons are generated from precursors that proliferate and become specified within the VZ, whereas interneurons derive from a population originated from VZ, but afterwards migrate and become specified in the PWM. ML, molecular layer; PCL, Purkinje cell layer; IGL, internal granular layer; PWM, prospective white matter; DCN, deep cerebellar nuclei (Leto et al., 2012).

Glutamatergic neurons are originated from RL, including Granule cells, unipolar brush cells and large DCN projection neurons. The first cerebellar glutamatergic subtype that

leaves the RL consists of progenitors of DNC projection neurons, which migrate to subpial position (Fink et al., 2006; Hoshino, 2012). In contrast, unipolar brush cells and granule cells leave the RL at middle to late stage of embryonic development (Consalez and Hawkes, 2013; Hoshino, 2012; Leto et al., 2012). The postmitotic DNC projection neurons express a characteristic set of transcription factors, such as TBR1, IXR3, MEIS2, LHX2 and LHX9 (Fink et al., 2006; Morales and Hatten, 2006). In contrast, TBR2 is strongly expressed in the unipolar brush cells (Englund, 2006). The Granule cells represent the majority of neurons in the entire brain, being the smallest and the most densely packed neuronal type (Goodlett and Mittleman, 2016; Wagner et al., 2017). The signals from this important cerebellar glutamatergic subtype appear to be critical for the final maturation stages of Purkinje cells, when extensive dendritic arbors and synapses are being developed (Baptista et al., 1994; Rakic and Sidman, 1973). Therefore, Purkinje cells and Granule cells seem to be the most important inhibitory and excitatory neurons present in the human cerebellum.

I.3 CEREBELLAR ATAXIAS

The dysfunction of the cerebellum is translated into ataxia, a symptom detected in different neurodegenerative disorders consisting in motor dysfunction, balance problems, and limb movement and gait abnormalities. Thus, cerebellar ataxias comprise a phenotypically and genotypically heterogeneous group of disorders.

Given their heterogeneity, cerebellar ataxias can be further subdivided into sporadic, acquired and inherited (Anheim et al., 2012; Manto and Marmolino, 2009b). The sporadic ataxias usually present adult-onset progressive ataxia, in which does not exist an obvious familial background and both non-genetic and genetic causes should be considered (Klockgether, 2010). On the other hand, in acquired ataxias the genetic basis is still unclear and the causes are variable including stroke, immune disorders, toxicity, infectious diseases,

and metabolic causes (Manto and Marmolino, 2009b; Nachbauer et al., 2015). Inherited ataxias comprise the autosomal recessive and dominant cerebellar ataxias. Recessive ataxias are multisystem disorders that are manifested mostly in children and young adults and are usually associated with loss of protein function (Anheim et al., 2012; Taroni and DiDonato, 2004). In contract, autosomal dominant ataxias, usually known as spinocerebellar ataxias (SCA), typically have a late-onset (usually between 30 and 50 years of age), involving a progressive neurodegeneration with a fatal stage (Carlson et al., 2009; Dueñas et al., 2006; Schöls et al., 2004).

No cure is currently available for this group of severe disorders. Symptomatic treatments have been applied, but since cerebellar ataxias are very heterogeneous, universal treatment does not exist (Jones et al., 2014; Marmolino and Manto, 2010). For restoring the cerebellar function, different approaches have been used, such as the anti-ataxic medications using neuromodulators, motor rehabilitation therapy and non-invasive cerebellar stimulation (Benussi et al., 2015; Grimaldi et al., 2014). Even though patients showed some motor improvements using these treatments, the majority of those were applied only for the cases of infarction, metabolic/toxic and immune-mediated diseases and some cerebellar malformations (Mitoma and Manto, 2016). In contrast, for degenerative cerebellar ataxias, therapies are still missing, since the treatments used until now provide few benefits. Furthermore, most of presently used therapies are only able to promote the recovery at the early stages of cerebellar atrophy (Mitoma and Manto, 2016). Therefore, efforts to better understand the mechanisms involved in the neuropathology of the cerebellar ataxias should be done in order to design new potential therapies and create effective treatments with proven efficacy.

Disease model systems for cerebellar ataxias

The different model systems used until now played important role in providing information about the function of the cerebellum, the pathogenesis of cerebellar disorders and also by giving some cues about therapies for cerebellar dysfunction. In fact, most of the current knowledge on neuronal phenotypes associated to neurogenerative disorders is based on primary cultures, animal models and immortalized cell lines (Tiscornia et al., 2011). The access to live brain tissue is very limited and usually unavailable in amounts appropriate for research. The reliability of readouts from *post mortem* tissues is highly variable depending on the *post mortem* interval (J Siney et al., 2018), making disease progression and development difficult to understand.

To study cerebellar ataxias, a high number of animal models, including genetically engineered animals and those with spontaneous mutations, are used routinely in many laboratories (Manto and Marmolino, 2009a). The golden standard in cerebellar ataxias modeling are mouse models with massive Purkinje cell degeneration leading to histological defects and behavioral alterations (Cendelin et al., 2014; Grüsser-Cornehls and Bäurle, 2001). Despite the fact that models of cerebellar degenerative disorders have shown some similarities with human disease, the observed differences have greatly limited their research applications (Cendelin et al., 2014). Indeed, many candidate drugs that showed promising results and significant effects in animal models failed to promote relevant positive effects in clinical trials (Bart van der Worp et al., 2010; Hackam and Redelmeier, 2006; Pound, 2004). The interspecies differences, human brain complexity (Clowry et al., 2010; Oberheim et al., 2006) and disease-specific phenotypes make it difficult to accurately simulate human neurodegenerative diseases in animal models (Bart van der Worp et al., 2010).

In addition to human *post mortem* tissues and animal models, immortalized cell lines are also used to model cerebellar ataxias (Nascimento-Ferreira et al., 2011; Ziv et al., 1989).

Immortalized human cell lines are usually used for high-throughput drug screening because they are easy to grow and maintain with low associated costs, and they represent a homogeneous population with reproducible results. However, they do not reflect accurately normal physiological conditions (Durnaoglu et al., 2011; Ebert and Svendsen, 2010).

Now, alternative models have been developed based on the recent advances in stem cell research. First, human neural stem cell (NSCs), isolated in the 1990's for the first time (Eriksson et al., 1998; Kukekov et al., 1999) have been applied to provide a more realistic model of human disorders (Jakel et al., 2004). However, since these cells need to be isolated from human tissues, they are very difficult to isolate and the available amounts are not sufficient (Jakel et al., 2004). Although improvements in NSCs culture and expansion have been done (Skogh et al., 2001), NSCs expansion is still very limited and their capacity for unlimited self-renewal and plasticity remains unclear (Sterneckert et al., 2014). As an alternative, human pluripotent stem cells (PSCs) provide a new human cell source that has demonstrated great potential for disease modeling, drug screening and toxicology, since they have unlimited *in vitro* expansion potential and differentiation capacity (Kropp et al., 2017; Yamamoto et al., 2018).

I.4 HUMAN INDUCED PLURIPOTENT STEM CELLS AS A SOURCE FOR MODELING NEURODEGENERATIVE DISORDERS

The concept of "stem cells" was first introduced some time ago (Till et al., 1964), and is now defined as a population of undifferentiated cells characterized by their ability to self-renew and to differentiate giving rise to specialized cell types (De Los Angeles et al., 2015; Weissman, 2000). As different stem cells vary in their ability to differentiate into different cell types, they can be categorized by their differentiation potential in: totipotent, pluripotent and multipotent stem cells. Therefore, totipotent stem cells have the ability to generate an entire

organism (all embryonic and extra-embryonic cell types) and only zygote and early blastomeres are included in this classification. Pluripotent stem cells (PSCs) can originate cells from the three germ layers: ectoderm, endoderm and mesoderm. Lastly, multipotent stem cells, such as neural or hematopoietic stem cells, present a more restricted differentiation capacity, being already committed to give rise to cells of a limited spectrum of lineages (Durnaoglu et al., 2011; De Los Angeles et al., 2015).

Human PSCs have great potential for modeling human diseases and development, due to their ability to differentiate into most if not all embryonic and adult cell lineages. Moreover, they can, in theory, be indefinitely expanded maintaining an undifferentiated state (Kropp et al., 2017). In 1981, Gail Martin in parallel to Evans and Kaufman isolated and cultured PSCs for the first time, the mouse embryonic stem cells (ESCs) (Evans and Kaufman, 1981; Martin, 1981). Only in 1998, the first human ESCs were isolated from the inner cell mass (ICM) of the *in vitro* produced human blastocysts and were expanded *in vitro* (Thomson, 1998). The reported isolation and expansion of human ESCs opened the possibility to perform new *in vitro* studies for understanding normal human embryogenesis, disease-associated developmental abnormalities, for drug screenings and regenerative medicine (Gearhart, 1998).

Until twelve years ago, human disease-specific PSCs used for disease modeling were obtained from human ESCs by genetic modification of already existing ESCs or by isolation of human ESCs from embryos carrying monogenic disease-associated mutations detectable via pre-implantation genetic diagnosis (PGD) (Colman and Dreesen, 2009; Maury et al., 2012). Genetically modified human ESCs were reported for the first time in 2004 (Urbach et al., 2004). However, the methods used for generating these modifications showed low efficiency of gene targeting. By using PGD embryos, only in few studies the disease-associated phenotypes have been recapitulated (Maury et al., 2012). Besides that, only in 2007, Eiges et al. were able to demonstrate novel early developmental information using

disease-derived human ESCs obtained from PGD embryos. Therefore, some barriers should be overcome in human ESC-derived disease modeling, including the limited number of diseases captured by PGD, inefficient methods for generating modified human ESC lines, ethical issues regarding the use of embryos and lack of consistency of human ESC-derived models.

Induced Pluripotent stem cells (iPSCs)

The development of human induced pluripotent stem cell (iPSC) technology has greatly improved the prospects for disease modeling and regenerative medicine. Takahashi and Yamanaka were the first to demonstrate the possibility to reprogram somatic cells into embryonic state-like cells by introducing a cocktail of four transcription factors (Octamer-binding transcription factor 4, OCT4; Sex determining region Y-box 2, SOX2; Krüppel-like factor 4, KLF4; and v-myc avian myeolocytomatosis viral oncogene homolog; c-MYC) in mouse fibroblasts (Takahashi and Yamanaka, 2006). Building on their earlier report, the reprogramming was then applied to human cells (Takahashi et al., 2007; Yu et al., 2007). Takahashi and Yamanaka introduced exactly the same cocktail in human fibroblast (Takahashi et al., 2007). Simultaneously, Yu et al. also reported the generation of human iPSCs from fibroblasts, but replacing the oncogene c-MYC by a post-transcriptional regulator, lin-28 homolog A (LIN28) (Yu et al., 2007). In both studies, the generated human iPSCs showed similar proprieties to human ESCs, having the same morphology and proliferation capacity when cultured *in vitro*. Besides that, both cell types shared the same transcriptional and epigenetic features (Takahashi et al., 2007; Yu et al., 2007).

Many critical issues involved in the process of generation of iPSCs influence the efficiency of the reprogramming and the quality of the obtained cells, including: the somatic cell type used for the reprogramming, the factors used to induce the pluripotency features

as well as the technology used to deliver these factors (Brouwer et al., 2016; Durnaoglu et al., 2011). For that reason, efforts to improve efficiency and quality of human iPSCs have been made in the last years. In addition to fibroblasts, other somatic cell sources have been reported (Singh et al., 2015). According to the cell type used for reprogramming, differences in efficiencies (Aasen et al., 2008), as well as in the tendency to form teratomas (Miura et al., 2009), were observed. Furthermore, alterations in the cocktail of the reprogramming factors have been also performed (Brouwer et al., 2016; Singh et al., 2015). The main objective is to successfully reprogram the cells in the absence of oncogenic potential. Therefore, new reprogramming factors that do not present tumorigenicity have been used, including small molecules (Huangfu et al., 2008; Lee et al., 2012) and microRNAs (Judson et al., 2009; Marson et al., 2008) that enhance the reprogramming efficiency and replace the potentially oncogenic reprograming factors used initially, particularly c-MYC. Lastly, different methodologies has been used for delivering the reprograming factors, including integrative viral vector systems and non-integrating methods (Brouwer et al., 2016; Singh et al., 2015). Although many methods have been used that avoid the random integration into the genome of reprogramed cells as seen in the integrative methods (Zhou and Zeng, 2013), integrating viral vectors is still mostly used because of higher reprogramming efficiencies (Bellin et al., 2012). In conclusion, there are crucial points that should be considered in the reprogramming process to have high efficiencies with a minimal risks associated.

Although the exact mechanism involved in the reprogramming process of iPSCs generation is still unclear, valuable iPSC contributions to uncover the pathological mechanisms associated with disease manifestation and to potential disease treatment are well-recognized. Cell-based therapies, drug discovery and screening, toxicological studies, and disease and human developmental modeling are the most encouraging applications of iPSC technology (**Figure I.5**).

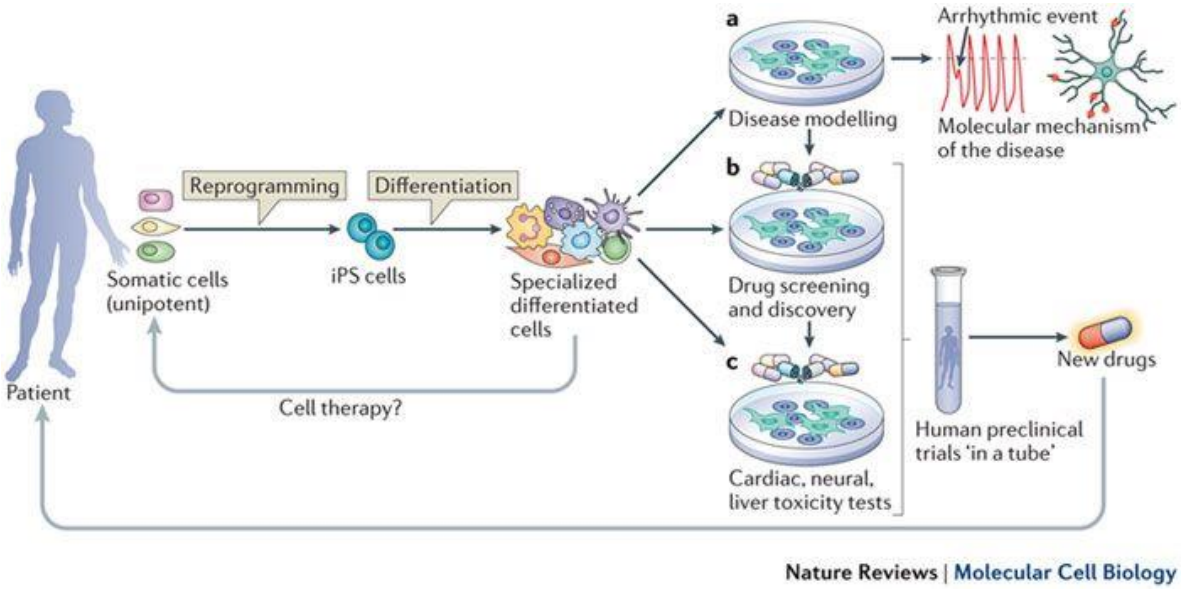

Figure I.5. Applications of iPSC technology. Induced pluripotent stem cells (iPSCs) can be generated by reprogramming from adult somatic cells derived from patients. *In vitro* differentiation of patient-derived iPSCs can provide a valuable tool for disease modeling (a), drug screening and discovery (b) and toxicity tests (c; Bellin et al., 2012).

For the first time in 2008, Park and colleagues generated disease-derived iPSCs from patients that suffered from a variety of genetic diseases giving the opportunity to recapitulate both healthy and disease-associated human tissue formation *in vitro* (Park et al., 2008). In fact, this ability to generate human iPSCs from patient-derived somatic cells provides the most relevant cell source for drug screening and human disease study by reproducing the patient's background.

Human iPSCs for modeling cerebellar ataxias

The knowledge about neural differentiation and regional specification has provided a base for establishment of different protocols for directing PSC differentiation to specific cortical, striatal, midbrain, spinal cord neurons and glia (Aubry et al., 2008; Gunhanlar et al.,

2018; Hu and Zhang, 2009; Junghyun Jo et al., 2016; Rodrigues et al., 2017). Consequently, the application of these new approaches to model neurogenerative disorders has been improved. However, for cerebellar disorders, only few studies have reported the use of patient-derived iPSCs to study cerebellar dysfunction (Lukovic et al., 2017). Moreover, the majority of studies have generated non-cerebellar neurons (Bird et al., 2014; Koch et al., 2011a; Nayler et al., 2012) as well as others disease-associated cell types (Hick et al., 2013; Igoillo-Esteve et al., 2015; Liu et al., 2011a), and only three reports have described protocols to generate cerebellar neurons from patient-derived iPSCs (Ishida et al., 2016; Morino et al., 2015; Nayler et al., 2017).

In 2010, Ku and others were the first to report a possible molecular explanation for repeated nucleotide expansion in Friedreich ataxia (FRDA), which is an autosomal recessive ataxia associated with cardiomyopathy (Delatycki et al., 2000) usually caused by an expansion of a GAA trinucleotide repeat in the first intron of the frataxin (*FXN*) gene (Lodi et al., 1999), based on alterations in FRDA-derived iPSCs (Ku et al., 2010). Neural differentiation of patient-derived iPSCs was not performed in this study. Afterwards, in addition to FRDA, iPSC-derived cerebellar ataxia modeling was implemented for SCAs and ataxia-telangiectasia (A-T), which is a autosomal recessive disorder characterized by prominent loss of cerebellar Purkinje cells caused by homozygous or compound heterozygous mutations in the ataxia-telangiectasia mutated (*ATM*) gene (Herrup et al., 2014).

In iPSC-derived FRDA models, relevant disease-associated phenotypes were detected in different cell types, including neural progenitors, neurons, cardiomyocytes and β-cells (Bird et al., 2014; Du et al., 2012; Eigentler et al., 2013; Hick et al., 2013; Igoillo-Esteve et al., 2015; Lee et al., 2014; Liu et al., 2011b; Shan et al., 2014; Soragni et al., 2014). The mitochondrial dysfunction and the reduction of *FXN* mRNA and protein levels were detected in most of the studies (Eigentler et al., 2013; Hick et al., 2013; Igoillo-Esteve

et al., 2015; Lee et al., 2014). In addition to these important findings unveiling pathological mechanisms of FRDA, approaches for reverting the disease phenotype were also explored in iPSC-derived models (Igoillo-Esteve et al., 2015; Soragni et al., 2014). Soragni and colleagues reported the use of FRDA iPSC-derived neurons to determine the efficacy of a modulator of *FXN* gene expression and chromatin histone modifications that were further used in phase I clinical trial (Soragni et al., 2014). Positive effects were observed in FRDA patients with increased *FXN* mRNA levels (Soragni et al., 2014).

For A-T, the first report of patient-derived iPSCs was published in 2012, in which observed low efficiency of reprogramming was attributed to characteristic chromosomal instability caused by ATM mutation(s) (Nayler et al., 2012). Later, the hypersensitivity to X-ray irradiation in A-T iPSCs was confirmed by Fukawatase and others. However, while chromosomal instability was also detected in parental cells, iPSCs derived from A-T patients did not exhibit the same deregulation (Fukawatase et al., 2014). Even with a reduced reprogramming efficiency, A-T iPSCs were efficiently differentiated into neural progenitors (Lee et al., 2013) and neurons (Carlessi et al., 2014; Nayler et al., 2012, 2017), showing defects in DNA damage responses and alterations in the synaptic and neuronal maturation markers. Only in 2017, A-T iPSCs were for the first time differentiated into cerebellar neurons (Nayler et al., 2017). The authors showed that patient-derived cerebellar neurons exhibit disrupted gene regulatory networks associated with synaptic vesicle dynamics and oxidative stress (Nayler et al., 2017). This study revealed important molecular insights about the early cerebellar pathogenesis of A-T, however the most significant cerebellar cell type involved in the neuropathological manifestation of A-T, the Purkinje cells, was not generated and evaluated.

Until now, all studies for SCA modeling using iPSCs were focused on polyglutamine SCAs, including SCA 2, 3, 6 and 7 (Ishida et al., 2016; Koch et al., 2011b; Luo et al., 2012; Xia et al., 2012), which are associated with the expansion of a CAG repeat in the respective

causative gene. Morino et al. were pioneers in successfully differentiating SCA patient-derived iPSCs into Purkinje cells (Morino et al., 2015). However, disease phenotype was not determined and no significant differences in Purkinje cell morphology was observed between control and disease-derived cells (Morino et al., 2015). Recently, the most interesting and enthusiastic study described derivation of Purkinje cells to examine disease phenotype (Ishida et al., 2016). Additionally to contributing for understanding disease pathology, the generated iPSC-derived disease model for SCA6 was also used for investigating new promising drugs for rescuing the neuropathology.

Despite cerebellar cells, mainly Purkinje cells, exhibit high developmental complexity, and the generation of functional cerebellar neurons from iPSCs is still very difficult, recent and encouraging progress in this field has been made. Therefore, it is possible that in the near future the use of iPSC-derived models will help to understand the molecular and cellular mechanisms underlying human cerebellar degeneration more precisely and thus provide valuable cues for prevention and treatment of cerebellar dysfunction.

Cerebellar differentiation from PSCs

In the last years, advances in our understanding of cerebellar development and differentiation have fostered generation of techniques for obtaining different types of cerebellar neurons from PSCs. Sue and colleagues reported for the first time the generation of Granule and Purkinje cells from mouse embryonic stem cells (ESCs) (Su et al., 2006). Following neural induction, neural progenitors were treated with BMP4/WNT3a leading to the generation of ATOH1^{+} cerebellar granular progenitors, achieved by the caudalization and dorsalization effect of WNT3a and BMP4. After cell sorting, ATOH1^{+} progenitors were efficiently differentiated into Granule cells (PAX6^{+}) by co-culturing with mouse embryonic EGL precursors. In addition to Granule cells, Purkinje cells (Calbindin^{+} and L7^{+}) were also

obtained at a lower percentage (1-3% of total differentiated neurons) using the same methodology, but replacing WNT3a by FGF8 (Su et al., 2006). Salero et al. applied the same approach to differentiate mouse ESC into cerebellar granule cells by using FGF8 and RA ("cerebellar organizers" that promote mid-hindbrain commitment), followed by WNTS, BMP7, GDF7, and BMP6 (signals that induce dorsal cerebellar neuroepithelium), SHH and JAG1 (ligands promoting proliferation of granular progenitors), and medium conditioned by cerebellar glial cells (Salero and Hatten, 2007). Among a vast number of cells expressing granular markers obtained in this study, cells with staining for Purkinje cell and Bergman cell markers were also found. However, the conditions for the differentiation of these cell types were not optimized.

In 2010, the protocol was reproduced in human ESCs using different inductive signals that induce early cerebellar patterning followed by the application of various factors, which promoted the differentiation into different cerebellar cells, including granule neurons, Purkinje cells, interneurons and glial cells (Erceg et al., 2010). The efficiency of Purkinje cell differentiation was significantly higher than in mouse ESC-based protocols, achieving about 11% of cells expressing L7 marker (Erceg et al., 2010). Although functional electrophysiological activity in the mixture of the generated cells was demonstrated, only few cells exhibited staining for L7 and their morphology was not similar to that of Purkinje cell.

In order to improve Purkinje cell differentiation efficiency, Tao and colleagues proposed the use of a co-culture system for increasing the survival and maturation of mouse Purkinje cells. In fact, the number of surviving Purkinje cells was significantly increased (two-fold to nine-fold) when the co-culture with whole postnatal cerebellum-derived cells was used (Tao et al., 2010). Although a correct morphology of Purkinje cells was observed in both co-cultured and feeder-free conditions, the maturation was incomplete or abnormal when cells were cultured without feeder cells or even when cultured with neonatal cerebellar

feeders. Only the co-culture system using postnatal cerebellum was capable of achieving the morphology and synaptogenesis of mature Purkinje cells (Tao et al., 2010). The reported variability in the efficiency to obtain mature Purkinje cells using different feeder cells sources was demonstrated later by Wang et al. (Wang et al., 2015b). These authors showed the generation of mature functional Purkinje cells from human iPSCs, by sorting KIRREL2^{+} GABAergic progenitors and further use of feeder layers to promote maturation. However, by using different sources of feeder cells the observed results were significantly different. Feeder-free and co-culturing with rat granular progenitors completely failed to achieve maturation. In contrast, by using rat cerebellar slices, the obtained cells showed a correct morphology but without appropriated membrane features, since no action potential and spontaneous post-synaptic currents were detected. Only the co-cultured cells with human fetal cerebellar slices showed right morphological proprieties and were electrophysiologically functional Purkinje neurons (Wang et al., 2015b). Therefore, it is still unclear which is the most permissive feeder cell source to provide the correct environment for the generation of functional Purkinje cells.

Muguruma and coworkers showed for the first time the possibility of using both mouse and human ESCs for *in vitro* recreation of the organized structure as seen during cerebellar ontogenesis by using a strategy that can mimic the initial cerebellar development associated with the specification of isthmic organizer (Muguruma, 2018; Muguruma et al., 2010, 2015). The initial neural commitment is achieved in floating aggregates by using a transforming growth factor β (TGFβ) inhibitor, which prevents mesenchymal differentiation and induces neuroectodermal commitment. Furthermore, by using FGF2 and insulin, which act as moderate caudalizing factors, the authors promoted an up-regulation of FGF8 and WNT1 expression, leading to an efficient generation of mid-hindbrain progenitors (EN2^{+} and GBX2^{+}). After 35 days in culture, about 28% of the generated cells expressed KIRREL2. For Purkinje cell differentiation and maturation, KIRREL2^{+} cells were separated by cell sorting

and afterwards co-cultured with mouse RL-derived granule cells. In fact, an efficient Purkinje cell maturation was shown, demonstrated by elaborated morphology and functional proprieties, and other types of cerebellar neurons were also obtained, including Golgi cells and interneurons (Muguruma et al., 2015). The same approach was applied for Granule cells generation, and, in contract to mouse ESCs (Muguruma et al., 2010), human ESCs did not need the BMP4-inducing effect for granular progenitor generation (Muguruma et al., 2015). Further maturation of migratory granule cell progenitors (PSA-NCAM$^+$ cells purified by FACS) was promoted from day 42 by co-culturing with mouse RL-derived granule cells (Muguruma et al., 2015).

Besides using FGF2 and insulin treatment together with co-culturing to generate different cerebellar neurons, the authors were capable of promoting the self-organization of cerebellar neuroepithelium derived from human ESCs. The sequential addition of FGF19 and SDF1 to the floating aggregates promoted not only the self-formation of mid-hindbrain structures with apico-basal polarity, but also the further re-organization into larger cerebellar neuroepithelium composed by three different cell layers. These layers included an apical layer occupied by SOX2$^+$/KIRREL2$^+$/PFT1$^+$ cells, similar to cerebellar VZ, an intermediate layer with Purkinje cell progenitors (OLIG2$^+$, LHX5$^+$, CORL2$^+$ and GAD$^+$) and a basal layer similar to RL zone, containing ATOH1$^+$/BARLH1$^+$ cells (Muguruma et al., 2015).

Further optimizations were performed more recently to simplify the generation of early neuroepithelium and the maturation of Purkinje cells (Holmes and Heine, 2017; Watson et al., 2018). However, these improvements were not significant, since the generated neuroepithelium did not show an organized structure (Holmes and Heine, 2017). Besides that, the maturation of Purkinje cells was once again achieved by co-culturing with mouse cerebellar cells and was not assessed for functionality by electrophysiology (Watson et al., 2018).

Thus, the most efficient method for the generation of functional Purkinje cells reported until now involves the co-culture with feeder cells, which is debatable method that introduces significant variability between experiments, so future studies are required to create a new culture system with higher efficiency and reproducibility. To overcome these limitations distinct bioengineering approaches can be used to manipulate stem cell differentiation and direct *in vitro* morphogenesis.

I.5 DESIGN PRINCIPLES FOR PLURIPOTENT STEM CELL-DERIVED ORGANOIDS ENGINEERING

The application of the biomimicry concept, defined as the imitation of biological systems, to biomedical research has contributed to a significant innovation in regenerative medicine during the last years. This concept is usually associated with new approaches that aim to achieve the recapitulation of the natural form or function, natural processes or natural systems (Simunovic and Brivanlou, 2017; Zhang, 2012). In the bioengineering field, efforts have been made to mimic the natural forms and functions of the human body *in vitro*, from the molecular to the cellular level, in an attempt to recreate the highest complexity level, the organism.

Recently, with the discovery of the ability of PSCs to coordinate various key signals and to recapitulate different structures as seen *in vivo*, including tissue- and mini organ-like structures, our knowledge about human development and morphogenesis in healthy and disease context has been greatly improved (Lancaster et al., 2012; Sasai, 2013). With the recapitulation of human organogenesis *in vitro*, the concept “organoid” emerged. In 1946, the “organoid” term was employed for the first time to define a tumor-derived mass isolated from a human tissue (Smith and Cochrane, 1946). Subsequently, all tissue masses resultant

from transplants were defined as “organoids” (Waddell, 1949; Yoshida et al., 1980) and the concept evolved to include cultures that were generated from dissociation and aggregation of animal- and tissue-derived cells (Elkasaby et al., 1991; Ridgeway et al., 1986; Schröter-Kermani et al., 1991). With the recent advances in human PSC expansion culture and direct differentiation, the “organoid” definition followed the same evolution, nowadays referring to an *in vitro* 3D multicellular structure containing different cell types with self-organization, as seen in human tissues, typically derived from stem cells (Simunovic and Brivanlou, 2017). Frequently, organoids display spherical or irregular shapes in suspension, or are embedded in different types of matrices (Lou and Leung, 2018).

The recreation of functional and structural mimicry within the organoid requires a minimal number of design components inspired on the original biological system. These include cellular and non-cellular parameters, such as cell type, microenvironmental and physical parameters, as well as the resulting internal and external interactions, like cell-cell, cell-matrix, and cell-microenvironment interactions (Yin et al., 2016). The ultimate goal is to reestablish some of the features of human tissues, particularly the presence of different cell types to recapitulate the multicellular heterogeneity, control the microenvironment to recreate a high level of organization, and promoting organoid maturation to achieve tissue functionality (Lou and Leung, 2018). Thus, the application of bioengineering strategies to manipulate cellular and non-cellular components may become a powerful tool to direct 3D human organoid morphogenesis.

The remarkable progress in organoid generation has provided the possibility to use these novel platforms for understanding human development and complex processes involved in organogenesis. The use of organoids in drug screening and toxicological testing could also improve the safety and efficiency of drugs before reaching clinical trials, making the drug development process more cost-effective. Lastly, disease-derived organoids could

also offer a valuable platform to study the mechanisms involved in disease manifestation and to identify possible therapeutic targets.

Here, we review distinct bioengineering approaches to direct the stem cell commitment and further self-organization of cells, recapitulating tissue morphogenesis *in vitro*. First, the self-organization capacity of cells is explored based on cell-cell and cell-matrix interaction. Afterwards, as self-organization is based on three different cell-associated capacities, including self-assembly, self-patterning and self-morphogenesis, we highlight examples of bioengineering methodologies to control the initial state and the spatiotemporal positioning of cells, and lastly the growth and remodeling of multicellular aggregates to achieve complex structures.

Self-organization in PSC-derived organoids

The ability of human PSCs to produce highly organized structures that reproduce features similar to the embryo and adult tissues was first detected in the teratomas formed after the injection of human ESCs in immune-deficient mice (reviewed in Przyborski, 2005). The “self-organization” capacity involves three different categories, first the control of relative cell position, named “self-assembly”, second the spatiotemporal control of the cell stage, defined as “self-patterning”, and lastly the capacity to promote deformation, growth and remodeling, which is termed “self-morphogenesis” (Li et al., 2014). This intrinsic ability of organization is strongly dependent of physical and morphological proprieties of cells, the autologous and exogenous signals that they receive, and also the mechanical features of the system.

Cell-Cell adhesive interactions

During embryogenesis, the cell-cell interactions play a critical role in the dynamic changes of cell sorting, arrangement and migration that originate different tissue morphologies. The adhesive forces between cells are crucial for the assembly and organization into a 3D structure. The most important and global mechanism of cell adhesive interactions is mediated by cadherins, which are Ca^{2+}-dependent transmembrane proteins that facilitate homophilic cell-cell adhesion by their extracellular domains, whereas the intracellular domain interacts with their partner proteins, the catenins (Gumbiner, 1996). Following cell-cell adhesion, a protein complex is formed composed by the catenin polypeptide from α-, β- or γ-catenins (Marie et al., 2014). Subsequently, α-catenin mediates physical interaction to the actin cytoskeleton, demonstrating that cadherins can also guide cell cytoskeletal anchoring (Itoh et al., 1997; Rimm et al., 1995). Different cadherins are expressed in different tissues and the best-studied are the classical vertebrate cadherins, including N-cadherin, highly expressed in the neuronal tissue, and E-cadherin, mostly expressed in the epithelial cells (Takeichi, 1987). Non-classical cadherins can be found in other human tissues, for instance VE-cadherin, which is the vascular-endothelial cadherin, and R-cadherin, expressed in the retinal tissue (Gumbiner, 2005).

During morphogenesis, different mechanisms involving cadherins appear to influence cell sorting and therefore alter the spatial organization of cells. The expression of different types of cadherins in different cell types promotes the selective recognition and connection of cells expressing the same type of cadherin leading to cell sorting and separation into different tissues (Friedlander et al., 1989; Price et al., 2002; Suzuki et al., 1997; Takeichi, 1995). For instance, N-cadherin expression in neural cells allows the separation from epithelial cells that express E-cadherin (Gumbiner, 2005; Katsamba et al., 2009; **Figure I.6-A**). In other cases, independently of cadherin type expression, cell sorting is also observed

based on differential levels of cadherin expression (Duguay et al., 2003; Friedlander et al., 1989; Godt and Tepass, 1998). The epithelial–mesenchymal transition (EMT), the reverse of epithelization, is a strong example of self-assembly capacity of cells mediated by cadherin expression and regulation (Hay and Zuk, 1995; **Figure I.6-B**). This process is achieved by altering cell-cell contact and promoting cell migration. In particular, E-cadherin is down-regulated during the transition to mesenchymal state, leading to decrease of cell-cell interactions (Cano et al., 2000; Moore et al., 2014). Simultaneously, an alteration on cellular signaling profiles and a re-modulation of cytoskeleton is observed, allowing cell migration (Lamouille et al., 2014).

In addition, other physiological factors that interact with cadherin-mediated signaling can influence cell sorting independently of cadherins expression. During development, anterior-posterior axis is created leading to the formation of compartment boundaries. Although epithelial cells express high levels of E-cadherin, selective adhesion is observed creating different boundaries in response to Hedgehog (Hh) signaling (Dahmann and Basler, 2000; Tepass et al., 2002) (**Figure I.6-C**). Activation of Hh expression in posterior cells conduces to diffusion of signals across the anterior-posterior boundary that determine the sorting of some anterior cells next to the boundary, which are not capable of receiving Hh and are sorted toward the posterior region (Tepass et al., 2002). Besides that, the dynamic regulation of cadherin adhesions may drive cell re-arrangements and migration. By breaking and reforming cadherin adhesive bonds, the convergent extension movements (**Figure I.6-D**) contribute to tissue morphogenesis by changing local cellular arrangement with respect to neighboring cells (Gumbiner, 1992; Zhong et al., 1999).

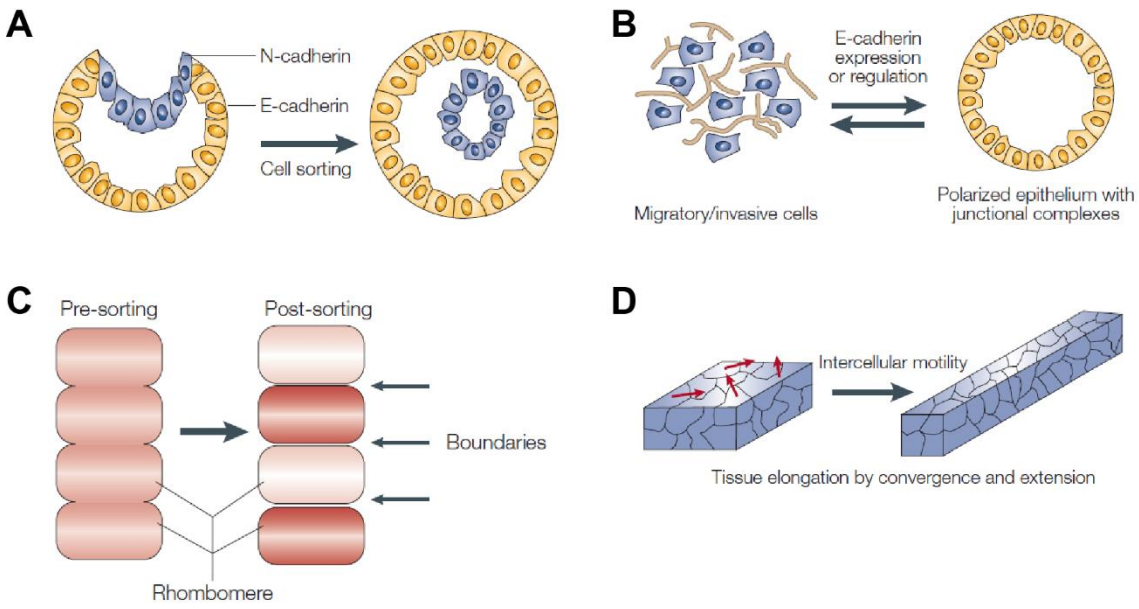

Figure I.6. Involvement of cadherins in tissue morphogenesis. A) Cell sorting based on differential expression of cadherins. **B)** Epithelial–mesenchymal transition (EMT) and its reverse, the mesenchymal–epithelial transition. **C)** Formation of boundaries between developmental compartments in a tissue. **D)** Cell rearrangements based on breaking and reforming of cadherin. (Adapted from (Gumbiner, 2005).

Besides the important function of cadherins during morphogenesis, it was already demonstrated their critical role in cell aggregate formation and further differentiation. By inhibition of E-cadherin mediated adhesion the agglomeration of ESCs in cell aggregates is prevented as well as their differentiation (Dang, 2004; Dasgupta et al., 2005; Fok and Zandstra, 2005). Hence, technologies to control stem cell differentiation by manipulating cell-cell interactions have been created (Alimperti and Andreadis, 2015). For example, surface engineering by immobilization of cadherins has been used to manipulate cadherin-mediated signaling pathways and thus direct stem cell fate decisions (Alimperti and Andreadis, 2015; Beckstead et al., 2006).

Cell-Matrix interaction

Not only cell-cell interactions provide important signals in the cell niche, but also other structural, physical, electrical, or biochemical signals present in the complex microenvironment during the embryonic development affect cell fate decisions (Gattazzo et al., 2014). The extracellular matrix (ECM) is an important component that gives the structural support to the cell niche and also contributes for mediating signaling for cell migration, retention and polarization (Peerani and Zandstra, 2010). The ECM is composed primarily by glycosaminoglycans and fibrous proteins that are secreted by the cells to generate their own physical scaffold (Bratt-Leal et al., 2009; Gattazzo et al., 2014). Cells interact with ECM molecules via integrins, which are cell adhesion receptors, regulating the cellular behavior (Legate et al., 2009).

Integrins present a family of heterodimeric transmembrane glycoproteins where heterodimers are composed by non-covalently connected α and β subunits (Hynes, 2002; Tamkun et al., 1986). In vertebrates, 24 different heterodimers resulting from different assembly of 18 α subunits and 8 β subunits have been described (Barczyk et al., 2010). Based on their subunit composition, integrins can be assembled in different subgroups. Under certain conditions, each cell type exhibits a specific integrin signature, including subgroup and quantity of integrins. However, this is a dynamic process, and both developmental stage and microenvironmental conditions can change the integrin repertoire (Barczyk et al., 2010). While the extracellular domain of integrins interacts with components of ECM including fibronectin, laminin and collagens, the intracellular domain links to cytoskeletal and regulatory proteins, such as α-actinin, filamin, calreticulin and cytohesin (Darribére et al., 2000). It is also known that the same component of ECM interacts with different integrin receptors, and in the same way a specific integrin receptor may recognize different ECM components (Barczyk et al., 2010; Darribére et al., 2000).

The role of integrins during embryogenesis has been extensively studied and the data accumulated so far are already enough to place integrins as important players in fertilization, cell migration in gastrulation, adhesion in embryo implantation, and generation of different organ systems, like the nervous system (Darribére et al., 2000). Additionally, it was already shown that the composition of ECM is able to influence ESCs behavior in the development of 3D structures as well as their differentiation. For example, fibronectin was reported to strongly stimulate endothelial and vascular cell differentiation, while laminin promotes the generation of beating cardiomyocytes (Battista et al., 2005). The matrix that is most commonly used for PSCs differentiation and generation of different types of organoids is Matrigel, which is a gelatinous protein mixture extracted from Englebreth-Holm-Swarm mouse sarcoma cells (Kleinman and Martin, 2005; Orkin et al., 1977), prone to lot-to-lot variation (Picollet-D'hahan et al., 2017). There are few studies that try to address the exact mechanism by which Matrigel supports organoid development. Although the manipulation of integrin signaling to direct stem cell fate is still very difficult, some groups have been studying the involvement of specific integrins in PSCs differentiation, with a focus on identification of ECM components directly interacting with a specific integrin subgroup and promoting selective endoderm, mesoderm or ectoderm differentiation (Wang et al., 2015a).

In addition to these chemical cues from the ECM, also mechanical and physical stimuli, like porosity and stiffness, exert their influence on cellular commitment (Evans et al., 2009). The matrix stiffness can be sensed by cells through mechanoreceptors that also include integrins, regulating cellular behavior (Humphrey et al., 2014). While intermediate substrate stiffness favors the endodermal lineage, softer subtracts originate ectodermal tissues (Zoldan et al., 2011). It was also demonstrated that mesodermal differentiation is very sensitive to mechanical proprieties of the ECM (Przybyla et al., 2016). While soft substrates enhance mesoderm commitment, stiff matrices induce only minimal mesoderm differentiation (Przybyla et al., 2016). In this latter study, authors showed that on a soft

substrate, human ESCs present β-catenin accumulation at cell-cell adhesions leading to enhanced WNT signaling and subsequent WNT-dependent mesoderm differentiation. In contrast, stiff materials promote the integrin-dependent β-catenin degradation and thus inhibit mesoderm commitment (Przybyla et al., 2016). Therefore, by playing with biochemical components of the ECM, as well as its mechanical and physical parameters, cell proliferation and differentiation can be manipulated in the 3D microenvironments.

Breaking symmetry

Symmetry breaking is a pivotal phenomenon in animal development that precedes pattern formation, allowing the generation of higher morphological and functional specialization. *In vivo*, symmetry is broken at the single cell level, where cellular cytoskeleton and membrane associated proteins are redistributed to create apico-basal polarity (**Figure I.7**). One example is while integrins accumulate at the basal side of the cell, a ring of actin filaments is formed at the apical side. The actin ring contraction can drive apical constriction leading to cell shape alteration and epithelial sheet bending (Pohl, 2015; Simunovic and Brivanlou, 2017; Spracklen and Peifer, 2015). In addition, symmetry breaking also occurs at the multicellular level, as seen in the early mouse embryo (**Figure I.7**). This morphological event called compaction process transforms the embryo from a loose cluster of spherical non-polarized cells into a tightly packed mass, in which cell-cell contacts are strengthened and cell polarization is achieved. Several mechanisms are involved in the compaction process: cell-cell adhesive interactions, involving the redistribution of E-cadherin; cortical tension, generated by actomyosin networks contractility determining the cell shape; and extension of long membrane protrusions (Simunovic and Brivanlou, 2017; White et al., 2016).

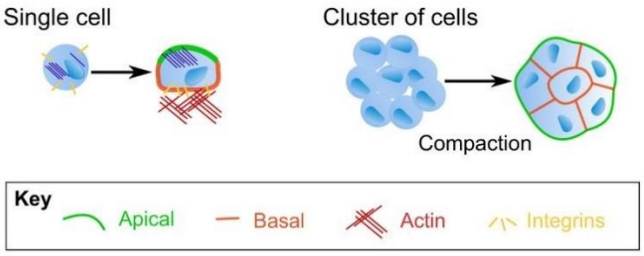

Figure I.7. Symmetry breaking *in vivo*. Symmetry breaking at the level of a single cell (left) and multicellular level (right), involving a process of compaction (Adapted from Simunovic and Brivanlou, 2017).

The precise molecular and physical features, as well as the precise timing in which symmetry breaking occurs is still poorly understood. Some events appear to be cell-autonomous, depending on asymmetric gene expression in embryonic cells, and others caused by morphogen gradients. The latter can be modeled by reaction-diffusion mechanisms, where symmetry is broken by a homogeneous distribution of a morphogen (Simunovic and Brivanlou, 2017). In a reaction-diffusion model, the self-organization capacity of cells leads to symmetry breaking activated by a stochastic disturbance of the system without a requirement of a dominant 'master factor' (Wennekamp et al., 2013). Therefore, cell characteristics, including gene expression and cell polarity, and local interactions between cells, can by themselves be responsible for lineage establishment. Reported studies already demonstrated that a uniform aggregate of stem cells is capable to originate a high organization level, comparable to what is observed in native tissues (reviewed in Ishihara and Tanaka, 2018). Some organoid models with minimal but sufficient complexity are able to undergo spontaneous symmetry breaking in the absence of spatial cues (reviewed in Ishihara and Tanaka, 2018). In this case, a specific pattern is created including rostral-caudal polarization in cortical organoids (Takata et al., 2017), anterior-posterior patterning in 3D gastruloids (Turner et al., 2017) and dorsal-ventral patterning in neural tube organoids (Ishihara et al., 2017; Meinhardt et al., 2014).

Therefore, symmetry breaking events can be attained *in vitro* by addition of a single morphogen, through a diffusion-reaction mechanism (**Figure I.8-A**), or by using more sophisticated bioengineering approaches to create symmetry breaking based on local morphogen delivery (**Figure I.8-B**).

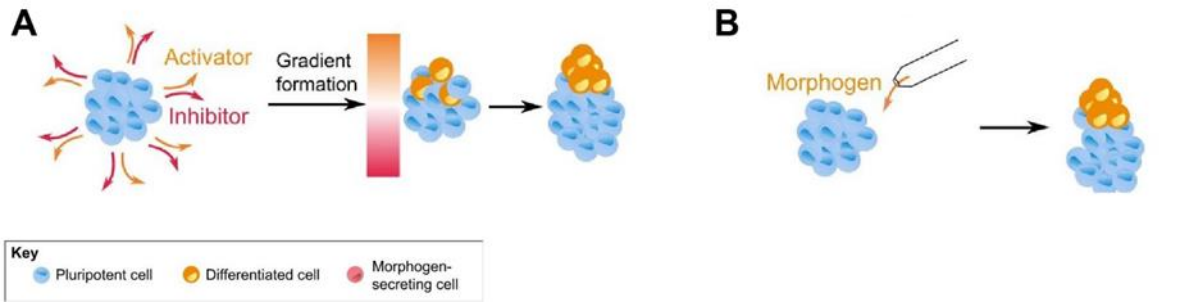

Figure I.8. Approaches for symmetry breaking *in vitro*. A) Breaking symmetry with a diffusion-reaction mechanism. **B)** Bioengineering approaches can be used to create morphogen gradient or to locally deliver a morphogen, inducing symmetry breaking. (Adapted from Simunovic and Brivanlou, 2017).

Controlled assembly of PSCs

The generation of organoids starts by promoting the assembly of PSC into a 3D structure. Similar to the human embryo, the earliest cell fate decision is based on the spatial orientation of cells (Mihajlović and Bruce, 2017). Therefore, methodologies to control cell arrangement during the initial organoid assembly can affect further morphogenesis induction. The assembly process can be achieved based on the self-assembly proprieties of cells in a scaffold-free tissue engineering approach and using different bioengineering strategies to direct and control the arrangement of cells.

Scaffold-free approaches

The generation of organoids in a scaffold-free manner is based on the "self-organization" propriety of stem cells, in which cells have the ability to assembly in a 3D structure. Different methodologies have been applied to form 3D aggregates of PSCs (**Figure I.9**), with the embryoid bodies (EBs) formation by the hanging drop method the first to be used for the production of homogeneous cell aggregates. This technique is based on gravity to force the cells to aggregate and consists on creating small drops of medium with cells suspended on a lid (Kurosawa et al., 2003) To overcome the manipulation limitations that could disturb the EBs, this technique was adapted to V-bottomed and round-bottomed multi-well plates, in which cells are forced to rapidly aggregate by applying a rotational force (Ng et al., 2005). However, this methodology does not avoid the individual manipulation of the cell aggregates. Therefore, different microwells fabricated by lithographic techniques have been used to simultaneously generate 100's to 1000's of cell aggregates by centrifugation, allowing the scaling up of the multi-well plate technique (Moeller et al., 2008; Mohr et al., 2006; Ungrin et al., 2008). In addition, microfluidic channels have also been used for continuous formation of cell aggregates, being a powerful tool for high-throughput applications (Torisawa et al., 2007).

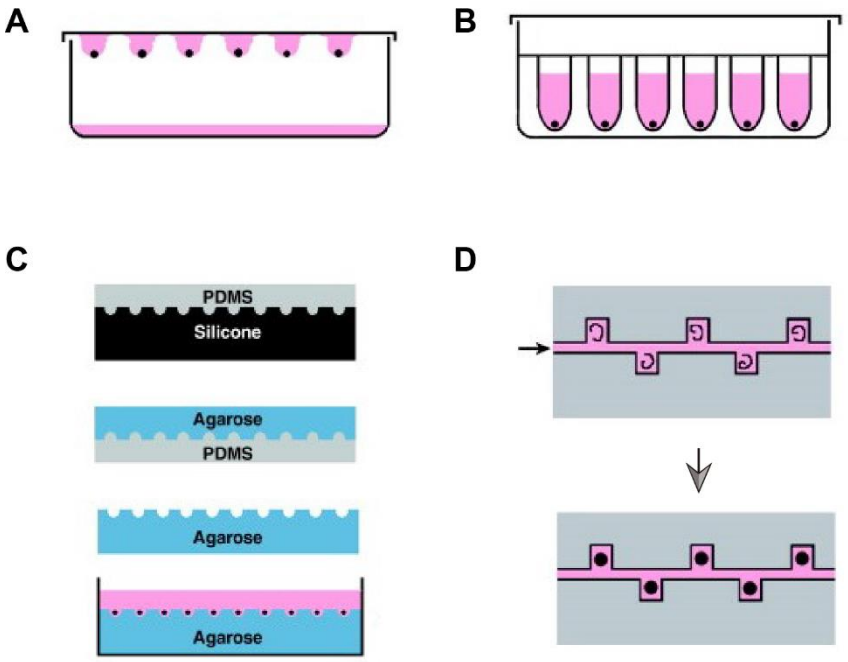

Figure I.9. Methods for generating cell-derived 3D aggregates. A) Hanging drop technique. **B)** V-bottomed and round-bottomed multi-well plates. **C)** Microwell array from micro-patterned agarose wells. **D)** Microfluidic system (Adapted from Fennema et al., 2013).

In these scaffold-free methodologies, the most important parameter to be controlled is the size of the generated aggregates. It was demonstrated that the size of the cell niche influences the differentiation trajectories because of its impact on the microenvironmental parameters, including spatial gradient of soluble molecules, and cell-cell and cell-matrix interactions (Bauwens et al., 2008; Bratt-Leal et al., 2009; Peerani et al., 2007). Thus, since variations in cell number are translated to different aggregate sizes, controlling the cell aggregate size can influence the signaling pathways conducing to a more efficient commitment and differentiation. In fact, different research groups have been optimizing the aggregate diameter to improve the mesoderm or neuroectodermal induction, achieving higher yields of neuronal and cardiac cells (Chen et al., 2015; Fonoudi et al., 2015; Miranda et al., 2015).

More recently, Xie and coworkers reported that not only the size of cell aggregates can influence the differentiation toward different lineages but also the self-assembly kinetics. The study showed that the aggregation kinetics altered the EB structure, particularly, slower kinetics originated EBs with higher porosity facilitating the exposure of cells to growth factors. Ultimately, faster aggregation appears to favor ectodermal commitment whereas slower aggregation promotes mesoendodermal differentiation (Xie et al., 2017).

Scaffolds for imposing external and internal architecture

Cellular organization within an engineering tissue involves the assembly of cells into a specific arrangement for mimicking the architecture of the native tissue. To mimic the *in vivo* physical and biochemical properties of the tissue microenvironment different matrices can be used, including those from natural sources or artificially synthesized. A specific architecture can be externally imposed by using different approaches to manipulate the tissue shape, like molds and scaffolds. As previously referred, micro-contact printing can provide different molds from different materials like agarose, polydimethylsiloxane or polyacrylamide, with minimal adhesive proprieties, only to force cells to aggregate and acquire a specific shape (Dahlmann et al., 2013; Youssef et al., 2011). Besides that, this technique can be used to introduce some functionalization by directly depositing some proteins or ECM components onto a partially polymerized subtract (Perl et al., 2009; Yin et al., 2016). Furthermore, the control of shape, size, space and organizational symmetry of nanometer-scale features in different biomaterials has been achieved by using different nanolithography strategies. Among different nanotopography approaches, the electrospinning allows the formation of nanofibrous substrates from natural or synthetic polymers, while electron-beam, selective etching and nanoimprinting have been used to create nanopits, nanopillars or nanochannels on various materials. By applying these

different approaches, the natural dimensions of basement-membrane fibers and pore sizes can be reached allowing to mimic the porosity of the natural ECM (Murphy et al., 2014).

The scaffolds used for imposing the external shape and mimicking the natural ECM mostly have a fixed morphology. However, human development starts on a micro-scale and considerable morphologic changes have to occur to achieve the final morphogenesis (Gilbert, 2007). Therefore, it is very important to try to dynamically control the organoid morphology in order to reach a correct tissue-like organization. The application of different types of hydrogels has been able to improve the control of the 3D microscale morphology of organoids. Hydrogels are hydrophilic 3D polymeric networks with natural or synthetic origin that are insoluble due to the presence of chemical or physical crosslinks (Lutolf and Hubbell, 2005; Peppas et al., 2000; Van Vlierberghe et al., 2011). The internal structure of the hydrogel can be manipulated by using different techniques, including 3D printing and sacrificial molding, being possible to regulate the morphology of the generated structures (Marti-Figueroa and Ashton, 2017).

In the last years, significant improvements have been made concerning mechanical performance and functionality in the 3D printing of hydrogels. There are different reported hydrogel composite 3D printing techniques that allow to fabricate complex and highly customizable scaffold structures, including nozzle based-, laser based- and inkjet based-3D printing systems (Jang et al., 2018). The nozzle based-3D printing is the most used approach, in which viscous liquids or melted polymers are forced and extruded out of a nozzle, syringe or orifice in order to sequentially build a 3D structure based on a pre-designed path created by computer modeling (Jang et al., 2018). Recently, Hinton and colleagues reported an adaptable and cost-effective nozzle based-3D printing, termed freeform reversible embedding of suspended hydrogels (FRESH) that uses a thermo-reversible support bath to enable deposition of hydrogels. Based on 3D imaging data from whole organs, FRESH is able to print scaffolds with complex internal and external

architectures, including 3D CAD model of the embryonic heart (Hinton et al., 2015), demonstrating a valuable applicability in organogenesis. In addition, the laser-based 3D printing systems are also capable of building 3D structures but in photo-treatable hydrogels under the deposition of laser energy, normally UV light, in specific designed patterns (Billiet et al., 2012). Finally, inkjet printing is a non-contact printing technique used to create ink droplets onto a material platform (Cui et al., 2012). Even though biological molecules and structures are fragile and sensitive, this approach appears to be appropriate to introduce biological modification onto generated scaffolds, since it was successfully used to transfer biomolecules like nucleic acids to solid supports (Goldmann and Gonzalez, 2000).

Miller and others were the first to report the generation of cylindrical networks within different hydrogels by using 3D filament networks of carbohydrate glass as a sacrificial template (Miller et al., 2012). Therefore, they were able to pattern vascular networks into 3D tissue constructs by molding channels. Following this study, this sacrificial molding technique was also used by other groups to create internal cavities of micro- to macro-scale dimensions within a variety of hydrogel materials by applying different molds, including calcium alginate and poly-vinyl alcohol (PVOH) templates (Tocchio et al., 2015; Wang et al., 2014). Briefly, the sacrificial molding technique is based on encapsulating a dissolvable or degradable material within a second hydrogel material. After the composite hydrogel formation, the internal sacrificial material is removed and a hydrogel with defined internal architecture is created (Marti-Figueroa and Ashton, 2017). This internal architecture manipulation in the hydrogels provides an important tool not only to create vascularized tissues but also for organoid encapsulation, in which the internal spaces allow the growth, deformation, and remodeling of the organoids to generate a defined morphology.

Bioengineering approaches to manipulate organoid assembly

Several bioengineering approaches have been applied to guide cell assembly in order to achieve a desired cell arrangement and organoid shape. In 2015, Todhunter et al. reported a DNA-programmed assembly of cells (DPAC), in which size, shape, composition and spatial heterogeneity is programmed, thereby recreating the multicellular organization of organoids (Todhunter et al., 2015). In DPAC, 2D DNA-patterned substrates are used to guide cellular organization by presenting complimentary lipid-modified oligonucleotides. After this programmed assembly, a DNase treatment is performed to release a well-organized cell aggregate, followed by encapsulation within ECM gels (Todhunter et al., 2015, 2016; **Figure I.10**).

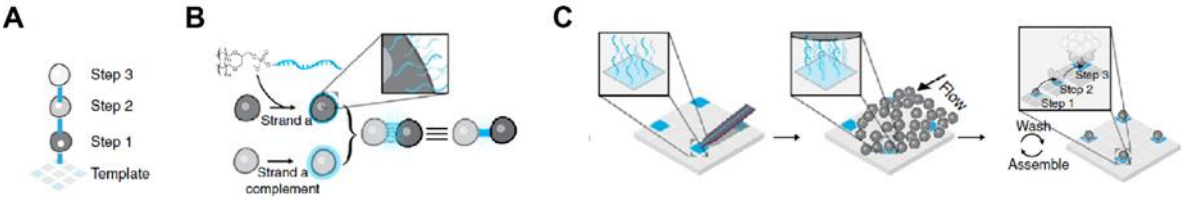

Figure I.10. DNA-programmed assembly of cells (DPAC). A) Multistep assembly based on different DNA spots and DNA-programmed connectivity. **B)** Cell incubation with lipid-modified oligonucleotides to remodel the cell surface with desired oligonucleotides. **C)** Assembly of cells using the complementarity of cell-surface oligonucleotides for DNA spots (Todhunter et al., 2015).

As previously described for fabrication of scaffold structures, 3D printing techniques have been also applied to control cell assembly by the deposition of single or multiple combination of cells with different supportive matrices. This type of bioprintring methodology involves different approaches, like inkjet bioprinting, microextrusion systems and laser-based direct-write techniques (**Figure I.11**), in which different actuation methods are applied (Garreta et al., 2017; Li et al., 2016). In inkjet bioprinting, two different actuation methods are used, piezoelectric and thermal, where by either acoustic waves or thermal forces,

respectively, liquid droplets are prepared (Cui et al., 2012; Garreta et al., 2017). While in the thermal approach a variable size of droplets is obtained, in piezoelectric technology regular and equal sizes are generated (Li et al., 2016; Nakamura et al., 2005; Saunders et al., 2008). This is a low-cost technology with high resolution and printing speed, however it has some limitations regarding the type of materials that can be printed (Garreta et al., 2017). Although some thermal and mechanical stress can be introduced to the cells, this technology was already successfully used in different mammalian cells with a viability above 85% (Saunders et al., 2008). On the other hand, the microextrusion technique is derived from modification of inkjet printers, which are pressure-assisted robotic apparatus that can extrude cell-laden hydrogels by pneumatic or mechanical dispensing onto a substrate (Mandrycky et al., 2016; Murphy and Atala, 2014). Human chondrocytes and osteogenic progenitors in combination with alginate hydrogel were already extruded by using a pneumatic syringe dispenser, demonstrating the ability to create 3D structures with high cell viability (Fedorovich et al., 2012).

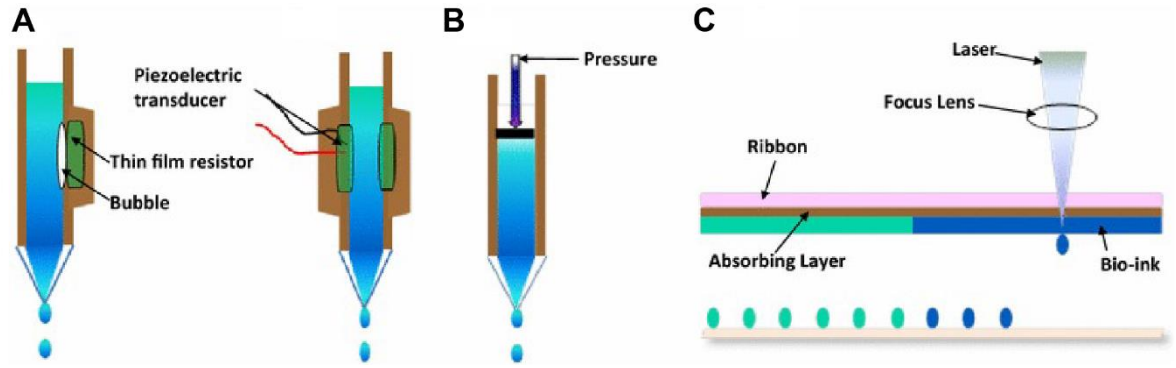

Figure I.11. 3D bioprinting techniques. A) Thermal and piezoelectric inkjet bioprinting. **B)** Pressure-assisted bioprinting. **C)** Laser-associated bioprinting. (Li et al., 2016).

Laser-based direct-writing technique is the most applied bioprinting technology. This technique uses a laser beam that is focused in a support layer underlying a cell containing matrix on the donor print ribbon, forcing its rapid volatilization and allowing the cell to be

transferred onto an adjacently localized receiving substrate (Schiele et al., 2010). High cell viabilities have been reported using this technique, due to low shear stress, and its high resolution allows single-cell deposition, yielding scaffold-free 3D cell constructs (Garreta et al., 2017). For cell-based applications, the most common laser-based techniques are biological laser processing (BioLP), matrix-assisted pulsed laser evaporation direct writing (MAPLE-DW), laser-induced forward transfer (LIFT), absorbing film-assisted laser-induced forward transfer (AFALIFT), and laser-guided direct writing (LG-DW) (Schiele et al., 2010). MAPLE-DW was successfully used to deposit patterns of different cell types onto and within Matrigel, demonstrating that spatial coherence can be achieved (Patz et al., 2006; Schiele et al., 2009). Furthermore, human osteosarcoma cells were printed by BioLP and transferred into Matrigel, producing a 3D cellular construct with 95% of cell viability (Barron et al., 2004). This method was later improved reaching 100% viable cells and single-cell resolution (Barron et al., 2005). Thus, a high control in cell assembly is reached, allowing to manipulate cellular arrangement and composition within an organoid with a defined 3D micro-scale morphology.

Directed organoid patterning and morphogenesis

The knowledge about the signaling pathways involved in pluripotency maintenance, as well as the generation of different germ layers has allowed the manipulation and control of PSC commitment to different lineages and further differentiation into specific cell types. For instance, neuroectoderm commitment is easily achieved by manipulating TGFβ signaling (Suzuki and Vanderhaeghen, 2015). The most efficient method for neural induction from hiPSCs is dual SMAD inhibition of BMP and Activin signaling, which are antagonized by Noggin and Lefty respectively (Chambers et al., 2009; Suzuki and Vanderhaeghen, 2015). Other chemical antagonists have been used to promote BMP signaling inhibition, like

dorsomorphin and LDN-193189, blocking the commitment towards trophectoderm (Chambers et al., 2009; Sanvitale et al., 2013). For Nodal/Activin signaling inhibition, a chemical antagonist SB431542 is efficient to prevent the mesoendodermal differentiation by blocking the TGFβ signaling (Chambers et al., 2009; Laping et al., 2002; **Figure I.12**).

Oppositely, the activation of dual SMAD regulators, as well as the WNT signaling, appears to be critical for the initial mesoendoderm commitment, giving rise to Brachyury$^+$ and MIXL1$^+$ cells (Lian et al., 2013; Murry and Keller, 2008). Following mesoendoderm induction, further differentiation towards mesoderm or endoderm lineages is associated with the expression levels of FOXA2 (Murry and Keller, 2008). While WNT activation generates cells with lower expression of FOXA2, activin leads to the development of a population with higher expression of FOXA2 (Gadue et al., 2006). Interestingly, BMP is not required for the mesoendoderm commitment, but alone is capable of inducing the development of a population with low expression of FOXA2 (Murry and Keller, 2008; Nostro et al., 2008). Therefore, based on the different levels of FOXA2, two different populations can be specified, the FLK-1$^+$ mesoderm and FOXA2$^+$ endoderm (Ema et al., 2006; Gouon-Evans et al., 2006; Tada, 2005; **Figure I.12**). In mesodermal differentiation, different cell types, including hematopoietic, vascular and cardiac cells, are originated from different subpopulations. While WNT, BMP and activin appear to be important for mesoderm specification and further generation of hematopoietic cells, the inhibition of WNT signaling is essential to promote cardiac differentiation (Lian et al., 2012; Murry and Keller, 2008; Trompouki et al., 2011). On the other hand, after the establishment of activin-induced definitive endoderm, various cell populations can arise, such as hepatocytes and pancreatic cells. BMP and WNT signaling pathways have an important role in the generation of the pancreatic lineage, while the specification of insulin-producing cells can be achieved by FGF signaling (Johannesson et al., 2009; Nostro et al., 2011). The combination of FGF and BMP4 signaling is related with hepatic fate (Gouon-Evans et al., 2006).

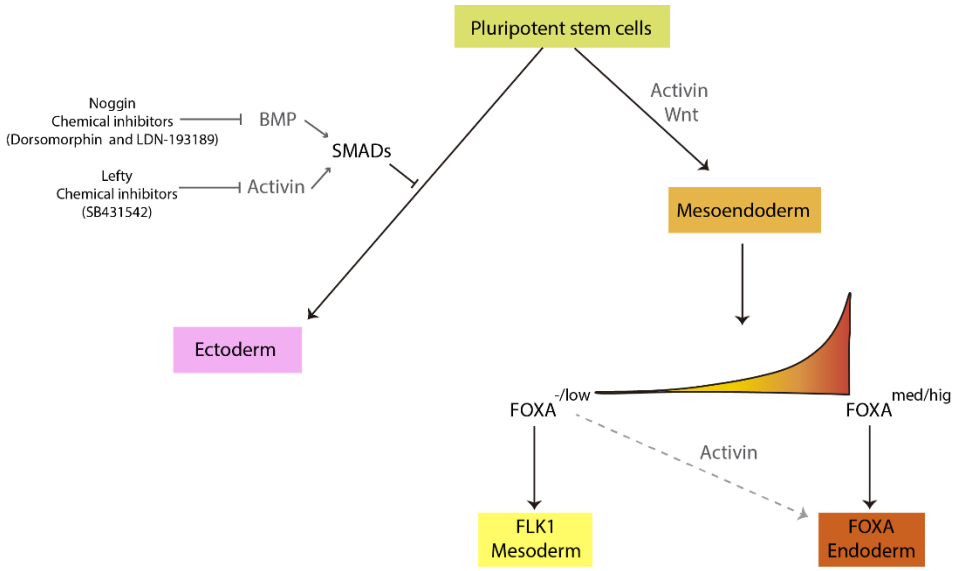

Figure I.12. Lineage specification from PSCs. Neural induction is achieved by dual SMAD inhibition, whereas mesoendoderm differentiation is based on activation of dual SMAD regulators and WNT signaling.

Based on the manipulation of the previously described signaling pathways, as well as on the "self-organization" capacity of stem cells, organoids from different lineages have been produced including brain, kidney, liver, pancreas, lung and gut (Dye et al., 2016; Kim et al., 2016; Lancaster et al., 2012; Spence et al., 2010; Takasato et al., 2015; Takebe et al., 2014). Yoshiki Sasai and coworkers were the first to demonstrate the ability of PSCs to self-organize in cortical tissue and recapitulate embryonic brain development (Eiraku et al., 2008). Later, Lancaster et al. were able to direct human PSC differentiation into different cerebral cortex regions and apply this technique for disease modeling (Lancaster et al., 2012). A variety of well-organized neuronal organoids was later reported, including forebrain, midbrain, hypothalamus and cerebellum-like structures (Junghyun Jo et al., 2016; Karzbrun et al., 2018; Muguruma et al., 2015; Qian et al., 2018). In addition to brain organoids, by directing PSCs towards the intermediate mesoderm, organoids that recapitulate the first trimester of human fetal kidney were also generated. These organoids present individual nephron-like structures segmented into distal and proximal tubules

surrounded by endothelia and renal interstitium, demonstrating a well-organized structure (Takasato et al., 2015). These are some examples of the ability to recapitulate human organogenesis *in vitro* from PSCs by the addition of only a few signaling cues. However, differences between native organ and PSC-derived organoids can be observed because either the microenvironment components may not be the most appropriate, or the signals are static in both space and time. Therefore, a higher spatiotemporal control is required to achieve closer similarity to native microenvironment.

Bioengineering approach to spatiotemporal control of mechanical signals

As previously demonstrated, the mechanical proprieties of cellular microenvironment highly influence the cell differentiation as well as cellular proliferation and apoptosis (Gilbert et al., 2010; Nelson et al., 2005; Przybyla et al., 2016). Additionally, such mechanical features are specific for different organs or, even within the same organ, different components present distinct mechanical proprieties, allowing the modulation of cellular behavior and promoting multicomponent organogenesis (Engler et al., 2006; Lopez et al., 2011). Subsequently, for organoid generation, the spatial modulation of mechanical features is a critical issue that can be achieved by generating composite hydrogels. For instance, the functionalization of traditional hydrogels, such as Matrigel or collagen, with synthetic ECM analogs allows to manipulate the mechanical proprieties (Ehrbar et al., 2011; Gill et al., 2012). The incorporation of adhesion peptides permits to manipulate mobility, since long peptide tethers lead to cell attachment and spreading, whereas short peptide tethers induce cell adhesion resistance, resulting in cell clustering (Kuhlman et al., 2007). Also the incorporation of peptide substrates that are susceptible to enzymatic cleavage can also modulate hydrogel degradation by cells and therefore promote cell migration (Raeber et al., 2005). A modular design of silk protein-based porous scaffolds was also used to produce

combined hydrogels, recreating the six-layered architecture of the human cortex (**Figure I.13-A**). The reported approach consisted on adhesive-free assembly of concentric units to create the modular structures based on a jigsaw puzzle-like cutting process (**Figure I.13-B**). In this way, different layers were populated with distinct types of neurons and a functional 3D cortical tissue construction was reached (Tang-Schomer et al., 2014). An alternative route to produce complex structures with composite hydrogels is a DNA-directed assembly of shape-controlled units (**Figure I.13-C**). This technique presents the same principle as previously described to cell assembly, consisting in enrichment of different blocks with circle DNA strand "glues". Based on the complementarity of each DNA block, a programmable assembly of complex macroscale structures can be achieved (Qi et al., 2013).

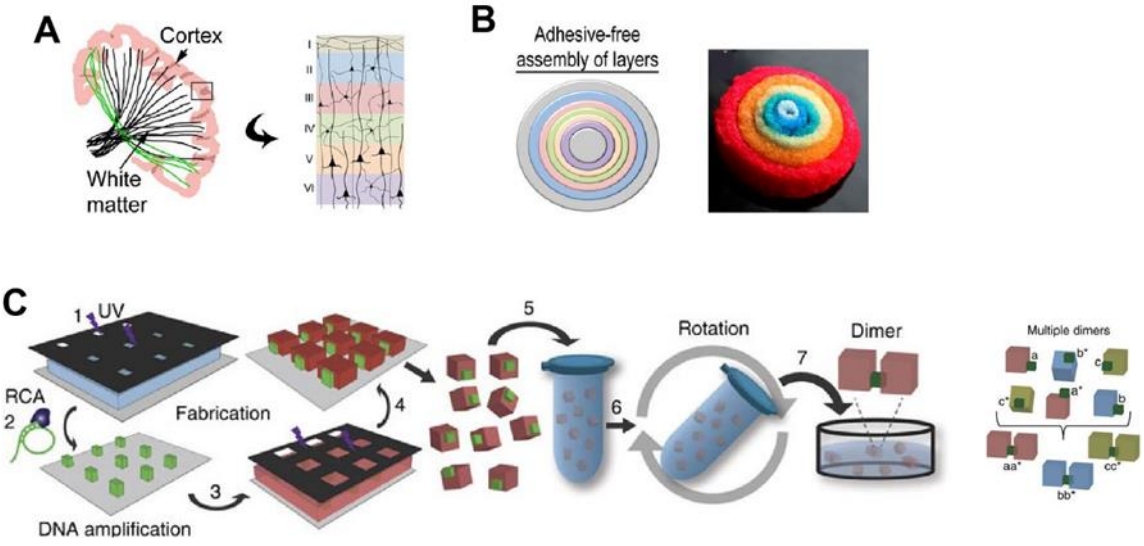

Figure I.13. Engineering hydrogels with spatial control. A) Human cerebral cortex composition: white matter and cortex, presenting a six-layered structure (Tang-Schomer et al., 2014). **B)** Design of adhesive-free assembly of concentric layers to mimic brain cortical tissue (Tang-Schomer et al., 2014). **C)** Assembly of different hydrogel cubes based on the complementarity between face-specific DNA glue modifications (Qi et al., 2013).

In addition to the reported technologies that allow the spatial modulation of mechanical features, further temporal guidance is possible to be generated by light-mediated patterning.

The formation of photodegradable hydrogels by incorporating photolabile moieties within the network backbone of an hydrogel, like poly(ethylene glycol), makes the manipulation of the physical features of the ECM possible by using light of different wavelengths. Then, upon light exposure, the local network crosslink density decreases and the hydrogel is cleaved, resulting in changes in physical proprieties, including stiffness, water content, diffusivity, or complete erosion, even in the presence of cells (Kloxin et al., 2009). In contrast to this local softening, the presence of a photoinitiator originates additional crosslinking after the exposure to ultraviolet light and providing local stiffening (Guvendiren and Burdick, 2012).

In addition to light-patterning, other approaches have been applied for tuning stiffness of hydrogels by using a combination of a pH-sensitive poly(2-(diisopropylamino)ethyl methacrylate) (PDPA) and biocompatible poly(2 (methacryloyloxy)ethyl phosphorylcholine) (PMPC) (Yoshikawa et al., 2011). With the careful adjustment of the pH the hydrogel film elasticity could be reversibly modulated allowing for the stiffening or softening of the material, and for the temporal dynamic manipulation of cell adhesion/detachment (Yoshikawa et al., 2011). This reversibly tunable stiffness can also be reached in cell-laden hydrogels based on supramolecular “host–guest” interactions. In this reported method, the stiffness is manipulated by non-covalent and reversible host–guest interactions between pendant “host” motifs, which are present in the primary hydrogel network and soluble polymers. Thus, when these soluble polymers are added, additional physical crosslinks are formed resulting in increased hydrogel crosslinking density and elastic modulus (Shih and Lin, 2016). Hydrogels can also be dynamically stiffened by using enzymatic reactions, in which a peptide linker with additional amino acids residues that are susceptible to a specific enzyme catalyzation is created. After enzyme exposure, specific dimer formation is achieved leading to additional crosslinks and final stiffening of the cell-laden hydrogel (Liu et al., 2017).

Therefore, based on these techniques, a spatiotemporal patterning of the mechanical features is straightforwardly reached. And by manipulating the matrix stiffness, the growth

of neighboring tissues and consequently the mechanical confinement as seen *in vivo* could be mimicked in the organoid microenvironment (Gjorevski et al., 2014).

Bioengineering approaches to spatiotemporal control of morphogens diffusion

Morphogens are molecules that are able to coordinate organ growth and patterning, establishing a graded concentration distribution and eliciting distinct cellular responses in a dose-dependent manner. They can be either cytoplasmatic proteins, able to promote a diffusion gradient within the cell, or secreted signaling molecules (Christian, 2012). The gradient of these signaling molecules appears to direct tissue patterns during embryogenesis (Crick, 1970; Wolpert, 1969). The formation of specific structures can be induced by the signaling gradients from the neighboring cells leading to differential expression, tissue patterning and morphogenesis (Muller et al., 2013). *In vitro*, various morphogens, including small molecules, growth factors and hormones, have been used to regulate cell fate within the organoids. Furthermore, with advances in the bioengineering field, the spatiotemporal control of the morphogen gradients within the organoid seems to be possible for instructing the correct morphogenesis.

As already mentioned above, light-mediated patterning approaches present also a promising application to control morphogenic signals in both time and space. Biomolecules can be introduced within the hydrogel at a desired location, protected by a photodegradable moiety (DeForest and Anseth, 2012; Wylie et al., 2011). At the proper timing, light exposure leads to a specific photo-releasing of the biomolecule. Beyond the spatial and temporal delivery control, for a given light exposure, the amount of biomolecule that is released can be predicted (DeForest and Anseth, 2012). Additionally, the use of microfluidic systems or micro/nanoparticles allows an efficient spatiotemporal control of morphogen gradients. Lithographic techniques can be used for the production of channels to create functional

microfluidic structures within hydrogels. Given the hydrodynamic properties of microchannels, following initial homogeneous distribution of biomolecules inside the channels, a concentration gradient is formed by adjusting the flow rate. The delivered biomolecules can be changed over time within the scaffold and the temporal modulation of these molecules can be achieved across the entire network in a spatially uniform manner. (Choi et al., 2007). These microfluidic devices were already successfully used to modulate neural tube patterning *in vitro*. Uzel et al. reported a microfluidic design to create orthogonal linear gradients in a 3D cell-embedded scaffold (Uzel et al., 2016). The authors used the reported device to generate gradients of RA and SAG, an agonist of SHH (Chen et al., 2002), across a 3D collagen hydrogel with mouse ESC-derived aggregates (Uzel et al., 2016; **Figure 1.14-A**). Since RA has a caudalizing effect on the neuroepithelium and SHH is secreted in the most ventral part of the neural tube (Dessaud et al., 2008; Maden, 2007), a combinatorial effect of these two morphogens specifies progenitor cells into caudal and ventral identities leading to subsequent formation of ventral spinal cord neurons (Uzel et al., 2016). A similar approach was also used by Demers and coworkers. In addition to RA and SHH signaling, they introduced a BMP4 gradient in a microdevice capable to mimic the dorsal patterning of the neuroepithelium (Demers et al., 2016; **Figure I.14-B**). During neural differentiation, dorsal-ventral identity is achieved by opposite gradient delivery of SHH and BMP, whereas the orthogonal delivery of RA gradient allows the generation of rostral-caudal axis (Demers et al., 2016). These two different studies demonstrated the ability to generate temporally-controlled morphogen gradients that allow the spatial patterning in stem cell-derived 3D structures.

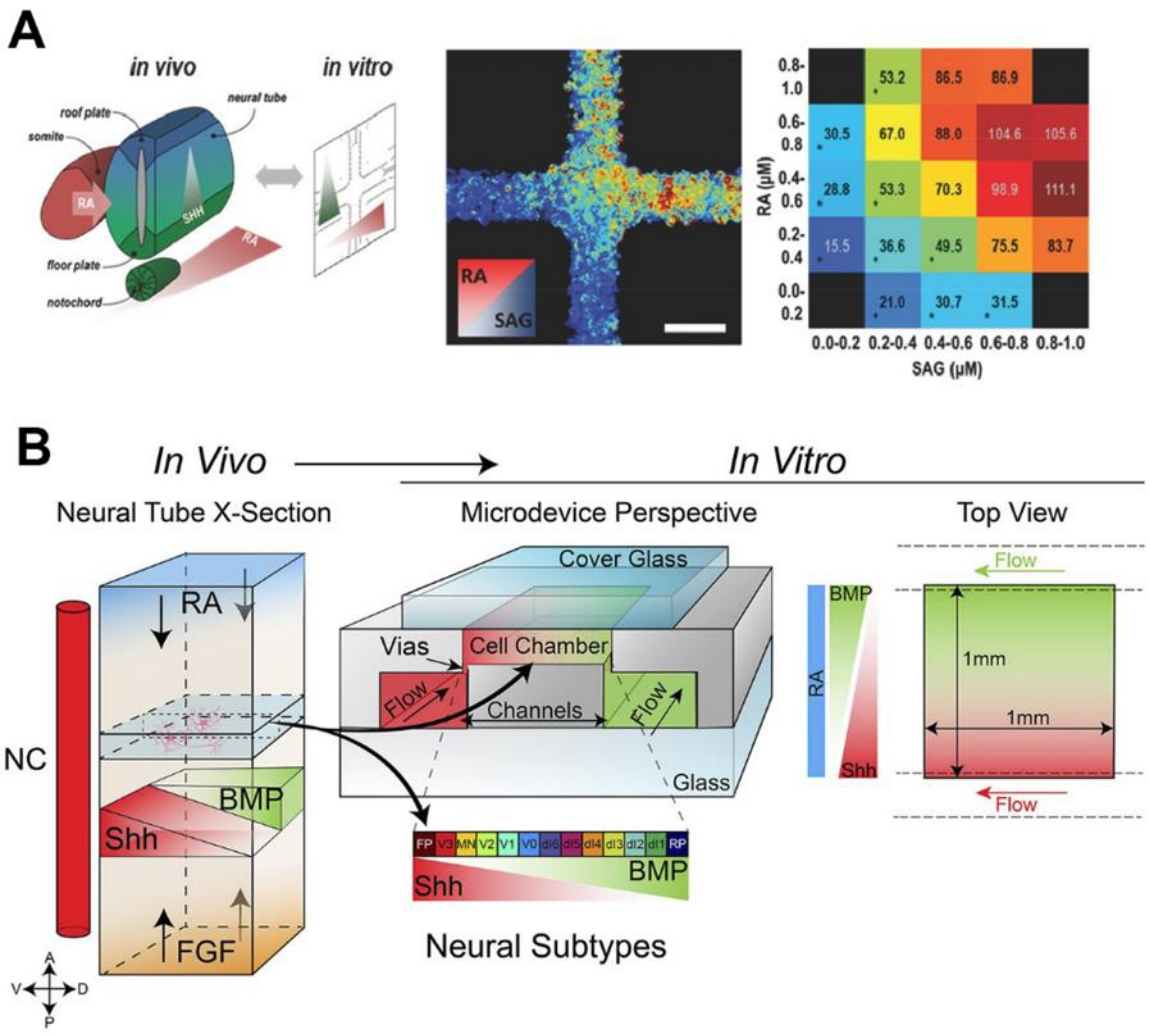

Figure I.14. Induction of morphogen gradients within organoids. A) Orthogonal gradients of RA and SAG for generation of motor neurons, which can achieve a wide range of concentrations (Uzel et al., 2016). **B)** Schematic overview of the microfluidic reconstruction of the neural tube patterning (Demers et al., 2016).

Thus, the use of microfluidics can provide a trans-organoid morphogen gradient, along with the immobilization of biomolecules in the biomaterial for spatial control (Marti-Figueroa and Ashton, 2017). In fact, direct integration of biomolecules into the scaffold allows to manipulate cell attachment, migration and fate, but when combined with a delivery vehicle, like micro/nanoparticles, the controlled release of biomolecules is possible, allowing the generation of spatial gradients (Van Rijt and Habibovic, 2017). Mahoney and Saltzman were

the first to assemble cells with controlled-release of polymeric microparticles to develop tissues with programmable synthetic extracellular microenvironments (Mahoney and Saltzman, 2001). This technology was later applied to promote the controlled release of morphogens within organoids (Carpenedo et al., 2009). Degradable PLGA microspheres, containing RA, were incorporated within ESC-derived aggregates to achieve a controlled morphogen presentation and cystic spheroids formation (Carpenedo et al., 2009). An efficient cell differentiation and morphogenesis by the generation of structures that resemble the early mouse embryos (E6.75), with an exterior of visceral endoderm enveloping an epiblast-like layer was demonstrated (Carpenedo et al., 2009). Moreover, the combination of microparticles that present different kinetic releases allows a controlled and sequential morphogen presentation, and therefore pre-determinate the time course of delivery and accomplish an efficient induction (Dang et al., 2016). These approaches represent a versatile tool to create morphogen gradients that provide an accurate spatiotemporal regulation, being capable of inducing the symmetry breaking necessary for correct organoid morphogenesis.

Scaling up of organoids generation

Other parameters, beyond biochemical signals and physical proprieties of ECM, should be considered for organoid generation, including sufficient nutrient and oxygen supply. The organoid size increases with the complexity of the generated structures and it can range from 200 µm to 4 mm (Li et al., 2014). However, larger organoids usually present diffusion limitations making it hard to mimic some developmental features (Van Winkle et al., 2012). Based on the physics of diffusion, cell density, and lower range of reported metabolic consumption rates for oxygen, cerebral organoids can achieve a maximal diameter of 1.4 mm without presenting central necrosis (McMurtrey, 2016). However, the

predicted diameter is based only on the low metabolic activity present in the organoids, since spontaneous neural activity is infrequent (McMurtrey, 2016). The use of a dynamic system, like a spinning bioreactor, is able to support organoid growth due to an efficient transport of nutrients and oxygen diffusion, allowing the maintenance of large-size organoids, with about 4 mm, that efficiently recapitulate the cerebral structure (Lancaster et al., 2012). In fact, bioreactors have been largely applied to expand and differentiate PSCs toward mesoderm, endoderm and ectoderm lineage, but without a structural cellular arrangement within the stem cell-derived 3D aggregates (Kempf et al., 2016; Kropp et al., 2016; Miranda et al., 2016; Rigamonti et al., 2016; Vosough et al., 2013). Moreover, the protocols for organoid generation using bioreactors typically involve initial commitment in static conditions, and further embedding of the organoids within a hydrogel, followed by transferring organoids to the bioreactor (Lancaster et al., 2012; Ovando-Roche et al., 2018; Przepiorski et al., 2018; Qian et al., 2016). This methodology limits the potential scale up and the application of organoid culture in high-throughput processes for drug discovery and toxicology studies. Recently, a new platform was reported that allows capsule production through electrospraying using a matrigel core, yielding robust capsules with microenvironmental support and organoid growth through the generation of an outer alginate shell that protects the cell-matrigel core (Lu et al., 2017). However, the generation of controlled size aggregates and further differentiation into well-organized organoids using bioreactors, in a continuous process, remains a challenge. Moreover, how the bioreactor design can affect the organization and morphogenesis of the organoid is still not understood.

I.6 THESIS OUTLINE

The thesis organization shows an optimization of the conditions for the generation of cerebellar neurons in defined and reproducible conditions that can be used routinely. Based on the influence of feeder layers in the variability between different experiments, we attempted to create a new approach that allows to differentiate cerebellar neurons from human iPSCs without requiring co-culturing with other cell types. This technique was further optimized by promoting a more efficient differentiation into Purkinje cell progenitors and maturation of Purkinje neurons. Finally, the generation of large amounts of cerebellar organoids as well as functional cerebellar neurons in a 3D dynamic culture system using Single-Use Vertical-Wheel™ bioreactors was accomplished.

Chapter II: Generation of mature cerebellar neurons from human induced pluripotent stem cells under defined and feeder-free

In this chapter, a novel strategy that uses a defined neuronal medium to generate distinct subtypes of cerebellar neurons, including Purkinje cells, granule cells, interneurons, and deep cerebellar nuclei projection neurons, was described. The generated cerebellar neurons were able to establish functional neuronal networks that were maintained for up to 145 days in culture. Using this defined medium reported to mimic the microenvironment of the CNS, we successfully promoted the maturation of cerebellar progenitors into functional neurons, without the need for co-culturing.

Chapter III: Controlling the regional identity of human pluritpotent stem cell-derived cerebellar organoids

This chapter reflects the optimizations of the previously reported protocol in order to increase the number of cerebellar GABArgic precursors and the efficiency of Purkinje cell maturation. Therefore, we attempted to control the regional identity of cerebellar organoids by manipulating SHH signaling to promote the ventral commitment of the cerebellar neuroepithelium. This new methodology promoted the generation of a dense layer of $OLIG2^{+}$ cells, which is important for Purkinje cell specification during cerebellar development. In addition, 5-HT treatment during the maturation process appeared to have positive effect on Purkinje cell generation and maturation, since enhanced expression of Purkinje-specific markers, including L7 and GRID2, was detected.

Chapter IV: Scalable generation of mature cerebellar neurons from human pluripotent stem cells using Single-Use Vertical-Wheel™ bioreactors

Lastly, we present a reproducible and scalable generation of neural organoids as well as functional neurons under chemical defined conditions by using the novel PBS 0.1 (100 mL) Vertical-Wheel single-use bioreactors. In this system, the generated human iPSC-derived organoids acquired an efficient mid-hindbrain patterning and further on cerebellar identity. The obtained cerebellar precursors were able to mature, in a 3D structure, into different functional cerebellar neurons and to survive for up to 3 months, without feeder layers.

I.7 REFERENCES

Aasen, T., Raya, A., Barrero, M.J., Garreta, E., Consiglio, A., Gonzalez, F., Vassena, R., Bilić, J., Pekarik, V., Tiscornia, G., et al. (2008). Efficient and rapid generation of induced pluripotent stem cells from human keratinocytes. Nat. Biotechnol. 26, 1276–1284.

Adamaszek, M., D'Agata, F., Ferrucci, R., Habas, C., Keulen, S., Kirkby, K.C., Leggio, M., Mariën, P., Molinari, M., Moulton, E., et al. (2017). Consensus Paper: Cerebellum and Emotion. Cerebellum 16, 552–576.

Adams, K. a, Maida, J.M., Golden, J. a, and Riddle, R.D. (2000). The transcription factor Lmx1b maintains Wnt1 expression within the isthmic organizer. Development 127, 1857–1867.

Alimperti, S., and Andreadis, S.T. (2015). CDH2 and CDH11 act as regulators of stem cell fate decisions. Stem Cell Res. 14, 270–282.

Andreu, A., Crespo-Enriquez, I., and Echevarria, D. (2014). Molecular events directing the patterning and specification of the cerebellum. Eur. J. Anat. 18, 245–252.

Anheim, M., Tranchant, C., and Koenig, M. (2012). The Autosomal Recessive Cerebellar Ataxias. N. Engl. J. Med. 366, 636–646.

Aubry, L., Bugi, A., Lefort, N., Rousseau, F., Peschanski, M., and Perrier, A.L. (2008). Striatal progenitors derived from human ES cells mature into DARPP32 neurons in vitro and in quinolinic acid-lesioned rats. Proc. Natl. Acad. Sci. 105, 16707–16712.

Baptista, C. a, Hatten, M.E., Blazeski, R., and Mason, C. a (1994). Cell-cell interactions influence survival and differentiation of purified Purkinje cells in vitro. Neuron 12, 243–260.

Barczyk, M., Carracedo, S., and Gullberg, D. (2010). Integrins. Cell Tissue Res. 339, 269–280.

Barron, J.A., Spargo, B.J., and Ringeisen, B.R. (2004). Biological laser printing of three dimensional cellular structures. In Applied Physics A: Materials Science and Processing, pp. 1027–1030.

Barron, J.A., Krizman, D.B., and Ringeisen, B.R. (2005). Laser printing of single cells: Statistical analysis, cell viability, and stress. Ann. Biomed. Eng. 33, 121–130.

Bart van der Worp, H., Howells, D.W., Sena, E.S., Porritt, M.J., Rewell, S., O'Collins, V., and Macleod, M.R. (2010). Can animal models of disease reliably inform human studies? PLoS Med. 7, 1–8.

Basler, K., Edlund, T., Jessell, T.M., and Yamada, T. (1993). Control of cell pattern in the neural tube: Regulation of cell differentiation by dorsalin-1, a novel TGFβ family member. Cell 73, 687–702.

Bastianelli, E. (2003). Distribution of calcium-binding proteins in the cerebellum. Cerebellum 2, 242–262.

Battista, S., Guarnieri, D., Borselli, C., Zeppetelli, S., Borzacchiello, A., Mayol, L., Gerbasio, D., Keene, D.R., Ambrosio, L., and Netti, P.A. (2005). The effect of matrix composition of 3D constructs on embryonic stem cell differentiation. Biomaterials 26, 6194–6207.

Bauwens, C.L., Peerani, R., Niebruegge, S., Woodhouse, K. a., Kumacheva, E., Husain, M., and Zandstra, P.W. (2008). Control of Human Embryonic Stem Cell Colony and Aggregate Size Heterogeneity Influences Differentiation Trajectories. Stem Cells 26, 2300–2310.

Beckstead, B.L., Santosa, D.M., and Giachelli, C.M. (2006). Mimicking cell-cell interactions at the biomaterial-cell interface for control of stem cell differentiation. J. Biomed. Mater. Res. - Part A 79, 94–103.

Bellin, M., Marchetto, M.C., Gage, F.H., and Mummery, C.L. (2012). Induced pluripotent stem cells: the new patient? Nat. Rev. Mol. Cell Biol. 13, 713–726.

Ben-Arie, N., McCall, A.E., Berkman, S., Eichele, G., Bellen, H.J., and Zoghbi, H.Y. (1996). Evolutionary conservation of sequence and expression of the bHLH protein Atonal suggests a conserved role in neurogenesis. Hum. Mol. Genet. 5, 1207–1216.

Ben-Arie, N., Bellen, H.J., Armstrong, D.L., McCall, A.E., Gordadze, P.R., Guo, Q., Matzuk, M.M., and Zoghbi, H.Y. (1997). Math1 is essential for genesis of cerebellar granule neurons. Nature 390, 169–172.

Benussi, A., Koch, G., Cotelli, M., Padovani, A., and Borroni, B. (2015). Cerebellar transcranial direct current stimulation in patients with ataxia: A double-blind, randomized, sham-controlled study. Mov. Disord. 30, 1701–1705.

Billiet, T., Vandenhaute, M., Schelfhout, J., Van Vlierberghe, S., and Dubruel, P. (2012). A review of trends and limitations in hydrogel-rapid prototyping for tissue engineering. Biomaterials 33, 6020–6041.

Bird, M.J., Needham, K., Frazier, A.E., Rooijen, J., Leung, J., Hough, S., Denham, M., Thornton, M.E., Parish, C.L., Nayagam, B.A., et al. (2014). Functional characterization of Friedreich ataxia iPS-derived neuronal progenitors and their integration in the adult brain. PLoS One 9, e101718.

Bratt-Leal, A.M., Carpenedo, R.L., and McDevitt, T.C. (2009). Engineering the embryoid body microenvironment to direct embryonic stem cell differentiation. Biotechnol. Prog. 25, 43–51.

Broccoli, V., Boncinelli, E., and Wurst, W. (1999). The caudal limit of Otx2 expression positions the isthmic organizer. Nature 401, 164–168.

Brouwer, M., Zhou, H., and Nadif Kasri, N. (2016). Choices for Induction of Pluripotency: Recent Developments in Human Induced Pluripotent Stem Cell Reprogramming Strategies. Stem Cell Rev. 12, 54–72.

Butts, T., Green, M.J., and Wingate, R.J.T. (2014). Development of the cerebellum: simple steps to make a “little brain.” Development 141, 4031–4041.

Cano, A., Pérez-Moreno, M.A., Rodrigo, I., Locascio, A., Blanco, M.J., Del Barrio, M.G., Portillo, F., and Nieto, M.A. (2000). The transcription factor Snail controls epithelial-mesenchymal transitions by repressing E-cadherin expression. Nat. Cell Biol. 2, 76–83.

Carlessi, L., Poli, E.F., Bechi, G., Mantegazza, M., Pascucci, B., Narciso, L., Dogliotti, E., Sala, C., Verpelli, C., Lecis, D., et al. (2014). Functional and molecular defects of hiPSC-derived neurons from patients with ATM deficiency. Cell Death Dis. 5, e1342.

Carletti, B., and Rossi, F. (2007). Neurogenesis in the Cerebellum. Neurosci. 14, 91–100.

Carlson, K.M., Andresen, J.M., and Orr, H.T. (2009). Emerging pathogenic pathways in the spinocerebellar ataxias. Curr. Opin. Genet. Dev. 19, 247–253.

Carpenedo, R.L., Bratt-Leal, A.M., Marklein, R.A., Seaman, S.A., Bowen, N.J., McDonald, J.F., and McDevitt, T.C. (2009). Homogeneous and organized differentiation within embryoid bodies induced by microsphere-mediated delivery of small molecules. Biomaterials 30, 2507–2515.

Cendelin, J., Schmahmann, J., Sherman, J., Manto, M., Manto, M., Marmolino, D., Phillips, R., Zuo, J., Jager, P. De, Takahasi, K., et al. (2014). From mice to men: lessons from mutant ataxic mice. Cerebellum & Ataxias 1, 4.

Chambers, S.M., Fasano, C.A., Papapetrou, E.P., Tomishima, M., Sadelain, M., and Studer, L. (2009). Highly efficient neural conversion of human ES and iPS cells by dual inhibition of SMAD signaling. Nat. Biotechnol. 27, 275–280.

Chen, J.K., Taipale, J., Young, K.E., Maiti, T., and Beachy, P.A. (2002). Small molecule modulation of Smoothened activity. Proc. Natl. Acad. Sci. 99, 14071–14076.

Chen, V.C., Ye, J., Shukla, P., Hua, G., Chen, D., Lin, Z., Liu, J. chang, Chai, J., Gold, J., Wu, J., et al. (2015). Development of a scalable suspension culture for cardiac differentiation from human pluripotent stem cells. Stem Cell Res. 15, 365–375.

Chiang, C., Litingtung, Y., Lee, E., Young, K.E., Corden, J.L., Westphal, H., and Beachy, P.A. (1996). Cyclopia and defective axial patterning in mice lacking Sonic hedgehog gene function. Nature 383, 407–413.

Chizhikov, V. V., and Millen, K.J. (2013). Neurogenesis in the Cerebellum. In Comprehensive Developmental Neuroscience: Patterning and Cell Type Specification in the Developing CNS and PNS, pp. 417–434.

Cho, K.H., Rodríguez-Vázquez, J.F., Kim, J.H., Abe, H., Murakami, G., and Cho, B.H. (2011). Early fetal development of the human cerebellum. Surg. Radiol. Anat. 33, 523–530.

Choi, N.W., Cabodi, M., Held, B., Gleghorn, J.P., Bonassar, L.J., and Stroock, A.D. (2007). Microfluidic scaffolds for tissue engineering. Nat Mater 6, 908–915.

Christian, J.L. (2012). Morphogen gradients in development: From form to function. Wiley Interdiscip. Rev. Dev. Biol. 1, 3–15.

Clowry, G., Molnár, Z., and Rakic, P. (2010). Renewed focus on the developing human neocortex. J. Anat. 217, 276–288.

Colas, J.-F., and Schoenwolf, G.C. (2001). Towards a cellular and molecular understanding of neurulation. Dev. Dyn. 221, 117–145.

Colman, A., and Dreesen, O. (2009). Pluripotent Stem Cells and Disease Modeling. Cell Stem Cell 5, 244–247.

Consalez, G.G., and Hawkes, R. (2013). The compartmental restriction of cerebellar interneurons. Front. Neural Circuits 6, 123.

Crick, F. (1970). Diffusion in embryogenesis. Nature 225, 420–422.

Crossley, P.H., and Martin, G.R. (1995). The mouse Fgf8 gene encodes a family of polypeptides and is expressed in regions that direct outgrowth and patterning in the developing embryo. Development 121, 439–451.

Cui, X., Boland, T., and Lotz, D.D.D. and M.K. (2012). Thermal Inkjet Printing in Tissue Engineering and Regenerative Medicine. Recent Pat. Drug Deliv. Formul. 6, 149–155.

Dahlmann, J., Kensah, G., Kempf, H., Skvorc, D., Gawol, A., Elliott, D. a., Dräger, G., Zweigerdt, R., Martin, U., and Gruh, I. (2013). The use of agarose microwells for scalable embryoid body formation and cardiac differentiation of human and murine pluripotent stem cells. Biomaterials 34, 2463–2471.

Dahmann, C., and Basler, K. (2000). Opposing transcriptional outputs of Hedgehog signaling and Engrailed control compartmental cell sorting at the Drosophila A/P boundary. Cell 100, 411–422.

Dang, S.M. (2004). Controlled, Scalable Embryonic Stem Cell Differentiation Culture. Stem Cells 22, 275–282.

Dang, P.N., Dwivedi, N., Phillips, L.M., Yu, X., Herberg, S., Bowerman, C., Solorio, L.D., Murphy, W.L., and Alsberg, E. (2016). Controlled Dual Growth Factor Delivery From Microparticles Incorporated Within Human Bone Marrow-Derived Mesenchymal Stem Cell Aggregates for Enhanced Bone Tissue Engineering via Endochondral Ossification. Stem Cells Transl. Med. 5, 206–217.

Danielian, P.S., and McMahon, A.P. (1996). Engrailed-1 as a target of the Wnt-1 signalling pathway in vertebrate midbrain development. Nature 383, 332–334.

Darribére, T., Skalski, M., Cousin, H., Gaultier, A., Montmory, C., and Alfandari, D. (2000). Integrins: Regulators of embryogenesis. Biol. Cell 92, 5–25.

Dasgupta, A., Hughey, R., Lancin, P., Larue, L., and Moghe, P. V. (2005). E-cadherin synergistically induces hepatospecific phenotype and maturation of embryonic stem cells in conjunction with hepatotrophic factors. Biotechnol. Bioeng. 92, 257–266.

Dastjerdi, F. V., Consalez, G.G., and Hawkes, R. (2012). Pattern formation during development of the embryonic cerebellum. Front. Neuroanat. 6, 10.

DeForest, C.A., and Anseth, K.S. (2012). Photoreversible patterning of biomolecules within click-based hydrogels. Angew. Chemie - Int. Ed. 51, 1816–1819.

Delatycki, M.B., Williamson, R., and Forrest, S.M. (2000). Friedreich ataxia: an overview. J. Med. Genet. 37, 1–8.

Demers, C.J., Soundararajan, P., Chennampally, P., Cox, G.A., Briscoe, J., Collins, S.D., and Smith, R.L. (2016). Development-on-chip: in vitro neural tube patterning with a microfluidic device. Development 143, 1884–1892.

Dessaud, E., McMahon, A.P., and Briscoe, J. (2008). Pattern formation in the vertebrate neural tube: a sonic hedgehog morphogen-regulated transcriptional network. Development 135, 2489–2503.

Dickinson, M.E., Selleck, M. a, McMahon, a P., and Bronner-Fraser, M. (1995). Dorsalization of the neural tube by the non-neural ectoderm. Development 121, 2099–2106.

Du, J., Campau, E., Soragni, E., Ku, S., Puckett, J.W., Dervan, P.B., and Gottesfeld, J.M. (2012). Role of mismatch repair enzymes in GAA•TTC triplet-repeat expansion in friedreich ataxia induced pluripotent stem cells. J. Biol. Chem. 287, 29861–29872.

Dueñas, A.M., Goold, R., and Giunti, P. (2006). Molecular pathogenesis of spinocerebellar ataxias. Brain 129, 1357–1370.

Duguay, D., Foty, R.A., and Steinberg, M.S. (2003). Cadherin-mediated cell adhesion and tissue segregation: Qualitative and quantitative determinants. Dev. Biol. 253, 309–323.

Durnaoglu, S., Genc, S., and Genc, K. (2011). Patient-Specific Pluripotent Stem Cells in Neurological Diseases. Stem Cells Int. 2011, 1–17.

Dye, B.R., Dedhia, P.H., Miller, A.J., Nagy, M.S., White, E.S., Shea, L.D., and Spence, J.R. (2016). A bioengineered niche promotes in vivo engraftment and maturation of pluripotent stem cell derived human lung organoids. Elife 5, e19732.

Ebert, A.D., and Svendsen, C.N. (2010). Human stem cells and drug screening: opportunities and challenges. Nat. Rev. DRUG Discov. 9, 1–6.

Ehrbar, M., Sala, A., Lienemann, P., Ranga, A., Mosiewicz, K., Bittermann, A., Rizzi, S.C., Weber, F.E., and Lutolf, M.P. (2011). Elucidating the role of matrix stiffness in 3D cell migration and remodeling. Biophys. J. 100, 284–293.

Eigentler, A., Boesch, S., Schneider, R., Dechant, G., and Nat, R. (2013). Induced Pluripotent Stem Cells from Friedreich Ataxia Patients Fail to Upregulate Frataxin During In Vitro Differentiation to Peripheral Sensory Neurons. Stem Cells Dev. 22, 3271–3282.

Eiraku, M., and Sasai, Y. (2012). Self-formation of layered neural structures in three-dimensional culture of ES cells. Curr. Opin. Neurobiol. 22, 768–777.

Eiraku, M., Watanabe, K., Matsuo-Takasaki, M., Kawada, M., Yonemura, S., Matsumura, M., Wataya, T., Nishiyama, A., Muguruma, K., and Sasai, Y. (2008). Self-Organized Formation of Polarized Cortical Tissues from ESCs and Its Active Manipulation by Extrinsic Signals. Cell Stem Cell 3, 519–532.

Elkasaby, A., Xu, D., Schroter-Kermani, C., and Merker, H.J. (1991). Morphology, differentiation and matrix production of liver cells in organoid cultures (high density cultures) of fetal rat livers. Histol. Histopathol. 217–228.

Ema, M., Takahashi, S., and Rossant, J. (2006). Deletion of the selection cassette, but not cis-acting elements, in targeted Flk1-lacZ allele reveals Flk1 expression in multipotent mesodermal progenitors. Blood 107, 111–117.

Engler, A.J., Sen, S., Sweeney, H.L., and Discher, D.E. (2006). Matrix Elasticity Directs Stem Cell Lineage Specification. Cell 126, 677–689.

Englund, C. (2006). Unipolar Brush Cells of the Cerebellum Are Produced in the Rhombic Lip and Migrate through Developing White Matter. J. Neurosci. 26, 9184–9195.

Erceg, S., Ronaghi, M., Zipancic, I., Lainez, S., Roselló, M.G., Xiong, C., Moreno-Manzano, V., Rodríguez-Jiménez, F.J., Planells, R., Alvarez-Dolado, M., et al. (2010). Efficient differentiation of human embryonic stem cells into functional cerebellar-like cells. Stem Cells Dev. 19, 1745–1756.

Eriksson, P.S., Perfilieva, E., Bjork-Eriksson, T., Alborn, A.M., Nordborg, C., Peterson, D.A., and Gage, F.H. (1998). Neurogenesis in the adult human hippocampus. Nat Med 4, 1313–1317.

Evans, M.J., and Kaufman, M.H. (1981). Establishment in culture of pluripotential cells from mouse embryos. Nature 292, 154–156.

Evans, N.D., Minelli, C., Gentleman, E., LaPointe, V., Patankar, S.N., Kallivretaki, M., Chen, X., Roberts, C.J., and Stevens, M.M. (2009). Substrate stiffness affects early differentiation events in embryonic stem cells. Eur. Cells Mater. 18, 1–13.

Fennema, E., Rivron, N., Rouwkema, J., van Blitterswijk, C., and De Boer, J. (2013). Spheroid culture as a tool for creating 3D complex tissues. Trends Biotechnol. 31, 108–115.

Fink, A.J., Englund, C., Daza, R. a M., Pham, D., Lau, C., Nivison, M., Kowalczyk, T., and Hevner, R.F. (2006). Development of the deep cerebellar nuclei: transcription factors and cell migration from the rhombic lip. J. Neurosci. 26, 3066–3076.

Fok, E.Y.L., and Zandstra, P.W. (2005). Shear-Controlled Single-Step Mouse Embryonic Stem Cell Expansion and Embryoid Body-Based Differentiation. Stem Cells 23, 1333–1342.

Fonoudi, H., Ansari, H., Abbasalizadeh, S., Larijani, M.R., Kiani, S., Hashemizadeh, S., Zarchi, A.S., Bosman, A., Blue, G.M., Pahlavan, S., et al. (2015). A Universal and Robust Integrated Platform for the Scalable Production of Human Cardiomyocytes From Pluripotent Stem Cells. Stem Cells Transl. Med. 4, 1482–1494.

Foster, A.C., and Kemp, J.A. (2006). Glutamate- and GABA-based CNS therapeutics. Curr. Opin. Pharmacol. 6, 7–17.

Friedlander, D.R., Mège, R.M., Cunningham, B.A., and Edelman, G.M. (1989). Cell sorting-out is modulated by both the specificity and amount of different cell adhesion molecules (CAMs) expressed on cell surfaces. Proc. Natl. Acad. Sci. U. S. A. 86, 7043–7047.

Fukawatase, Y., Toyoda, M., Okamura, K., Nakamura, K.I., Nakabayashi, K., Takada, S., Yamazaki-Inoue, M., Masuda, A., Nasu, M., Hata, K., et al. (2014). Ataxia telangiectasia derived iPS cells show preserved x-ray sensitivity and decreased chromosomal instability. Sci. Rep. 4, 5421.

Furutama, D., Morita, N., Takano, R., Sekine, Y., Sadakata, T., Shinoda, Y., Hayashi, K., Mishima, Y., Mikoshiba, K., Hawkes, R., et al. (2010). Expression of the IP3R1 promoter-driven nls-LacZ transgene in Purkinje cell parasagittal arrays of developing mouse cerebellum. J. Neurosci. Res. 88, 2810–2825.

Gadue, P., Huber, T.L., Paddison, P.J., and Keller, G.M. (2006). Wnt and TGF-beta signaling are required for the induction of an in vitro model of primitive streak formation using embryonic stem cells. Proc. Natl. Acad. Sci. U. S. A. 103, 16806–16811.

Gammill, L.S., and Bronner-Fraser, M. (2003). Neural crest specification: Migrating into genomics. Nat. Rev. Neurosci. 4, 795–805.

Garda, A.L., Echevarría, D., and Martínez, S. (2001). Neuroepithelial co-expression of Gbx2 and Otx2 precedes Fgf8 expression in the isthmic organizer. Mech. Dev. 101, 111–118.

Garreta, E., Oria, R., Tarantino, C., Pla-Roca, M., Prado, P., Fernández-Avilés, F., Campistol, J.M., Samitier, J., and Montserrat, N. (2017). Tissue engineering by decellularization and 3D bioprinting. Mater. Today 20, 166–178.

Gattazzo, F., Urciuolo, A., and Bonaldo, P. (2014). Extracellular matrix: A dynamic microenvironment for stem cell niche. Biochim. Biophys. Acta - Gen. Subj. 1840, 2506–2519.

Gavalas, a, Davenne, M., Lumsden, a, Chambon, P., and Rijli, F.M. (1997). Role of Hoxa-2 in axon pathfinding and rostral hindbrain patterning. Development 124, 3693–3702.

Gearhart, J. (1998). New potential for human embryonic stem cells. Science 282, 1061–1062.

Gilbert, S. (2007). Developmental Biology. Dev. Biol. 311, 691.

Gilbert, P.M., Havenstrite, K.L., Magnusson, K.E.G., Sacco, A., Leonardi, N.A., Kraft, P., Nguyen, N.K., Thrun, S., Lutolf, M.P., and Blau, H.M. (2010). Substrate elasticity regulates skeletal muscle stem cell self-renewal in culture. Science 329, 1078–1081.

Gill, B.J., Gibbons, D.L., Roudsari, L.C., Saik, J.E., Rizvi, Z.H., Roybal, J.D., Kurie, J.M., and West, J.L. (2012). A synthetic matrix with independently tunable biochemistry and mechanical properties to study epithelial morphogenesis and EMT in a lung adenocarcinoma model. Cancer Res. 72, 6013–6023.

Gjorevski, N., Ranga, A., and Lutolf, M.P. (2014). Bioengineering approaches to guide stem cell-based organogenesis. Development 141, 1794–1804.

Glickstein, M. (1993). Motor skills but not cognitive tasks. Trends Neurosci. 16, 450–451.

Godt, D., and Tepass, U. (1998). Drosophila oocyte localization is mediated by differential cadherin- based adhesion. Nature 395, 387–391.

Goldmann, T., and Gonzalez, J.S. (2000). DNA-printing: Utilization of a standard inkjet printer for the transfer of nucleic acids to solid supports. J. Biochem. Biophys. Methods 42, 105–110.

Goodlett, C.R., and Mittleman, G. (2016). The Cerebellum, pp. 191-212.

Gouon-Evans, V., Boussemart, L., Gadue, P., Nierhoff, D., Koehler, C.I., Kubo, A., Shafritz, D.A., and Keller, G. (2006). BMP-4 is required for hepatic specification of mouse embryonic stem cell-derived definitive endoderm. Nat. Biotechnol. 24, 1402–1411.

Grimaldi, G., Argyropoulos, G.P., Boehringer, A., Celnik, P., Edwards, M.J., Ferrucci, R., Galea, J.M., Groiss, S.J., Hiraoka, K., Kassavetis, P., et al. (2014). Non-invasive cerebellar stimulation - A consensus paper. Cerebellum 13, 121–138.

Grüsser-Cornehls, U., and Bäurle, J. (2001). Mutant mice as a model for cerebellar ataxia. Prog. Neurobiol. 63, 489–540.

Gumbiner, B.M. (1992). Epithelial morphogenesis. Cell 69, 385–387.

Gumbiner, B.M. (1996). Cell adhesion: The molecular basis of tissue architecture and morphogenesis. Cell 84, 345–357.

Gumbiner, B.M. (2005). Regulation of cadherin-mediated adhesion in morphogenesis. Nat. Rev. Mol. Cell Biol. 6, 622–634.

Gunhanlar, N., Shpak, G., van der Kroeg, M., Gouty-Colomer, L.A., Munshi, S.T., Lendemeijer, B., Ghazvini, M., Dupont, C., Hoogendijk, W.J.G., Gribnau, J., et al. (2018). A simplified protocol for differentiation of electrophysiologically mature neuronal networks from human induced pluripotent stem cells. Mol. Psychiatry 23, 1336–1344.

Guo, C., Qiu, H.-Y., Huang, Y., Chen, H., Yang, R.-Q., Chen, S.-D., Johnson, R.L., Chen, Z.-F., and Ding, Y.-Q. (2007). Lmx1b is essential for Fgf8 and Wnt1 expression in the isthmic organizer during tectum and cerebellum development in mice. Development 134, 317–325.

Guvendiren, M., and Burdick, J.A. (2012). Stiffening hydrogels to probe short- and long-term cellular responses to dynamic mechanics. Nat. Commun. 3, 792.

Hackam, D.G., and Redelmeier, D.A. (2006). Translation of Research Evidence From Animals to Humans. JAMA 296, 1727.

Harland, R. (2000). Neural induction. Curr. Opin. Genet. Dev. 10, 357–362.

Hay, E.D., and Zuk, A. (1995). Transformations between epithelium and mesenchyme: Normal, pathological, and experimentally induced. Am. J. Kidney Dis. 26, 678–690.

Heikinheimo, M., Lawshé, A., Shackleford, G.M., Wilson, D.B., and MacArthur, C.A. (1994). Fgf-8 expression in the post-gastrulation mouse suggests roles in the development of the face, limbs and central nervous system. Mech. Dev. 48, 129–138.

Herculano-Houzel (2010). Coordinated scaling of cortical and cerebellar numbers of neurons. Front. Neuroanat 4,12.

Herrup, K., Chen, J., Li, J., and Plummer, M.R. (2014). Ataxia-Telangiectasia and the Biology of Ataxia-Telangiectasia Mutated (ATM). In Movement Disorders: Genetics and Models: Second Edition, pp. 1025–1032.

Hick, A., Wattenhofer-Donzé, M., Chintawar, S., Tropel, P., Simard, J.P., Vaucamps, N., Gall, D., Lambot, L., André, C., Reutenauer, L., et al. (2013). Neurons and cardiomyocytes derived from induced pluripotent stem cells as a model for mitochondrial defects in Friedreich's ataxia. Dis. Model. Mech. 6, 608–621.

Hinton, T.J., Jallerat, Q., Palchesko, R.N., Park, J.H., Grodzicki, M.S., Shue, H.J., Ramadan, M.H., Hudson, A.R., and Feinberg, A.W. (2015). Three-dimensional printing of complex biological structures by freeform reversible embedding of suspended hydrogels. Sci. Adv. 1, e1500758.

Holmes, D.B., and Heine, V.M. (2017). Simplified 3D protocol capable of generating early cortical neuroepithelium. Biol. Open 6, 402–406.

Hoshino, M. (2012). Neuronal subtype specification in the cerebellum and dorsal hindbrain. Dev. Growth Differ. 54, 317–326.

Hoshino, M., Nakamura, S., Mori, K., Kawauchi, T., Terao, M., Nishimura, Y. V., Fukuda, A., Fuse, T., Matsuo, N., Sone, M., et al. (2005). Ptf1a, a bHLH transcriptional gene, defines GABAergic neuronal fates in cerebellum. Neuron 47, 201–213.

Hu, B.-Y., and Zhang, S.-C. (2009). Differentiation of spinal motor neurons from pluripotent human stem cells. Nat. Protoc. 4, 1295–1304.

Huangfu, D., Maehr, R., Guo, W., Eijkelenboom, A., Snitow, M., Chen, A.E., and Melton, D.A. (2008). Induction of pluripotent stem cells by defined factors is greatly improved by small-molecule compounds. Nat. Biotechnol. 26, 795–797.

Humphrey, J.D., Dufresne, E.R., and Schwartz, M.A. (2014). Mechanotransduction and extracellular matrix homeostasis. Nat. Rev. Mol. Cell Biol. 15, 802–812.

Hynes, R.O. (2002). Integrins: Bidirectional, allosteric signaling machines. Cell 110, 673–687.

Igoillo-Esteve, M., Gurgul-Convey, E., Hu, A., Dos Santos, L.R.B., Abdulkarim, B., Chintawar, S., Marselli, L., Marchetti, P., Jonas, J.C., Eizirik, D.L., et al. (2015). Unveiling a common mechanism of apoptosis in beta-cells and neurons in Friedreich's ataxia. Hum. Mol. Genet. 24, 2274–2286.

Imaizumi, K., Sone, T., Ibata, K., Fujimori, K., Yuzaki, M., Akamatsu, W., and Okano, H. (2015). Controlling the Regional Identity of hPSC-Derived Neurons to Uncover Neuronal Subtype Specificity of Neurological Disease Phenotypes. Stem Cell Reports 5, 1010–1022.

Irioka, T., Watanabe, K., Mizusawa, H., Mizuseki, K., and Sasai, Y. (2005). Distinct effects of caudalizing factors on regional specification of embryonic stem cell-derived neural precursors. Dev. Brain Res. 154, 63–70.

Irving, C., and Mason, I. (2000). Signalling by FGF8 from the isthmus patterns anterior hindbrain and establishes the anterior limit of Hox gene expression. Development 127, 177–186.

Ishida, Y., Kawakami, H., Kitajima, H., Nishiyama, A., Sasai, Y., Inoue, H., and Muguruma, K. (2016). Vulnerability of Purkinje Cells Generated from Spinocerebellar Ataxia Type 6 Patient-Derived iPSCs. Cell Rep. 17, 1482–1490.

Ishihara, K., and Tanaka, E.M. (2018). Spontaneous symmetry breaking and pattern formation of organoids. Curr. Opin. Syst. Biol. ISSN 2452-3100.

Ishihara, K., Ranga, A., Lutolf, M.P., Tanaka, E.M., and Meinhardt, A. (2017). Reconstitution of a patterned neural tube from single mouse embryonic stem cells. In Methods in Molecular Biology, pp. 43–55.

Ito, M. (1984). The modifiable neuronal network of the cerebellum. Jpn. J. Physiol. 34, 781–792.

Itoh, M., Nagafuchi, A., Moroi, S., and Tsukita, S. (1997). Involvement of ZO-1 in cadherin-based cell adhesion through its direct binding to a-catenin and actin filaments. J Cell Biol 138, 181–192.

J Siney, E., Kurbatskaya, K., Chatterjee, S., Prasannan, P., Mudher, A., and Willaime-Morawek, S. (2018). Modelling neurodegenerative diseases in vitro: Recent advances in 3D iPSC technologies. AIMS Cell Tissue Eng. 2, 1–23.

Jakel, R.J., Schneider, B.L., and Svendsen, C.N. (2004). Using human neural stem cells to model neurological disease. Nat. Rev. Genet. 5, 136–144.

Jang, T.-S., Jung, H.-D., Pan, H.M., Han, W.T., Chen, S., and Song, J. (2018). 3D printing of hydrogel composite systems: Recent advances in technology for tissue engineering. Int. J. Bioprinting 4, 126.

Johannesson, M., Ståhlberg, A., Ameri, J., Sand, F.W., Norrman, K., and Semb, H. (2009). FGF4 and retinoic acid direct differentiation of hESCs into PDX1-expressing foregut endoderm in a time- and concentration-dependent manner. PLoS One 4, e4794.

Jones, T.M., Shaw, J.D., Sullivan, K., and Zesiewicz, T. a (2014). Treatment of cerebellar ataxia. Neurodegener. Dis. Manag. 4, 379–392.

Joyner, A.L. (1996). Engrailed, Wnt and Pax genes regulate midbrain-hindbrain development. Trends Genet. 12, 15–20.

Joyner, A.L., Liu, A., and Millet, S. (2000). Otx2, Gbx2 and Fgf8 interact to position and maintain a mid-hindbrain organizer. Curr. Opin. Cell Biol. 12, 736–741.

Judson, R.L., Babiarz, J.E., Venere, M., and Blelloch, R. (2009). Embryonic stem cell-specific microRNAs promote induced pluripotency. Nat. Biotechnol. 27, 459–461.

Junghyun Jo, A., Xiao, Y., Xuyang Sun, A., King Tan, E., Shawn Je, H., and Ng, H.-H. (2016). Midbrain-like Organoids from Human Pluripotent Stem Cells Contain Functional Dopaminergic and Neuromelanin-Producing Neurons. 1–10.

Kandel, E.R., Schwartz, J.H., and Jessell, T.M. (2000). Principles of Neural Science.

Karzbrun, E., Kshirsagar, A., Cohen, S.R., Hanna, J.H., and Reiner, O. (2018). Human brain organoids on a chip reveal the physics of folding. Nat. Phys. 14, 515–522.

Katsamba, P., Carroll, K., Ahlsen, G., Bahna, F., Vendome, J., Posy, S., Rajebhosale, M., Price, S., Jessell, T.M., Ben-Shaul, A., et al. (2009). Linking molecular affinity and cellular specificity in cadherin-mediated adhesion. Proc Natl Acad Sci USA 106, 11594–11599.

Kempf, H., Andree, B., and Zweigerdt, R. (2016). Large-scale production of human pluripotent stem cell derived cardiomyocytes. Adv. Drug Deliv. Rev. 96, 18–30.

Kim, Y., Kim, H., Ko, U.H., Oh, Y., Lim, A., Sohn, J.W., Shin, J.H., Kim, H., and Han, Y.M. (2016). Islet-like organoids derived from human pluripotent stem cells efficiently function in the glucose responsiveness in vitro and in vivo. Sci. Rep. 6, 35145.

Kirkeby, A., Grealish, S., Wolf, D.A., Nelander, J., Wood, J., Lundblad, M., Lindvall, O., and Parmar, M. (2012). Generation of Regionally Specified Neural Progenitors and Functional Neurons from Human Embryonic Stem Cells under Defined Conditions. Cell Rep. 1, 703–714.

Kleinman, H.K., and Martin, G.R. (2005). Matrigel: Basement membrane matrix with biological activity. Semin. Cancer Biol. 15, 378–386.

Klockgether, T. (2010). Sporadic ataxia with adult onset: classification and diagnostic criteria. Lancet Neurol. 9, 94–104.

Klockgether, T. (2011). Update on degenerative ataxias. Curr. Opin. Neurol. 24, 339–345.

Kloxin, A.M., Kasko, A.M., Salinas, C.N., and Anseth, K.S. (2009). Photodegradable hydrogels for dynamic tuning of physical and chemical properties. Science (80-.). 324, 59–63.

Koch, P., Breuer, P., Peitz, M., Jungverdorben, J., Kesavan, J., Poppe, D., Doerr, J., Ladewig, J., Mertens, J., Tüting, T., et al. (2011a). Excitation-induced ataxin-3 aggregation in neurons from patients with Machado–Joseph disease. Nature 0–5.

Koch, P., Breuer, P., Peitz, M., Jungverdorben, J., Kesavan, J., Poppe, D., Doerr, J., Ladewig, J., Mertens, J., Tüting, T., et al. (2011b). Excitation-induced ataxin-3 aggregation in neurons from patients with Machado-Joseph disease. Nature 480, 543–546.

Kropp, C., Kempf, H., Halloin, C., Robles-Diaz, D., Franke, A., Scheper, T., Kinast, K., Knorpp, T., Joos, T.O., Haverich, A., et al. (2016). Impact of Feeding Strategies on the

Scalable Expansion of Human Pluripotent Stem Cells in Single-Use Stirred Tank Bioreactors. Stem Cells Transl. Med. 5, 1289–1301.

Kropp, C., Massai, D., and Zweigerdt, R. (2017). Progress and challenges in large-scale expansion of human pluripotent stem cells. Process Biochem. 59, 244–254.

Ku, S., Soragni, E., Campau, E., Thomas, E.A., Altun, G., Laurent, L.C., Loring, J.F., Napierala, M., and Gottesfeld, J.M. (2010). Friedreich's ataxia induced pluripotent stem cells model intergenerational GAATTC triplet repeat instability. Cell Stem Cell 7, 631–637.

Kuhlman, W., Taniguchi, I., Griffith, L.G., and Mayes, A.M. (2007). Interplay between PEO tether length and ligand spacing governs cell spreading on RGD-modified PMMA-g-PEO comb copolymers. Biomacromolecules 8, 3206–3213.

Kukekov, V.G., Laywell, E.D., Suslov, O., Davies, K., Scheffler, B., Thomas, L.B., O'Brien, T.F., Kusakabe, M., and Steindler, D.A. (1999). Multipotent stem/progenitor cells with similar properties arise from neurogenic regions of adult human brain. Exp. Neurol. 156, 333–344.

Kurosawa, H., Imamura, T., Koike, M., Sasaki, K., and Amano, Y. (2003). A simple method for forming embryoid body from mouse embryonic stem cells. J. Biosci. Bioeng. 96, 409–411.

Lamouille, S., Xu, J., and Derynck, R. (2014). Molecular mechanisms of epithelial-mesenchymal transition. Nat. Rev. Mol. Cell Biol. 15, 178–196.

Lancaster, M. a, Renner, M., Martin, C., Wenzel, D., Bicknell, L.S., Hurles, M.E., Homfray, T., Penninger, J.M., Jackson, A.P., Knoblich, J.A., et al. (2012). Cerebral organoids model human brain development and microcephaly. Nature 501, 373–379.

Laping, N.J., Grygielko, E., Mathur, A., Butter, S., Bomberger, J., Tweed, C., Martin, W., Fornwald, J., Lehr, R., Harling, J., et al. (2002). Inhibition of transforming growth factor (TGF)-beta1-induced extracellular matrix with a novel inhibitor of the TGF-beta type I receptor kinase activity: SB-431542. Mol. Pharmacol. 62, 58–64.

Larouche, M., Che, P.M., and Hawkes, R. (2006). Neurogranin expression identifies a novel array of Purkinje cell parasagittal stripes during mouse cerebellar development. J. Comp. Neurol. 494, 215–227.

Lee, J., Xia, Y., Son, M.Y., Jin, G., Seol, B., Kim, M.J., Son, M.J., Do, M., Lee, M., Kim, D., et al. (2012). A novel small molecule facilitates the reprogramming of human somatic cells into a pluripotent state and supports the maintenance of an undifferentiated state of human pluripotent stem cells. Angew. Chemie - Int. Ed. 51, 12509–12513.

Lee, P., Martin, N.T., Nakamura, K., Azghadi, S., Amiri, M., Ben-David, U., Perlman, S., Gatti, R.A., Hu, H., and Lowry, W.E. (2013). SMRT compounds abrogate cellular phenotypes of ataxia telangiectasia in neural derivatives of patient-specific hiPSCs. Nat. Commun. 4, 1824.

Lee, Y.K., Ho, P.W.L., Schick, R., Lau, Y.M., Lai, W.H., Zhou, T., Li, Y., Ng, K.M., Ho, S.L., Esteban, M.A., et al. (2014). Modeling of Friedreich ataxia-related iron overloading cardiomyopathy using patient-specific-induced pluripotent stem cells. Pflugers Arch. Eur. J. Physiol. 466, 1831–1844.

Legate, K.R., Wickström, S.A., and Fässler, R. (2009). Genetic and cell biological analysis of integrin outside-in signaling. Genes Dev. 23, 397–418.

Leto, K., and Rossi, F. (2012). Specification and differentiation of cerebellar GABAergic neurons. In Cerebellum, pp. 434–435.

Leto, K., Rolando, C., and Rossi, F. (2012). The Genesis of Cerebellar GABAergic Neurons: Fate Potential and Specification Mechanisms. Front. Neuroanat. 6, 6.

Leto, K., Arancillo, M., Becker, E.B.E., Buffo, A., Chiang, C., Ding, B., Dobyns, W.B., Dusart, I., Haldipur, P., Hatten, M.E., et al. (2016). Consensus Paper: Cerebellar Development. The Cerebellum 15, 789–828.

Levine, A.J., and Brivanlou, A.H. (2007). Proposal of a model of mammalian neural induction. Dev. Biol. 308, 247–256.

Li, J., Chen, M., Fan, X., and Zhou, H. (2016). Recent advances in bioprinting techniques: Approaches, applications and future prospects. J. Transl. Med. 14, 271.

Li, Y., Xu, C., and Ma, T. (2014). In vitro organogenesis from pluripotent stem cells. Organogenesis 10, 159–163.

Lian, X., Hsiao, C., Wilson, G., Zhu, K., Hazeltine, L.B., Azarin, S.M., Raval, K.K., Zhang, J., Kamp, T.J., and Palecek, S.P. (2012). Robust cardiomyocyte differentiation from human pluripotent stem cells via temporal modulation of canonical Wnt signaling. Proc. Natl. Acad. Sci. 109, E1848–E1857.

Lian, X., Zhang, J., Zhu, K., Kamp, T.J., and Palecek, S.P. (2013). Insulin inhibits cardiac mesoderm, not mesendoderm, formation during cardiac differentiation of human pluripotent stem cells and modulation of canonical wnt signaling can rescue this inhibition. Stem Cells 31, 447–457.

Liu, H.Y., Greene, T., Lin, T.Y., Dawes, C.S., Korc, M., and Lin, C.C. (2017). Enzyme-mediated stiffening hydrogels for probing activation of pancreatic stellate cells. Acta Biomater. 48, 258–269.

Liu, J., Verma, P.J., Evans-Galea, M. V, Delatycki, M.B., Michalska, A., Leung, J., Crombie, D., Sarsero, J.P., Williamson, R., Dottori, M., et al. (2011a). Generation of induced pluripotent stem cell lines from Friedreich ataxia patients. Stem Cell Rev 7, 703–713.

Liu, J., Verma, P.J., Evans-Galea, M. V., Delatycki, M.B., Michalska, A., Leung, J., Crombie, D., Sarsero, J.P., Williamson, R., Dottori, M., et al. (2011b). Generation of Induced Pluripotent Stem Cell Lines from Friedreich Ataxia Patients. Stem Cell Rev. Reports 7, 703–713.

Lodi, R., Cooper, J.M., Bradley, J.L., Manners, D., Styles, P., Taylor, D.J., and Schapira, a H. (1999). Deficit of in vivo mitochondrial ATP production in patients with Friedreich ataxia. Proc. Natl. Acad. Sci. U. S. A. 96, 11492–11495.

Lopez, J.I., Kang, I., You, W.K., McDonald, D.M., and Weaver, V.M. (2011). In situ force mapping of mammary gland transformation. Integr. Biol. 3, 910–921.

De Los Angeles, A., Ferrari, F., Xi, R., Fujiwara, Y., Benvenisty, N., Deng, H., Hochedlinger, K., Jaenisch, R., Lee, S., Leitch, H.G., et al. (2015). Hallmarks of pluripotency. Nature 525, 469–478.

Lou, Y.R., and Leung, A.W. (2018). Next generation organoids for biomedical research and applications. Biotechnol. Adv. 36, 132–149.

Lu, Y.-C., Fu, D.-J., An, D., Chiu, A., Schwartz, R., Nikitin, A.Y., and Ma, M. (2017). Scalable Production and Cryostorage of Organoids Using Core-Shell Decoupled Hydrogel Capsules. Adv. Biosyst. 1700165.

Lukovic, D., Moreno-Manzano, V., Rodriguez-Jimenez, F.J., Vilches, A., Sykova, E., Jendelova, P., Stojkovic, M., and Erceg, S. (2017). HiPSC Disease Modeling of Rare Hereditary Cerebellar Ataxias: Opportunities and Future Challenges. Neuroscientist 23, 554–566.

Luo, Y., Fan, Y., Zhou, B., Xu, Z., Chen, Y., and Sun, X. (2012). Generation of Induced Pluripotent Stem Cells from Skin Fibroblasts of a Patient with Olivopontocerebellar Atrophy. Tohoku J. Exp. Med. 226, 151–159.

Lutolf, M.P., and Hubbell, J.A. (2005). Synthetic biomaterials as instructive extracellular microenvironments for morphogenesis in tissue engineering. Nat. Biotechnol. 23, 47–55.

MacHold, R., and Fishell, G. (2005). Math1 is expressed in temporally discrete pools of cerebellar rhombic-lip neural progenitors. Neuron 48, 17–24.

Maden, M. (2007). Retinoic acid in the development, regeneration and maintenance of the nervous system. Nat. Rev. Neurosci. 8, 755–765.

Mahoney, M.J., and Saltzman, W.M. (2001). Transplantation of brain cells assembled around a programmable synthetic microenvironment. Nat. Biotechnol. 19, 934–939.

Manto, M., and Marmolino, D. (2009a). Animal models of human cerebellar ataxias: A cornerstone for the therapies of the twenty-first century. Cerebellum 8, 137–154.

Manto, M., and Marmolino, D. (2009b). Cerebellar ataxias. Curr. Opin. Neurol. 22, 419–429.

Maricich, S.M., and Herrup, K. (1999). Pax-2 expression defines a subset of GABAergic interneurons and their precursors in the developing murine cerebellum. J. Neurobiol. 41, 281–294.

Marie, P.J., Haÿ, E., Modrowski, D., Revollo, L., Mbalaviele, G., and Civitelli, R. (2014). Cadherin-mediated cell-cell adhesion and signaling in the skeleton. Calcif. Tissue Int. 94, 46–54.

Marmolino, D., and Manto, M. (2010). Past, Present and Future Therapeutics for Cerebellar Ataxias. Curr. Neuropharmacol. 8, 41–61.

Marson, A., Levine, S.S., Cole, M.F., Frampton, G.M., Brambrink, T., Johnstone, S., Guenther, M.G., Johnston, W.K., Wernig, M., Newman, J., et al. (2008). Connecting microRNA Genes to the Core Transcriptional Regulatory Circuitry of Embryonic Stem Cells. Cell 134, 521–533.

Marti-Figueroa, C.R., and Ashton, R.S. (2017). The case for applying tissue engineering methodologies to instruct human organoid morphogenesis. Acta Biomater. 54, 35–44.

Martin, G.R. (1981). Isolation of a pluripotent cell line from early mouse embryos cultured in medium conditioned by teratocarcinoma stem cells (embryonic stem cells/inner cell masses/differentiation in vsitro/embryonal carcinoma cells/growth factors). Dev. Biol. 78, 7634–7638.

Martinez, S., Andreu, A., Mecklenburg, N., and Echevarria, D. (2013). Cellular and molecular basis of cerebellar development. Front. Neuroanat. 7, 18.

Martínez, S., Puelles, E., Puelles, L., and Echevarria, D. (2012). Molecular Regionalization of the Developing Neural Tube. In The Mouse Nervous System, pp. 2–18.

Marzban, H., Bigio, M.R. Del, Alizadeh, J., Ghavami, S., Zachariah, R.M., and Rastegar, M. (2015). Cellular commitment in the developing cerebellum. 8, 1–26.

Matsunaga, E., Katahira, T., and Nakamura, H. (2002). Role of Lmx1b and Wnt1 in mesencephalon and metencephalon development. Development 129, 5269–5277.

Maury, Y., Gauthier, M., Peschanski, M., and Martinat, C. (2012). Human pluripotent stem cells for disease modelling and drug screening. BioEssays 34, 61–71.

McLachlan, N.M., and Wilson, S.J. (2017). The contribution of brainstem and cerebellar pathways to auditory recognition. Front. Psychol. 8, 265.

McMurtrey, R.J. (2016). Analytic Models of Oxygen and Nutrient Diffusion, Metabolism Dynamics, and Architecture Optimization in Three-Dimensional Tissue Constructs with Applications and Insights in Cerebral Organoids. Tissue Eng. Part C Methods 22, 221–249.

Meinhardt, A., Eberle, D., Tazaki, A., Ranga, A., Niesche, M., Wilsch-Bräuninger, M., Stec, A., Schackert, G., Lutolf, M., and Tanaka, E.M. (2014). 3D reconstitution of the patterned neural tube from embryonic stem cells. Stem Cell Reports 3, 987–999.

Mihajlović, A.I., and Bruce, A.W. (2017). The first cell-fate decision of mouse preimplantation embryo development: Integrating cell position and polarity. Open Biol. 7, 170210.

Millen, K.J., Wurst, W., Herrup, K., and Joyner, A.L. (1994). Abnormal embryonic cerebellar development and patterning of postnatal foliation in two mouse Engrailed-2 mutants. Development 120, 695–706.

Miller, J.S., Stevens, K.R., Yang, M.T., Baker, B.M., Nguyen, D.H.T., Cohen, D.M., Toro, E., Chen, A.A., Galie, P.A., Yu, X., et al. (2012). Rapid casting of patterned vascular networks for perfusable engineered three-dimensional tissues. Nat. Mater. 11, 768–774.

Millet, S., Campbell, K., Epstein, D.J., Losos, K., Harris, E., and Joyner, A.L. (1999). A role for Gbx2 in repression of Otx2 and positioning the mid/hindbrain organizer. Nature 401, 161–164.

Miranda, C.C., Fernandes, T.G., Pascoal, J.F., Haupt, S., Brüstle, O., Cabral, J.M.S., and Diogo, M.M. (2015). Spatial and temporal control of cell aggregation efficiently directs human pluripotent stem cells towards neural commitment. Biotechnol. J. 10, 1612–1624.

Miranda, C.C., Fernandes, T.G., Diogo, M.M., and Cabral, J.M.S. (2016). Scaling up a chemically-defined aggregate-based suspension culture system for neural commitment of human pluripotent stem cells. Biotechnol. J. 11, 1628–1638.

Mitoma, H., and Manto, M. (2016). The physiological basis of therapies for cerebellar ataxias. Ther. Adv. Neurol. Disord. 9, 396–413.

Miura, K., Okada, Y., Aoi, T., Okada, A., Takahashi, K., Okita, K., Nakagawa, M., Koyanagi, M., Tanabe, K., Ohnuki, M., et al. (2009). Variation in the safety of induced pluripotent stem cell lines. Nat. Biotechnol. 27, 743–745.

Mizuhara, E., Minaki, Y., Nakatani, T., Kumai, M., Inoue, T., Muguruma, K., Sasai, Y., and Ono, Y. (2010). Purkinje cells originate from cerebellar ventricular zone progenitors positive for Neph3 and E-cadherin. Dev. Biol. 338, 202–214.

Moeller, H.C., Mian, M.K., Shrivastava, S., Chung, B.G., and Khademhosseini, A. (2008). A microwell array system for stem cell culture. Biomaterials 29, 752–763.

Mohr, J.C., de Pablo, J.J., and Palecek, S.P. (2006). 3-D microwell culture of human embryonic stem cells. Biomaterials 27, 6032–6042.

Moore, R., Tao, W., Meng, Y., Smith, E.R., and Xu, X.-X. (2014). Cell adhesion and sorting in embryoid bodies derived from N- or E-cadherin deficient murine embryonic stem cells. Biol. Open 3, 121–128.

Morales, D., and Hatten, M.E. (2006). Molecular Markers of Neuronal Progenitors in the Embryonic Cerebellar Anlage. J. Neurosci. 26, 12226–12236.

Morino, H., Matsuda, Y., Muguruma, K., Miyamoto, R., Ohsawa, R., Ohtake, T., Otobe, R., Watanabe, M., Maruyama, H., Hashimoto, K., et al. (2015). A mutation in the low voltage-gated calcium channel CACNA1G alters the physiological properties of the channel, causing spinocerebellar ataxia. Mol. Brain 8, 89.

Muguruma, K. (2018). Self-Organized Cerebellar Tissue from Human Pluripotent Stem Cells and Disease Modeling with Patient-Derived iPSCs. Cerebellum 17, 37–41.

Muguruma, K., Nishiyama, A., Ono, Y., Miyawaki, H., Mizuhara, E., Hori, S., Kakizuka, A., Obata, K., Yanagawa, Y., Hirano, T., et al. (2010). Ontogeny-recapitulating generation and tissue integration of ES cell-derived Purkinje cells. Nat. Neurosci. 13, 1171–1180.

Muguruma, K., Nishiyama, A., Kawakami, H., Hashimoto, K., and Sasai, Y. (2015). Self-Organization of Polarized Cerebellar Tissue in 3D Culture of Human Pluripotent Stem Cells. Cell Rep. 10, 537–550.

Muller, P., Rogers, K.W., Yu, S.R., Brand, M., and Schier, A.F. (2013). Morphogen transport. Development 140, 1621–1638.

Murphy, W.L., McDevitt, T.C., and Engler, A.J. (2014). Materials as stem cell regulators. Nat. Mater. 13, 547–557.

Murry, C.E., and Keller, G. (2008). Differentiation of Embryonic Stem Cells to Clinically Relevant Populations: Lessons from Embryonic Development. Cell 132, 661–680.

Nachbauer, W., Eigentler, A., and Boesch, S. (2015). Acquired ataxias: the clinical spectrum, diagnosis and management. J. Neurol. 262, 1385–1393.

Nascimento-Ferreira, I., Santos-Ferreira, T., Sousa-Ferreira, L., Auregan, G., Onofre, I., Alves, S., Dufour, N., Colomer Gould, V.F., Koeppen, A., Déglon, N., et al. (2011). Overexpression of the autophagic beclin-1 protein clears mutant ataxin-3 and alleviates Machado-Joseph disease. Brain 134, 1400–1415.

Nayler, S., Gatei, M., Kozlov, S., Gatti, R., Mar, J.C., Wells, C.A., Lavin, M., and Wolvetang, E. (2012). Induced pluripotent stem cells from ataxia-telangiectasia recapitulate the cellular phenotype. Stem Cells Transl. Med. 1, 523–535.

Nayler, S.P., Powell, J.E., Vanichkina, D.P., Korn, O., Wells, C.A., Kanjhan, R., Sun, J., Taft, R.J., Lavin, M.F., and Wolvetang, E.J. (2017). Human iPSC-Derived Cerebellar Neurons from a Patient with Ataxia-Telangiectasia Reveal Disrupted Gene Regulatory Networks. Front. Cell. Neurosci. 11, 321.

Nelson, C.M., Jean, R.P., Tan, J.L., Liu, W.F., Sniadecki, N.J., Spector, A.A., and Chen, C.S. (2005). Emergent patterns of growth controlled by multicellular form and mechanics. Proc. Natl. Acad. Sci. 102, 11594–11599.

Ng, E.S., Davis, R.P., Azzola, L., Stanley, E.G., and Elefanty, A.G. (2005). Forced aggregation of defined numbers of human embryonic stem cells into embryoid bodies fosters robust, reproducible hematopoietic differentiation. Blood 106, 1601–1603.

Nostro, M.C., Cheng, X., Keller, G.M., and Gadue, P. (2008). Wnt, Activin, and BMP Signaling Regulate Distinct Stages in the Developmental Pathway from Embryonic Stem Cells to Blood. Cell Stem Cell 2, 60–71.

Nostro, M.C., Sarangi, F., Ogawa, S., Holtzinger, A., Corneo, B., Li, X., Micallef, S.J., Park, I.-H., Basford, C., Wheeler, M.B., et al. (2011). Stage-specific signaling through TGFβ family members and WNT regulates patterning and pancreatic specification of human pluripotent stem cells. Development 138, 1445–1445.

Oberdick, J., Smeyne, R.J., Mann, J.R., Zackson, S., and Morgan, J.I. (1990). A promoter that drives transgene expression in cerebellar Purkinje and retinal bipolar neurons. Science (80-.). 248, 223–226.

Oberheim, N.A., Wang, X., Goldman, S., and Nedergaard, M. (2006). Astrocytic complexity distinguishes the human brain. Trends Neurosci. 29, 547–553.

Orkin, R.W., Gehron, P., McGoodwin, E.B., Martin, G.R., Valentine, T., and Swarm, R. (1977). A murine tumor producing a matrix of basement membrane. J. Exp. Med. 145, 204–220.

Ovando-Roche, P., West, E.L., Branch, M.J., Sampson, R.D., Fernando, M., Munro, P., Georgiadis, A., Rizzi, M., Kloc, M., Naeem, A., et al. (2018). Use of bioreactors for culturing human retinal organoids improves photoreceptor yields. Stem Cell Res. Ther. 9, 156.

Ozol, K., Hayden, J.M., Oberdick, J., and Hawkes, R. (1999). Transverse zones in the vermis of the mouse cerebellum. J. Comp. Neurol. 412, 95–111.

Park, I.-H., Arora, N., Huo, H., Maherali, N., Ahfeldt, T., Shimamura, A., Lensch, M.W., Cowan, C., Hochedlinger, K., and Daley, G.Q. (2008). Disease-specific induced pluripotent stem cells. Cell 134, 877–886.

Patz, T.M., Doraiswamy, A., Narayan, R.J., He, W., Zhong, Y., Bellamkonda, R., Modi, R., and Chrisey, D.B. (2006). Three-dimensional direct writing of B35 neuronal cells. J. Biomed. Mater. Res. - Part B Appl. Biomater. 78, 124–130.

Peerani, R., and Zandstra, P.W. (2010). Enabling stem cell therapies through synthetic stem cell-niche engineering. J. Clin. Invest. 120, 60–70.

Peerani, R., Rao, B.M., Bauwens, C., Yin, T., Wood, G. a, Nagy, a, Kumacheva, E., and Zandstra, P.W. (2007). Niche-mediated control of human embryonic stem cell self-renewal and differentiation. EMBO J. 26, 4744–4755.

Peppas, N.A., Bures, P., Leobandung, W., and Ichikawa, H. (2000). Hydrogels in pharmaceutical formulations. Eur. J. Pharm. Biopharm. 50, 27–46.

Perl, A., Reinhoudt, D.N., and Huskens, J. (2009). Microcontact printing: Limitations and achievements. Adv. Mater. 21, 2257–2268.

Picollet-D'hahan, N., Dolega, M.E., Freida, D., Martin, D.K., and Gidrol, X. (2017). Deciphering Cell Intrinsic Properties: A Key Issue for Robust Organoid Production. Trends Biotechnol. 35, 1035–1048.

Pohl, C. (2015). Cytoskeletal symmetry breaking and chirality: From reconstituted systems to animal development. Symmetry (Basel). 7, 2062–2107.

Pound, P. (2004). Where is the evidence that animal research benefits humans? BMJ 328, 514–517.

Price, S.R., De Marco Garcia, N. V., Ranscht, B., and Jessell, T.M. (2002). Regulation of motor neuron pool sorting by differential expression of type II cadherins. Cell 109, 205–216.

Przepiorski, A., Sander, V., Tran, T., Hollywood, J.A., Sorrenson, B., Shih, J.-H., Wolvetang, E.J., McMahon, A.P., Holm, T.M., and Davidson, A.J. (2018). A Simple Bioreactor-Based Method to Generate Kidney Organoids from Pluripotent Stem Cells. Stem Cell Reports 11, 470-484.

Przyborski, S.A. (2005). Differentiation of Human Embryonic Stem Cells After Transplantation in Immune-Deficient Mice. Stem Cells 23, 1242–1250.

Przybyla, L., Lakins, J.N., and Weaver, V.M. (2016). Tissue Mechanics Orchestrate Wnt-Dependent Human Embryonic Stem Cell Differentiation. Cell Stem Cell 19, 462–475.

Qi, H., Ghodousi, M., Du, Y., Grun, C., Bae, H., Yin, P., and Khademhosseini, A. (2013). DNA-directed self-assembly of shape-controlled hydrogels. Nat. Commun. 4, 2275.

Qian, X., Nguyen, H.N., Song, M.M., Hadiono, C., Ogden, S.C., Hammack, C., Yao, B., Hamersky, G.R., Jacob, F., Zhong, C., et al. (2016). Brain-Region-Specific Organoids Using Mini-bioreactors for Modeling ZIKV Exposure. Cell 1–17.

Qian, X., Jacob, F., Song, M.M., Nguyen, H.N., Song, H., and Ming, G. (2018). Generation of human brain region–specific organoids using a miniaturized spinning bioreactor. Nat. Protoc. 13, 565–580.

Raeber, G.P., Lutolf, M.P., and Hubbell, J.A. (2005). Molecularly engineered PEG hydrogels: A novel model system for proteolytically mediated cell migration. Biophys. J. 89, 1374–1388.

Rakic, P., and Sidman, R.L. (1973). Organization of cerebellar cortex secondary to deficit of granule cells in weaver mutant mice. J. Comp. Neurol. 152, 133–161.

Ridgeway, R.D., Hamilton, J.W., and MacGregor, R.R. (1986). Characteristics of bovine parathyroid cell organoids in culture. Vitr. Cell. Dev. Biol. 22, 91–99.

Rigamonti, A., Repetti, G.G., Sun, C., Price, F.D., Reny, D.C., Rapino, F., Weisinger, K., Benkler, C., Peterson, Q.P., Davidow, L.S., et al. (2016). Large-Scale Production of Mature Neurons from Human Pluripotent Stem Cells in a Three-Dimensional Suspension Culture System. Stem Cell Reports 6, 993–1008.

Van Rijt, S., and Habibovic, P. (2017). Enhancing regenerative approaches with nanoparticles. J. R. Soc. Interface 14, 20170093.

Rimm, D.L., Koslov, E.R., Kebriaei, P., Cianci, C.D., and Morrow, J.S. (1995). Alpha 1(E)-catenin is an actin-binding and -bundling protein mediating the attachment of F-actin to the membrane adhesion complex. Proc. Natl. Acad. Sci. 92, 8813–8817.

Rodrigues, G.M.C., Gaj, T., Adil, M.M., Wahba, J., Rao, A.T., Lorbeer, F.K., Kulkarni, R.U., Diogo, M.M., Cabral, J.M.S., Miller, E.W., et al. (2017). Defined and Scalable Differentiation of Human Oligodendrocyte Precursors from Pluripotent Stem Cells in a 3D Culture System. Stem Cell Reports 8, 1770–1783.

Ruigrok, T.J.H., Sillitoe, R. V., and Voogd, J. (2014). Cerebellum and Cerebellar Connections. In The Rat Nervous System: Fourth Edition, pp. 133–205.

Sadler, T.W. (2005). Embryology of neural tube development. In American Journal of Medical Genetics - Seminars in Medical Genetics, pp. 2–8.

Salero, E., and Hatten, M.E. (2007). Differentiation of ES cells into cerebellar neurons. Proc. Natl. Acad. Sci. U. S. A. 104, 2997–3002.

Sanvitale, C.E., Kerr, G., Chaikuad, A., Ramel, M.-C., Mohedas, A.H., Reichert, S., Wang, Y., Triffitt, J.T., Cuny, G.D., Yu, P.B., et al. (2013). A New Class of Small Molecule Inhibitor of BMP Signaling. PLoS One 8, e62721.

Sasai, Y. (2013). Next-generation regenerative medicine: Organogenesis from stem cells in 3D culture. Cell Stem Cell 12, 520–530.

Schiele, N.R., Koppes, R.A., Corr, D.T., Ellison, K.S., Thompson, D.M., Ligon, L.A., Lippert, T.K.M., and Chrisey, D.B. (2009). Laser direct writing of combinatorial libraries of idealized cellular constructs: Biomedical applications. Appl. Surf. Sci. 255, 5444–5447.

Schiele, N.R., Corr, D.T., Huang, Y., Raof, N.A., Xie, Y., and Chrisey, D.B. (2010). Laser-based direct-write techniques for cell printing. Biofabrication 2, 032001.

Schmahmann, J.D. (1997). Rediscovery of an Early Concept. 3–27.

Schöls, L., Bauer, P., Schmidt, T., Schulte, T., and Riess, O. (2004). Autosomal dominant cerebellar ataxias: Clinical features, genetics, and pathogenesis. Lancet Neurol. 3, 291–304.

Schröter-Kermani, C., Hinz, N., Risse, P., Zimmermann, B., and Merker, H.J. (1991). The Extracellular Matrix in Cartilage Organoid Culture: Biochemical, Immunomorphological and Electron Microscopic Studies. Matrix 11, 428–441.

Shan, B., Xu, C., Zhang, Y., Xu, T., Gottesfeld, J.M., and Yates, J.R. (2014). Quantitative proteomic analysis identifies targets and pathways of a 2-aminobenzamide HDAC inhibitor in Friedreichs ataxia patient iPSC-derived neural stem cells. J. Proteome Res. 13, 4558–4566.

Shih, H., and Lin, C.C. (2016). Tuning stiffness of cell-laden hydrogel: Via host-guest interactions. J. Mater. Chem. B 4, 4969–4974.

Simunovic, M., and Brivanlou, A.H. (2017). Embryoids, organoids and gastruloids: new approaches to understanding embryogenesis. Development 144, 976–985.

Singec, I., Knoth, R., Ditter, M., Frotscher, M., and Volk, B. (2003). Neurogranin expression by cerebellar neurons in rodents and non-human primates. J. Comp. Neurol. 459, 278–289.

Singh, V.K., Kalsan, M., Kumar, N., Saini, A., and Chandra, R. (2015). Induced pluripotent stem cells: applications in regenerative medicine, disease modeling, and drug discovery. Front Cell Dev Biol 3, 2.

Skogh, C., Eriksson, C., Kokaia, M., Meijer, X.C., Wahlberg, L.U., Wictorin, K., and Campbell, K. (2001). Generation of regionally specified neurons in expanded glial cultures derived from the mouse and human lateral ganglionic eminence. Mol. Cell. Neurosci. 17, 811–820.

Smith, E., and Cochrane, W.J. (1946). Cystic organoid teratoma; report of a case. Can Med Assoc J. 151.

Soragni, E., Miao, W., Iudicello, M., Jacoby, D., De Mercanti, S., Clerico, M., Longo, F., Piga, A., Ku, S., Campau, E., et al. (2014). Epigenetic Therapy for Friedreich ataxia. Ann. Neurol. 76, 489–508.

Spence, J., Mayhew, C., Rankin, S., Kuhar, M., Vallance, J., Tolle, K., Hoskins, E., Kalinichenko, V., Wells, S., Zorn, A., et al. (2010). Directed differentiation of human pluripotent stem cells into intestinal tissue in vitro. Nature 470, 105–109.

Spracklen, A.J., and Peifer, M. (2015). Actin and Apical Constriction: Some (Re)-Assembly Required. Dev. Cell 35, 662–664.

Stern, C.D. (2001). Initial patterning of the central nervous system: How many organizers? Nat. Rev. Neurosci. 2, 92–98.

Sterneckert, J.L., Reinhardt, P., and Schöler, H.R. (2014). Investigating human disease using stem cell models. Nat. Rev. Genet. 15, 625–639.

Stiles, J., and Jernigan, T.L. (2010). The basics of brain development. Neuropsychol. Rev. 20, 327–348.

Su, H.L., Muguruma, K., Matsuo-Takasaki, M., Kengaku, M., Watanabe, K., and Sasai, Y. (2006). Generation of cerebellar neuron precursors from embryonic stem cells. Dev. Biol. 290, 287–296.

Suzuki, I.K., and Vanderhaeghen, P. (2015). Is this a brain which I see before me? Modeling human neural development with pluripotent stem cells. Development 142, 3138–3150.

Suzuki, S.C., Inoue, T., Kimura, Y., Tanaka, T., and Takeichi, M. (1997). Neuronal circuits are subdivided by differential expression of type-II classic cadherins in postnatal mouse brains. Mol. Cell. Neurosci. 9, 433–447.

Tada, S. (2005). Characterization of mesendoderm: a diverging point of the definitive endoderm and mesoderm in embryonic stem cell differentiation culture. Development 132, 4363–4374.

Takahashi, S., and Yamanaka, K. (2006). Induction of Pluripotent Stem Cells from Mouse Embryonic and Adult Fibroblast Cultures by Defined Factors. Cell 126, 663–676.

Takahashi, K., Tanabe, K., Ohnuki, M., Narita, M., Ichisaka, T., Tomoda, K., and Yamanaka, S. (2007). Induction of Pluripotent Stem Cells from Adult Human Fibroblasts by Defined Factors. Cell 131, 861–872.

Takasato, M., Er, P.X., Chiu, H.S., Maier, B., Baillie, G.J., Ferguson, C., Parton, R.G., Wolvetang, E.J., Roost, M.S., De Sousa Lopes, S.M.C., et al. (2015). Kidney organoids from human iPS cells contain multiple lineages and model human nephrogenesis. Nature 526, 564–568.

Takata, N., Sakakura, E., Eiraku, M., Kasukawa, T., and Sasai, Y. (2017). Self-patterning of rostral-caudal neuroectoderm requires dual role of Fgf signaling for localized Wnt antagonism. Nat. Commun. 8, 1339.

Takebe, T., Zhang, R.R., Koike, H., Kimura, M., Yoshizawa, E., Enomura, M., Koike, N., Sekine, K., and Taniguchi, H. (2014). Generation of a vascularized and functional human liver from an iPSC-derived organ bud transplant. Nat. Protoc. 9, 396–409.

Takeichi, M. (1987). Cadherins: a molecular family essential for selective cell-cell adhesion and animal morphogenesis. Trends Genet. 3, 213–217.

Takeichi, M. (1995). Morphogenetic roles of classic cadherins. Curr. Opin. Cell Biol. 7, 619–627.

Tamkun, J.W., DeSimone, D.W., Fonda, D., Patel, R.S., Buck, C., Horwitz, A.F., and Hynes, R.O. (1986). Structure of integrin, a glycoprotein involved in the transmembrane linkage between fibronectin and actin. Cell 46, 271–282.

Tang-Schomer, M.D., White, J.D., Tien, L.W., Schmitt, L.I., Valentin, T.M., Graziano, D.J., Hopkins, A.M., Omenetto, F.G., Haydon, P.G., and Kaplan, D.L. (2014). Bioengineered functional brain-like cortical tissue. Proc. Natl. Acad. Sci. 111, 13811–13816.

Tao, O., Shimazaki, T., Okada, Y., Naka, H., Kohda, K., Yuzaki, M., Mizusawa, H., and Okano, H. (2010). Efficient generation of mature cerebellar Purkinje cells from mouse embryonic stem cells. J. Neurosci. Res. 88, 234–247.

Taroni, F., and DiDonato, S. (2004). Pathways to motor incoordination: the inherited ataxias. Nat. Rev. Neurosci. 5, 641–655.

Tepass, U., Godt, D., and Winklbauer, R. (2002). Cell sorting in animal development: Signalling and adhesive mechanisms in the formation of tissue boundaries. Curr. Opin. Genet. Dev. 12, 572–582.

Thomson, J.A. (1998). Embryonic Stem Cell Lines Derived from Human Blastocysts. Science 282, 1145–1147.

Till, J.E., McCulloch, E.A., and Siminovitch, L. (1964). A stochastic model of stem cell proliferation, based on the growth of spleen colony-forming cells. Proc. Natl. Acad. Sci. USA 51, 29–36.

Tiscornia, G., Vivas, E.L., and Belmonte, J.C.I. (2011). Diseases in a dish: Modeling human genetic disorders using induced pluripotent cells. Nat. Med. 17, 1570–1576.

Tocchio, A., Tamplenizza, M., Martello, F., Gerges, I., Rossi, E., Argentiere, S., Rodighiero, S., Zhao, W., Milani, P., and Lenardi, C. (2015). Versatile fabrication of vascularizable scaffolds for large tissue engineering in bioreactor. Biomaterials 45, 124–131.

Todhunter, M.E., Jee, N.Y., Hughes, A.J., Coyle, M.C., Cerchiari, A., Farlow, J., Garbe, J.C., LaBarge, M.A., Desai, T.A., and Gartner, Z.J. (2015). Programmed synthesis of three-dimensional tissues. Nat. Methods 12, 975–981.

Todhunter, M.E., Weber, R.J., Farlow, J., Jee, N.Y., Cerchiari, A.E., and Gartner, Z.J. (2016). Fabrication of 3-D Reconstituted Organoid Arrays by DNA-Programmed Assembly of Cells (DPAC). Curr. Protoc. Chem. Biol. 8, 147–178.

Torisawa, Y.S., Chueh, B.H., Huh, D., Ramamurthy, P., Roth, T.M., Barald, K.F., and Takayama, S. (2007). Efficient formation of uniform-sized embryoid bodies using a compartmentalized microchannel device. Lab Chip 7, 770–776.

Trompouki, E., Bowman, T. V., Lawton, L.N., Fan, Z.P., Wu, D.C., Dibiase, A., Martin, C.S., Cech, J.N., Sessa, A.K., Leblanc, J.L., et al. (2011). Lineage regulators direct BMP and Wnt pathways to cell-specific programs during differentiation and regeneration. Cell 147, 577–589.

Turner, D.A., Girgin, M., Alonso-Crisostomo, L., Trivedi, V., Baillie-Johnson, P., Glodowski, C.R., Hayward, P.C., Collignon, J., Gustavsen, C., Serup, P., et al. (2017). Anteroposterior polarity and elongation in the absence of extraembryonic tissues and spatially localised signalling in Gastruloids, mammalian embryonic organoids. Development dev.150391.

Ulloa, F., and Martí, E. (2010). Wnt won the war: Antagonistic role of Wnt over Shh controls dorso-ventral patterning of the vertebrate neural tube. Dev. Dyn. 239, 69–76.

Ungrin, M.D., Joshi, C., Nica, A., Bauwens, C., and Zandstra, P.W. (2008). Reproducible, Ultra High-Throughput Formation of Multicellular Organization from Single Cell Suspension-Derived Human Embryonic Stem Cell Aggregates. PLoS One 3, e1565.

Urbach, a, Schuldiner, M., and Benvenisty, N. (2004). Modeling for Lesch-Nyhan disease by gene targeting in human embryonic stem cells. Stem Cells 22, 635–641.

Uzel, S.G.M., Amadi, O.C., Pearl, T.M., Lee, R.T., So, P.T.C., and Kamm, R.D. (2016). Simultaneous or Sequential Orthogonal Gradient Formation in a 3D Cell Culture Microfluidic Platform. Small 12, 612–622.

Van Vlierberghe, S., Dubruel, P., and Schacht, E. (2011). Biopolymer-based hydrogels as scaffolds for tissue engineering applications: A review. Biomacromolecules 12, 1387–1408.

Vosough, M., Omidinia, E., Kadivar, M., Shokrgozar, M.-A., Pournasr, B., Aghdami, N., and Baharvand, H. (2013). Generation of Functional Hepatocyte-Like Cells from Human Pluripotent Stem Cells in a Scalable Suspension Culture. Stem Cells Dev. 22, 2693–2705.

Waddell, W.R. (1949). Organoid differentiation of the fetal lung; a histologic study of the differentiation of mammalian fetal lung in utero and in transplants. Arch. Pathol. (Chic.) 227–247.

Wagner, M.J., Kim, T.H., Savall, J., Schnitzer, M.J., and Luo, L. (2017). Cerebellar granule cells encode the expectation of reward. Nature 544, 96–100.

Wang, V.Y., and Zoghbi, H.Y. (2001). Genetic regulation of cerebellar development. Nat. Rev. Neurosci. 2, 484–491.

Wang, H., Luo, X., and Leighton, J. (2015a). Extracellular Matrix and Integrins in Embryonic Stem Cell Differentiation. Biochem. Insights 15, 15-21.

Wang, S., Wang, B., Pan, N., Fu, L., Wang, C., Song, G., An, J., Liu, Z., Zhu, W., Guan, Y., et al. (2015b). Differentiation of human induced pluripotent stem cells to mature functional Purkinje neurons. Sci. Rep. 5, 9232.

Wang, V.Y., Rose, M.F., and Zoghbi, H.Y. (2005). Math1 expression redefines the rhombic lip derivatives and reveals novel lineages within the brainstem and cerebellum. Neuron 48, 31–43.

Wang, X.Y., Jin, Z.H., Gan, B.W., Lv, S.W., Xie, M., and Huang, W.H. (2014). Engineering interconnected 3D vascular networks in hydrogels using molded sodium alginate lattice as the sacrificial template. Lab Chip 14, 2709–2716.

Wassarman, K.M., Lewandoski, M., Campbell, K., Joyner, A.L., Rubenstein, J.L., Martinez, S., Martin, G.R., Abbott, L., Jacobowitz, D., Acampora, D., et al. (1997). Specification of the anterior hindbrain and establishment of a normal mid/hindbrain organizer is dependent on Gbx2 gene function. Development 124, 2923–2934.

Watson, L.M., Wong, M.M.K., and Becker, E.B.E. (2015). Induced pluripotent stem cell technology for modelling and therapy of cerebellar ataxia. Open Biol. 5, 150056.

Watson, L.M., Wong, M.M.K., Vowles, J., Cowley, S.A., and Becker, E.B.E. (2018). A Simplified Method for Generating Purkinje Cells from Human-Induced Pluripotent Stem Cells. Cerebellum 17, 419-427.

Weaver, A.H. (2005). Reciprocal evolution of the cerebellum and neocortex in fossil humans. Proc. Natl. Acad. Sci. 102, 3576–3580.

Weinstein, D.C., and Hemmati-Brivanlou, A. (1999). Neural Induction. Annu. Rev. Cell Dev. Biol. 15, 411–433.

Weissman, I.L. (2000). Stem cells: Units of development, units of regeneration, and units in evolution. Cell 100, 157–168.

Wennekamp, S., Mesecke, S., Nédélec, F., and Hiiragi, T. (2013). A self-organization framework for symmetry breaking in the mammalian embryo. Nat. Rev. Mol. Cell Biol. 14, 454–461.

White, J.J., and Sillitoe, R. V. (2013). Development of the cerebellum: From gene expression patterns to circuit maps. Wiley Interdiscip. Rev. Dev. Biol. 2, 149–164.

White, M.D., Bissiere, S., Alvarez, Y.D., and Plachta, N. (2016). Mouse Embryo Compaction. In Current Topics in Developmental Biology, pp. 235–258.

Whitney, E.R., Kemper, T.L., Rosene, D.L., Bauman, M.L., and Blatt, G.J. (2008). Calbindin-D28k is a more reliable marker of human Purkinje cells than standard Nissl stains: A stereological experiment. J. Neurosci. Methods 168, 42–47.

Wilson, S.W., and Houart, C. (2004). Early steps in the development of the forebrain. Dev. Cell 6, 167–181.

Van Winkle, A.P., Gates, I.D., and Kallos, M.S. (2012). Mass transfer limitations in embryoid bodies during human embryonic stem cell differentiation. Cells Tissues Organs 196, 34–47.

Wolpert, L. (1969). Positional information and the spatial pattern of cellular differentiation. J. Theor. Biol. 25, 1–47.

Wurst, W., Bally-Cuif, L., and Bally-Cuif, L. (2001). Neural plate patterning: Upstream and downstream of the isthmic organizer. Nat. Rev. Neurosci. 2, 99–108.

Wylie, R.G., Ahsan, S., Aizawa, Y., Maxwell, K.L., Morshead, C.M., and Shoichet, M.S. (2011). Spatially controlled simultaneous patterning of multiple growth factors in three-dimensional hydrogels. Nat. Mater. 10, 799–806.

Xia, G., Santostefano, K., Hamazaki, T., Liu, J., Subramony, S.H., Terada, N., and Ashizawa, T. (2012). Generation of Human-Induced Pluripotent Stem Cells to Model Spinocerebellar Ataxia Type 2 In vitro. J. Mol. Neurosci. 29, 237–248.

Xie, A.W., Binder, B.Y.K., Khalil, A.S., Schmitt, S.K., Johnson, H.J., Zacharias, N.A., and Murphy, W.L. (2017). Controlled Self-assembly of Stem Cell Aggregates Instructs Pluripotency and Lineage Bias. Sci. Rep. 7, 14070.

Yamamoto, T., Takenaka, C., Yoda, Y., Oshima, Y., Kagawa, K., Miyajima, H., Sasaki, T., and Kawamata, S. (2018). Differentiation potential of Pluripotent Stem Cells correlates to the level of CHD7. Sci. Rep. 8, 241.

Yawata, S., Tsuchida, H., Kengaku, M., and Hirano, T. (2006). Membrane-proximal region of glutamate receptor delta2 subunit is critical for long-term depression and interaction with protein interacting with C kinase 1 in a cerebellar Purkinje neuron. J. Neurosci. 26, 3626–3633.

Yin, X., Mead, B.E., Safaee, H., Langer, R., Karp, J.M., and Levy, O. (2016). Engineering Stem Cell Organoids. Cell Stem Cell 18, 25–38.

Yoshida, Y., Hilborn, V., and Freeman, A.E. (1980). Fine structural identification of organoid mouse lung cells cultured on a pigskin substrate. In Vitro 994–1006.

Yoshikawa, H.Y., Rossetti, F.F., Kaufmann, S., Kaindl, T., Madsen, J., Engel, U., Lewis, A.L., Armes, S.P., and Tanaka, M. (2011). Quantitative evaluation of mechanosensing of cells on dynamically tunable hydrogels. J. Am. Chem. Soc. 133, 1367–1374.

Youssef, J., Nurse, A.K., Freund, L.B., and Morgan, J.R. (2011). Quantification of the forces driving self-assembly of three-dimensional microtissues. Proc. Natl. Acad. Sci. 108, 6993–6998.

Yu, J., Vodyanik, M. a, Smuga-Otto, K., Antosiewicz-Bourget, J., Frane, J.L., Tian, S., Nie, J., Jonsdottir, G. a, Ruotti, V., Stewart, R., et al. (2007). Induced pluripotent stem cell lines derived from human somatic cells. Science (80-.). 318, 1917–1920.

Zervas, M., Millet, S., Ahn, S., and Joyner, A.L. (2004). Cell behaviors and genetic lineages of the mesencephalon and rhombomere 1. Neuron 43, 345–357.

Zhang, G. (2012). Biomimicry in biomedical research. Organogenesis 8, 101–102.

Zhang, L., and Goldman, J.E. (1996). Generation of cerebellar interneurons from dividing progenitors in white matter. Neuron 16, 47–54.

Zhong, Y., Brieher, W.M., and Gumbiner, B.M. (1999). Analysis of C-cadherin regulation during tissue morphogenesis with an activating antibody. J. Cell Biol. 144, 351–359.

Zhou, Y., and Zeng, F. (2013). Integration-free Methods for Generating Induced Pluripotent Stem Cells. Genomics. Proteomics Bioinformatics 11, 284–287.

Ziv, Y., Danieli, T., Amiel, A., Ravia, Y., Shiloh, Y., Etkin, S., Trakhtenbrot, L., and Jaspers, N.G.J. (1989). Cellular and Molecular Characteristics of an Immortalized Ataxia-Telangiectasia (Group AB) Cell Line. Cancer Res. 49, 2495–2501.

Zoldan, J., Karagiannis, E.D., Lee, C.Y., Anderson, D.G., Langer, R., and Levenberg, S. (2011). The influence of scaffold elasticity on germ layer specification of human embryonic stem cells. Biomaterials 32, 9612–9621.

II. GENERATION OF MATURE CEREBELLAR NEURONS FROM HUMAN PLURIPOTENT STEM CELLS UNDER DEFINED AND FEEDER-FREE CONDITIONS

The content of this chapter was adapted from the publication:

Silva, T.P., Bekman, E., Fernandes, T.G., Vaz, S.H., Rodrigues, C.A.V., Diogo, M.M., Cabral, J.M.S., Carmo-Fonseca, M., "Human pluripotent stem cell-derived cerebellum organoids yield mature neurons in feeder-free cultures", *submitted*.

II.1 ABSTRACT

The cerebellum plays a critical role in all vertebrates, and many neurological disorders such as ataxias are associated with cerebellum dysfunction. A major limitation in cerebellar research has been the lack of adequate disease models. As an alternative to animal models, cerebellar neurons have been differentiated from human induced pluripotent stem cells (iPSCs). However, previous studies were able to produce only limited amounts of Purkinje cells. These cells are strongly involved with the development of cerebellar ataxias and are thus required for studying these diseases. Moreover, *in vitro* generation of Purkinje cells required co-culture systems, which may introduce unknown components to the system. Here we describe a novel 3D differentiation strategy that uses defined medium to generate Purkinje cells, granule cells, interneurons, and deep cerebellar nuclei projection neurons. The distinct types of cerebellar neurons self-formed and matured into functional cells that were maintained in cultures for up to 145 days. Using a defined basal medium optimized for neuronal cell culture, we successfully promoted the maturation of cerebellar precursors without the need for co-culturing. We anticipate that our findings can be translated into better models for the study of cerebellar dysfunctions, and represent a valuable advance towards the development of autologous replacement strategies for treating cerebellar degenerative diseases.

Keywords: cerebellum, ataxia, Purkinje cells, feeder-free culture, human pluripotent stem cells

II.2 INTRODUCTION

The cerebellum plays a critical role in maintaining balance and posture, coordination of voluntary movements, and motor learning in all vertebrates (for a recent review see McLachlan and Wilson, 2017). Emerging evidence indicates that this brain structure also plays a role in auditory processing tasks, reward expectation (Wagner et al., 2017), and other forms of emotional processing (Adamaszek et al., 2017). Therefore, it is not surprising that many neurological disorders are associated with abnormal changes in the cerebellum (Schöls et al., 2004; Taroni and DiDonato, 2004). This association has generated a great interest in the study of cerebellum development and function.

A major limitation in cerebellar research has been the lack of adequate experimental models that could help identify essential molecular and cellular pathways and thus could be used to improve our understanding of cerebellum dysfunction. Indeed, much of the current knowledge about the mechanisms of cerebellar diseases has been based on human postmortem studies, which do not inform on disease development or progression. Alternatively, animal models and immortalized human cell lines have been used (Manto and Marmolino, 2009). While these models permit in-depth investigation, they do not fully reflect the physiology and metabolism of human tissues. Thus, there is a great need for better models for the study of the human cerebellum.

The generation of cerebellar neurons using human induced pluripotent stem cells (iPSCs) aims to recapitulate early cerebellar development during human embryogenesis (Andreu et al., 2014; Butts et al., 2014; Leto et al., 2016). Pioneer studies worked on the formation of embryoid body-like structures derived from human or mouse embryonic stem cells that did differentiate into cerebellar-like cells (Erceg et al., 2010, 2012; Salero and Hatten, 2007; Su et al., 2006) but nevertheless showed only a small number of immature Purkinje cells. Considering that most cerebellar disorders, namely ataxias, are associated

with a loss of Purkinje cells, this technical limitation compromises the use of such embryoid bodies as a model for studying cerebellar biology and pathology.

Recent studies have generated bona fide Purkinje cells from mouse embryonic stem cells (Muguruma et al., 2010), human pluripotent stem cells (Muguruma et al., 2015), or spinocerebellar ataxia patient-derived iPSCs (Ishida et al., 2016). However, the maturation into functional Purkinje neurons has been achieved by co-culturing cells with either cerebellar granule cell precursors isolated from mouse embryos (Ishida et al., 2016; Muguruma et al., 2015) or fetal cerebellar slices (Wang et al., 2015). Co-culture systems can be problematic because feeder cells add significant variability to the system, which may in turn affect its reproducibility and the experimental results (Akopian et al., 2010; Wang et al., 2015). Thus, establishing long-term culture systems that are able to support complete maturation of human cerebellar neurons in feeder-free conditions is highly needed.

Here we present a novel differentiation strategy to generate distinct types of cerebellar cells that self-formed and matured into functional neurons in a defined medium. The possibility of efficiently generating cerebellar neurons from patient-derived iPSCs will facilitate drug screening and the study of specific pathways involved in disease development and progression.

II.3 METHODS

Maintenance of human iPSCs

We used two distinct human iPSC lines. A cell line, termed F002.1A.13, was derived from a healthy female donor using a standard protocol (Takahashi et al., 2007). Karyotyping of these cells revealed no abnormalities, and upon subcutaneous injection into immune-deficient mice they induced the formation of tumoral masses reminiscent of teratomas (Hentze et al., 2009), thus confirming their *in vivo* differentiation potential (**Figure II.1**). Besides the F002.1A.13, the Gibco® Human Episomal iPSC line (iPSC6.2) was also used (Burridge et al., 2011). Both human iPSCs were cultured on Matrigel™ (Corning)-coated plates with either Essential 8™ Medium (Life Technologies) or mTeSR™1 Medium (StemCell Technologies). Medium was changed daily. Cells were passaged every three to four days (when the colonies covered approximately 85% of the surface area of the culture dish) using 0.5mM EDTA dissociation buffer (Life Technologies). Two to three passages were performed before starting the differentiation process.

Teratoma assay

Animal experimentation at Instituto de Medicina Molecular was conducted strictly within the rules of the Portuguese official veterinary directorate, which complies with the European Guideline 86/609/EC concerning laboratory animal welfare, according to a protocol approved by the Institute's Animal Ethics Committee. To assess capacity of the F002.1A.13 cells to form teratoma, cells were collected using 0.5 mM EDTA dissociation buffer and $2x10^6$ cells, resuspended in mTeSR™1/Matrigel 1:1, were subcutaneously injected into the flanks of 8-week-old immunocompromised mice (NGS). Animals were sacrificed with anesthetic overdose and necropsy was performed. Subcutaneous tumor and

ipsilateral inguinal lymph node were harvested, fixed in 10% neutral-buffered formalin, embedded in paraffin, and 3µm sections were stained with hematoxylin and eosin. Tissue sections were examined by a pathologist blinded to experimental groups in a Leica DM2500 microscope coupled to a Leica MC170 HD microscope camera.

Karyotyping of human iPSCs

F002.1A.13 cells were incubated with colcemid (10µg/ml; Life Technologies) for 4 hours to arrest cells in metaphase. Next, cells were collected and incubated with hypotonic potassium chloride solution for 15 min at 37 °C. Finally, cells were resuspended and fixed in glacial acetic acid and methanol (1:3). Karyotype analysis was performed by Genomed SA (Lisbon, Portugal).

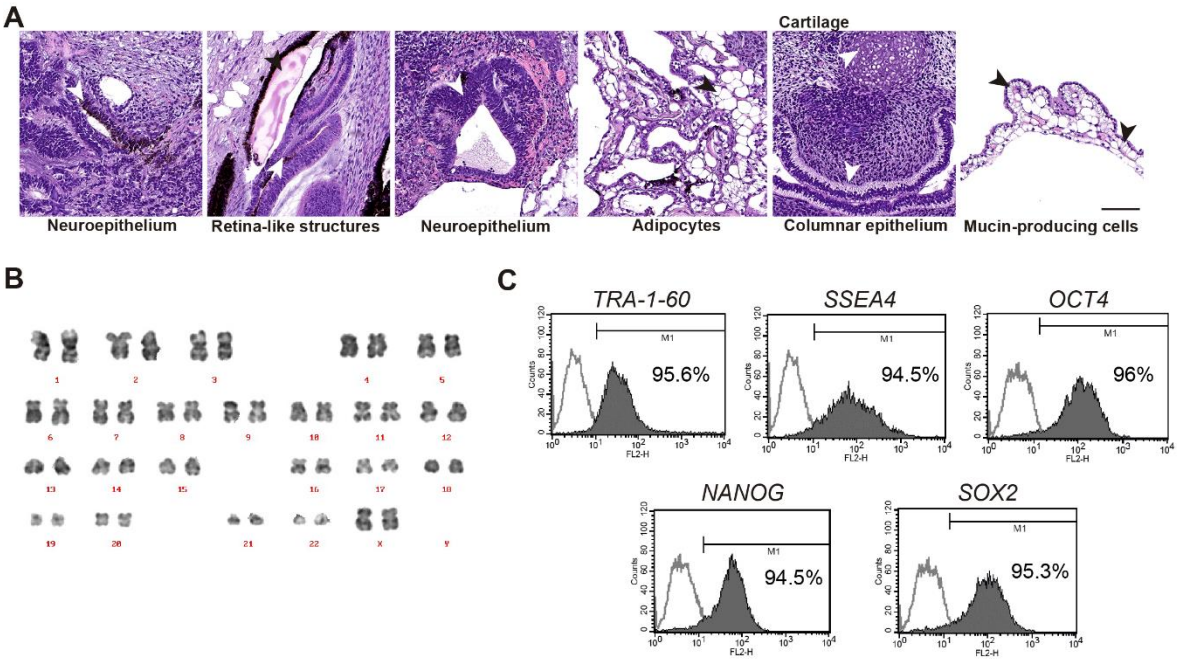

Figure II.1. F002.1A.13 cell line characterization. A) Representative histological sections of teratomas stained with hematoxylin and eosin. Tumors contained cell types derived from the three embryonic germ layers, including ectodermal components corresponding to neuroepithelium with melanin pigment, retina-like pigmented structures, and neuroepithelium consisting of small hyperchromatic cells arranged in rosettes; mesodermal

components corresponding to adipocytes and cartilage; and endodermal components corresponding to columnar epithelium and mucin-producing cells. **B)** Karyotype performed by Giemsa Trypsin banding. C) Flow cytometry analysis for the indicated pluripotency markers on day zero of differentiation.

3-D culture of cerebellar organoids

To promote human iPSC aggregation in embryoid body-like floating structures, both cell lines used in this study were incubated with ROCK inhibitor (ROCKi, Y-27632, 10μM, StemCell Technologies) for 1 h at 37 ºC and then treated with accutase (Sigma) for 5 min at 37ºC. After dissociation, cells were quickly re-aggregated using microwell plates (AggreWell™800, StemCell Technologies) according to the manufacturer's instructions. Cells were plated at a density of 1.8 x 10^6 cells/well (6,000 cells/microwell) in 1.5 mL/well of mTeSR™1 supplemented with 10μM ROCKi. Twenty-four hours later the entire medium was replaced and cells were maintained in mTeSR™1 without ROCKi for another 24 hours.

The day on which the aggregate culture was started was defined as day 0. The basal differentiation medium used during days 2–21 was growth-factor-free chemically defined medium (gfCDM) (Muguruma et al., 2015), consisting of Isocove's modified Dulbecco's medium/Ham's F-12 (Life Technologies) 1:1, chemically defined lipid concentrate (1% v/v, Life Technologies), monothioglycerol (450μM, Sigma), apo-transferrin (15μg/ml, Sigma), crystallization-purified BSA (5mg/ml, >99%, Sigma), and 50U/ml penicillin/50μg/ml streptomycin (PS, Life Technologies). The medium was also supplemented with insulin (7μg/ml, Sigma).

Recombinant human basic FGF (FGF2, 50ng/ml, PeproTech) and SB431542 (SB, 10μM, Sigma) were added to culture on day 2. The entire medium was replaced by gfCDM (supplemented with insulin, FGF2 and SB) on day 5. On day 7, the floating aggregates were transferred from microwell plates to ultra-low attachment 6-well plates (Costar, Corning) and cultured at a density of 1 × 106 cells/mL in 1.8 mL/well. Medium was replaced and 2/3 of the

initial amount of FGF2 and SB was added. Recombinant human FGF19 was added to culture on day 14, and the entire medium was replaced by gfCDM (supplemented with insulin and FGF19) on day 18. From day 21 onwards, the aggregates were cultured in Neurobasal medium (Life Technologies) supplemented with GlutaMax I (Life Technologies), N2 supplement (Life Technologies), and PS. The entire medium was then replaced weekly. Recombinant human SDF1 (300ng/ml, PeproTech) was added to culture on day 28 (**Figure II.4**).

Maturation of cerebellar neurons

On day 35 of differentiation, aggregates were dissociated using accutase (Sigma) and re-plated on wells coated with poly-L-ornithine (15µg/mL, Sigma) and Laminin (20µg/mL, Sigma), at a seeding density between 20,000 – 200,000 cells/cm^2. Both floating and re-plated aggregates were cultured in BrainPhys™ Neuronal Medium (StemCell Technologies), supplemented with NeuroCult™ SM1 Neuronal Supplement (StemCell Technologies), N2 Supplement-A (StemCell Technologies), Recombinant Human Brain Derived Neurotrophic Factor (BDNF, PeproTech, 20ng/mL), Recombinant Human Glial-Derived Neurotrophic Factor (GDNF, PeproTech, 20ng/mL), dibutyryl cAMP (1mM, Sigma), and ascorbic acid (200nM, Sigma). One-third of the total volume was replaced at every 2–3 days.

Organoid size analysis

To monitor organoid sizes throughout time in culture, several images were acquired at different time-points using a Leica DMI 3000B microscope with a Nikon DXM 1200F digital

camera. The organoid diameter was calculated based on determined area using the Mathworks computer tool (MATLAB), as described (Miranda et al., 2015).

Tissue preparation and Immunostaining

Organoids were fixed in 4% paraformaldehyde (PFA, Sigma) for 20 min at 4 ºC followed by washing in Phosphate buffered saline (PBS, 0.1M) and overnight incubation in 15% sucrose at 4 ºC. Organoids were embedded in 7.5% gelatin/15% sucrose and frozen in isopenthane at -80 ºC. Sections (approximately 12µm thick) were cut on a cryostat-microtome (Leica CM3050S, Leica Microsystems), collected on Superfrost™ Microscope Slides (Thermo Scientific), and stored at -20 ºC. Sections were de-gelatinized for 45 min in PBS at 37 ºC before being submitted to immunohistochemistry.

For immunostaining, sections and cells plated on coverslips were incubated in 0.1 M Glycine (Millipore) for 10 min at room temperature (RT), permeabilized with 0.1% Triton X-100 (Sigma) for 10 min at RT, and blocked with 10% fetal goat serum (FGS, Life Technologies) in TBST (20mM Tris-HCl pH 8.0, 150mM NaCl, 0.05% Tween-20, Sigma) for 30 min at RT. Next, they were incubated overnight at 4 ºC with the primary antibodies (**Table II.1**) diluted in blocking solution. Secondary antibodies were added to sections for 30 min (goat anti-mouse or goat anti-rabbit IgG, Alexa Fluor®–488 or –546, 1:400 v/v dilution, Molecular Probes) at RT and nuclear counterstaining was performed using 4',6-diamidino-2-phenylindole (DAPI, 1.5µg/mL; Sigma). For phalloidin staining, cells were incubated with Alexa Fluor® 488 Phalloidin (1:40 in PBS, Life Technologies). After brief drying, sections and coverslips were mounted in Mowiol (Sigma). Fluorescence images were acquired with Zeiss LSM 710 or Zeiss LSM 880 Confocal Laser Point-Scanning Microscopes.

Table II-1. List of primary antibodies and dilutions used for immunostaining

Antibody	Company	Host species	Dilution
BARHL1	Atlas	rabbit	1:500
CALBINDIN	Swant	rabbit	1:500
CORL2	Atlas	rabbit	1:100
GAD65	BD Pharmingen	mouse	1:100
MAP2	Sigma	mouse	1:1000
N-CADHERIN	BD Transduction	mouse	1:1000
NESTIN	R&D	mouse	1:400
NEUROGRANIN	Millipore	rabbit	1:200
PARVALBUMIN	Sigma	mouse	1:200
PAX6	Covance	rabbit	1:400
SOX2	R&D	mouse	1:200
TBR1	Millipore	rabbit	1:200
TUJ1	Biolegend	mouse	1:1000
V-GLUT1	Abcam	rabbit	1:100

Quantitative real time (qRT)-PCR

Total RNA was extracted at different time-points of differentiation using High Pure RNA Isolation Kit (Roche) and converted into complementary cDNA with Transcriptor High Fidelity cDNA Synthesis Kit (Roche). Taqman® Gene Expression Assays (20X, Applied Biosystems) were selected for *NANOG* (HS02387400-g1), *OCT4* (HS00999634-sh), *PAX6* (HS00240871-m1), *SOX1* (HS01057642-s1), *EN2* (Hs00171321_m1), *KIRREL2* (Hs00375638_m1), and *GAPDH* (HS02758991-g1). *ATOH1*, *BARHL1*, *FGF8*, *GAD65*, *GRID2*, *NESTIN*, *NEUROGRANIN*, *OLIG2*, *OTX2*, *PARVALBUMIN*, *PAX2*, *TBR1*, and *V-GLUT1* were analyzed using SYBR® green chemistry (**Table II.2**). All PCR reactions were done in duplicate or triplicate, using the StepOneTM or ViiA™ 7 RT-PCR Systems (Applied BioSystems). Reactions were normalized to the housekeeping gene GAPDH and results were analyzed with StepOne™ or QuantStudio™ RT-PCR Software. Relative expression values were used for ClustVis analysis, an in silico tool that clustered different conditions that have similar gene expression at different time points (Metsalu and Vilo, 2015).

Table II-2. Primers used for qRT-PCR

Gene	Forward	Reverse
ATOH1	TGTTATCCCGTCGTTCAACAAC	TGGGCGTTTGTAGCAGCTC
BARHL1	GAGCGGCAGAAGTACCTGAG	GTAGAAATAAGGCGACGGGAAC
CALBINDIN	AGTGGTTACCTGGAAGGAAAGG	AGCAGGAAATTCTCTTCTGTGG
CORL2	CCAGGTGTTAAAAGGAAACACA	GCTCCCTTTTCATCTGATCCT
FGF8	GAGCCTGGTGACGGATCAG	CGTTGCTCTTGGCGATCAG
GAD65	GTCTCCAGCTCGCATACACA	CGAAAGACCAAAAGCCAGAG
GRID2	AGCTCTTCCTCTCTTGGTTTCC	GCCCCACGTTGCCTAGAAAT
NESTIN	GAAACAGCCATAGAGGGCAAA	TGGTTTTCCAGAGTCTTCAGTGA

NEUROGRANIN	TCAAAGTTCCCGAGGAGAGA	CTAAAAGGGCACGGACTCAG
OLIG2	GACAAGCTAGGAGGCAGTGG	CGGCTCTGTCATTTGCTTCTTG
OTX2	AGAGGACGACGTTCACTCG	TCGGGCAAGTTGATTTTCAGT
PARVALBUMIN	TTCTCCCCAGATGCCAGAGA	GAGATTGGGTGTTCAGGGCA
PAX2	AACGACAGAACCCGACTATGT	GAGCGAGGAATCCCCAGGA
TBR1	CGTCTGCAGCGAATAAGTGC	AATGTGGAGGCCGAGACTTG
VGLUT1	TACACGGCTCCTTTTTCTGG	CTGAGGGGATCAGCATGTTT

Flow cytometry

Eppendorf tubes were coated with 1% v/v bovine serum albumin (BSA; Life Technologies) solution in PBS for 15 min. Samples previously stored in 2% PFA (Sigma) were centrifuged at 1000 rpm for 5 min and washed twice with PBS. For surface staining, cells were resuspended in primary antibody diluted in FACS buffer, at approximately 500,000 cells per condition, and incubated for 30 min at RT. Afterwards, cells were washed with PBS and resuspended in FACS buffer and incubated with secondary antibodies for another 15 min, at room temperature. Finally, cells were washed twice with PBS and resuspended in PBS, for flow cytometry analysis (FACSCalibur, Becton Dickinson). For intracellular staining, cells were then resuspended in 3% normal goat serum (NGS, Sigma), at 0.5–1x10^6 cells per condition. The cell suspension was centrifuged once again at 1000 rpm for 3 min. The cell membrane was then permeabilized using a solution 1:1 of 3% NGS and 1% saponin (Sigma) for 15 min, at RT. After washing three times with 1% NGS, cells were resuspended in primary antibody solution (in 3% NGS) and incubated for 1.5h at room temperature. Cells were then washed three times with 1% NGS, and incubated for 45 min in the dark with the secondary antibody (in 3% NGS). Finally, after another washing step, cells were resuspended in PBS and analyzed in the flow cytometer (Becton Dickinson).

Antibodies used for flow cytometry were: Tra-1-60-PE (Miltenyi Biotec, 1:50), SEEA-4-PE (Miltenyi Biotec, 1:10), SOX2 (Sigma, 1:150), OCT4 (Invitrogen, 1:300), NANOG (Millipore, 1:300), and KIRREL2 (R&D Systems, 1:50). Secondary antibodies included goat anti-mouse and anti-rabbit IgG Alexa Fluor – 488 (Invitrogen, 1:300), and anti-mouse IgG-PE (1:300, Miltenyi Biotec), all used as negative control for their tested counterpart.

Single cell calcium imaging

For single cell calcium imaging, organoids were dissociated using accutase (Sigma) and re-plated on glass bottom microwell chambers previously coated with poly-D-lysine (MatTek) and Laminin (20µg/mL, Sigma), at a seeding density of 80 000 cells/cm2. At different time-points of differentiation, dissociated cells were loaded with 5µM Fura-2 AM (Invitrogen) in Krebs solution (132mM NaCl, 4mM KCl, 1.4mM MgCl2, 2.5mM CaCl2, 6mM glucose, 10mM HEPES, pH 7.4) for 45 min at 37 ºC in an incubator with 5% CO2 and 95% atmospheric air. Dishes were washed in Krebs solution and then mounted on an inverted microscope with epifluorescence optics (Axiovert 135TV, Zeiss). Cells were continuously perfused with Krebs solution and stimulated by applying high-potassium Krebs solution (containing 10-100mM KCl, isosmotic substitution with NaCl), 2µM ionomycin, or 100µM histamine. Ratio images were obtained from image pairs acquired every 200ms by exciting the cells at 340nm and 380nm. Excitation wavelengths were changed through a high-speed switcher (Lambda DG4, Sutter Instrument, Novato, CA, United States). The emission fluorescence was recorded at 510nm by a cooled CDD camera (Photometrics CoolSNAP fx). Images were processed and analyzed using the software MetaFluor (Universal Imaging, West Chester, PA, United States). Regions of interest were defined manually.

Dendritic spine classification

After phalloidin-staining, cell images were acquired using Zeiss LSM 880 Confocal Laser Point-Scanning Microscopes. Representative images were used to measure dendritic spine head width and neck length using ImageJ software.

Patch-clamp recordings

Whole-cell patch-clamp recordings were obtained from generated cerebellar neurons visualized with an upright microscope (Zeiss Axioskop 2FS) equipped with differential interference contrast optics using a Zeiss AxioCam MRm camera and an x40 IR-Achroplan objective. During recordings, cells were continuously superfused with artificial cerebrospinal fluid (aCSF) containing124mM NaCl, 3 mM KCl, 1.2 mM NaH_2PO_4, 25 mM $NaHCO_3$, 2 mM $CaCl_2$, 1 mM $MgSO_4$, and 10 mM glucose, which was continuously gassed with 95%O_2/5% CO_2. Recordings were performed at room temperature in current-clamp or voltage-clamp mode [holding potential (Vh) = −60 mV] with an Axopatch 200B (Axon Instruments) amplifier, as performed elsewhere (Felix-Oliveira et al., 2014). Synaptic currents and action potential activity were recorded using patch pipettes with 4 to 7 MΩ resistance filled with an internal solution containing 125 mM K-gluconate, 11 mM KCl, 0.1 mM $CaCl_2$, 2 mM $MgCl_2$, 1mM EGTA, 10 mM HEPES, 2mM MgATP, 0.3mM NaGTP, and 10mM phosphocreatine, pH 7.3, adjusted with 1 M NaOH, 280-290 mOsm. Acquired signals were filtered using an in-built, 2-kHz, three-pole Bessel filter, and data were digitized at 5 kHz under control of the pCLAMP 10 software program. The junction potential was not compensated for, and offset potentials were nulled before gigaseal formation. The resting membrane potential was measured immediately upon establishing whole-cell configuration. Spontaneous miniature postsynaptic currents were recorded in aCSF solution for 5 minutes. After this period, the sCSF solution was supplemented with 500nM TTX (tetrodotoxin, a voltage-dependent

sodium channel blocker), 5µM CNQX (6-cano-7-nitroquinoxaline-2, 3-dione, a glutamate AMPA receptor antagonist), and 50µM DL-APV (DL-(−)-2-amino-5-phosphonopentanoic acid, a glutamate NMDA receptor antagonist), for the specific recording of miniature inhibitory post-synaptic currents, mIPSCs (Rombo et al., 2016). To silence mIPSCs and confirm their GABAergic nature, 10µM bicuculline (a $GABA_A$ receptor antagonist) was used at the end of the recording. Analysis was performed off line using the spontaneous event detection parameters of the Synaptosoft Minianalysis software, the amplitude threshold for event detection being set at 3x the average root-mean-square noise.

II.4 RESULTS

Generation of controlled-size aggregates and size characterization of iPSC-derived organoids

The ability to recapitulate aspects of human developmental processes *in vitro* using hPSCs have been largely studied in the last few years (Ungrin et al., 2008). Mimicking the embryonic development *in vitro* requires that appropriate spatial, temporal and mechanical cues are provided to assure correct differentiation in functional hPSC-derived progenitors. For recapitulating some of the *in vivo* developmental cues, many differentiation protocols using hPSCs begin by promoting cell aggregation in 3D aggregates (Bauwens et al., 2008; Peerani et al., 2007). Thus, we first focused on establishing optimal initial conditions to obtain a homogeneous population of aggregates from different iPSC lines, which then could be differentiated into cerebellar organoids. Since aggregates size is a significant parameter influencing the differentiation towards specific cell lineages (Bratt-Leal et al., 2009), we controlled the initial cell number per aggregate by promoting the iPSC aggregation in microwell plates (Miranda et al., 2015). Size-controlled aggregates were obtained by plating 6 000 cells per microwell, as shown in **Figure II.2**.

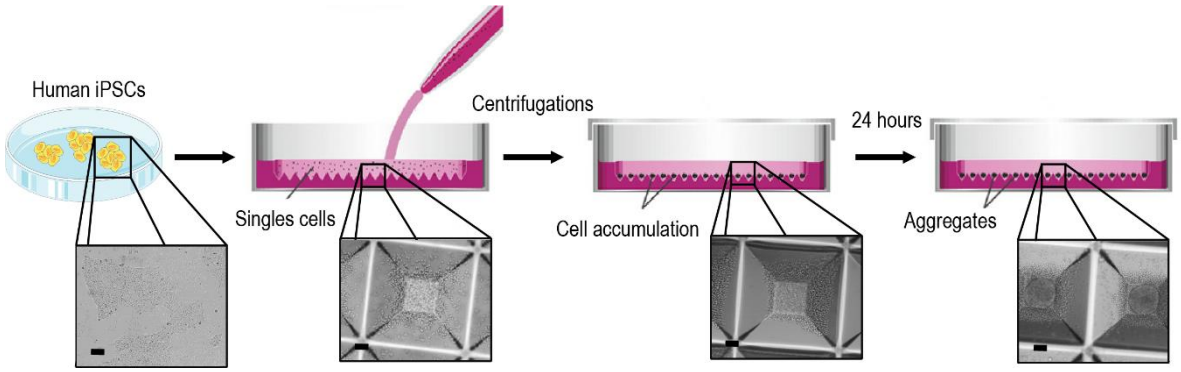

Figure II.2. Schematic representation of a controlled iPSC aggregation at day 0 using Aggrewell^{TM}800 plates. Cells were seeded at concentration of 6 000 cells per microwell and aggregated by centrifugation. After 24 hours, aggregates with homogeneous size were observed. Scale bar, 100 µm. Adapted from (Dahlmann et al., 2013).

Aggregates exhibited homogeneous size and shape when they were maintained in the microwell plates until day 8 after initiating the differentiation. After being transferred from the microwells to low-attachment plates, organoids presented greater variability in both size and shape (**Figure II.3-A**). For evaluating the organoids size distribution along the differentiation protocol, an assessment of the organoids diameter was performed at different time points of culture. The culture displays an increase of aggregate diameter along time by using different iPSC lines (**Figure II.3-B**). The relative frequencies of measured diameters on day 8 presents well-defined distribution, becoming more heterogeneous along time, with widespread distribution on day 35. This means that, while at day 8 most aggregates have approximately the same diameter range, on day 35 several “subsets” of organoids can be identified, thus an increasing of organoids diameter variability during time in culture can be observed (**Figure II.3-C**).

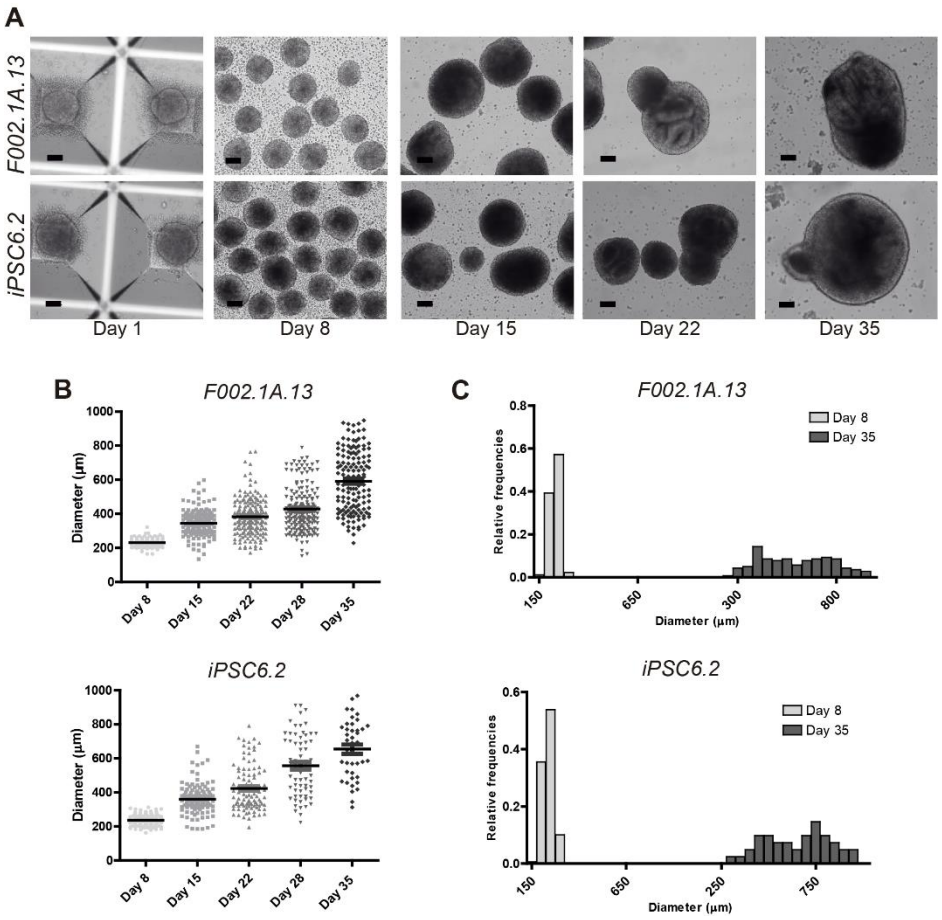

Figure II.3. Generation of 3D organoids derived from human iPSCs. A) Bright field photomicrograph showing floating aggregates during cerebellar differentiation. Scale bar, 100 µm. **B)** The diameter of floating aggregates was estimated at the indicated time-points. **C)** Distribution of floating aggregate diameters was determined at the indicated time-points.

Induction of cerebellar differentiation in human iPSCs-derived 3D organoids

To generate cerebellar progenitors, human iPSCs were induced to spontaneously self-assemble in suspension culture. Cells were cultured in chemically defined medium and fibroblast growth factor 2 (FGF2), insulin, transforming growth factor β-receptor blocker SB431542, fibroblast growth factor 19 (FGF19), and stromal cell-derived factor 1 (SDF1) were added sequentially, as previously described (Muguruma et al., 2015). On day 2, the

mTESR1 medium was replaced with gfCDM and then with neurobasal medium on day 21 (**Figure II.4**).

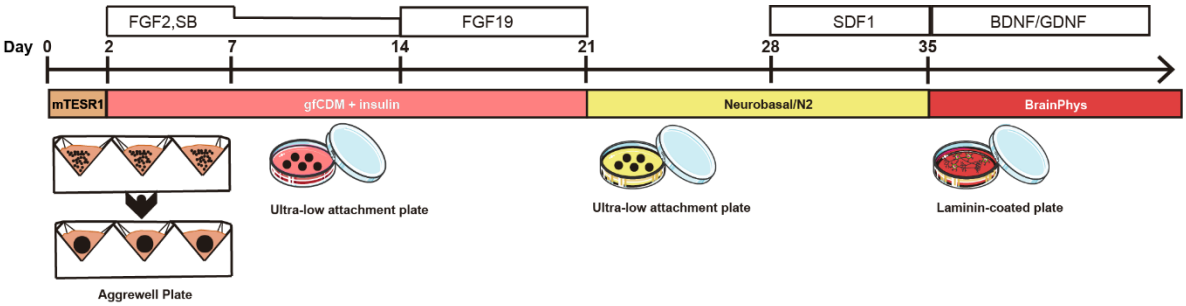

Figure II.4. Schematics illustrating the culture procedure to induce differentiation of iPSCs to cerebellar progenitors. F002.1A.13 and iPSC6.2 cells were induced to aggregate and develop into 3D organoids. On day 2, fibroblast growth factor 2 (FGF2), insulin, and transforming growth factor β-receptor blocker SB431542 were added. Starting on day 14 until day 21, fibroblast growth factor 19 (FGF19) was added to the culture. Lastly, stromal cell-derived factor 1 (SDF1) was added on day 28 until day 35. After day 35, maturation of cerebellar progenitors was promoted by using BrainPhys™ supplemented with BDNF and GDNF.

Schematics illustrating the culture procedure to induce differentiation of iPSCs to cerebellar progenitors. F002.1A.13 and iPSC6.2 cells were induced to aggregate and develop into 3D organoids. On day 2, fibroblast growth factor 2 (FGF2), insulin, and transforming growth factor β-receptor blocker SB431542 were added. Starting on day 14 until day 21, fibroblast growth factor 19 (FGF19) was added to the culture. Lastly, stromal cell-derived factor 1 (SDF1) was added on day 28 until day 35. After day 35, maturation of cerebellar progenitors was promoted by using BrainPhys™ supplemented with BDNF and GDNF.

As expected, on day zero of differentiation human iPSCs expressed the pluripotency and self-renewal genes *OCT4* and *NANOG* (**Figure II.5-A**). By day 7, their mRNA levels were significantly reduced whereas by day 14 they were almost undetectable, indicating that cells were committed to differentiate. Starting on day 7 and going onwards until day 35,

organoids progressively expressed higher mRNA levels of the neural stem cell markers *SOX1* and *NESTIN* (**Figure II.5-B**). Immunofluorescence analysis further revealed that most cells within the aggregates expressed NESTIN and detected small neural rosettes structures staining for PAX6 and SOX2 (**Figure II.5-C**). Besides that, cell expressing TUJ1 were detected on the organoid surface, basally to neural rosettes (**Figure II.5-C**). Altogether these results support the neural commitment of the iPSC-derived organoids.

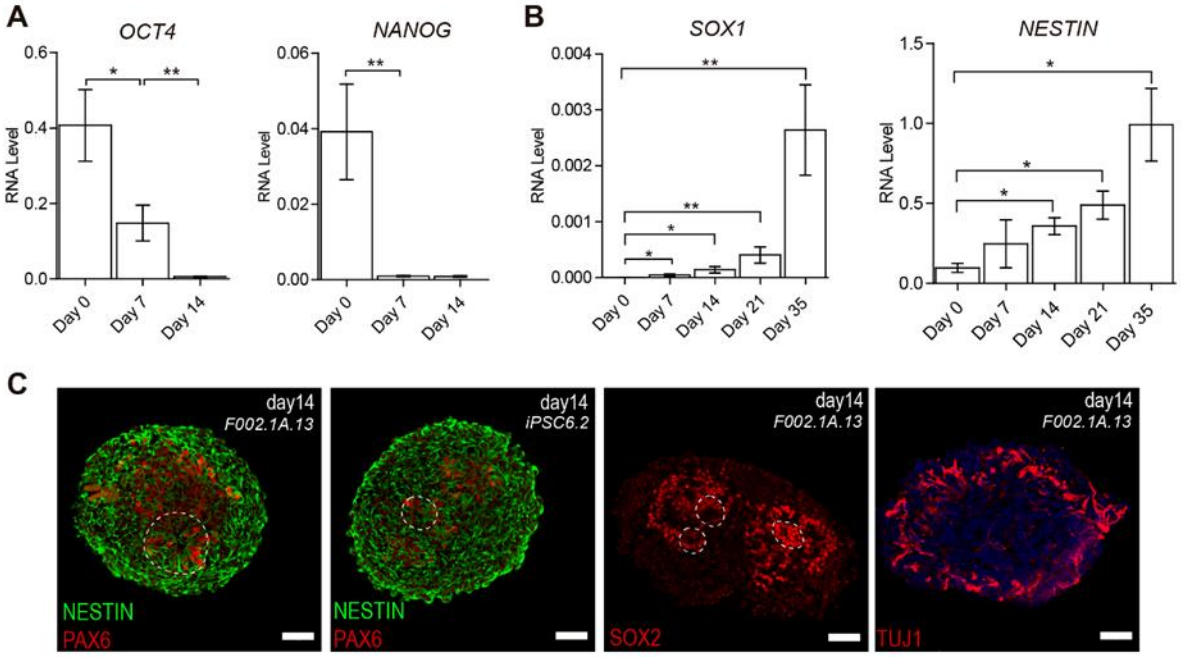

Figure II.5. Efficient neural induction in iPSC-derived organois. qRT-PCR analysis of *NANOG* and *OCT*4 (**A**), *SOX1* and *NESTIN* (**B**) mRNA levels relative to *GAPDH* levels at different time-points. For all graphics depicted, data were obtained from 5 independent differentiation experiments using F002.1A.13 cells. Student´s t-test (two-tailed) statistics, * p<0.05, ** p<0.01; error bars represent SEM. **C)** Immunofluorescence for NESTIN, PAX6, SOX2 and TUJ1 on day 14 of differentiation (scale bar, 50µm).

As shown in **Figure II.6**, RNA levels of *FGF8*, a gene encoding a signaling protein required for early cerebellum development (Chi et al., 2003), is at its highest on day 7 of differentiation and then declines thereafter. **Figure II.6** shows a significant increase in the mRNA levels of *OTX2* (a homeobox gene required for cerebellum development and which

is inhibited by FGF8, Frantz et al., 1994; Larsen et al., 2010) on day 35. As expected, *OTX2* levels increase only after *FGF8* mRNA has been significantly down-regulated (**Figure II.6**). On days 14 through 35, we also detected the expression of *EN2* (**Figure II.6**), another homeobox gene required to generate a fully functional cerebellum (Zec et al., 1997). Having established that iPSCs-derived organoids were expressing critical genes required for early cerebellum morphogenesis, we next focused on detecting specific cerebellar progenitors. Starting on day 14 (and increasing onwards), we detected significantly higher levels of *PAX6* mRNA (**Figure II.6**), which is an essential transcription factor for the development of all cerebellar glutamatergic neurons (Yeung et al., 2016).

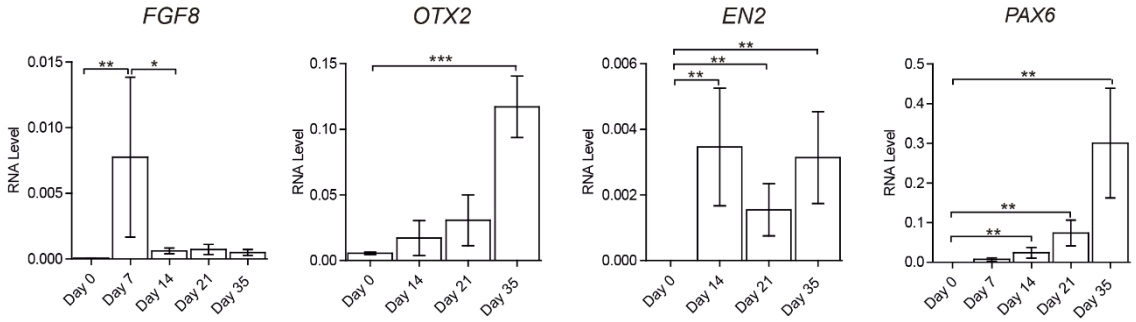

Figure II.6. Efficient cerebellar commitment in iPSC-derived organoids. qRT-PCR analysis of *FGF8, OTX2, EN2* and *PAX6* mRNA levels relative to *GAPDH* levels at the indicated time-points. For all graphics depicted, data were obtained from 5 independent differentiation experiments using F002.1A.13 cells. Student´s t-test (two-tailed) statistics, * p<0.05, ** p<0.01, *** p<0.001; error bars represent SEM.

As **Figure II.7-A** shows, the expression levels of *KIRREL2*, which is a cell adhesion molecule found on the surface of cerebellar GABAergic progenitors, including Purkinje cell precursors (Mizuhara et al., 2010), significantly and progressively increased starting on day 14. The fact that KIRREL2 is found on the cell surface allowed us to do flow cytometry analysis. The results show that on day 35, 87% and 37% of cells in F002.1A.13 and iPSC6.2-derived organoids corresponded to GABAergic progenitors (**Figure II.7-B**).

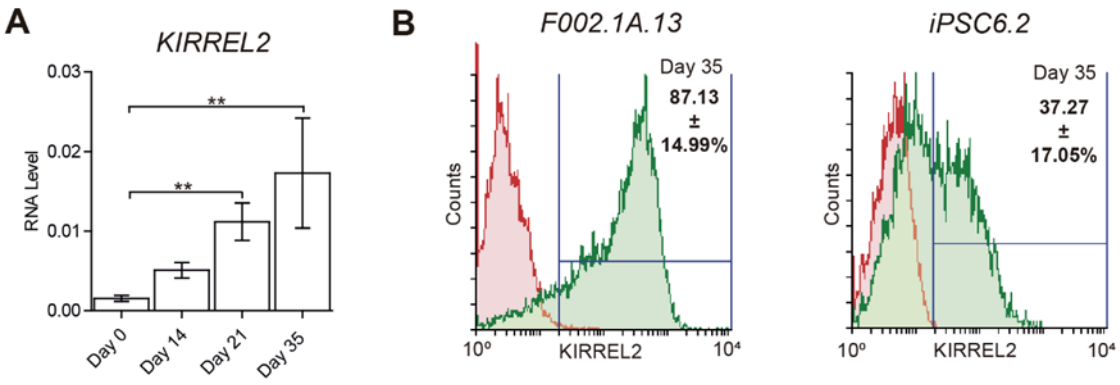

Figure II.7. Generation of GABAergic progenitors. A) qRT-PCR analysis of *KIRREL2* mRNA levels relative to *GAPDH* levels at the indicated time-points. For all graphics depicted, data were obtained from 5 independent differentiation experiments using F002.1A.13 cells. Student´s t-test (two-tailed) statistics, * $p<0.05$, ** $p<0.01$; error bars represent SEM. **B)** Flow cytometry analysis of KIRREL2^{+} cells on day 35. Estimates of the proportion of KIRREL2+ cells were based on 2 independent differentiation experiments.

Cerebellar progenitors in 3D organoids self-organize into polarized neuroepithelium

On day 21, organoids derived from both human iPSC lines displayed characteristic hollow structures with a radial organization (neural rosettes) reminiscent of the neural tube. These structures showed apical-basal polarity, with the apical side surrounded by a strong signal of N-cadherin (**Figure II.8-A**). Furthermore, iPSC-derived organoids exhibited most of cells expressing NESTIN and PAX6, essential to further neuronal and cerebellar development (Lendahl et al., 1990; Yeung et al., 2016), and TUJ1 on the basal surface, staining new born immature neurons (Von Bohlen Und Halbach, 2007) (**Figure II.8-A**).

Polarized neuroepithelial structures were more prominent on day 35, with proliferating cerebellar progenitors expressing PAX6 and SOX2 on the apical (luminal) side, confirmed by presence of cells in metaphase stage during the mitotic phase, and more mature post-mitotic neurons on the basal side (**Figure II.8-B**). Cells located in the basal compartment expressed neuron-specific class III beta-tubulin TUJ1, early markers for granule, BARHL1,

and Purkinje cells, OLIG2 and CORL2, and the marker for maturing GABAergic neurons GAD65 (**Figure II.8-B**).

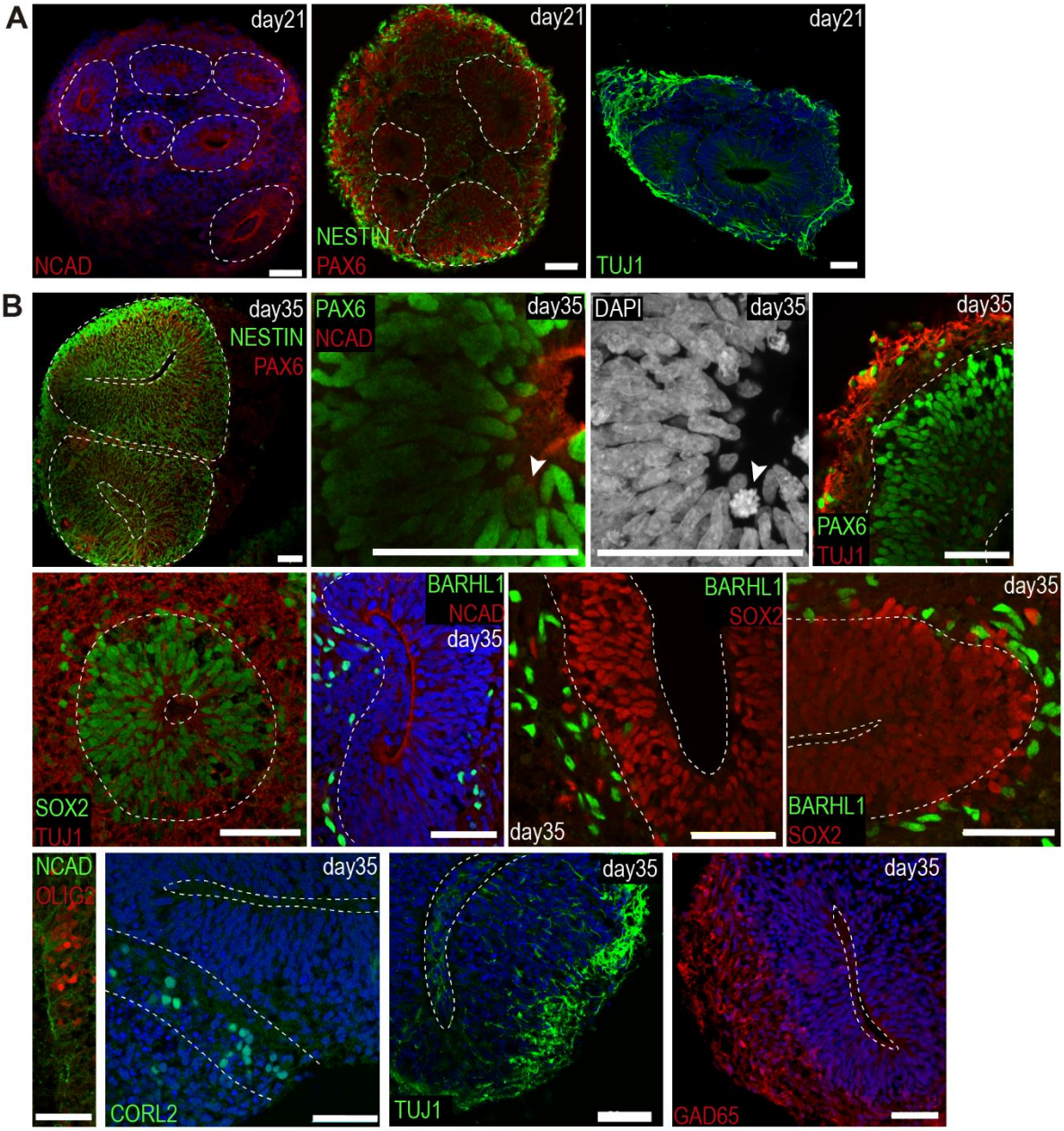

Figure II.8. Cerebellar progenitors self-organize into neural-tube-like structures. A) Immunofluorescence on day 21 of differentiation (F002.1A.13 cells) for indicated proteins. Nuclei are stained with DAPI. Neural rosettes are delineated by white dashes. **B)** Immunofluorescence of proteins (as indicated for each image) on day 35 of differentiation (F002.1A.13 cells). Different zones are delineated by white dashes. White arrowhead demonstrate a cell in metaphase present in the proliferating layer. Scale bars, 50µm.

High expression of specific markers for different types of cerebellar neurons was further detected by qRT-PCR analysis of organoids on day 35 (**Figure II.9**). These markers were: *BARHL1*, *CORL2*, *OLIG2*, *GAD65*, the transcription factors *ATOH1* (required for the differentiation of cerebellar granule neurons), *PAX2* (expressed in cerebellar interneurons), and *TBR1* (expressed in deep cerebellar nuclei).

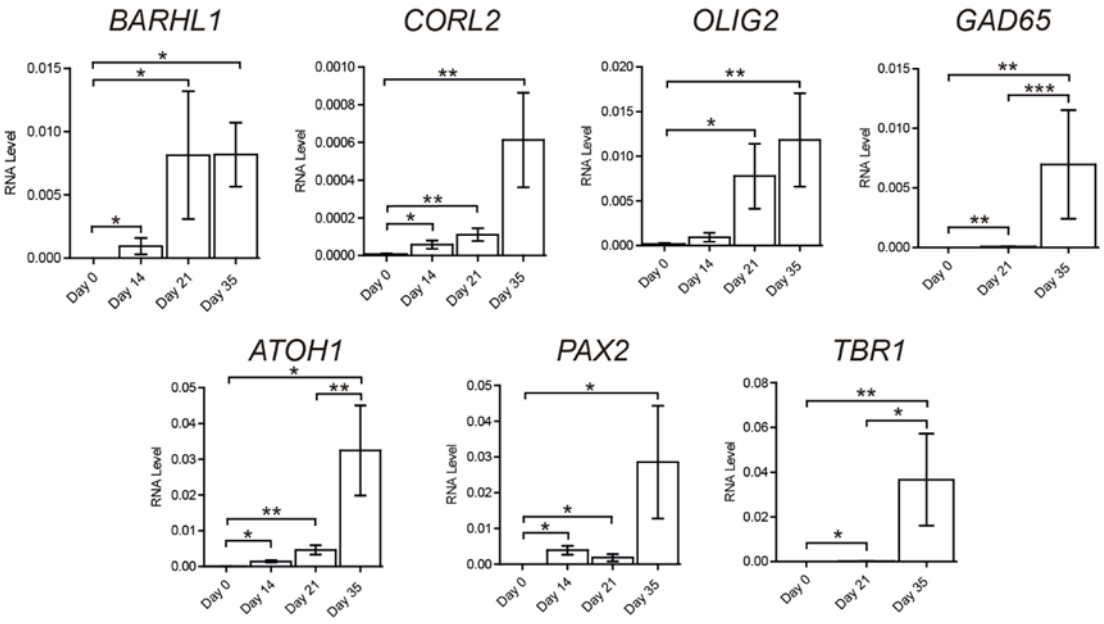

Figure II.9. Efficient cerebellar differentiation. mRNA levels relative to *GAPDH* levels at the indicated time-points. Data based on five independent differentiation experiments using F002.1A.13 cells. Student´s t-test (two-tailed) statistics, * p<0.05, ** p<0.01; error bars represent SEM.

Cerebellar neurons undergo maturation in feeder-free culture

To promote further maturation of cerebellar neurons, organoids were dissociated on day 35. Cells were then transferred to laminin-coated plates and cultured in serum-free BrainPhys™ medium (Bardy et al., 2015) supplemented with BDNF and GDNF. On day 56 of differentiation (21 days after organoid dissociation and re-plating), cultures derived from

the iPSC6.2 cell line already contained a dense meshwork of neurons expressing either the GABAergic marker GAD65 or the glutamatergic marker VGLUT1 (**Figure II.10-A**). On day 81, *GAD65* and *VGLUT1* RNA levels were both significantly increased (**Figure II.10-B**).

Because the morphology of dendritic spines changes during neuronal maturation (Hering and Sheng, 2001; Risher et al., 2014), we measured spine head width and neck length as shown on representative images of our cultured neurons (**Figure II.10-C**). Dendritic spines were classified as follows: Filopodia (length > 2µm); Long thin (length < 2µm); Thin (length < 1µm); Stubby (length/width ratio < 1µm); Mushroom (width > 0.6µm), and Branched (2 or more heads), as previously described (Risher et al., 2014). As shown in Figure 2.10-C, the relative proportion of more mature branched spines increased from day 56 to day 81 of differentiation, indicating that neurons matured over time.

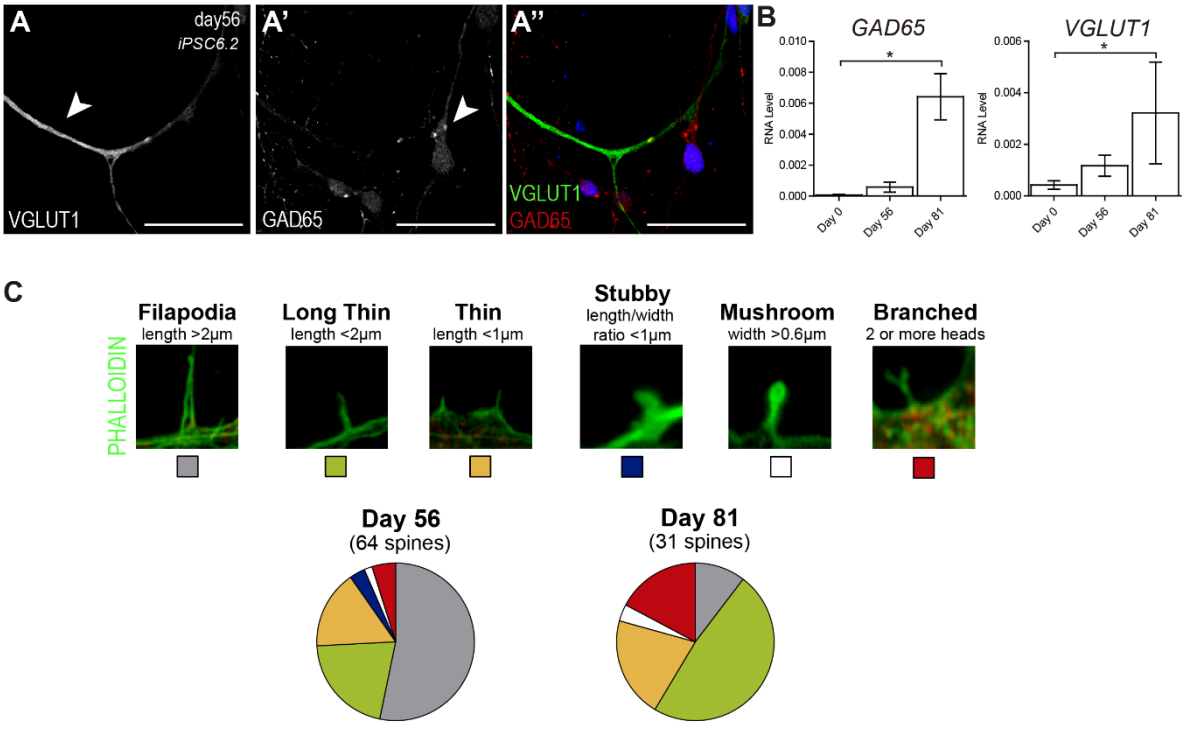

Figure II.10. Maturation of GABAergic and glutamatergic neurons. A) Immunofluorescence for V-GLUT1 and GAD65 in iPSC6.2-derived cultures on day 56 of differentiation (scale bars, 50µm). **B)** qRT-PCR analysis of *GAD65* and *V-GLUT* mRNA levels relative to *GAPDH* at the indicated time-points. Data were obtained from

four independent differentiation experiments using F002.1A.13 cells. Student´s t-test (two-tailed) statistics, * $p<0.05$; error bars represent SEM. **C)** Representative images of dendritic spine morphologies. The two pie-charts depict the relative proportion of the different dendritic spine morphologies observed on days 56 and 81 of differentiation.

Immunofluorescence analysis using an antibody to calbindin (CALB), a calcium-binding protein highly expressed in Purkinje cells, revealed multiple cells with the characteristic long axon and highly arborized dendrites with numerous, well-developed spines (**Figure II.11-A**). These cells were consistently observed in cultures differentiated from both iPSC6.2 and F002.1A.13 cell lines on days 81 through 145 (**Figure II.11-A**). Other neurons did not stain for CALB but were recognized by anti-parvalbumin antibodies (**Figure II.11-B**, red staining), indicating that they were likely the precursors of GABAergic interneurons. Another group of morphologically distinct neurons had their nucleus stained for PAX6 (**Figure II.11-C**) and BARHL1 (**Figure II.11-D**) suggesting that they were granule cell precursors. Other neurons were positive for neurogranin (**Figure II.11-E**), which is a marker of either Golgi cells or unipolar brush cells, depending on the species (Singec et al., 2004). Finally, anti-TBR1 antibodies identified precursors of deep cerebellar nuclei projection neurons (**Figure II.11-F**).

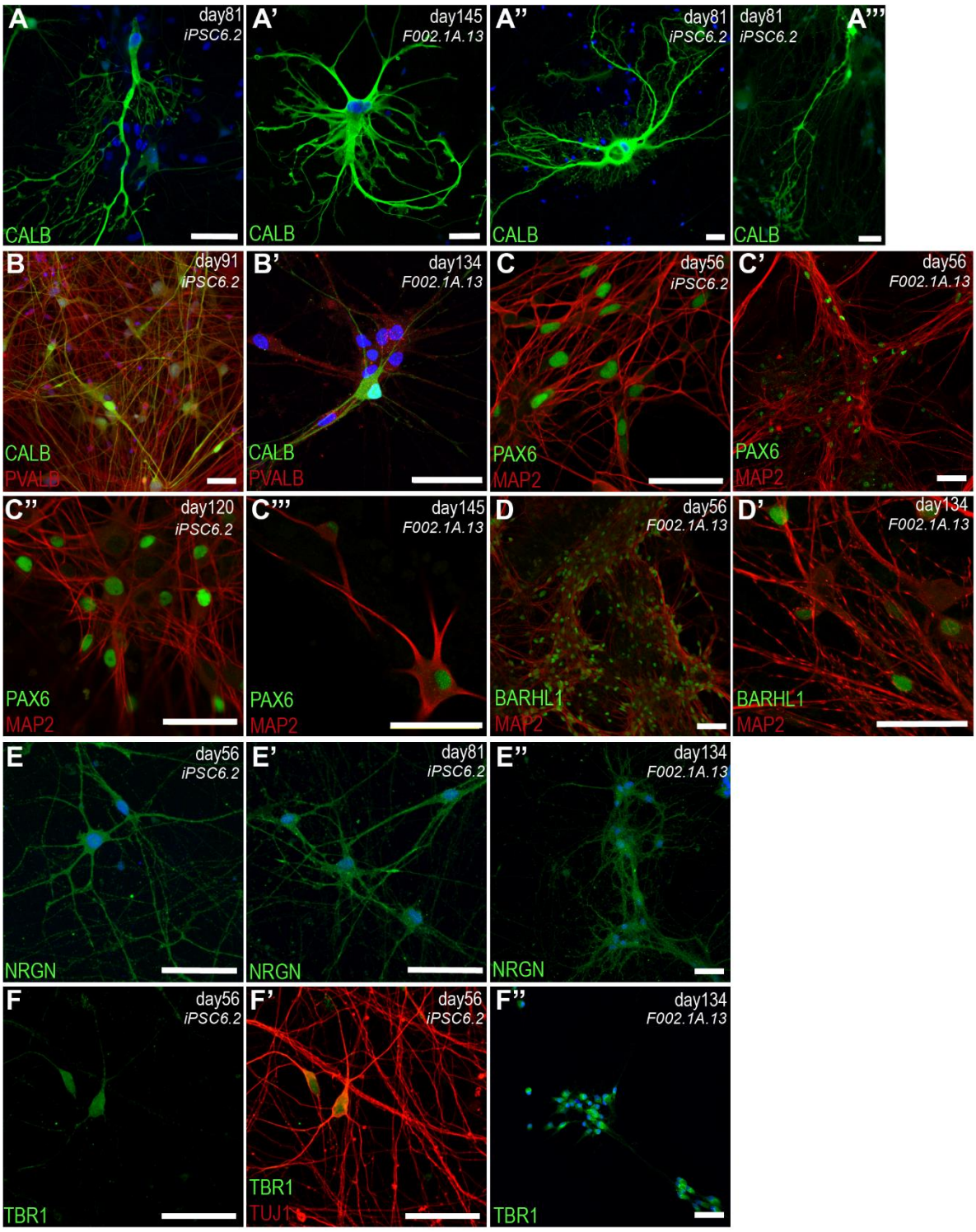

Figure II.11. Generation of distinct types of cerebellar neurons. Identification of distinct types of cerebellar neurons by immunofluorescence. Day of differentiation and the derived cell line are indicated at the top right of each image. **A)** Purkinje cells stained for calbindin (CALB) in the cytoplasm; nuclei stained by DAPI. **B)** GABAergic interneurons positive for parvalbumin (PVALB) and negative for calbindin; nuclei stained by DAPI.

Granule cells stained in the nucleus for PAX6 (**C**) or BARHL1 (**D**) and in the cytoplasm for MAP2. **E)** Golgi or unipolar brush cells positive for neurogranin (NRGN); nuclei stained by DAPI. **F)** Deep cerebellar nuclei projection neurons stained for TBR1 in the nucleus and TUJ1 in the cytoplasm. Scale bars, 50µm

Analysis of mRNA levels corresponding to transcription factors *PAX2*, *BARHL1*, and *TBR1* peaked on day 56 of differentiation and decreased thereafter, which is consistent with their temporally controlled expression during embryonic cerebellar development (Fink et al., 2006; Joyner, 1996; Li, 2004). In contrast, the levels of mRNAs encoding hallmark proteins of differentiated neurons kept increasing until day 81 (**Figure II.12**). These proteins included the glutamate ionotropic receptor *GRID2*, the calcium-binding protein *PVALB*, and the calmodulin-binding protein *NRGN*.

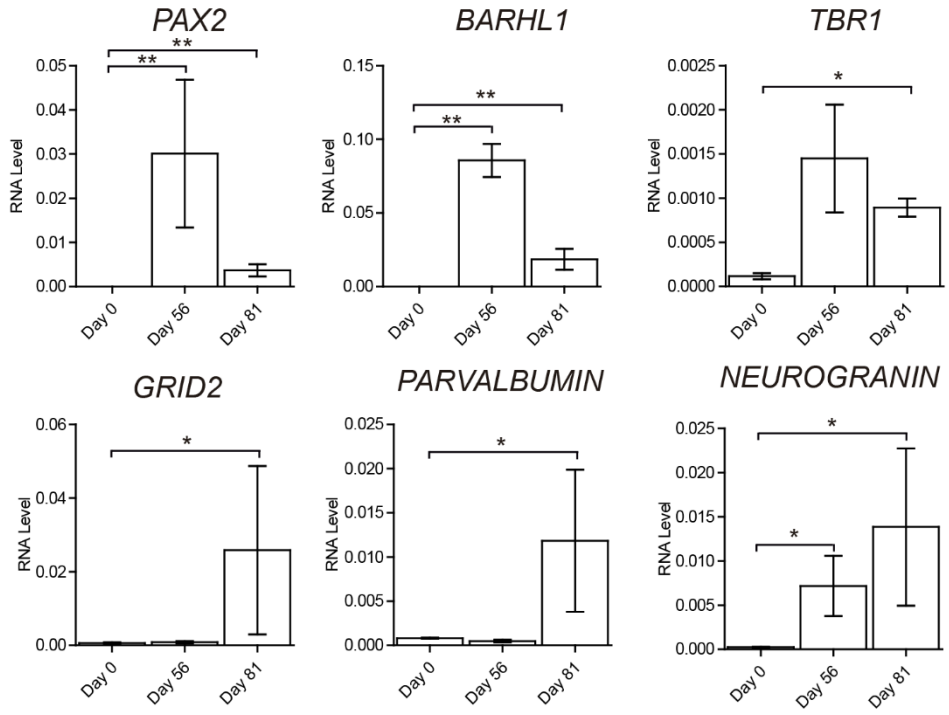

Figure II.12. Generation of distinct types of cerebellar neurons. qRT-PCR analysis of *PAX2*, *BARHL1*, *TBR1*, *GRID2*, *PARVALBUMIN*, and *NEUROGRANIN* mRNA levels relative to *GAPDH* at the indicated time-points. Data were obtained from four independent differentiation experiments using F002.1A.13 cells. Student´s t-test (two-tailed) statistics, * p<0.05, ** p<0.01; error bars represent SEM.

In order to assess the functionality of the cerebellar neurons, we next performed single cell calcium imaging. Cells were pre-loaded with the calcium indicator fluorescent dye Fura-2 that switches its excitation peak from 340nm to 380nm in response to calcium binding, allowing the concentration of intracellular calcium to be determined based on the ratio of fluorescence emission after sequential excitation at 340nm and 380nm (Grienberger and Konnerth, 2012). Cells were stimulated by exposure to KCl at different time-points. If cells were differentiated into excitable neurons, high KCl concentrations were expected to induce the opening of voltage sensitive calcium channels resulting in massive influx of calcium to the cytoplasm (Ambrósio et al., 2000; Macías et al., 2001). Elevations in cytosolic calcium concentration (visualized by increased fluorescence ratios) were indeed observed in cells cultured for 49 days (**Figure II.13**). These results confirm that excitable neurons formed in our human iPSC-derived cultures.

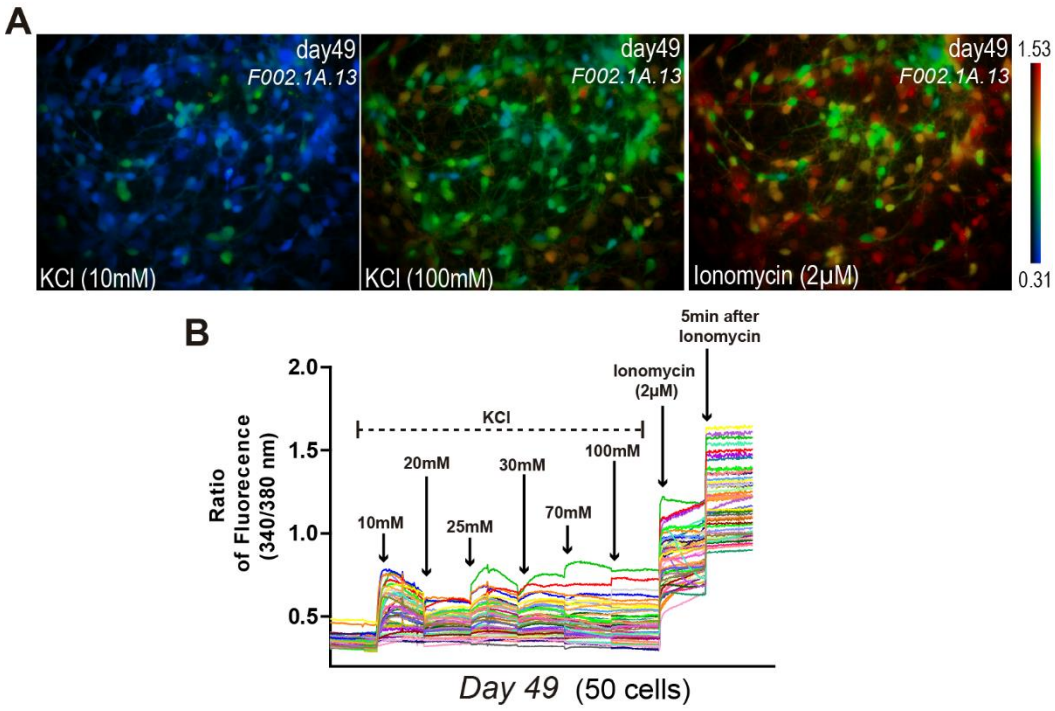

Figure II.13. Single cell calcium imaging. Representative ratio images (**A**) and fluorescence ratio profiles (**B**) of individual F002.1A.13-derived neurons on day 49. Images were taken immediately after cells received the indicated stimulus.

In contrast to mature neurons, neuronal progenitors express functional histamine receptors (Agasse et al., 2008; Molina-Hernández and Velasco, 2008; Rodríguez-Martínez et al., 2012). KCl depolarization causes an increase in calcium concentration in neurons, whereas stimulation with histamine leads to an increase in calcium concentration in stem/progenitor cells (Agasse et al., 2008; Rodrigues et al., 2017). We therefore measured variations in intracellular free calcium concentration following 50mM KCl and 100µM histamine stimulation to discriminate between immature cells and functional neurons in our cultures (**Figure II.14**).

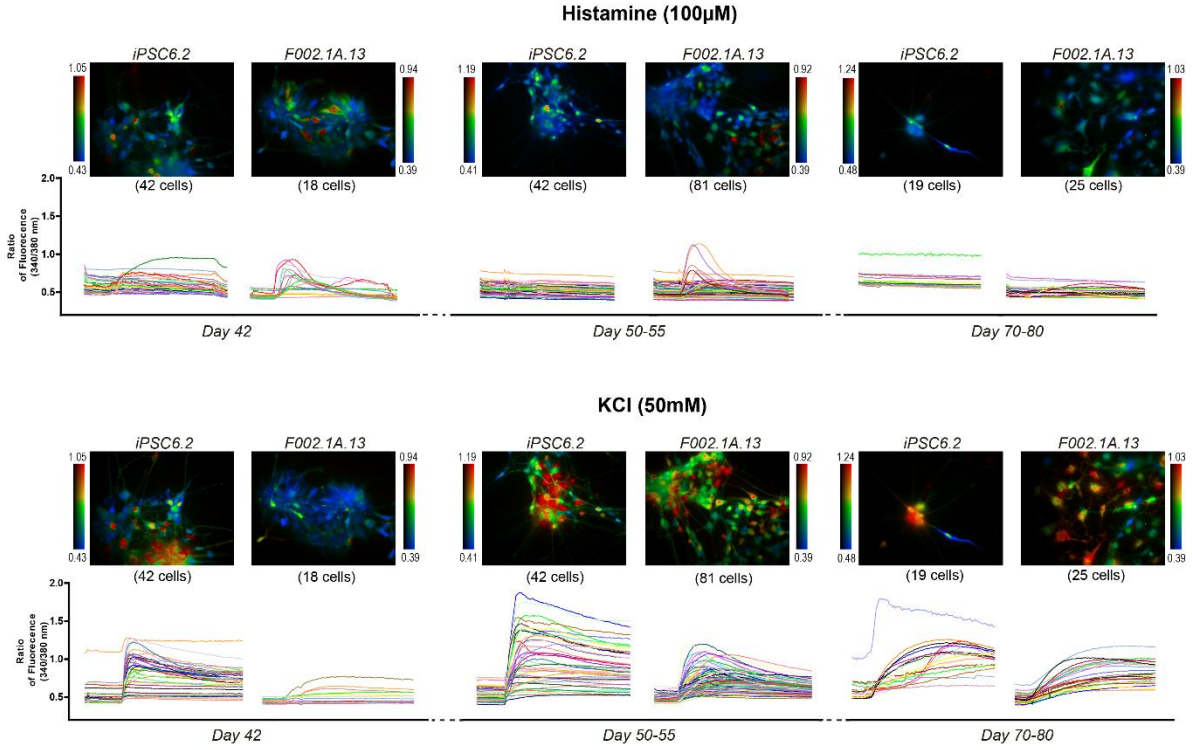

Figure II.14. Single cell calcium imaging. Representative ratio images and fluorescence ratio profiles after histamine and KCl stimulation of iPCS6.2- and F002.1A.13-derived neurons.

Histamine/KCl ratios were calculated using the corresponding peak values given by the normalized ratios of fluorescence at 340/380 nm. Mature neurons typically depict ratios below 0.8 whereas immature cells have ratios between 1 and 1.3 (Agasse et al., 2008;

Rodrigues et al., 2017). Quantification of the percentage of cells displaying a Histamine/KCl ratio below 0.8 showed that on day 42 of differentiation, the iPSC6.2-derived culture exhibited about 80% of mature neurons while the F002.1A.13-derived culture presented about 33% (**Figure II.15**). From day 50 of differentiation, a progress was observed in maturation of the F002.1A.13-derived culture, and by days 70–80 of culture most cells in either culture corresponded to mature neurons (**Figure II.15**).

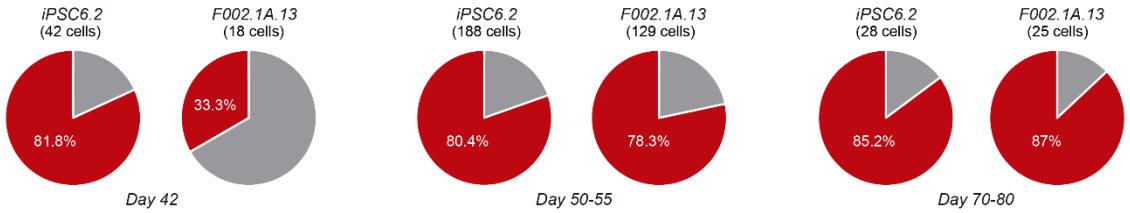

Figure II.15. Single cell calcium imaging. Percentage of cells displaying a Histamine/KCl ratio below 0.8 (red slices).

Finally, we evaluated the electrophysiological properties of differentiated cells by using whole-cell path clamp recordings. Cells analyzed on days 56 through 118 presented typical neuronal fire action potentials upon a current injection and were also able to depolarize, repolarize and recover, responding to a second current injection (**Figure II.16-A, B**). Most cells analyzed were spiking and showed high amplitude action potential (indicative of expression of voltage-dependent Na^+ channels) and reduced spike width (indicative of abundant K^+ channels), as expected for mature neurons. Furthermore, spontaneous currents were recorded, which indicates the presence of synaptic connections (**Figure II.16-C**). A subset of these currents remained in the presence of the sodium channel blocker TTX (indicative that they are independent of action potential generation) and of specific antagonists of ionotropic glutamate receptors, CNQX and DL-APV, suggestive of the existence of functional GABAergic synapses. Addition of the $GABA_A$ receptor antagonist

bicuculline completely abolished all activity (**Figure II.16-C, D**), confirming that the previously recorded miniature events indeed resulted from the spontaneous activity of GABAergic synapses. These data show that neurons in culture established functional connections, suggesting that a mature neuronal network had been created.

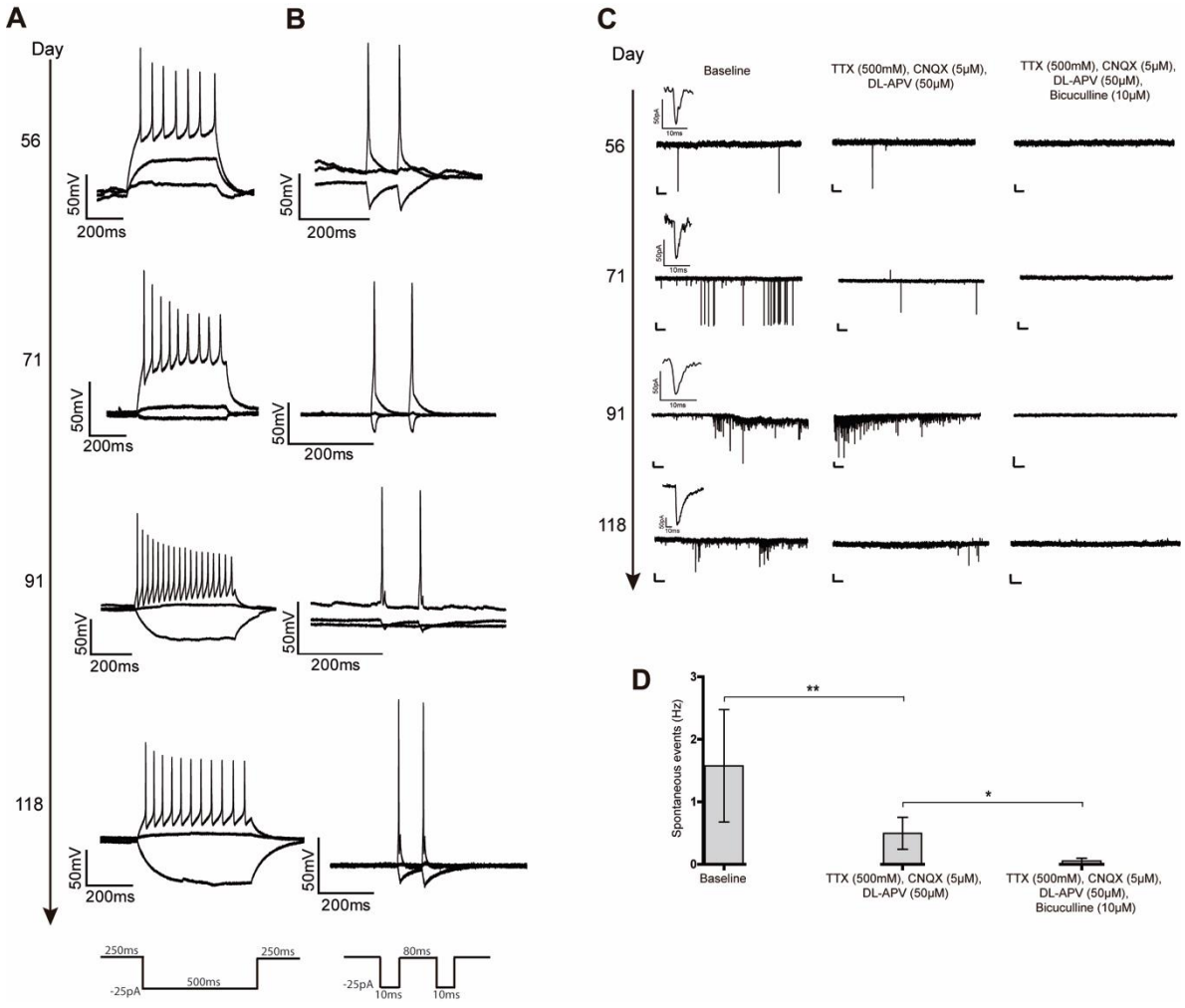

Figure II.16. Patch-clamp recordings. A-C) Whole-cell patch clamp recordings. **A)** Representative traces of firing responses evoked under current-clamp mode by injection of a 500ms current pulse (-25 to +275pA in 12.5- or 25pA increments) from an initial holding potential (Vh) of -70mV. **B)** Firing responses to two independent current injections (10ms) separated by 80ms. **C)** Representative traces of spontaneous postsynaptic currents recorded without any treatment (an example of a miniature postsynaptic current is also shown in each case; see figure), after blocking voltage dependent sodium channels using TTX and ionotropic glutamate receptors with CNQX and DL-APV (middle), and $GABA_A$ receptors with bicuculline (right). Recordings in each row are from the same cell at the indicated days in culture. Scale bars correspond to 50pA and 2000ms. **D)** Frequency of spontaneous events recorded without any treatment (baseline) and after addition of the indicated blockers. Data

from three independent differentiation experiments using iPCS6.2-derived cells. Student´s t-test (two-tailed) statistics, * $p<0.05$, ** $p<0.01$; error bars represent SEM.

3D Culture efficiently supports cerebellar maturation

An efficient maturation of cerebellar neurons was achieved after cerebellar organoids re-plating at day 35. Nevertheless, 3D culture systems seem to better mimic the biological cues when compared to 2D systems (Laschke and Menger, 2017). Therefore, we maintained organoids until day 91 of differentiation and promoted the cerebellar maturation using BrainPhys^{TM} medium supplemented with BDNF and GDNF, the same formulation used for re-plated cells. In this 3D culture system, an efficient generation of mature cerebellar neurons, including GABAergic (Purkinje cells) and glutamatergic (Granule cells) neurons, was observed. MAP2^{+} fibers was detected in mature neurons at days 81 and 91 (**Figure II.17-A**). Furthermore, immunofluorescence analysis revealed the presence of CALB, suggesting the presence of Purkinje cells (**Figure II.17-A**). Granule cells were also identified in cerebellar organoids, by co-localization of PAX6/BARHL1 and MAP2 (**Figure II.17-A**). On day 91, *GAD65* and *VGLUT1* mRNA levels, GABAergic and glutamatergic markers respectively, were both significantly increased (**Figure II.17-B**). In addition, a significantly higher expression of specific markers for different types of cerebellar neurons was further detected by qRT-PCR analysis of organoids on day 91 (**Figure II.17-C**). These markers were: *PAX2, BARHL1, TBR1, GRID2, PARVALBUMIN*, and *NEUROGRANIN*.

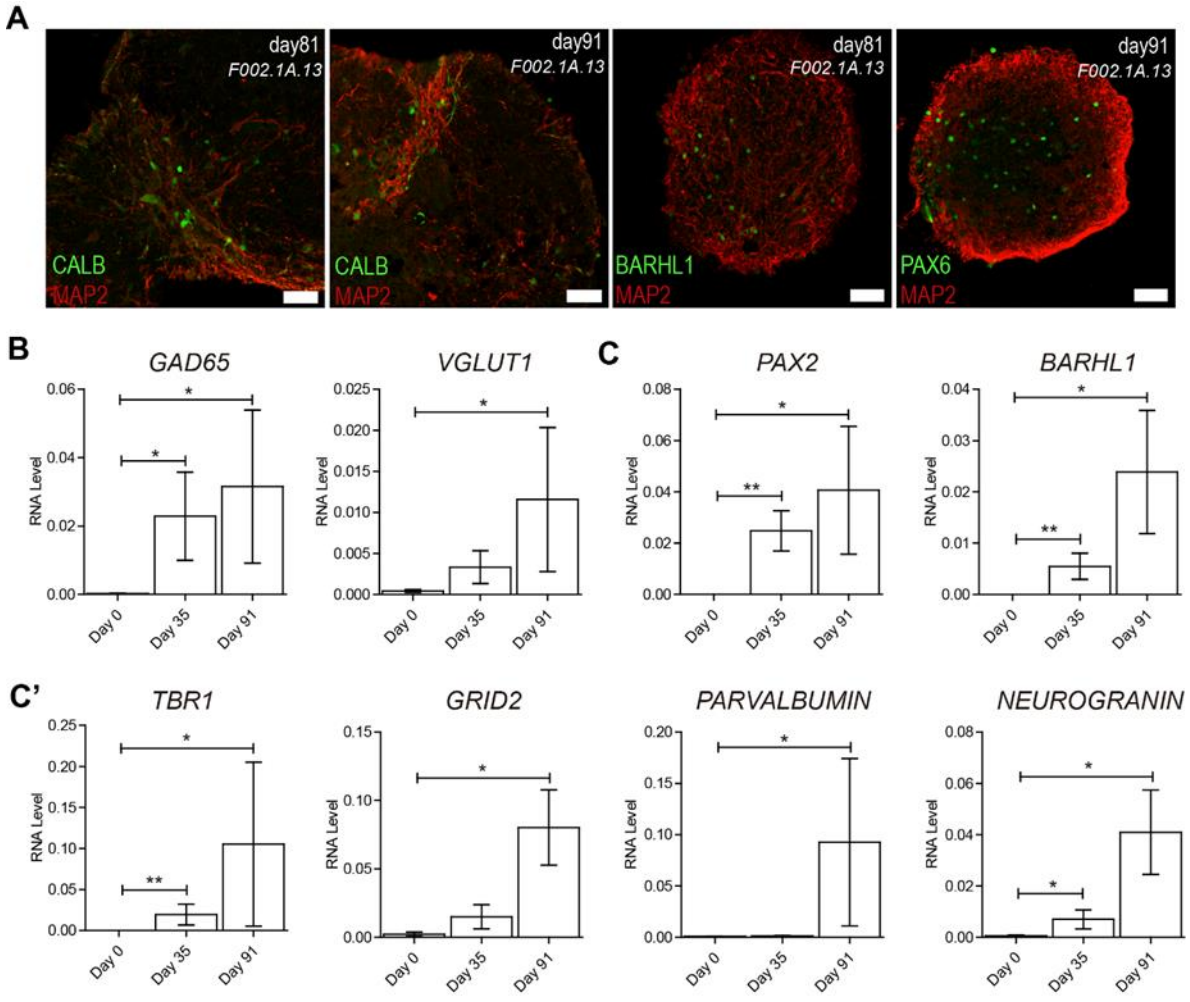

Figure II.17. Maturation of iPSC-derived cerebellar organoids. A) Immunofluorescence for CALB, MAP2, BARHL1 and PAX6 on days 81 and 91 of differentiation (F002.1A.13). qRT-PCR analysis of *GAD65* and *VGLUT1* (**B**), and *PAX2*, *BARHL1*, *TBR1*, *GRID2*, *PARVALBUMIN* and *NEUROGRANIN* (**C**) mRNA levels relative to *GAPDH* at the indicated time-points. Data were obtained from three independent differentiation experiments using F002.1A.13 cells. Student´s t-test (two-tailed) statistics, * p<0.05, ** p<0.01; error bars represent SEM.

We compared the maturation efficiency of re-plated cells and organoids by gene expression analysis for different cerebellar neurons markers. The difference in gene expression between re-plated cells and organoids is evident, with higher levels of mRNA for mature cerebellar genes in floating organoids at day 90, including GABAergic and glutamatergic types (**Figure II.18-A**). Principal Component Analysis (PCA), which is a

method that reduces the dimensionality of the data and retains most of its variation (Ringnér and Ringner, 2008), confirms a considerable difference between re-plated cells and floating cerebellar organoids (**Figure II.18-B**). The percentage of variance for all data is explained by PCs. As seen in the PCA, PC1 had the largest variance, explaining 98.6%, followed by 3.2% captured by PC2 (**Figure II.18-B**). Furthermore, the 2D system (re-plated cells) groups closer to the initial stages of differentiation (day 0, iPSCs) for the selected mature genes (**Figure II.18-B**). These results suggest that 3D culture supports more efficiently the cerebellar organoids differentiation and further maturation in cerebellar neurons when compared with the 2D system.

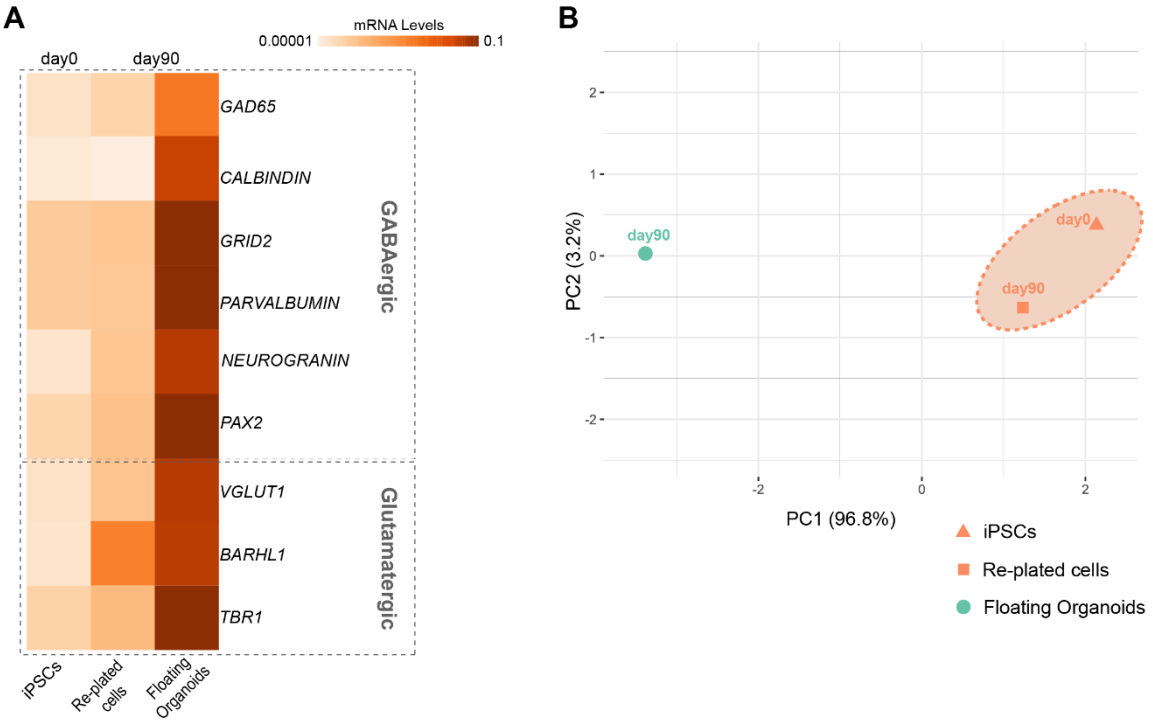

Figure II.18. 3D condition enables cerebellar neurons maturation. A) Temporal ClustVis analysis of qRT-PCR gene expression after iPSC-derived organoids were matured in 2D (replated cells) and 3D (floating organoids) conditions. mRNA levels were relative to *GAPDH* at the indicated time-points and conditions. **B)** Principal Component Analysis (PCA) for relative gene expression of both culture systems. X and Y axis show PC1 and PC2 that explain 96.8% and 3.2% of the total variance, respectively. Data were obtained from three independent differentiation experiments using F002.1A.13 cells.

II.5 DISCUSSION

Using a defined medium only and without the need for co-culturing, we successfully generated reproducible mature networks of cerebellar neurons with established functional connections.

In our work, we controlled the size of 3D cell aggregates as previously described (Ungrin et al., 2008), leading to an efficient neuronal commitment (Bauwens et al., 2008; Miranda et al., 2015). Our procedure allows the production of hundreds of organoids per cm2, which is a significant increase over the 96-well plates used by most cerebellar differentiation protocols previously described (Bratt-Leal et al., 2009; Muguruma et al., 2015; Ungrin et al., 2008; Wang et al., 2015). Cells were cultured in chemically defined medium and we sequentially added FGF2, SB, FGF19, and SDF1 in order to promote a spontaneous formation of cerebellar plate neuroepithelium, which has been described as differentiating into a multilayered structure reminiscent of cerebellar ontogenesis *in vivo* (Ishida et al., 2016; Muguruma et al., 2015).

The initial stage of cerebellar commitment in organoids was detected on day 7, when expression of *FGF8* mRNA was at its highest but declined thereafter. This behavior observed in 3D cultures recapitulates the cerebellar ontogenesis *in vivo* (reviewed in Marzban et al., 2015). Indeed, previous studies have shown that at early embryonic stages FGF signaling is required to establish the cerebellar territory, however, its suppression afterwards is essential for cerebellar development (Butts et al., 2014; Suzuki-Hirano et al., 2010).

In our study, organoids also formed neural tube-like structures organized in layers with apico-basal polarity. Most important, compared to findings from a previous study (Muguruma et al., 2015), the organoids in our cultures exhibited an earlier neuronal maturation pattern. On day 35, we found cells positive for OLIG2, CORL2, BARHL1, TBR1, and GAD65. CORL2

is the earliest marker for Purkinje cells (Seto et al., 2014); it is specifically expressed in post-mitotic Purkinje cell precursors shortly after exiting the cell cycle (Minaki et al., 2008) and it plays an essential role in Purkinje cell development (Nakatani et al., 2014; Wang et al., 2011). OLIG2 is another marker for Purkinje cell progenitors that is involved with cell cycle exit and differentiation into post-mitotic neurons (Ju et al., 2016; Seto et al., 2014; Takebayashi et al., 2002). In contrast, BARHL1 is expressed in migrating granule cell progenitors (Bulfone et al., 2000), while TBR1 is expressed in migrating progenitors of deep cerebellar nuclei projection neurons (Fink et al., 2006). *In vivo*, the protein glutamic acid decarboxylase isoform 65 (GAD65), which is a rate-limiting GABA synthesizing enzyme, localizes primarily on presynaptic boutons (Esclapez et al., 1994). Because the onset of GAD65 expression in the cerebellum occurs after synaptogenesis (Greif et al., 1991), we conclude that an interconnected neuronal network has been formed in organoids by day 35.

Our innovative strategy uses a defined basal medium optimized for neuronal cell culture (Bardy et al., 2015). Upon dissociation of organoids and re-plating on a laminin-coated surface, we promoted the maturation of cerebellar precursors without the need for co-culturing. Remarkably, our cultures remained viable for up to 145 days. The presence of cells displaying a characteristic long axon and highly arborized dendrites, and which stained positive for calbindin, a calcium-binding protein highly expressed in Purkinje cells (Nag and Wadhwa, 1999; Whitney et al., 2008), strongly indicates that our cultures support the maturation of Purkinje cells. Other neurons had a distinctive morphology and were positive for PAX6 in the nucleus and for microtubule-associated protein 2 (MAP2) in the cytoplasm, suggesting that these were granule cells. Additional types of neurons in our cultures were either negative for calbindin while expressing parvalbumin, which suggests that they corresponded to GABAergic interneurons (Bastianelli, 2003), or showed a strong positive signal for neurogranin, which is highly expressed in Golgi cells in the mouse cerebellum and in unipolar brush cells in the monkey cerebellum (Singec et al., 2004). Furthermore, cells

with nuclei positive for the transcription factor TBR1 and elaborate cellular processes positive for the neuron-specific class III beta-tubulin TUJ1 (Lee et al., 1990), revealed the formation of deep cerebellar nuclei projection neurons in our cultures (Fink, 2006).

Taken together, the data obtained with dendritic spine morphology analyses, calcium imaging, and electrophysiological evaluation strongly indicate that we have achieved an efficient maturation of cerebellar precursors in our cultures, both at the individual cell level and at the level of network connectivity. In particular, the presence of synaptic connections shows that a mature neuronal network has been generated. However, our cells did not reach the level of neuronal maturation equivalent to that occurring in post-natal human cerebellum. This is particularly evident for Purkinje cells, which in our cultures did not form the elaborated dendritic branches observed *in vivo*. Further studies should investigate which signaling molecules may be missing, and which are necessary, for our cells to fully recapitulate the entire maturation process similar to that occurring in the human cerebellum after birth.

Here we show for the first time that is possible to generate different types of electrophysiologically functional cerebellar neurons in long-term cultures that are feeder-free. Our findings represent an important contribution towards the development of autologous replacement strategies for the treatment of cerebellar degenerative diseases. Additionally, functional cerebellar neurons are an important cell source for drug screening and for the study of specific pathways involved with the development of cerebellar diseases such as ataxias, a group of disorders that affect many children and adults worldwide.

However, 2D single cell systems do not mimic what occurs *in vivo* and a 3D approach can exhibit improved cell-cell contact and therefore enhanced intracellular functions (Laschke and Menger, 2017). In fact, we observed that our organoids present enhancements in cerebellar maturation when compared with our re-plated cells. Although an efficient cerebellum differentiation and further maturation is achieved in these 3D conditions, we found that in static conditions these cerebellar organoids tend to coalesce

forming large structures with mass transfer limitations that lead to the formation of necrotic zones if nutrients and oxygen are unable to reach the aggregate center. In the future, these limitations should be minimized by using a dynamic approach (Miranda et al., 2016; Rigamonti et al., 2016), with the possibility of scaling up the production of mature cerebellar neurons in 3D structures.

II.6 REFERENCES

Adamaszek, M., D'Agata, F., Ferrucci, R., Habas, C., Keulen, S., Kirkby, K.C., Leggio, M., Mariën, P., Molinari, M., Moulton, E., et al. (2017). Consensus Paper: Cerebellum and Emotion. Cerebellum 16, 552–576.

Agasse, F., Bernardino, L., Silva, B., Ferreira, R., Grade, S., and Malva, J.O. (2008). Response to histamine allows the functional identification of neuronal progenitors, neurons, astrocytes, and immature cells in subventricular zone cell cultures. Rejuvenation Res. 11, 187–200.

Akopian, V., Andrews, P.W., Beil, S., Benvenisty, N., Brehm, J., Christie, M., Ford, A., Fox, V., Gokhale, P.J., Healy, L., et al. (2010). Comparison of defined culture systems for feeder cell free propagation of human embryonic stem cells. In Vitro Cell. Dev. Biol. Anim. 46, 247–258.

Ambrósio, A.F., Silva, A.P., Malva, J.O., Mesquita, J.F., Carvalho, A.P., and Carvalho, C.M. (2000). Role of desensitization of AMPA receptors on the neuronal viability and an the [Ca2+](i) changes in cultured rat hippocampal neurons. Eur. J. Neurosci. 12, 2021–2031.

Andreu, A., Crespo-Enriquez, I., and Echevarria, D. (2014). Molecular events directing the patterning and specification of the cerebellum. Eur. J. Anat. 18, 245–252.

Bardy, C., van den Hurk, M., Eames, T., Marchand, C., Hernandez, R. V, Kellogg, M., Gorris, M., Galet, B., Palomares, V., Brown, J., et al. (2015). Neuronal medium that supports basic synaptic functions and activity of human neurons in vitro. Proc. Natl. Acad. Sci. U. S. A. 112, E2725–E2734.

Bastianelli, E. (2003). Distribution of calcium-binding proteins in the cerebellum. Cerebellum 2, 242–262.

Bauwens, C.L., Peerani, R., Niebruegge, S., Woodhouse, K. a., Kumacheva, E., Husain, M., and Zandstra, P.W. (2008). Control of Human Embryonic Stem Cell Colony and Aggregate Size Heterogeneity Influences Differentiation Trajectories. Stem Cells 26, 2300–2310.

Von Bohlen Und Halbach, O. (2007). Immunohistological markers for staging neurogenesis in adult hippocampus. Cell Tissue Res. 329, 409–420.

Bratt-Leal, A.M., Carpenedo, R.L., and McDevitt, T.C. (2009). Engineering the embryoid body microenvironment to direct embryonic stem cell differentiation. Biotechnol. Prog. 25, 43–51.

Bulfone, a, Menguzzato, E., Broccoli, V., Marchitiello, a, Gattuso, C., Mariani, M., Consalez, G.G., Martinez, S., Ballabio, a, and Banfi, S. (2000). Barhl1, a gene belonging to a new subfamily of mammalian homeobox genes, is expressed in migrating neurons of the CNS. Hum. Mol. Genet. 9, 1443–1452.

Burridge, P.W., Thompson, S., Millrod, M.A., Weinberg, S., Yuan, X., Peters, A., Mahairaki, V., Koliatsos, V.E., Tung, L., and Zambidis, E.T. (2011). A universal system for highly efficient cardiac differentiation of human induced pluripotent stem cells that eliminates interline variability. PLoS One 6, e18293.

Butts, T., Green, M.J., and Wingate, R.J.T. (2014). Development of the cerebellum: simple steps to make a “little brain.” Development 141, 4031–4041.

Chi, C.L., Martinez, S., Wurst, W., and Martin, G.R. (2003). The isthmic organizer signal FGF8 is required for cell survival in the prospective midbrain and cerebellum. Development 130, 2633–2644.

Dahlmann, J., Kensah, G., Kempf, H., Skvorc, D., Gawol, A., Elliott, D. a., Dr??ger, G., Zweigerdt, R., Martin, U., and Gruh, I. (2013). The use of agarose microwells for scalable embryoid body formation and cardiac differentiation of human and murine pluripotent stem cells. Biomaterials 34, 2463–2471.

Erceg, S., Ronaghi, M., Zipancic, I., Lainez, S., Roselló, M.G., Xiong, C., Moreno-Manzano, V., Rodríguez-Jiménez, F.J., Planells, R., Alvarez-Dolado, M., et al. (2010). Efficient differentiation of human embryonic stem cells into functional cerebellar-like cells. Stem Cells Dev. 19, 1745–1756.

Erceg, S., Lukovic, D., Moreno-Manzano, V., Stojkovic, M., and Bhattacharya, S.S. (2012). Derivation of Cerebellar Neurons from Human Pluripotent Stem Cells. In Current Protocols in Stem Cell Biology, (Hoboken, NJ, USA: John Wiley & Sons, Inc.), chapter 1.

Esclapez, M., Tillakaratne, N.J., Kaufman, D.L., Tobin, a J., and Houser, C.R. (1994). Comparative localization of two forms of glutamic acid decarboxylase and their mRNAs in rat brain supports the concept of functional differences between the forms. J. Neurosci. 14, 1834–1855.

Felix-Oliveira, A., Dias, R.B., Colino-Oliveira, M., Rombo, D.M., and Sebastiao, A.M. (2014). Homeostatic plasticity induced by brief activity deprivation enhances long-term potentiation in the mature rat hippocampus. J. Neurophysiol. 112, 3012–3022.

Fink, a. J. (2006). Development of the Deep Cerebellar Nuclei: Transcription Factors and Cell Migration from the Rhombic Lip. J. Neurosci. 26, 3066–3076.

Fink, A.J., Englund, C., Daza, R. a M., Pham, D., Lau, C., Nivison, M., Kowalczyk, T., and Hevner, R.F. (2006). Development of the deep cerebellar nuclei: transcription factors and cell migration from the rhombic lip. J. Neurosci. 26, 3066–3076.

Frantz, G.D., Weimann, J.M., Levin, M.E., and McConnell, S.K. (1994). Otx1 and Otx2 define layers and regions in developing cerebral cortex and cerebellum. J. Neurosci. 14, 5725–5740.

Greif, K.F., Erlander, M.G., Tillakaratne, N.J.K., and Tobin, A.J. (1991). Postnatal expression of glutamate decarboxylases in developing rat cerebellum. Neurochem. Res. 16, 235–242.

Grienberger, C., and Konnerth, A. (2012). Imaging Calcium in Neurons. Neuron 73, 862–885.

Hentze, H., Soong, P.L., Wang, S.T., Phillips, B.W., Putti, T.C., and Dunn, N.R. (2009). Teratoma formation by human embryonic stem cells: Evaluation of essential parameters for future safety studies. Stem Cell Res. 2, 198–210.

Hering, H., and Sheng, M. (2001). Dentritic spines: structure, dynamics and regulation. Nat. Rev. Neurosci. 2, 880–888.

Ishida, Y., Kawakami, H., Kitajima, H., Nishiyama, A., Sasai, Y., Inoue, H., and Muguruma, K. (2016). Vulnerability of Purkinje Cells Generated from Spinocerebellar Ataxia Type 6 Patient-Derived iPSCs. Cell Rep. 17, 1482–1490.

Joyner, A.L. (1996). Engrailed, Wnt and Pax genes regulate midbrain-hindbrain development. Trends Genet. 12, 15–20.

Ju, J., Liu, Q., Zhang, Y., Liu, Y., Jiang, M., Zhang, L., He, X., Peng, C., Zheng, T., Lu, Q.R., et al. (2016). Olig2 regulates Purkinje cell generation in the early developing mouse cerebellum. Sci. Rep. 6, 30711.

Larsen, K.B., Lutterodt, M.C., Møllgård, K., and Møller, M. (2010). Expression of the homeobox genes OTX2 and OTX1 in the early developing human brain. J. Histochem. Cytochem. 58, 669–678.

Laschke, M.W., and Menger, M.D. (2017). Life is 3D: Boosting Spheroid Function for Tissue Engineering. Trends Biotechnol. 35, 133–144.

Lee, M.K., Rebhun, L.I., and Frankfurter, A. (1990). Posttranslational modification of class III beta-tubulin. Proc. Natl. Acad. Sci. 87, 7195–7199.

Lendahl, U., Zimmerman, L.B., and McKay, R.D. (1990). CNS stem cells express a new class of intermediate filament protein. Cell 60, 585–595.

Leto, K., Arancillo, M., Becker, E.B.E., Buffo, A., Chiang, C., Ding, B., Dobyns, W.B., Dusart, I., Haldipur, P., Hatten, M.E., et al. (2016). Consensus Paper: Cerebellar Development. The Cerebellum 15, 789–828.

Li, S. (2004). Barhl1 Regulates Migration and Survival of Cerebellar Granule Cells by Controlling Expression of the Neurotrophin-3 Gene. J. Neurosci. 24, 3104–3114.

Macías, W., Carlson, R., Rajadhyaksha, A., Barczak, A., and Konradi, C. (2001). Potassium chloride depolarization mediates CREB phosphorylation in striatal neurons in an NMDA receptor-dependent manner. Brain Res. 890, 222–232.

Manto, M., and Marmolino, D. (2009). Animal models of human cerebellar ataxias: A cornerstone for the therapies of the twenty-first century. Cerebellum 8, 137–154.

Marzban, H., Bigio, M.R. Del, Alizadeh, J., Ghavami, S., Zachariah, R.M., and Rastegar, M. (2015). Cellular commitment in the developing cerebellum. 8, 1–26.

McLachlan, N.M., and Wilson, S.J. (2017). The contribution of brainstem and cerebellar pathways to auditory recognition. Front. Psychol. 8, 265.

Metsalu, T., and Vilo, J. (2015). ClustVis: A web tool for visualizing clustering of multivariate data using Principal Component Analysis and heatmap. Nucleic Acids Res. 43, W566–W570.

Minaki, Y., Nakatani, T., Mizuhara, E., Inoue, T., and Ono, Y. (2008). Identification of a novel transcriptional corepressor, Corl2, as a cerebellar Purkinje cell-selective marker. Gene Expr. Patterns 8, 418–423.

Miranda, C.C., Fernandes, T.G., Pascoal, J.F., Haupt, S., Brüstle, O., Cabral, J.M.S., and Diogo, M.M. (2015). Spatial and temporal control of cell aggregation efficiently directs human pluripotent stem cells towards neural commitment. Biotechnol. J. 10, 1612–1624.

Miranda, C.C., Fernandes, T.G., Diogo, M.M., and Cabral, J.M.S. (2016). Scaling Up a Chemically-Defined Aggregate-Based Suspension Culture System for Neural Commitment of Human Pluripotent Stem Cells. Biotechnol. J. 11, 1628-1638.

Mizuhara, E., Minaki, Y., Nakatani, T., Kumai, M., Inoue, T., Muguruma, K., Sasai, Y., and Ono, Y. (2010). Purkinje cells originate from cerebellar ventricular zone progenitors positive for Neph3 and E-cadherin. Dev. Biol. 338, 202–214.

Molina-Hernández, A., and Velasco, I. (2008). Histamine induces neural stem cell proliferation and neuronal differentiation by activation of distinct histamine receptors. J. Neurochem. 106, 706–717.

Muguruma, K., Nishiyama, A., Ono, Y., Miyawaki, H., Mizuhara, E., Hori, S., Kakizuka, A., Obata, K., Yanagawa, Y., Hirano, T., et al. (2010). Ontogeny-recapitulating generation and tissue integration of ES cell-derived Purkinje cells. Nat. Neurosci. 13, 1171–1180.

Muguruma, K., Nishiyama, A., Kawakami, H., Hashimoto, K., and Sasai, Y. (2015). Self-Organization of Polarized Cerebellar Tissue in 3D Culture of Human Pluripotent Stem Cells. Cell Rep. 10, 537–550.

Nag, T.C., and Wadhwa, S. (1999). Calbindin immunoreactivity in the developing and adult human cerebellum. J. Chem. Neuroanat. 17, 1–12.

Nakatani, T., Minaki, Y., Kumai, M., Nitta, C., and Ono, Y. (2014). The c-Ski family member and transcriptional regulator Corl2/Skor2 promotes early differentiation of cerebellar Purkinje cells. Dev. Biol. 388, 68–80.

Peerani, R., Rao, B.M., Bauwens, C., Yin, T., Wood, G. a, Nagy, a, Kumacheva, E., and Zandstra, P.W. (2007). Niche-mediated control of human embryonic stem cell self-renewal and differentiation. EMBO J. 26, 4744–4755.

Rigamonti, A., Repetti, G.G., Sun, C., Price, F.D., Reny, D.C., Rapino, F., Weisinger, K., Benkler, C., Peterson, Q.P., Davidow, L.S., et al. (2016). Large-Scale Production of Mature Neurons from Human Pluripotent Stem Cells in a Three-Dimensional Suspension Culture System. Stem Cell Reports 6, 993–1008.

Ringnér, M., and Ringner, M. (2008). What is principal component analysis? Nat Biotechnol 26, 303–304.

Risher, W.C., Ustunkaya, T., Alvarado, J.S., and Eroglu, C. (2014). Rapid golgi analysis method for efficient and unbiased classification of dendritic spines. PLoS One 9, e107591.

Rodrigues, R.S., Ribeiro, F.F., Ferreira, F., Vaz, S.H., Sebastião, A.M., and Xapelli, S. (2017). Interaction between cannabinoid type 1 and type 2 receptors in the modulation of subventricular zone and dentate gyrus neurogenesis. Front. Pharmacol. 8, 516.

Rodríguez-Martínez, G., Velasco, I., García-López, G., Solís, K.H., Flores-Herrera, H., Díaz, N.F., and Molina-Hernández, A. (2012). Histamine is required during neural stem cell proliferation to increase neuron differentiation. Neuroscience 216, 10–17

Rombo, D.M., Dias, R.B., Duarte, S.T., Ribeiro, J.A., Lamsa, K.P., and Sebastião, A.M. (2016). Adenosine A1 Receptor Suppresses Tonic GABAA Receptor Currents in Hippocampal Pyramidal Cells and in a Defined Subpopulation of Interneurons. Cereb. Cortex 26, 1081–1095.

Salero, E., and Hatten, M.E. (2007). Differentiation of ES cells into cerebellar neurons. Proc. Natl. Acad. Sci. U. S. A. 104, 2997–3002.

Schöls, L., Bauer, P., Schmidt, T., Schulte, T., and Riess, O. (2004). Autosomal dominant cerebellar ataxias: Clinical features, genetics, and pathogenesis. Lancet Neurol. 3, 291–304.

Seto, Y., Ishiwata, S., and Hoshino, M. (2014). Characterization of Olig2 expression during cerebellar development. Gene Expr. Patterns 15, 1–7.

Singec, I., Knoth, R., Ditter, M., Volk, B., and Frotscher, M. (2004). Neurogranin is expressed by principal cells but not interneurons in the rodent and monkey neocortex and hippocampus. J. Comp. Neurol. 479, 30–42.

Su, H.L., Muguruma, K., Matsuo-Takasaki, M., Kengaku, M., Watanabe, K., and Sasai, Y. (2006). Generation of cerebellar neuron precursors from embryonic stem cells. Dev. Biol. 290, 287–296.

Suzuki-Hirano, A., Harada, H., Sato, T., and Nakamura, H. (2010). Activation of Ras-ERK pathway by Fgf8 and its downregulation by Sprouty2 for the isthmus organizing activity. Dev. Biol. 337, 284–293.

Takahashi, K., Tanabe, K., Ohnuki, M., Narita, M., Ichisaka, T., Tomoda, K., and Yamanaka, S. (2007). Induction of Pluripotent Stem Cells from Adult Human Fibroblasts by Defined Factors. Cell 131, 861–872.

Takebayashi, H., Ohtsuki, T., Uchida, T., Kawamoto, S., Okubo, K., Ikenaka, K., Takeichi, M., Chisaka, O., and Nabeshima, Y.I. (2002). Non-overlapping expression of Olig3 and Olig2 in the embryonic neural tube. Mech. Dev. 113, 169–174.

Taroni, F., and DiDonato, S. (2004). Pathways to motor incoordination: the inherited ataxias. Nat. Rev. Neurosci. 5, 641–655.

Ungrin, M.D., Joshi, C., Nica, A., Bauwens, C., and Zandstra, P.W. (2008). Reproducible, Ultra High-Throughput Formation of Multicellular Organization from Single Cell Suspension-Derived Human Embryonic Stem Cell Aggregates. PLoS One 3, e1565.

Wagner, M.J., Kim, T.H., Savall, J., Schnitzer, M.J., and Luo, L. (2017). Cerebellar granule cells encode the expectation of reward. Nature 544, 96–100.

Wang, B., Harrison, W., Overbeek, P.A., and Zheng, H. (2011). Transposon mutagenesis with coat color genotyping identifies an essential role for Skor2 in sonic hedgehog signaling and cerebellum development. Development 138, 4487–4497.

Wang, S., Wang, B., Pan, N., Fu, L., Wang, C., Song, G., An, J., Liu, Z., Zhu, W., Guan, Y., et al. (2015). Differentiation of human induced pluripotent stem cells to mature functional Purkinje neurons. Sci. Rep. 5, 9232.

Whitney, E.R., Kemper, T.L., Rosene, D.L., Bauman, M.L., and Blatt, G.J. (2008). Calbindin-D28k is a more reliable marker of human Purkinje cells than standard Nissl stains: A stereological experiment. J. Neurosci. Methods 168, 42–47.

Yeung, J., Ha, T.J., Swanson, D.J., and Goldowitz, D. (2016). A Novel and Multivalent Role of Pax6 in Cerebellar Development. J. Neurosci. 36, 9057–9069.

Zec, N., Rowitch, D.H., Bitgood, M.J., and Kinney, H.C. (1997). Expression of the homeobox-containing genes EN1 and EN2 in human fetal midgestational medulla and cerebellum. J. Neuropathol. Exp. Neurol. 56, 236–242.

III. CONTROLLING THE REGIONAL IDENTITY OF HUMAN PLURIPOTENT STEM CELL-DERIVED CEREBELLAR ORGANOIDS

III.1 ABSTRACT

The human cerebellum contains the majority of neurons in the central nervous system (CNS), being composed by diverse neuronal subtypes. Cerebellar diseases represent a heterogeneous group of disorders characterized by the dysfunction of the cerebellum, in which different types of cerebellar neurons can be affected. Notwithstanding the recent development of *in vitro* models for cerebellar ataxias employing human pluripotent stem cells (PSCs), specific cerebellar neuronal subtypes are still difficult to obtain. Purkinje cells, a GABAergic neuronal subtype present in the cerebellum, have been generated by co-culturing, but only a limited number of cells can be obtained. Previously, we reported the generation of human PSC-derived Purkinje cells under defined and feeder-free conditions. However, the reported protocols showed a moderated dorsalization, with a limited amount of GABAergic progenitors. Therefore, we attempted to control the regional identity of cerebellar organoids, promoting the generation of ventral cerebellar neuroepithelium and thus increasing the number of GABAergic progenitors. This system successfully promoted the generation of a dense layer of $OLIG2^{+}$cells, which is important for Purkinje cell differentiation. In addition, 5-HT treatment during the maturation process was able to enhance the expression of Purkinje-specific markers, including L7 and GRID2.

Keywords: cerebellum, ventral region, GABAergic progenitors, Purkinje cells

III.2 INTRODUCTION

Most of the current knowledge about human neurodegenerative disorders has been based on human postmortem tissues and animal models that do not allow to investigate disease progression and development, and do not reflect the physiological characteristics of human tissues (J Siney et al., 2018; Tiscornia et al., 2011). Modeling these complex diseases with human induced pluripotent stem cells (iPSCs), which can be reprogrammed from patient somatic cells (Park et al., 2008; Takahashi et al., 2007), has great potential to understand the pathological mechanisms, as well as to generate powerful insights about possible effective therapies. The application of iPSC technology was already reported to model different neurodegenerative disorders, including Alzheimer's disease (Ochalek et al., 2017; Yang et al., 2016), Parkinson's disease (Imaizumi et al., 2012; Nguyen et al., 2011), Huntington's disease (Lim et al., 2017; Liu et al., 2016), and autism (Andoh-Noda et al., 2015; Fernandes et al., 2015). Based on diverse neuropathology manifestations, distinct areas of central nervous systems (CNS) and neuronal subtypes are affected in different neurodegenerative diseases. Efforts have been made to direct PSC differentiation to specific regions of the CNS, including cortical, striatal, midbrain and spinal cord neurons (Aubry et al., 2008; Gunhanlar et al., 2018; Hu and Zhang, 2009; Junghyun Jo et al., 2016). However, it has been difficult to establish a pathological mechanism using the specific disease-associated neuronal subtype, since only few neuronal subtypes can be generated from iPSCs and direct induction for a specific subtype can originate a limited amount of neurons. Another limitation is variability between experiments and different cell lines, including differentiation efficiency and maturity (Imaizumi and Okano, 2014; Okano and Yamanaka, 2014; Su et al., 2006; Wang et al., 2015). For unknown reasons, the dysfunction of cerebellum involves a prominent loss of Purkinje neurons, the most elaborate inhibitory GABAergic neuronal subtype of the cerebellar cortex (Taroni and DiDonato, 2004). The

generation of these cerebellar neurons from PSCs was already reported (Muguruma et al., 2015; Su et al., 2006; Tao et al., 2010; Wang et al., 2015). However a low efficiency of functional Purkinje cell generation was achieved, which is expectable since the Purkinje cell number in the cerebellum is far less than that of other cerebellar neurons, <1/1000 (Keller and Heinrichs, 1975; Tomomura et al., 2001)

Here, we attempted to address this problem by manipulating the regional identity of generated cerebellar neurons and supporting the Purkinje cell maturation. For this, sonic hedgehog (SHH) signaling (Chiang et al., 1996; Martínez et al., 2012) was modulated to control dorsal-ventral identity of cerebellar progenitors in order to increase the efficiency of ventral differentiation and the number of GABAergic progenitors. Furthermore, the role of serotonin (5-hydroxytryptoamine, 5-HT) was also reported in the regulation of morphological maturation of Purkinje cells (Kondoh et al., 2004; Oostland and van Hooft, 2013). The 5-HT receptor knockout mice exhibited abnormal dendritic tree morphology of Purkinje cells and impaired short-term plasticity at Purkinje cell synapses (Oostland et al., 2013). Therefore, we hypothesized that 5-HT treatment during the maturation protocol could lead to a higher efficiency of morphological and physiological maturation of Purkinje cells. Indeed, inducing ventralizing signaling during cerebellar differentiation protocol demonstrated an enhanced expression of cerebellar ventral progenitors, *OLIG2* and *CORL2*, as well as the creation of a consistent layer of $OLIG2^{+}$ Purkinje cell progenitors. Further addition of 5-HT during the maturation protocol did not reveal a significant alteration in dendritic branch morphology of the generated Purkinje cells, but an increased expression of Purkinje cell markers, including L7 and GRID2, was detected. Our findings show important insights for the directed generation of specific cerebellar subtypes that can contribute to investigate phenotypes associated with cerebellar diseases and identify possible therapeutic targets.

III.3 METHODS

Maintenance of human iPSCs

Gibco® Human Episomal iPSC line (iPSC6.2), derived from $CD34^+$ cord blood was used (Burridge et al., 2011). Human iPSCs were cultured on Matrigel™ (Corning)-coated plates with mTeSR™1 Medium (StemCell Technologies). Medium was changed daily. Cells were passaged every three to four days (when the colonies covered approximately 85% of the surface area of the culture dish) using 0.5mM EDTA dissociation buffer (Life Technologies). Two to three passages were performed before starting the differentiation process.

Ventral cerebellar commitment

Before seeding, cells were incubated with ROCKi (Y-27632, 10μM, StemCell Technologies) for 1 h at 37ºC and then treated with accutase (Sigma) for 7 min at 37ºC. After dissociation, cells were re-aggregated using microwell plates (AggreWell™800, StemCell Technologies) according to the manufacturer's instructions. Cells were plated at a density of 1.8×10^6 cells/well (6,000 cells/microwell) in 1.5 mL/well of mTeSR™1 supplemented with 10μM ROCKi. After 24 hours, full volume of the medium was replaced, and aggregates were maintained in mTeSR™1 without ROCKi. Defining the day on which the cell seeding was performed as day 0, the basal differentiation medium used during days 2-21 was gfCDM (Muguruma et al., 2015). Recombinant human basic FGF (FGF2, 50ng/ml, PeproTech) and SB431542 (SB, 10μM, Sigma) were added to culture on day 2. Full-volume medium replacement with gfCDM (supplemented with insulin, FGF2 and SB) was performed on day 5. On day 7, the aggregates were transferred from microwells to ultra-low attachment

6-well plates (Costar, Corning) at a density of 1 x 10^6 cells/mL. Full volume of the medium was replaced and two-thirds of initial amount of FGF2 and SB was used. Recombinant human FGF19 (100ng/ml, PeproTech) and SAG (10µM, Millipore) were added to culture on day 14. At day 18, total volume of medium change was performed (gfCDM supplemented with insulin, FGF19 and SAG). From day 21, the aggregates were cultured in Neurobasal medium supplemented with GlutaMax I, N2 supplement and PS. Full-volume replacement was performed every 7 days. SAG was added to culture at day 21 when the medium was changed. Recombinant human SDF1 (300ng/ml, PeproTech) was added to culture on day 28 (**Figure III.1**).

Purkinje cells maturation

After 35 days of differentiation, aggregates were dissociated using accutase (Sigma) and re-plated on wells coated with poly-L-ornithine (15µg/mL, Sigma) and Laminin (20µg/mL, Sigma), at a seeding density of 80 000 cells/cm^2. Afterwards, re-plated cells were cultured in complete BrainPhys™ Neuronal Medium (StemCell Technologies) - supplemented with NeuroCult™ SM1 Neuronal Supplement (StemCell Technologies), N2 Supplement-A (StemCell Technologies), Recombinant Human Brain Derived Neurotrophic Factor (BDNF, PeproTech, 20ng/mL), Recombinant Human Glial-Derived Neurotrophic Factor (GDNF, PeproTech, 20ng/mL), dibutyryl cAMP (1mM, Sigma), and ascorbic acid (200nM, Sigma). Serotonin-Creatinin-sulfate monohydrate (2µM, 5-Hydroxy-tryptoamin-creatinin-sulfate) was also added to culture, from day 35 or day 56 of differentiation and was maintained until day 56 or until day 70, respectively (**Figure III.5**). One-third of the total volume was replaced at every 3 days using complete BrainPhys supplemented with Serotonin-Creatinin-sulfate monohydrate.

Tissue preparation and Immunofluorescence

Aggregates were fixed in 4% paraformaldehyde (PFA, Sigma) for 20 min at 4ºC followed by washing in Phosphate buffered saline (PBS, 0.1M) and overnight incubation in 15% (v/v) sucrose at 4ºC. Aggregates were embedded in 7.5%/15% (v/v) gelatin/sucrose and frozen in isopenthane at -80ºC. Twelve-µm sections were cut on a cryostat-microtome (Leica CM3050S, Leica Microsystems), collected on Superfrost™ Microscope Slides (Thermo Scientific) and stored at -20ºC. For immunostaining, sections were de-gelatinized for 45 min in PBS at 37ºC, incubated in 0.1 M Glycine (Millipore) for 10 min at room temperature (RT), permeabilized with 0.1% (v/v) Triton X-100 (Sigma) for 10 min at RT and blocked with 10 % (v/v) fetal goat serum (FGS, Gibco) in TBST (20 mM Tris-HCl pH 8.0, 150 mM NaCl, 0.05 % (v/v) Tween-20, Sigma) for 30 min. at RT. Sections were then incubated overnight at 4ºC with the primary antibodies (**Table III.1**) diluted in blocking solution. Secondary antibodies were added to sections for 30 min (goat anti-mouse or goat anti-rabbit IgG, Alexa Fluor®–488 or –546, 1:400 (v/v) dilution, Molecular Probes) at RT and nuclear counterstaining was performed using 4',6-diamidino-2-phenylindole (DAPI, 1.5µg/mL; Sigma). After brief drying, sections were mounted in Mowiol (Sigma). Fluorescence images were acquired with Zeiss LSM 710 Confocal Laser Point-Scanning Microscopes.

Table III-1. List of primary antibodies and dilutions used for immunostaining

Antibody	Company	Host species	Dilution
BARHL1	Atlas	rabbit	1:500
CALBINDIN	Swant	rabbit	1:500
GAD65	BD Pharmingen	mouse	1:100
MAP2	Sigma	mouse	1:1000
N-CADHERIN	BD Transduction	mouse	1:1000
NESTIN	R&D	mouse	1:400
OLIG2	Millipore	rabbit	1:500
PAX6	Covance	rabbit	1:400
SOX2	R&D	mouse	1:200
SYNAPSIN1	Abcam	rabbit	1:500

Quantitative Real-time PCR (qRT-PCR)

Total RNA was extracted at different time-points of differentiation using High Pure RNA Isolation Kit (Roche) and converted into complementary cDNA with Transcriptor High Fidelity cDNA Synthesis Kit (Roche). Taqman® Gene Expression Assays (20X, Applied Biosystems) were selected for *NANOG* (HS02387400-g1), *OCT4* (HS00999634-sh), *PAX6* (HS00240871-m1), *SOX1* (HS01057642-s1). Other transcripts were analyzed using SYBR® green chemistry (**Table III.2**). All PCR reactions were run in triplicate, using the StepOne™ or ViiA™7 RT-PCR Systems (Applied BioSystems). Reactions were normalized to the housekeeping gene GAPDH and results analyzed with StepOne™ or QuantStudio™ RT-PCR Software. The average of relative expression values were used for ClustVis analysis, an in silico tool that clustered different conditions that have similar gene expression at different time points (Metsalu and Vilo, 2015).

Table III-2. Primers used for qRT-PCR

Gene	Foward	Reverse
CORL2	CCAGGTGTTAAAAGGAAACACA	GCTCCCTTTTCATCTGATCCT
EN2	CCGGCGTGGGTCTACTGTA	GGCCGCTTGTCCTCTTTGTT
GAD65	GTCTCCAGCTCGCATACACA	CGAAAGACCAAAAGCCAGAG
GAD67	CCTGGAACTGGCTGAATACC	CCCTGAGGCTTTGTGGAATA
GBX2	GACGAGTCAAAGGTGGAAGAC	GATTGTCATCCGAGCTGTAGTC
GRID2	AGCTCTTCCTCTCTTGGTTTCC	GCCCCACGTTGCCTAGAAAT
KIRREL2	GGGGCTAGTTCAGTGGACTAA	CACGGGCCTAATGTGGAGG
L7	ACCAGGAGGGCTTCTTCAAT	CTGTCACACGTTGGTCATCC
NEUROGRANIN	TCAAAGTTCCCGAGGAGAGA	CTAAAAGGGCACGGACTCAG
OLIG2	GACAAGCTAGGAGGCAGTGG	CGGCTCTGTCATTTGCTTCTTG
OTX2	AGAGGACGACGTTCACTCG	TCGGGCAAGTTGATTTTCAGT
PARVALBUMIN	TTCTCCCCAGATGCCAGAGA	GAGATTGGGTGTTCAGGGCA

III.4 RESULTS

Efficient neural and cerebellar commitment is achieved in the targeted ventral differentiation

Sonic Hedgehog (SHH) signaling is involved in the specification of ventral neuronal subtypes along the dorsal-ventral (D-V) axis of the neural tube. SHH is a secreted protein produced by the cells of the ventral most floor plate of the neural tube, underlying notochord and forming a diffusion gradient in a direction of dorsal neural tube (Briscoe and Ericson, 1999; Chiang et al., 1996). Thus, SHH signaling is essential for the specification of ventral neuronal subtypes throughout whole CNS, the reason why in general, *in vitro* neuronal differentiation protocols usually generate more ventral identities. Purkinje cells are cerebellar GABAergic neurons originated from ventral region of cerebellar neuroepithelium. Therefore we explored the effect of the Smo receptor agonist SAG (a SHH agonist, Chen et al., 2002)

on mid-hindbrain committed progenitors. For that, SAG was added to culture at day 14 of differentiation, immediately after the initial neural induction and mid-hindbrain patterning (**Figure III.1**). Although FGF19, which is a human ortholog of mouse FGF15, is expressed in the mid-hindbrain region and seems to be involved in dorsal progenitor development (Fischer et al., 2011; Gimeno and Martinez, 2007), it was reported to be critical for promoting self-formation of continuous neuroepithelium in human PSC-derived organoids, as well as generation of different cerebellar progenitors (Muguruma et al., 2015). Therefore, a combination of FGF19 and SAG was used until day 21 to generate continuous neural tube-like structures with ventral identity (**Figure III.1**). Afterwards, SDF1 was added, on day 28, to create a laminated structure as seen during cerebellar neurogenesis (**Figure III.1**).

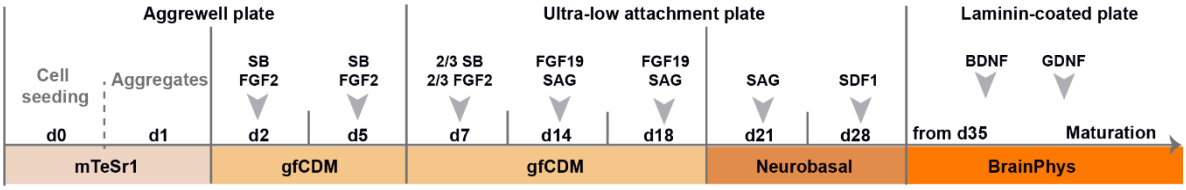

Figure III.1. Overview of the culture protocol. SHH signaling was modulated by using a Smo receptor agonist, SAG, to manipulate the regional identity of generated cerebellar progenitors.

Gene expression analysis demonstrated that pluripotency genes, including *OCT4* and *NANOG*, were expressed in human iPSCs at day 0. After neural induction they were down-regulated, being no longer expressed at day 14 of differentiation (**Figure III.2-A**). In the meantime, transcripts involved in the neural commitment were up-regulated, including *PAX6* and *SOX1*, starting to be expressed by day 14 and increasing until day 35 of differentiation (**Figure III.2-B**). In accordance, immunofluorescence on day 14 revealed that most of cells had positive staining for a neural marker NESTIN and neural tube-like structures were

detected expressing PAX6 and SOX2 (**Figure III.2-C**). Therefore, an effective neural commitment was confirmed by day 14, prior to ventral patterning.

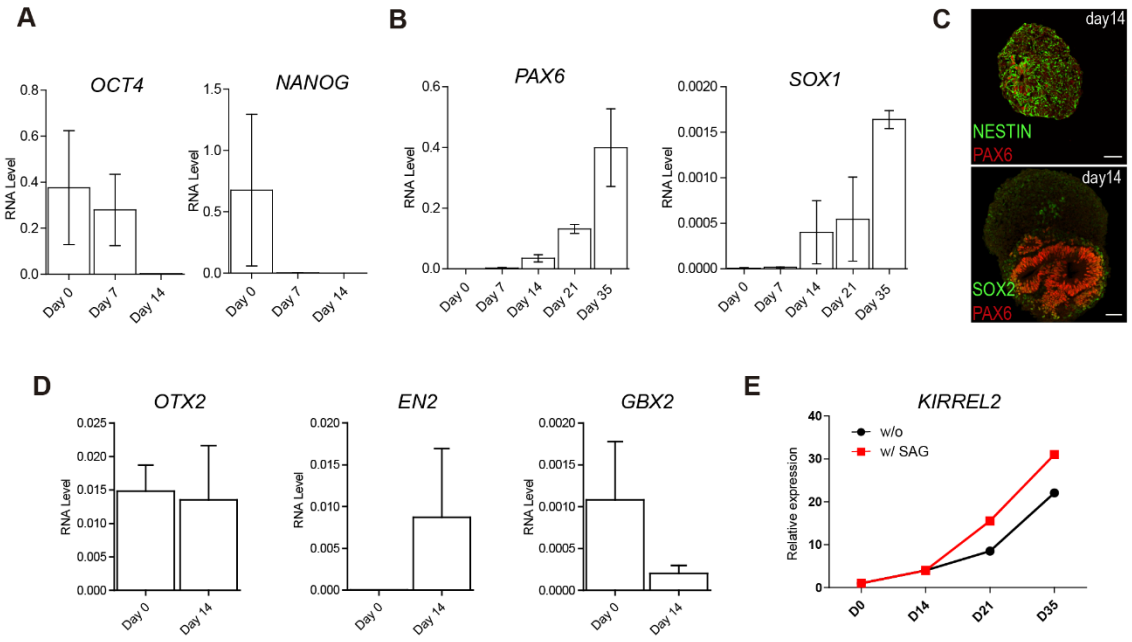

Figure III.2. Efficient neural induction and cerebellar commitment. qRT-PCR analysis of *OCT4* (**A**), *NANOG* (**A**), *PAX6* (**B**), *SOX1* (**B**), *OTX2* (**D**), *EN2* (**D**), and *GBX*2 (**D**) mRNA levels relative to *GAPDH* levels at different time-points. **C)** Immunofluorescence for NESTIN, PAX6, NCAD and SOX2 on day 14 of differentiation. Scale bars, 50µm. **E)** qRT-PCR analysis of *KIRREL2* mRNA levels, normalized to *GAPDH* levels and relative to day 0, at different time-points.

In order to verify if the initial neuroepithelial caudalization was not affected, we further investigated the gene expression for distinct markers expressed along rostral-caudal (R-C) axis of the neural tube, before starting specification along D-V direction. Indeed, qRT-PCR analysis showed that an efficient mid-hindbrain patterning was already achieved by day 14 (**Figure III.2-D**). While the expression of a midbrain and rostral hindbrain marker *EN2* (Joyner, 1996) was enhanced, *OTX2* and *GBX2* mRNA levels remained low at day 14 of differentiation (**Figure III.2-D**), denoting insignificant commitment to caudal forebrain and rostral hindbrain fates, respectively (Simeone et al., 1992; Wassarman et al., 1997). Thus, the addition of SAG to culture do not affect cerebellar commitment. Gene expression

analysis revealed that *KIRREL2* transcript, which is a marker of cerebellar territory (Mizuhara et al., 2010), was up-regulated during differentiation, with higher expression at day 35 (**Figure III.2-E**). A slightly increased expression was observed in organoids treated with SAG when compared with non-treated organoids from day 14 (**Figure III.2-E**), consistent with an effective ventral commitment, since KIRREL2 is expressed in cerebellar GABAergic progenitors (Mizuhara et al., 2010).

Generation of Purkinje cell progenitors upon enhanced SHH signaling

Following an efficient neural induction and mid-hindbrain patterning, we investigated the impact of SHH signaling modulation on the generation of Purkinje cell progenitors. OLIG2 protein is expressed during Purkinje cell specification in the cerebellar ventricular zone, representing a marker for neurogenic progenitors and nascent neurons (Ju et al., 2016; Seto et al., 2014). Other important transcriptional regulator of Purkinje cell development is CORL2 (also called SKOR2), selectively expressed in Purkinje cell lineage during embryonic development and afterwards in Purkinje cells during adult stages (Minaki et al., 2008; Nakatani et al., 2014). Gene expression analysis demonstrated that SAG addition promoted an enhanced expression of both *OLIG2* and *CORL2* transcripts when compared with non-treated organoids, on day 21 of differentiation (**Figure III.3-A**). Later on, *OLIG2* mRNA levels continued to increase until day 35 in SAG condition, being lower in the non-treated condition (**Figure III.3-A**). Oppositely, *CORL2* mRNA levels started to decrease after achieving the maximum level of expression on day 21, attaining by day 35 almost the same level of expression detected in organoids without ventral differentiation (**Figure III.3-A**). Immunostaining analysis confirmed the enhanced expression of OLIG2 in SAG treated-organoids (**Figure III.3-B**). Whereas in non-treated organoids few $OLIG2^{+}$ cells were found

dispersed within the human iPSC-derived organoids, a compact layer of OLIG2^{+} progenitors was produced under SHH signaling stimulation (**Figure III.3-B**).

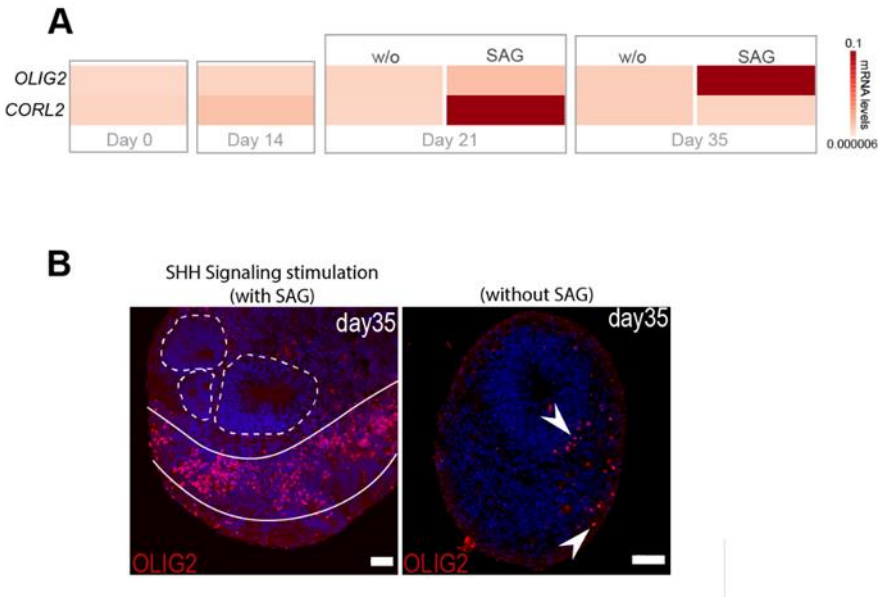

Figure III.3. Ventral patterning by SAG treatment. A) Temporal ClustVis analysis of qRT-PCR of *OLIG2 and CORL2* mRNA levels relative to *GAPDH* at the indicated time-points and conditions. **B)** Immunofluorescence for OLIG2 on day 35 of differentiation. Scale bars, 50µm.

As it was reported that SDF1 can induce a moderate dorsalization in the human PSC-derived neuroepithelium (Muguruma et al., 2015), we further attempted to detect distinct dorsal and ventral cerebellar progenitors by immunostaining at day 28 of differentiation, before adding SDF1 to culture. Modulation of SHH signaling induced the generation of OLIG2^{+} precursors in human iPSC-derived organoids (**Figure III.4**). Two different structural organization were observed in SAG-treated organoids. First, multiple flat-oval structures were detected, some of them expressing OLIG2, which formed a layer around the luminal side (**Figure III.4-A**). Second, some aggregates exhibited a continuous neuroepithelium with a dense layer of OLIG2^{+} progenitors on the surface of the organoid (**Figure III.4-B**).

Furthermore, polarized structures appeared in this last set of organoids, where a strong signal of the apical marker N-cadherin (NCAD) was detected on the superficial side of aggregates suggesting that it corresponds to the apical side of the neuroepithelium (**Figure III.4-B**). Consistent with these results, a dense layer $SOX2^+$ and $PAX6^+$ proliferative progenitors was detected on the organoid surface (apical side, **Figure III.4-C and D**). The OLIG2, which is expressed in cerebellar ventricular proliferating cells and particularly Purkinje progenitors (Ju et al., 2016), was found in the same layer of $SOX2^+$ cells, also suggesting the presence of mitotic progenitors (**Figure III.4-C**). On the other hand, post-mitotic neurons were located on the basal side, confirmed by the presence of few cells expressing BARHL1 located basally to proliferating progenitors (**Figure III.4-C**). Also, a weak staining for the neuronal marker $MAP2^+$ was detected inside of the organoid, in the basal compartment (**Figure III.4-D**). These results suggest that an efficient ventralization, as well as the development of a large structured neuroepithelium, can be achieved by enhancing SHH signaling.

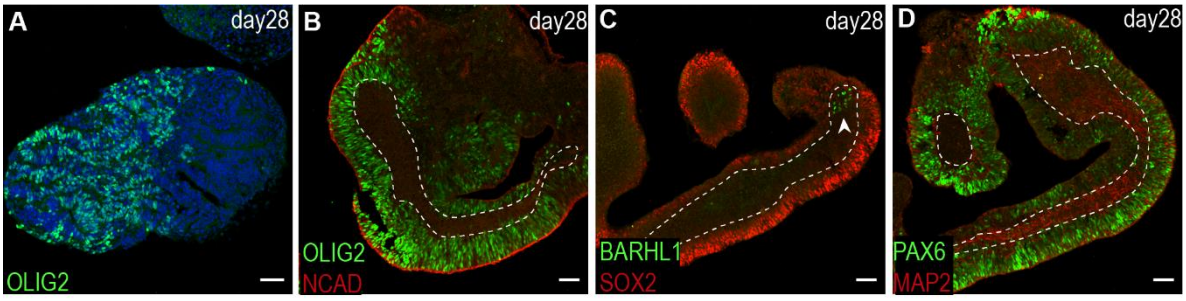

Figure III.4. Analysis of SAG treatment at day 28. Immunofluorescence for OLIG2, NCAD, BARHL1, SOX2, PAX6 and MAP2. Scale bars, 50µm.

5-HT treatment supports Purkinje cell survival during ventral cerebellar maturation

As 5-HT expression has been reported to have an important role in Purkinje cell maturation, stimulating dendritic growth and synapse formation (Oostland and van Hooft, 2013; Oostland et al., 2013), we evaluated the effect of 5-HT during the maturation process in our cultures, after early cerebellar specification. For that, cultures treated with SAG were afterwards exposed to 5-HT (**Figure III.5**). It was demonstrated that while lower concentration of 5-HT (2-20µM) increased dendrite formation in Purkinje cells from rat organotypic cultures along all cerebellar lobes, higher 5-HT concentrations of serotonin (20µM) conduced to decreased dendritic branches in Purkinje cells from anterior lobes (Kondoh et al., 2004). In order to avoid the inhibitory effect of 5-HT in some cerebellar lobes, the lower concentration (2µM) was used in our culture. In addition to concentration-dependent effect, also the temporal exposure can affect 5-HT action, presenting an inhibitory effect on dendritic growth in Purkinje cells from rat organotypic cultures after 7 days *in vitro* (Kondoh et al., 2004). Thus, we next evaluated as well the temporal effect of 5-HT treatment in cultures that were not treated with SAG (**Figure III.5**).

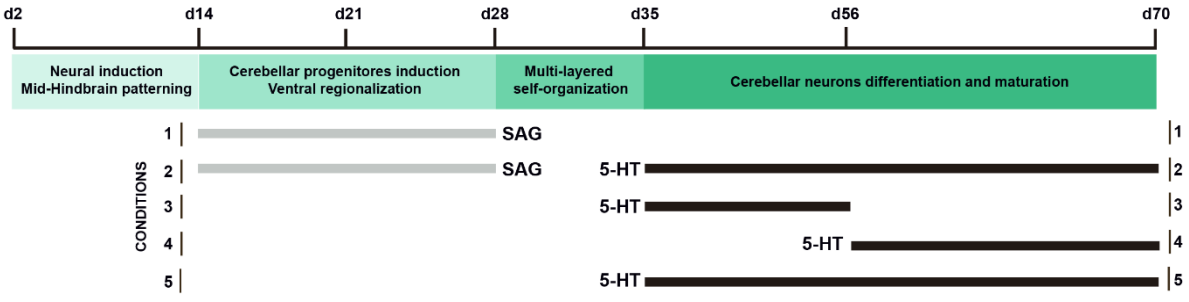

Figure III.5. Schematic strategy employed for inducing ventral commitment and manipulating Purkinje cell maturation.

As shown in **Figure III.6**, RNA levels for some markers of GABAergic neuronal subtype, including *GAD67* (enzyme converting glutamate into GABA), *PARVALBUMIN* (calcium-binding protein expressed in GABAergic interneurons) and *NEUROGRANIN* (calmodulin-binding protein expressed in Golgi cells), were increased by day 56 of differentiation in cells previously treated with SAG. Oppositely, *GAD65* (another glutamate-to-GABA converting enzyme), *L7* and *GRID2* (Purkinje cell-specific markers) were unaltered when compared with day 0. However, by day 70, the expression of the up-regulated markers in SAG condition returned to their initial levels, similar to day 0. This can be explained by a high neuronal cell death observed in this condition by day 70, suggesting that SAG-derived cells expressing these GABAergic markers were not able to survive until later stages.

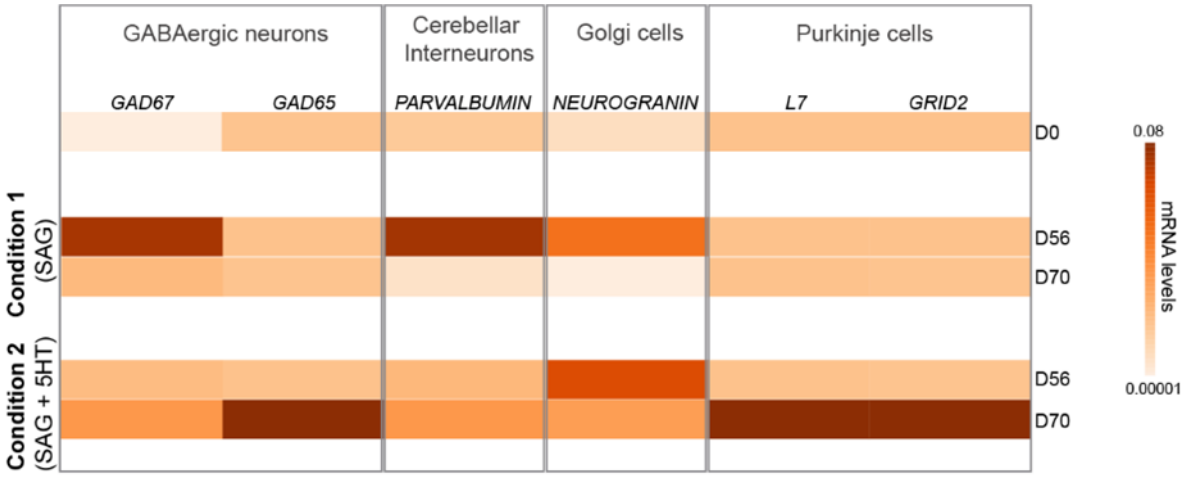

Figure III.6. Effect of 5-HT exposure in SAG-treated cell. Temporal ClustVis analysis of qRT-PCR of *GAD67*, *GAD65*, *PARVALBUMNIN*, *NEUROGRANIN*, *L7* and *GRID2* mRNA levels were relative to *GAPDH* at the indicated time-points and conditions.

In contrast, cells that were previously cultured with a SHH agonist and afterwards treated with 5-HT showed an up-regulation of mRNA levels for all GABAergic neuronal subtypes at day 70 (**Figure 3.6**), with a most prominent expression of *GAD65, L7* and *GRID2*

transcripts, demonstrating the presence of Purkinje cells at this time-point. Therefore, these results suggest that culturing SAG-treated neural progenitors with 5-HT during maturation stimulation can lead to increasing survival of GABAergic cerebellar neurons, particularly Purkinje cells.

Enhanced expression of Purkinje cell-specific markers in cerebellar progenitors exposed to 5-HT during maturation progression

To investigate whether 5-HT has any effect on Purkinje cell maturation, cerebellar progenitors generated from the standard protocol, reported in the previous chapter, were maturated by using Brainphys™ supplemented with BDNF and GDNF, and 5-HT was added to culture at different time-points (between 35-56, 56-70 and 35-70 days).

On day 56, we evaluated the action of 5-HT on the dendrite formation of Purkinje cells generated from organoid-derived cerebellar progenitors. By immunofluorescence analysis, no evident differences between non-treated and 5-HT-treated neurons were observed (**Figure III.7-A**). In both conditions, an efficient neuronal maturation was detected demonstrated by the presence of a pre-synaptic marker SYNAPSIN1 immunoreactive puncta distributed along the $GAD65^+$ dendrites (**Figure III.7-A**), suggesting the formation of GABAergic synaptic connections. Furthermore, Purkinje cells positively stained for calbindin (CALB) presenting the formation of dendritic branches, as well as a dense network of $CALB^+$ neurons, were detected in both cultures (**Figure III.7-A**). Although no differences were detected by immunostaining, further qRT-PCR analysis revealed that all GABAergic transcripts were highly expressed in 5HT-treated neurons, in comparison with non-treated neurons (**Figure III.7-B**), with the exception of *L7* RNA levels that were similar to both cases. Therefore, 5-HT treatment may potentially generate more GABAergic neurons. Even though no differences in L7 expression was detected, *GRID2* mRNA levels were higher in 5-HT-

treated cells (**Figure III.7-B**), suggesting that 5-HT may not be effective in Purkinje cell generation, but can stimulate Purkinje cell maturation, since GRID2 is an ionotropic glutamate receptor specifically expressed in spines of mature Purkinje cells, responsible for synapse formation and maintenance (Ichikawa et al., 2016; Yawata et al., 2006).

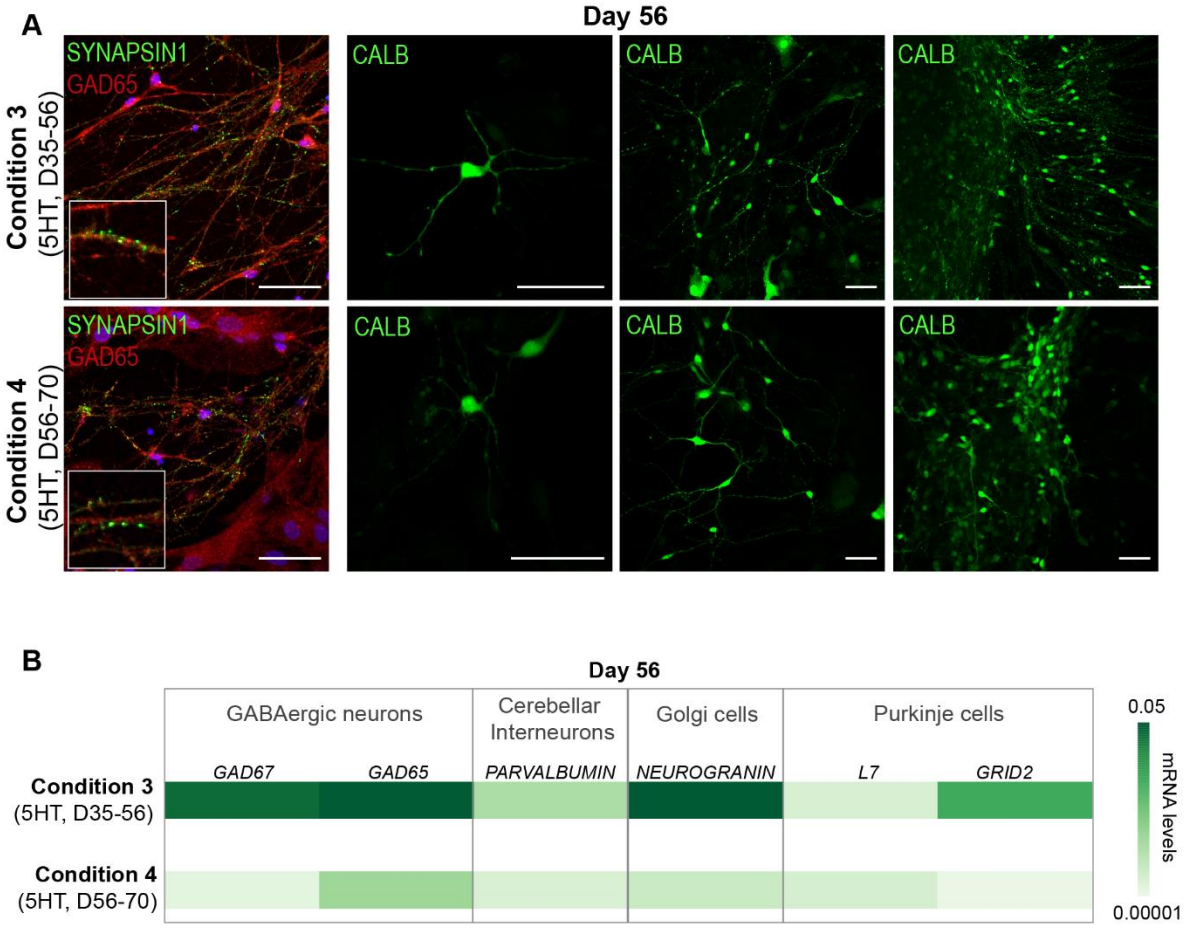

Figure III.7. Effect of 5-HT in Purkinje cell differentiation. A) Immunofluorescence for SYNAPSIN1, GAD65 and CALB on day 56 of differentiation. Scale bars, 50µm. **B)** Temporal ClustVis analysis of qRT-PCR of *GAD67*, *GAD65*, *PARVALBUMNIN*, *NEUROGRANIN*, *L7* and *GRID2* mRNA levels were relative to *GAPDH* on day 56 of differentiation at the indicated conditions.

By day 70 of differentiation, after 35 days in maturation medium, we evaluated the effect of different temporal exposures to 5-HT in Purkinje cell differentiation and maturation. No differences were detected in immunofluorescence using a CALB antibody between distinct temporal treatments (**Figure III.8-A**). All conditions exhibited neuronal network formation by neurons expressing CALB, demonstrating the presence of Purkinje cell on day 70 (**Figure III.8-A**). Nevertheless, qRT-PCR analysis for general GABAergic markers, as well as specific markers for distinct GABAergic cerebellar subtypes revealed that treatment with 5-HT at different time-points was able to induce differential gene expression (**Figure III.8-B**). The RNA levels of the majority of GABAergic markers appeared to be increased in condition 5, where 5-HT was added to culture during all maturation protocol (**Figure III.8-B**). In particular, expression of Purkinje cell markers was enhanced when 5-HT was present from day 35 until day 70 of differentiation. *L7* transcript was more expressed in conditions 3 and 5, corresponding to 5-HT treatment in the initial stages of maturation and during all maturation process, respectively (**Figure III.8-B**). Oppositely, the addition of 5-HT at later maturation stages did not seem to enhance Purkinje cell differentiation (**Figure III.8-B**). Although condition 3 and 5 were similar in terms of *L7* transcripts, in condition 5 mRNA levels for *GRID2* were much higher than condition 3, suggesting that the initial exposure is important for Purkinje cell differentiation, while the later exposure favors the maturation of previously generated Purkinje cells (**Figure III.8-B**).

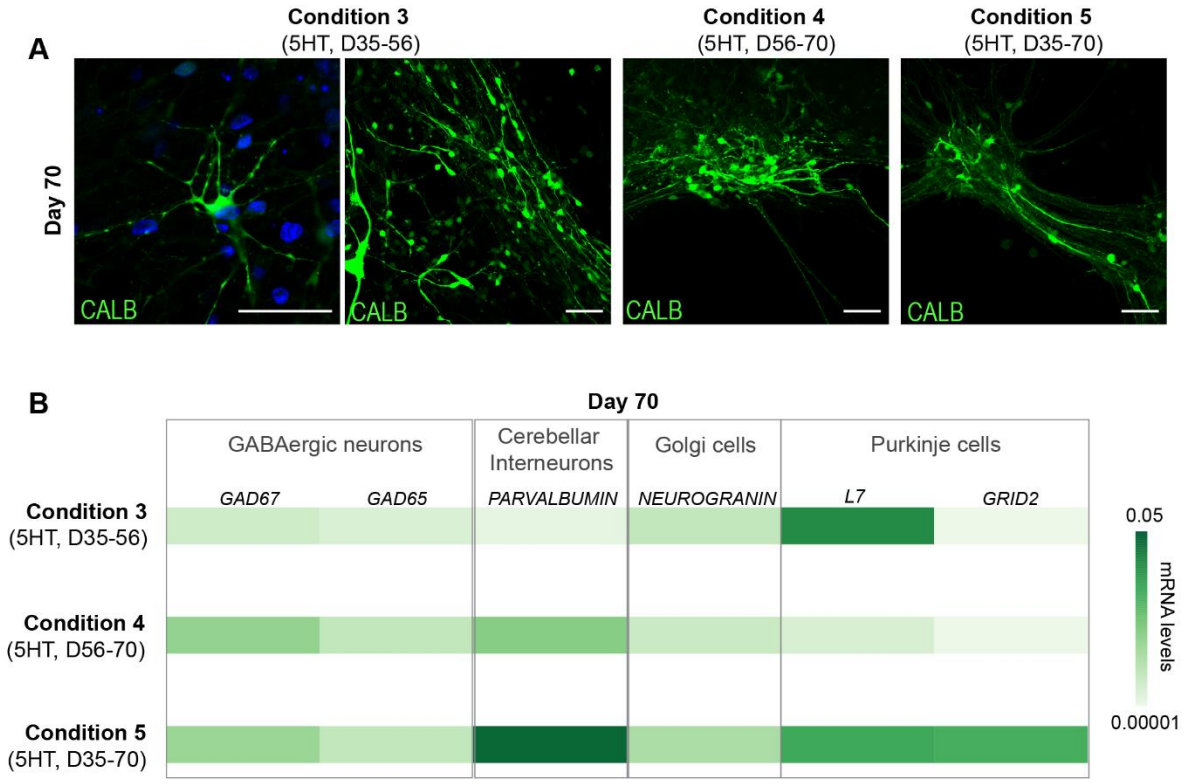

Figure III.8. Effect of different temporal exposures to 5-HT in Purkinje cell differentiation and maturation. **A)** Immunofluorescence for CALB on day 70 of differentiation. Scale bars, 50µm. **B)** Temporal ClustVis analysis of qRT-PCR of *GAD67*, *GAD65*, *PARVALBUMNIN*, *NEUROGRANIN, L7* and *GRID2*. mRNA levels were relative to GAPDH on day 70 of differentiation at the indicated conditions.

In conclusion, 5-HT treatment at the initial stages of maturation seems to be important for the establishment of a Purkinje cell population but is not sufficient to promote an efficient maturation. Exposure of 5-HT at later stages of maturation can lead to higher expression of general GABAergic markers and other GABAergic cerebellar neurons, like interneurons (PARVALBUMIN^{+}), but is tardily to promote Purkinje cell differentiation. Lastly, by adding 5-HT during all maturation process, not only the establishment of Purkinje cell population seems to be enhanced but also the maturation of generated Purkinje cells.

III.5 DISCUSSION

The majority of neurons in the human CNS are found in the cerebellum, since it contains 60 billion of granule cells representing more than all other brain neurons combined (Wagner et al., 2017). Moreover, cerebellum is characterized by a well-defined structure composed by diverse neuronal subtypes (Hoshino, 2012; Marzban et al., 2015; White and Sillitoe, 2013). These distinct cerebellar neurons were already successfully obtained from human PSC, as well as their use to model cerebellar dysfunction was also reported (Erceg et al., 2012; Ishida et al., 2016; Muguruma et al., 2015; Salero and Hatten, 2007; Su et al., 2006; Tao et al., 2010; Wang et al., 2015). Although cerebellar disorders are phenotypically heterogeneous, in which different types of cerebellar neurons are degenerated, Purkinje cells seem to be particularly affected (Taroni and DiDonato, 2004). Therefore, some groups have attempted to generate Purkinje cells from PSCs, but with low differentiation efficacies and high variability associated with feeder cell sources, used to promote their maturation (Muguruma et al., 2015; Su et al., 2006; Tao et al., 2010; Wang et al., 2015). Here, we presented evidences that the manipulation of SHH signaling during cerebellar commitment can increase the number of generated Purkinje cell progenitors ($OLIG2^{+}$). Furthermore, simultaneous treatment with 5-HT and maturation of cerebellar progenitors, under defined and feeder-free conditions, can enhance the expression of *L7* and *GRID2*, suggesting that 5-HT is able to support Purkinje cell differentiation and maturation.

The oligodendrocyte transcription factor OLIG2, was first identified in spinal cord and has a critical function in oligodendrocyte development (Park et al., 2002; Zhou et al., 2000). Nonetheless, it is known that OLIG2 is involved not only in oligodendrocyte specification but also in the development of some types of neurons, including motor neurons and Purkinje cells (Ju et al., 2016; Mizuguchi et al., 2001; Seto et al., 2014). During cerebellar development, OLIG2 is transiently expressed in the cerebellar ventricular zone (VZ), in both

proliferating VZ progenitors and newborn neurons, during Purkinje cell specification (Ju et al., 2016; Seto et al., 2014). Strong evidences suggest that SHH represents an important regulator of early stages of oligodendrocyte specification (Lu et al., 2000; Wang and Almazan, 2016). However, the use of SHH in combination with the dual-SMAD inhibitors, SB431542 and LDN193189, failed to efficiently generate oligodendrocytes from PSCs (Rodrigues et al., 2017). To efficiently produce $OLIG2^+$ oligodendrocyte progenitors, a combination of SHH and retinoic acid (RA) is essential (Rodrigues et al., 2017), since RA promotes a robust caudalization of the neuroepithelium (Okada et al., 2004) that is required to spinal cord commitment and further oligodendrocyte differentiation. Therefore, to ensure that most of $OLIG2^+$ cells that were generated in our differentiation protocol belong to cerebellar lineage, we proceeded to neural induction and stimulated mid-hindbrain patterning before modulating SHH signaling to promote the ventral commitment in the generated cerebellar progenitors. Indeed, an effective mid-hindbrain patterning was achieved before adding SAG to our culture system as well as an efficient cerebellar commitment. Besides that, the expression of *GBX2*, a hindbrain marker, was up-regulated at day 14 of differentiation, suggesting that spinal cord together with oligodendrocyte progenitors could not be obtained in our differentiation protocol.

During the generation of cerebellar progenitors, addition of SAG to the culture promoted an increased expression of *OLIG2* by day 21, which was maintained and peaked at day 35. On the other hand, *CORL2* was highly expressed at day 21 of differentiation, significantly increased in SAG-treated cells, but declining thereafter reaching an expression level similar to non-treated cells. Indeed, it was already reported that SDF1 treatment during cerebellar differentiation of human PSC leads to a significant down-regulation of ventral marker genes, suggesting to have a moderate dorsalizing effect (Muguruma et al., 2015). Although only a slight decrease of *CORL2* RNA levels, without significant differences between SDF1-treated and non-treated organoids, was promoted by SDF1 (Muguruma et

al., 2015), further studies are required to understand the effect of SDF1 in the cultures previously treated with SAG. Despite the presence of SDF1, the *OLIG2* levels were maintained high after SAG treatment until the end of organoid generation, and Purkinje cell differentiation was observed afterwards. While it was demonstrated that OLIG2 is required for a complete specification of Purkinje cells (Ju et al., 2016), CORL2 seems to be dispensable for initial specification of Purkinje cell fate (Nakatani et al., 2014), which explains the normal Purkinje cell generation even with reduced levels of *CORL2* at day 35. Moreover, the combination of FGF19 and SAG appeared to be sufficient to generate continuous cerebellar neuroepithelium, creating a dense layer of $OLIG2^{+}$ progenitors by day 28. Most likely 28 days in culture are sufficient for a robust production of Purkinje cell progenitors and SDF1 may not be required in this ventral cerebellar differentiation, a hypothesis that needs additional verification.

During the maturation protocol, we observed that organoids previously treated with SAG failed to generate mature Purkinje cells, most probably due to a low neuronal survival at later stages of maturation. It is known that Granule cells are potent regulators of Purkinje cell development, being able to initiate Purkinje cell differentiation (Hirai and Launey, 2000; Morrison and Mason, 1998). Moreover, when a pure population of Purkinje cells was isolated, they exhibited poor survival and differentiation, being rescued only by co-culturing with granule neurons, which promoted their survival and dendritic development (Baptista et al., 1994; Morrison and Mason, 1998). At previous stages of differentiation, we detected only a few cells staining for BARHL1 expressed in granular cell progenitors. It is likely that the ventralizing effect of SAG induced low generation of granule cell progenitors and thus granule neurons were not present during the maturation. Therefore, without granule neurons, Purkinje cells were not able to survive and differentiate. However, 5-HT treatment was capable of increasing Purkinje cell survival and differentiation, after the initial SAG-induced commitment. Indeed, it was reported that the 5-HT receptor expression by Granular

cells correlates with the expression patterns of these receptors in Purkinje cells during cerebellar development (Daval et al., 1987; Matthiessen et al., 1992, 1993; Miquel et al., 1994). It was proposed that, during the first postnatal week, Purkinje cell dendritic growth and formation is stimulated by the activation of 5-HT receptors expressed by both cell types (Oostland and van Hooft, 2013). Therefore, the addition of 5-HT to our cultures can mimic to some extent what happens in this cell-cell interaction process.

Furthermore, the addition of 5-HT to re-plated cells originated from cerebellar organoids stimulated an enhanced expression of Purkinje cell-specific markers, L7 and GRID2. During cerebellar development, 5-HT also stimulates dendritic growth of Purkinje cells, as well as synapse formation. Besides that it ensures the Purkinje cell synaptic plasticity and stabilization (Oostland and van Hooft, 2013). Therefore, further studies are needed to evaluate the effect of 5-HT on the development of morphological features of Purkinje cells and to investigate its effect on the functionality of the generated neurons. In addition to Purkinje cells, also the expression of other markers of GABAergic neurons were stimulated by 5-HT, including *PARVALBUMIN* and *NEUROGRANIN*. Based on the expression of 5-HT in both Golgi cells and molecular layer interneurons, it is expected that 5-HT treatment can support the development of all these types of cerebellar neurons (Geurts et al., 2002).

In conclusion, we reported important findings for the generation of higher amounts of cerebellar GABAergic neurons by manipulation SHH signaling. A more efficient Purkinje cell differentiation and maturation can be achieved by stimulating 5-HT receptors during the maturation process. Thus, a more robust and efficient differentiation of Purkinje cells can be obtained, which is the most important subtype of cerebellar neurons involved in cerebellum degeneration, providing a valuable cell source for modeling cerebellar disorders.

III.6 REFERENCES

Andoh-Noda, T., Akamatsu, W., Miyake, K., Matsumoto, T., Yamaguchi, R., Sanosaka, T., Okada, Y., Kobayashi, T., Ohyama, M., Nakashima, K., et al. (2015). Differentiation of multipotent neural stem cells derived from Rett syndrome patients is biased toward the astrocytic lineage. Mol. Brain 8, 31.

Aubry, L., Bugi, A., Lefort, N., Rousseau, F., Peschanski, M., and Perrier, A.L. (2008). Striatal progenitors derived from human ES cells mature into DARPP32 neurons in vitro and in quinolinic acid-lesioned rats. Proc. Natl. Acad. Sci. 105, 16707–16712.

Baptista, C. a, Hatten, M.E., Blazeski, R., and Mason, C. a (1994). Cell-cell interactions influence survival and differentiation of purified Purkinje cells in vitro. Neuron 12, 243–260.

Briscoe, J., and Ericson, J. (1999). The specification of neuronal identity by graded Sonic Hedgehog signalling. Semin Cell Dev Biol 10, 353–362.

Burridge, P.W., Thompson, S., Millrod, M.A., Weinberg, S., Yuan, X., Peters, A., Mahairaki, V., Koliatsos, V.E., Tung, L., and Zambidis, E.T. (2011). A universal system for highly efficient cardiac differentiation of human induced pluripotent stem cells that eliminates interline variability. PLoS One 6, e18293.

Chen, J.K., Taipale, J., Young, K.E., Maiti, T., and Beachy, P.A. (2002). Small molecule modulation of Smoothened activity. Proc. Natl. Acad. Sci. 99, 14071–14076.

Chiang, C., Litingtung, Y., Lee, E., Young, K.E., Corden, J.L., Westphal, H., and Beachy, P.A. (1996). Cyclopia and defective axial patterning in mice lacking Sonic hedgehog gene function. Nature 383, 407–413.

Daval, G., Vergé, D., Becerril, A., Gozlan, H., Spampinato, U., and Hamon, M. (1987). Transient expression of 5-HT1A receptor binding sites in some areas of the rat CNS during postnatal development. Int. J. Dev. Neurosci. 5, 171–180.

Erceg, S., Lukovic, D., Moreno-Manzano, V., Stojkovic, M., and Bhattacharya, S.S. (2012). Derivation of Cerebellar Neurons from Human Pluripotent Stem Cells. In Current Protocols in Stem Cell Biology, (Hoboken, NJ, USA: John Wiley & Sons, Inc.), chapter 1.

Fernandes, T.G., Duarte, S.T., Ghazvini, M., Gaspar, C., Santos, D.C., Porteira, A.R., Rodrigues, G.M.C., Haupt, S., Rombo, D.M., Armstrong, J., et al. (2015). Neural commitment of human pluripotent stem cells under defined conditions recapitulates neural development and generates patient-specific neural cells. Biotechnol. J. 10, 1578–1588.

Fischer, T., Faus-Kessler, T., Welzl, G., Simeone, A., Wurst, W., and Prakash, N. (2011). Fgf15-mediated control of neurogenic and proneural gene expression regulates dorsal midbrain neurogenesis. Dev. Biol. 350, 496–510.

Geurts, F.J., De Schutter, E., and Timmermans, J.P. (2002). Localization of 5-HT2A, 5-HT3, 5-HT5A and 5-HT7 receptor-like immunoreactivity in the rat cerebellum. J. Chem. Neuroanat. 24, 65–74.

Gimeno, L., and Martinez, S. (2007). Expression of chick Fgf19 and mouse Fgf15 orthologs is regulated in the developing brain by Fgf8 and Shh. Dev. Dyn. 236, 2285–2297.

Gunhanlar, N., Shpak, G., van der Kroeg, M., Gouty-Colomer, L.A., Munshi, S.T., Lendemeijer, B., Ghazvini, M., Dupont, C., Hoogendijk, W.J.G., Gribnau, J., et al. (2018). A

simplified protocol for differentiation of electrophysiologically mature neuronal networks from human induced pluripotent stem cells. Mol. Psychiatry 23, 1336–1344.

Hirai, H., and Launey, T. (2000). The regulatory connection between the activity of granule cell NMDA receptors and dendritic differentiation of cerebellar Purkinje cells. J. Neurosci. 20, 5217–5224.

Hoshino, M. (2012). Neuronal subtype specification in the cerebellum and dorsal hindbrain. Dev. Growth Differ. 54, 317–326.

Hu, B.-Y., and Zhang, S.-C. (2009). Differentiation of spinal motor neurons from pluripotent human stem cells. Nat. Protoc. 4, 1295–1304.

Ichikawa, R., Sakimura, K., and Watanabe, M. (2016). GluD2 Endows Parallel Fiber-Purkinje Cell Synapses with a High Regenerative Capacity. J. Neurosci. 36, 4846–4858.

Imaizumi, Y., and Okano, H. (2014). Modeling human neurological disorders with induced pluripotent stem cells. J. Neurochem. 129, 388–399.

Imaizumi, Y., Okada, Y., Akamatsu, W., Koike, M., Kuzumaki, N., Hayakawa, H., Nihira, T., Kobayashi, T., Ohyama, M., Sato, S., et al. (2012). Mitochondrial dysfunction associated with increased oxidative stress and α-synuclein accumulation in PARK2 iPSC-derived neurons and postmortem brain tissue. Mol. Brain 5, 35.

Ishida, Y., Kawakami, H., Kitajima, H., Nishiyama, A., Sasai, Y., Inoue, H., and Muguruma, K. (2016). Vulnerability of Purkinje Cells Generated from Spinocerebellar Ataxia Type 6 Patient-Derived iPSCs. Cell Rep. 17, 1482–1490.

J Siney, E., Kurbatskaya, K., Chatterjee, S., Prasannan, P., Mudher, A., and Willaime-Morawek, S. (2018). Modelling neurodegenerative diseases in vitro: Recent advances in 3D iPSC technologies. AIMS Cell Tissue Eng. 2, 1–23.

Joyner, A.L. (1996). Engrailed, Wnt and Pax genes regulate midbrain-hindbrain development. Trends Genet. 12, 15–20.

Ju, J., Liu, Q., Zhang, Y., Liu, Y., Jiang, M., Zhang, L., He, X., Peng, C., Zheng, T., Lu, Q.R., et al. (2016). Olig2 regulates Purkinje cell generation in the early developing mouse cerebellum. Sci. Rep. 6, 30711.

Junghyun Jo, A., Xiao, Y., Xuyang Sun, A., King Tan, E., Shawn Je, H., and Ng, H.-H. (2016). Midbrain-like Organoids from Human Pluripotent Stem Cells Contain Functional Dopaminergic and Neuromelanin-Producing Neurons. 1–10.

Keller, B., and Heinrichs, I. (1975). [Acoustic diagnosis of accessory lung]. Z. Kardiol. 64, 687–690.

Kondoh, M., Shiga, T., and Okado, N. (2004). Regulation of dendrite formation of Purkinje cells by serotonin through serotonin1A and serotonin2A receptors in culture. Neurosci. Res. 48, 101–109.

Lim, R.G., Quan, C., Reyes-Ortiz, A.M., Lutz, S.E., Kedaigle, A.J., Gipson, T.A., Wu, J., Vatine, G.D., Stocksdale, J., Casale, M.S., et al. (2017). Huntington's Disease iPSC-Derived Brain Microvascular Endothelial Cells Reveal WNT-Mediated Angiogenic and Blood-Brain Barrier Deficits. Cell Rep. 19, 1365–1377.

Liu, L., Huang, J.-S., Han, C., Zhang, G.-X., Xu, X.-Y., Shen, Y., Li, J., Jiang, H.-Y., Lin, Z.-C., Xiong, N., et al. (2016). Induced Pluripotent Stem Cells in Huntington's Disease: Disease Modeling and the Potential for Cell-Based Therapy. Mol. Neurobiol. 53, 6698–6708.

Lu, Q.R., Yuk, D.I., Alberta, J.A., Zhu, Z., Pawlitzky, I., Chan, J., McMahon, A.P., Stiles, C.D., and Rowitch, D.H. (2000). Sonic hedgehog-regulated oligodendrocyte lineage genes encoding bHLH proteins in the mammalian central nervous system. Neuron 25, 317–329.

Martínez, S., Puelles, E., Puelles, L., and Echevarria, D. (2012). Molecular Regionalization of the Developing Neural Tube. In The Mouse Nervous System, pp. 2–18.

Marzban, H., Bigio, M.R. Del, Alizadeh, J., Ghavami, S., Zachariah, R.M., and Rastegar, M. (2015). Cellular commitment in the developing cerebellum. 8, 1–26.

Matthiessen, L., Daval, G., Bailly, Y., Gozlan, H., Hamon, M., and Vergé, D. (1992). Quantification of 5-hydroxytryptamine1areceptors in the cerebellum of normal and X-irradiated rats during postnatal development. Neuroscience 51, 475–485.

Matthiessen, L., Kia, H.K., Daval, G., Riad, M., Hamon, M., and Verge, D. (1993). Immunocytochemical localization of 5-HT1A receptors in the rat immature cerebellum. Neuroreport 4, 763–766.

Metsalu, T., and Vilo, J. (2015). ClustVis: A web tool for visualizing clustering of multivariate data using Principal Component Analysis and heatmap. Nucleic Acids Res. 43, W566–W570.

Minaki, Y., Nakatani, T., Mizuhara, E., Inoue, T., and Ono, Y. (2008). Identification of a novel transcriptional corepressor, Corl2, as a cerebellar Purkinje cell-selective marker. Gene Expr. Patterns 8, 418–423.

Miquel, M.C., Kia, H.K., Boni, C., Doucet, E., Daval, G., Matthiessen, L., Hamon, M., and Verge, D. (1994). Postnatal development and localization of 5-HT1A receptor mRNA in rat forebrain and cerebellum. Brain Res Dev Brain Res 80, 149–157.

Mizuguchi, R., Sugimori, M., Takebayashi, H., Kosako, H., Nagao, M., Yoshida, S., Nabeshima, Y.I., Shimamura, K., and Nakafuku, M. (2001). Combinatorial roles of Olig2 and Neurogenin2 in the coordinated induction of pan-neuronal and subtype-specific properties of motoneurons. Neuron 31, 757–771.

Mizuhara, E., Minaki, Y., Nakatani, T., Kumai, M., Inoue, T., Muguruma, K., Sasai, Y., and Ono, Y. (2010). Purkinje cells originate from cerebellar ventricular zone progenitors positive for Neph3 and E-cadherin. Dev. Biol. 338, 202–214.

Morrison, M.E., and Mason, C.A. (1998). Granule neuron regulation of Purkinje cell development: striking a balance between neurotrophin and glutamate signaling. J. Neurosci. 18, 3563–3573.

Muguruma, K., Nishiyama, A., Kawakami, H., Hashimoto, K., and Sasai, Y. (2015). Self-Organization of Polarized Cerebellar Tissue in 3D Culture of Human Pluripotent Stem Cells. Cell Rep. 10, 537–550.

Nakatani, T., Minaki, Y., Kumai, M., Nitta, C., and Ono, Y. (2014). The c-Ski family member and transcriptional regulator Corl2/Skor2 promotes early differentiation of cerebellar Purkinje cells. Dev. Biol. 388, 68–80.

Nguyen, H.N., Byers, B., Cord, B., Shcheglovitov, A., Byrne, J., Gujar, P., Kee, K., Schüle, B., Dolmetsch, R.E., Langston, W., et al. (2011). LRRK2 mutant iPSC-derived da neurons demonstrate increased susceptibility to oxidative stress. Cell Stem Cell 8, 267–280.

Ochalek, A., Mihalik, B., Avci, H.X., Chandrasekaran, A., Téglási, A., Bock, I., Giudice, M. Lo, Táncos, Z., Molnár, K., László, L., et al. (2017). Neurons derived from sporadic Alzheimer's disease iPSCs reveal elevated TAU hyperphosphorylation, increased amyloid levels, and GSK3B activation. Alzheimer's Res. Ther. 9, 90.

Okada, Y., Shimazaki, T., Sobue, G., and Okano, H. (2004). Retinoic-acid-concentration-dependent acquisition of neural cell identity during in vitro differentiation of mouse embryonic stem cells. Dev. Biol. 275, 124–142.

Okano, H., and Yamanaka, S. (2014). IPS cell technologies: Significance and applications to CNS regeneration and disease. Mol. Brain 7, 22.

Oostland, M., and van Hooft, J.A. (2013). The role of serotonin in cerebellar development. Neuroscience 248, 201–212.

Oostland, M., Buijink, M.R., and van Hooft, J. a (2013). Serotonergic control of Purkinje cell maturation and climbing fibre elimination by 5-HT3 receptors in the juvenile mouse cerebellum. J. Physiol. 591, 1793–1807.

Park, H.C., Mehta, A., Richardson, J.S., and Appel, B. (2002). Olig2 is required for zebrafish primary motor neuron and oligodendrocyte development. Dev. Biol. 248, 356–368.

Park, I.-H., Arora, N., Huo, H., Maherali, N., Ahfeldt, T., Shimamura, A., Lensch, M.W., Cowan, C., Hochedlinger, K., and Daley, G.Q. (2008). Disease-specific induced pluripotent stem cells. Cell 134, 877–886.

Rodrigues, G.M.C., Gaj, T., Adil, M.M., Wahba, J., Rao, A.T., Lorbeer, F.K., Kulkarni, R.U., Diogo, M.M., Cabral, J.M.S., Miller, E.W., et al. (2017). Defined and Scalable Differentiation of Human Oligodendrocyte Precursors from Pluripotent Stem Cells in a 3D Culture System. Stem Cell Reports 8, 1770–1783.

Salero, E., and Hatten, M.E. (2007). Differentiation of ES cells into cerebellar neurons. Proc. Natl. Acad. Sci. U. S. A. 104, 2997–3002.

Seto, Y., Ishiwata, S., and Hoshino, M. (2014). Characterization of Olig2 expression during cerebellar development. Gene Expr. Patterns 15, 1–7.

Simeone, A., Acampora, D., Gulisano, M., Stornaiuolo, A., and Boncinelli, E. (1992). Nested expressiondomains of four homeobox genes in developing rostral brain. Nature 358, 687–690.

Su, H.L., Muguruma, K., Matsuo-Takasaki, M., Kengaku, M., Watanabe, K., and Sasai, Y. (2006). Generation of cerebellar neuron precursors from embryonic stem cells. Dev. Biol. 290, 287–296.

Takahashi, K., Tanabe, K., Ohnuki, M., Narita, M., Ichisaka, T., Tomoda, K., and Yamanaka, S. (2007). Induction of Pluripotent Stem Cells from Adult Human Fibroblasts by Defined Factors. Cell 131, 861–872.

Tao, O., Shimazaki, T., Okada, Y., Naka, H., Kohda, K., Yuzaki, M., Mizusawa, H., and Okano, H. (2010). Efficient generation of mature cerebellar Purkinje cells from mouse embryonic stem cells. J. Neurosci. Res. 88, 234–247.

Taroni, F., and DiDonato, S. (2004). Pathways to motor incoordination: the inherited ataxias. Nat. Rev. Neurosci. 5, 641–655.

Tiscornia, G., Vivas, E.L., and Belmonte, J.C.I. (2011). Diseases in a dish: Modeling human genetic disorders using induced pluripotent cells. Nat. Med. 17, 1570–1576.

Tomomura, M., Rice, D.S., Morgan, J.I., and Yuzaki, M. (2001). Purification of Purkinje cells by fluorescence-activated cell sorting from transgenic mice that express green fluorescent protein. Eur. J. Neurosci. 14, 57–63.

Wagner, M.J., Kim, T.H., Savall, J., Schnitzer, M.J., and Luo, L. (2017). Cerebellar granule cells encode the expectation of reward. Nature 544, 96–100.

Wang, L.-C., and Almazan, G. (2016). Role of Sonic Hedgehog Signaling in Oligodendrocyte Differentiation. Neurochem. Res. 41, 3289–3299.

Wang, S., Wang, B., Pan, N., Fu, L., Wang, C., Song, G., An, J., Liu, Z., Zhu, W., Guan, Y., et al. (2015). Differentiation of human induced pluripotent stem cells to mature functional Purkinje neurons. Sci. Rep. 5, 9232.

Wassarman, K.M., Lewandoski, M., Campbell, K., Joyner, A.L., Rubenstein, J.L., Martinez, S., Martin, G.R., Abbott, L., Jacobowitz, D., Acampora, D., et al. (1997). Specification of the anterior hindbrain and establishment of a normal mid/hindbrain organizer is dependent on Gbx2 gene function. Development 124, 2923–2934.

White, J.J., and Sillitoe, R. V. (2013). Development of the cerebellum: From gene expression patterns to circuit maps. Wiley Interdiscip. Rev. Dev. Biol. 2, 149–164.

Yang, J., Li, S., He, X.B., Cheng, C., and Le, W. (2016). Induced pluripotent stem cells in Alzheimer's disease: Applications for disease modeling and cell-replacement therapy. Mol. Neurodegener. 11, 39.

Yawata, S., Tsuchida, H., Kengaku, M., and Hirano, T. (2006). Membrane-proximal region of glutamate receptor delta2 subunit is critical for long-term depression and interaction with protein interacting with C kinase 1 in a cerebellar Purkinje neuron. J. Neurosci. 26, 3626–3633.

Zhou, Q., Wang, S., and Anderson, D.J. (2000). Identification of a novel family of oligodendrocyte lineage-specific basic helix-loop-helix transcription factors. Neuron 25, 331–343.

IV. SCALABLE GENERATION OF MATURE CEREBELLAR NEURONS FROM HUMAN INDUCED PLURIPOTENT STEM CELLS USING SINGLE-USE VERTICAL-WHEEL™ BIOREACTOR

IV.1 ABSTRACT

Human induced pluripotent stem cells (iPSCs) have great potential for disease modeling and provide a valuable source for regenerative approaches. However, generating human iPSC-derived models to study brain diseases remains a challenge. Previously, we described the long-term culture of cerebellar neuroepithelium formed from human iPSCs, recapitulating the early developmental events of the cerebellum. Additionally, an efficient maturation of re-plated cerebellar progenitors into distinct types of functional cerebellar neurons was also achieved under defined and feeder-free conditions. However, defining protocols that allow the production of large numbers of organoids and a high yield of mature neurons in these 3D culture systems is still difficult. We present a new approach for the reproducible and scalable generation of human iPSC-derived organoids under chemically defined conditions by using the novel PBS 0.1 (100 mL) Vertical-Wheel single-use bioreactors, in which organoids acquire cerebellar identity. In this system, human iPSC-derived organoids are able to mature into different cerebellar neurons and to survive for up to 3 months, without feeder layers.

Keywords: human induced pluripotent stem cells; cerebellar differentiation; scale-up; vertical-wheel bioreactors; feeder-free

IV.2 INTRODUCTION

The emergence of human pluripotent stem cells (PSCs) represents a promising tool for regenerative medicine and disease modeling, since this cell type can be differentiated into most of cell lineages of the human body (Takahashi et al., 2007; Thomson, 1998). Since their discovery, PSC differentiation using diverse approaches have been reported to model different diseases, including neurodegenerative disorders (Ishida et al., 2016; Lancaster et al., 2012; Liu and Zhang, 2010; Mariani et al., 2015). However, the reproducible generation of a desired neuronal type for disease modeling under defined conditions is still a challenge, aggravated by culture and line variability.

Until now, different methodologies have been reported to generate neural progenitors and functional neurons, starting either by monolayer culture or using embryoid bodies (EBs) (Amoroso et al., 2013; Boissart et al., 2013; Chambers et al., 2009; Eiraku et al., 2008; Hu and Zhang, 2009; Qu et al., 2014; Sasai et al., 2012). In a monolayer culture, a target differentiation is obtained producing homogeneous neural cell population (Chambers et al., 2009). However, it does not represent the human biological system because 3D structure is not recapitulated. Furthermore, the need for passaging neurons during the differentiation protocol, and the lack of evidence regarding the effect of this re-plating on the long-term viability and functionality of these cells makes it difficult to use this differentiation strategy to model neurodegenerative disorders (Chambers et al., 2009; Qu et al., 2014). In EB-based neural differentiation, a low efficiency was reported as well as the requirement of feeder layers to promote the survival of neurons in long-term cultures (Boulting et al., 2011; Hu and Zhang, 2009). Moreover, the EB cultures produce aggregates with variable size and shape, introducing low differentiation efficacies and variability both within the same experiment and between different experiments.

More recently, 3D cultures resembling the organ structure, including cerebral structures, were reported (Lancaster et al., 2012; Muguruma et al., 2015; Qian et al., 2018). The generation of these neural organoids from PSCs provides a valuable opportunity to model human development and neurodevelopmental disorders. In the reported protocols PSC-derived aggregates are produced by using a scaffold-free approach to generate controlled size and shape aggregates. However, this method is difficult to be applied for large scale production. To produce structures that are large enough to recapitulate tissue morphogenesis without the presence of necrosis inside the organoids, recent protocols rely upon the initial neural commitment in static conditions, with later transfer of hydrogel-embedded organoids to dynamic systems (Lancaster et al., 2012). Such approach may limit the potential scaling up of organoid production.

Previously, we reported the recapitulation of early cerebellar development in human iPSC-derived organoids and further maturation of cerebellar progenitors into functional cerebellar neurons after re-plating onto laminin-coated plates. In these conditions, when 3D structure is maintained, a more efficient generation of cerebellar neurons is achieved. Therefore, we decided to optimize culture conditions for 3D expansion and differentiation of human iPSCs into cerebellar neurons in single-use Vertical-Wheel agitated bioreactors (PBS Biotech's Vertical-Wheel™ Bioreactors). These novel vertical-wheel bioreactors were already successfully used for human mesenchymal stem cell and iPSC expansion (Rodrigues et al., 2018; Sousa et al., 2015), in which a large vertical impeller and a U-shaped bottom provide a more homogeneous shear distribution inside the bioreactor, allowing a gentle and uniform mixing and particle suspension with reduced power input and agitation speeds (Croughan et al., 2016). Here, we describe a new approach for the reproducible and scalable generation of neural organoids that adopt cerebellar identity and further maturation into cerebellar neurons under chemically defined and feeder-free conditions by using the novel PBS 0.1 (100 mL) Vertical-Wheel single-use bioreactors. In this system, an efficient

cell aggregation with shape and size-controlled aggregates can be obtained, which is important for a more homogeneous and efficient differentiation. Moreover, a larger amount of iPSC-derived aggregates can be generated without being excessively labor-intensive, achieving 431 ± 53.6 aggregates/mL at 24 hours after seeding. After differentiation, distinct types of cerebellar neurons can be generated, including Purkinje cells ($CALB^+$), granule cells ($PAX6^+/MAP2^+$), Golgi cells ($NRGN^+$), and deep cerebellar nuclei projection neurons ($TBR1^+$). These cells show signs of efficient maturation, changing intracellular Ca^{2+} concentration following KCl stimulation and exhibiting fire action potential upon current injection. In this system, human iPSC-derived organoids are able to mature into different cerebellar neurons and to survive for up to 3 months, without feeder layers, providing a novel source of human cerebellar neurons for disease modeling.

IV.3 METHODS

Maintenance of human iPSCs

We used two distinct human iPSC lines, F002.1A.13 and Gibco® Human Episomal iPSC line (iPSC6.2) (Burridge et al., 2011). Both human iPSCs were cultured on Matrigel™ (Corning)-coated plates with mTeSR™1 Medium (StemCell Technologies). Medium was changed daily. Cells were passaged every three to four days (when the colonies covered approximately 85% of the surface area of the culture dish) using 0.5mM EDTA dissociation buffer (Life Technologies). Two to three passages were performed before starting the differentiation protocol.

Generation, differentiation and maturation of human iPSC-derived aggregates using Vertical-Wheel Bioreactors

For single-cell inoculation, cells were incubated with ROCKi (Y-27632, 10μM, StemCell Technologies) for 1 h at 37ºC and then treated with accutase (Sigma) for 7 min at 37ºC. After dissociation, cells were cultured into PBS MINI 0.1L Vertical-Wheel Bioreactors (PBS Biotech, USA) at a density of 250 000 cells/mL in 60 mL of mTeSR™1 supplemented with 10μM ROCKi . To promote cell aggregation an agitation speed of 27 rpm was used. After 24 hours, full volume of the medium was replaced and aggregates were maintained in mTeSR™1 without ROCKi for another 24 hours at an agitation speed of 25 rpm.

Defining the day on which single-cell inoculation was performed as day 0, from day 2 to day 21 gfCDM was used as basal medium for the differentiation (Muguruma et al. 2015). This medium consists of Isocove's modified Dulbecco's medium/Ham's F-12 (Life Technology) 1:1, chemically defined lipid concentrate (1% v/v, Life Technology), monothioglycerol (450μM, Sigma), apo-transferrin (15μg/ml, Sigma), crystallization-purified

BSA (5mg/ml, >99%, Sigma) and 50U/ml penicillin/50µg/ml streptomycin (PS, Life Technology). The medium was also supplemented with insulin (7µg/ml, Sigma). Recombinant human basic FGF (FGF2, 50ng/ml, PeproTech) and SB431542 (SB, 10µM, Sigma) were added to culture on day 2. Full-volume medium replacement with gfCDM (supplemented with insulin, FGF2 and SB) was performed on day 5. On day 7, the agitation speed was changed to 30 rpm for both cell lines. Full volume of the medium was replaced and two-thirds of initial amount of FGF2 and SB was added. Recombinant human FGF19 (100ng/ml, PeproTech) was added to culture on day 14, and full-volume replacement with gfCDM (supplemented with insulin and FGF19) was performed on day 18. From day 21, the aggregates were cultured in BrainPhys™ Neuronal Medium (StemCell Technologies), supplemented with NeuroCult™ SM1 Neuronal Supplement (StemCell Technologies), N2 Supplement-A (StemCell Technologies) and PS. Full-volume replacement was performed every 7 days. Recombinant human SDF1 (300ng/ml, PeproTech) was added to culture on day 28.

After 35 days of differentiation, neuronal maturation was promoted by using BrainPhys™ Neuronal Medium (StemCell Technologies), supplemented with NeuroCult™ SM1 Neuronal Supplement (StemCell Technologies), N2 Supplement-A (StemCell Technologies), Recombinant Human Brain Derived Neurotrophic Factor (BDNF, PeproTech, 20ng/mL), Recombinant Human Glial-Derived Neurotrophic Factor (GDNF, PeproTech, 20ng/mL), dibutyryl cAMP (1mM, Sigma), and ascorbic acid (200nM, Sigma). One-third of the total volume was replaced every 3 days.

Aggregate size and biomass analysis

To monitor aggregate sizes throughout time in culture, several images were acquired at different time points using a Leica DMI 3000B microscope with a Nikon DXM 1200F digital

camera. The aggregate area was measured using ImageJ Software. Considering the aggregates as spheroids, diameters were calculated based on determined area according to the equation: $d = 2 \times \sqrt{\frac{A}{\pi}}$, in which *d* represents the diameter and *A* represents the area.

The homogeneity of aggregate size was evaluated by frequency distribution and measured by using the coefficient of variation (*Cv*), according to the equation: $Cv = {}^{\delta}/_{\mu}$, in which δ represents the standard deviation of aggregate diameter and μ is the average diameter.

To analyze the volume of biomass, volume was calculated based on determined diameter according to the equation: $V = \frac{4}{3} \times \pi \left(\frac{d}{2}\right)^3$. The number of aggregates was measured, and the volume of biomass was calculated and normalized to day 1.

Tissue preparation and Immunohistochemistry

Aggregates were fixed in 4% paraformaldehyde (PFA, Sigma) for 20 min at 4ºC followed by washing in Phosphate buffered saline (PBS, 0.1M) and overnight incubation in 15% (v/v) sucrose at 4ºC. Aggregates were embedded in 7.5%/15% (v/v) gelatin/sucrose and frozen in isopenthane at -80ºC. Twelve-µm sections were cut on a cryostat-microtome (Leica CM3050S, Leica Microsystems), collected on Superfrost™ Microscope Slides (Thermo Scientific) and stored at -20ºC. For immunostaining, sections were de-gelatinized for 45 min in PBS at 37ºC, incubated in 0.1 M Glycine (Millipore) for 10 min at room temperature (RT), permeabilized with 0.1% (v/v) Triton X-100 (Sigma) for 10 min at RT and blocked with 10% (v/v) fetal goat serum (FGS, Gibco) in TBST (20 mM Tris-HCl pH 8.0, 150 mM NaCl, 0.05 % v/v Tween-20, Sigma) for 30 min at RT. Sections were then incubated overnight at 4ºC with the primary antibodies diluted in blocking solution (**Table IV.1**). Secondary antibodies

were added to sections for 30 min (goat anti-mouse or goat anti-rabbit IgG, Alexa Fluor®–488 or –546, 1:400 v/v dilution, Molecular Probes) at RT and nuclear counterstaining was performed using 4',6-diamidino-2-phenylindole (DAPI, 1.5µg/mL; Sigma). After brief drying, sections were mounted in Mowiol (Sigma). Fluorescence images were acquired with Zeiss LSM 710 Confocal Laser Point-Scanning Microscopes.

Table IV-1. List of primary antibodies and dilutions used for immunostaining

Antibody	Company	Host species	Dilution
BARHL1	Atlas	rabbit	1:500
CALBINDIN	Swant	rabbit	1:500
GAD65	BD Pharmingen	mouse	1:100
GAD67	Millipore	mouse	1:500
MAP2	Sigma	mouse	1:1000
N-CADHERIN	BD Transduction	mouse	1:1000
NESTIN	R&D	mouse	1:400
NEUROGRANIN	Millipore	rabbit	1:200
OLIG2	Millipore	rabbit	1:500
PARVALBUMIN	Sigma	mouse	1:200
PAX6	Covance	rabbit	1:400
SOX2	R&D	mouse	1:200
TBR1	Millipore	rabbit	1:200
TUJ1	Biolegend	mouse	1:1000
V-GLUT1	Abcam	rabbit	1:100

Quantitative Real-time PCR (qRT-PCR)

Total RNA was extracted at different time points of differentiation using High Pure RNA Isolation Kit (Roche) and converted into complementary cDNA with Transcriptor High Fidelity cDNA Synthesis Kit (Roche). Gene expression was analyzed using SYBR® green chemistry (**Table IV.2**). All PCR reactions were run in duplicate, using the ViiA™7 RT-PCR System (Applied BioSystems). Reactions were normalized to the housekeeping gene *GAPDH* and results analyzed with QuantStudio™ RT-PCR Software.

Table IV-2. Primers used for qRT-PCR

Gene	Foward	Reverse
BARHL1	GAGCGGCAGAAGTACCTGAG	GTAGAAATAAGGCGACGGGAAC
CORL2	CCAGGTGTTAAAAGGAAACACA	GCTCCCTTTTCATCTGATCCT
EN2	CCGGCGTGGGTCTACTGTA	GGCCGCTTGTCCTCTTTGTT
FGF8	GAGCCTGGTGACGGATCAG	CGTTGCTCTTGGCGATCAG
GAD65	GTCTCCAGCTCGCATACACA	CGAAAGACCAAAAGCCAGAG
GAD67	CCTGGAACTGGCTGAATACC	CCCTGAGGCTTTGTGGAATA
GBX2	GACGAGTCAAAGGTGGAAGAC	GATTGTCATCCGAGCTGTAGTC
GRID2	AGCTCTTCCTCTCTTGGTTTCC	GCCCCACGTTGCCTAGAAAT
KIRREL2	GGGGCTAGTTCAGTGGACTAA	CACGGGCCTAATGTGGAGG
L7	ACCAGGAGGGCTTCTTCAAT	CTGTCACACGTTGGTCATCC
NEUROGRANIN	TCAAAGTTCCCGAGGAGAGA	CTAAAAGGGCACGGACTCAG
OCT4	GTGGAGGAAGCTGACAACAA	ATTCTCCAGGTTGCCTCTCA
OLIG2	GACAAGCTAGGAGGCAGTGG	CGGCTCTGTCATTTGCTTCTTG
OTX2	AGAGGACGACGTTCACTCG	TCGGGCAAGTTGATTTTCAGT
PARVALBUMIN	TTCTCCCCAGATGCCAGAGA	GAGATTGGGTGTTCAGGGCA
PAX2	AACGACAGAACCCGACTATGT	GAGCGAGGAATCCCCAGGA
PAX6	GAATCAGAGAAGACAGGCCA	GTGTAGGTATCATAACTCCG
TBR1	CGTCTGCAGCGAATAAGTGC	AATGTGGAGGCCGAGACTTG
VGLUT1	TACACGGCTCCTTTTTCTGG	CTGAGGGGATCAGCATGTTT

Single cell calcium imaging

Functional maturation was evaluated by single cell calcium imaging (SCCI) to analyze the intracellular variations of Ca^{2+} following stimulation with 50mM KCl and 100µM histamine (Sigma-Aldrich). Two to five days before, aggregates were re-plated on Glass Bottom Cell Culture Dish (Nest) previously coated with poly-L-ornithine (15µg/mL, Sigma) and Laminin (20µg/mL, Sigma). At different time points of differentiation, neurons were loaded with Fura-2 AM (5µM, in normal Krebs solution with the following composition: NaCl (132mM), KCl (4mM), $MgCl_2$ (1.4mM), $CaCl_2$ (2.5mM), D-(+)-glucose (6mM) and HEPES (10mM) - pH 7.4 adjusted with NaOH - and incubated at 37ºC for 45 min. Fura-2 AM loaded cells were sequentially excited both at 340 nm and 380 nm, for 250 ms at each wavelength, using an inverted microscope with epifluorescent optics and equipped with a high speed multiple excitation fluorimetric system (Lambda DG4, with a 175W Xenon arc lamp). The emission fluorescence was recorded at 510 nm by a CDD camera. Cells were stimulated by 100 µM histamine or high potassium Krebs solution (containing 50 mM KCl, isosmotic substitution with NaCl), as reported elsewhere (Agasse et al., 2008; Rodrigues et al., 2017).

Patch Electrophysiology

For electrophysiological evaluation, 2-5 days before the analysis aggregates were dissociated using accutase (Sigma) and re-plated on coverslips coated with poly-L-ornithine (15µg/mL, Sigma) and Laminin (20µg/mL, Sigma). Whole cell patch-clamp recordings were obtained from generated neurons using an upright microscope (Zeiss Axioskop 2FS) equipped with differential interference contrast optics using a Zeiss AxioCam MRm camera and a 40x IR-Achroplan objective. During recordings, cells were continuously superfused with artificial cerebrospinal fluid (aCSF) containing (in mM): 124 NaCl, 3 KCl, 1.2 NaH_2PO_4,

25 $NaHCO_3$, 2 $CaCl_2$, 1 $MgSO_4$ and 10 glucose, which was continuously gassed with 95%O_2/5% CO_2. Recordings were performed at room temperature in current-clamp or voltage-clamp mode [holding potential (Vh) = −60 mV] with an Axopatch 200B (Axon Instruments) amplifier, as performed in (Felix-Oliveira et al., 2014). Briefly, Patch pipettes with 4 to 7 MΩ resistance when filled with an internal solution containing (in mM): 125 K-gluconate, 11 KCl, 0.1 $CaCl_2$, 2 $MgCl_2$, 1 EGTA, 10 HEPES, 2 MgATP, 0.3 NaGTP, and 10 phosphocreatine, pH 7.3, adjusted with 1 M NaOH, 280-290 mOsm were used to record excitatory synaptic currents and action potential activity. Acquired signals were filtered using an in-built, 2-kHz, three-pole Bessel filter, and data were digitized at 5 kHz under control of the pCLAMP 10 software program. The junction potential was not compensated for, and offset potentials were nulled before gigaseal formation. The resting membrane potential was measured immediately upon establishing whole-cell configuration. Firing patterns of cerebellar neurons were determined in current-clamp mode immediately after achieving whole-cell configuration by a series of hyperpolarizing and depolarizing steps of current injection (500 ms). Firing potential were also determined through the application of two depolarizing steps of current injection of 10 ms, separated by 80 ms.

IV.4 RESULTS

Production of size-controlled human iPSC-derived aggregates using PBS MINI 0.1L bioreactor

The generation of human iPSC-derived organoids starts by cell aggregation to mimic the 3D structure and recapitulate both the structure and functionality of human organs. The cell aggregation is a critical step to obtain homogeneous outcome with high yield of viable

organoids and increased reproducibility of the differentiation protocol (Xie et al., 2017). We initiated the protocol by promoting cell aggregation using PBS MINI 0.1L bioreactor (**Figure IV.1-A**). Single-cell inoculation was performed and 250 000 cells/mL were seeded in 60 mL of medium with an agitation speed of 27 rpm. After 24 hours, cells were able to efficiently aggregate, with an aggregation efficiency of 54.1 ± 18.7% and 82 ± 14.1% (Mean ± SEM) obtained from F002.1A.13 (n=4) and iPSC6.2 cell line (n=2), respectively. In addition, homogeneous shape aggregates were obtained 24 hours after seeding (day 1, **Figure IV.1-B**), and were maintained until day 5 with a spheroid-like structure (**Figure IV.1-B**). Aggregate size distribution also revealed the presence of very homogeneous population at day 1 (**Figure IV.1-C**). Therefore, an efficient cell aggregation with shape and size-controlled aggregates can be obtained by using PBS MINI 0.1L bioreactor, as a first step towards a more homogeneous and efficient differentiation.

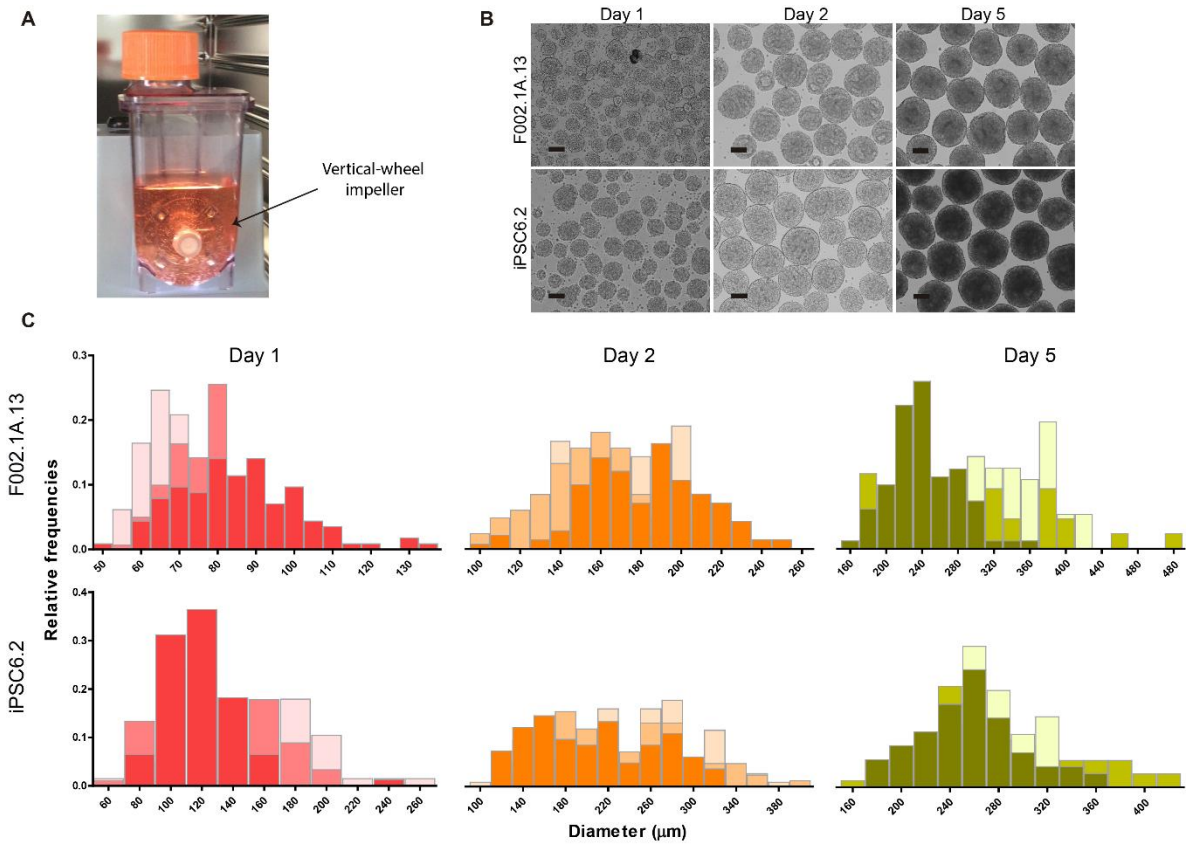

Figure IV.1. Figure 4.1. Generation of size-controlled aggregates using PBS MINI 0.1L bioreactor. A) Design features of a vertical-wheel bioreactor. **B)** Bright field photomicrograph showed aggregates with homogeneous shape and size between days 1 and 5. Scale bar, 100 µm. **C)** The distribution of floating aggregates diameters demonstrates that homogeneous size aggregates can be obtained from different iPSC lines by using PBS MINI 0.1L bioreactor.

Since the size of the cellular niche regulates the balance between differentiation-inducing and -inhibiting factors, and influences the spatial gradient of soluble factor-dependent signaling (Peerani et al., 2007), the aggregate size is an important physical parameter capable of prompting the cells to differentiate toward different lineages (Bauwens et al., 2008; Bratt-Leal et al., 2009). Besides that, there is a minimum size threshold that appears to favor differentiation (Arora et al., 2017). For that reason, based on the aggregate size previously obtained in static conditions (≈ 200 µm) and reported optimal aggregate diameter to promote efficient neural commitment (Miranda et al., 2015, 2016), we

maintained the generated aggregates in mTeSR1 medium at 25 rpm until reaching the desired diameter to start the differentiation. At day 2, the obtained average diameter was 221 ± 3.34 µm for F002.1A.13 cell line and 212.1 ± 2.53 µm (Mean ± SEM) for iPSC6.2 cell line, attaining the optimal aggregate size at this time-point. Distribution of aggregate diameter showed that aggregates continue to grow from day 1 to 5, and a homogeneous size distribution was observed when differentiation was initiated and in the initial days of the neural commitment, up to day 5 (**Figure IV.1-B**).

Expansion and size characterization of human iPSC-derived organoids

At day 2, after achieving the desired aggregate diameter, the neural differentiation was induced by SB, transforming growth factor β (TGF-β)-receptor inhibitor that promotes the neuroectodermal differentiation. For the first days of neural induction, the rotation speed of 25 rpm was used and increasing to 30 rpm after 7 days to avoid the accumulation and clumping of bigger aggregates (**Figure IV.2**).

Although an efficient cerebellum differentiation was demonstrated previously in static conditions, we found that organoids tend to coalesce forming large macroscopic structures resistant to diffusion of morphogens and nutrients (**Figure IV.2**). These structures become progressively necrotic and resilient to differentiation cues, being difficult to retain more than 35 days to achieve an efficient neuronal maturation in the static 3D culture system. During differentiation in the PBS MINI 0.1L, organoids showed a more pronounced epithelization similar to neural tube-like structures with luminal space when compared to static conditions, where a dense cell mass was observed at the final differentiation stages (**Figure IV.2**).

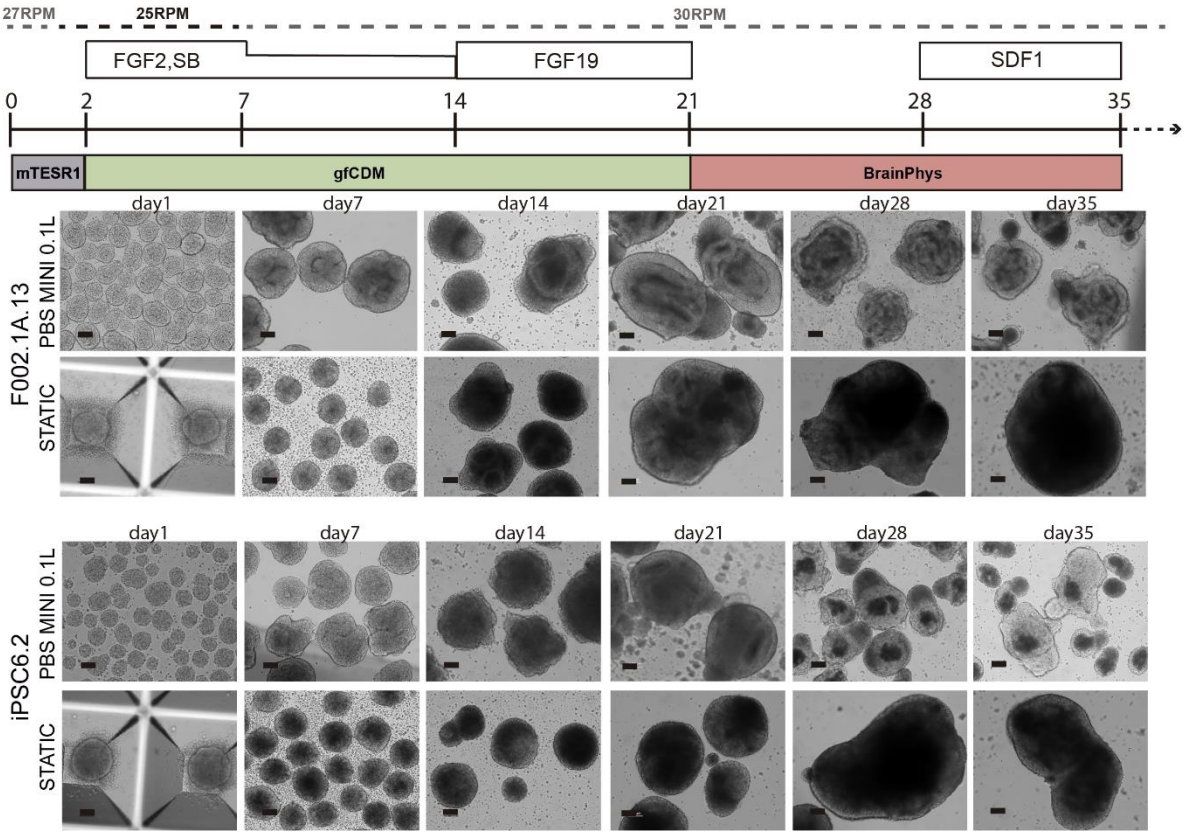

Figure IV.2. Generation of iPSC-derived organoids using PBS MINI 0.1L Bioreactor. Cells were seeded at the density of 250 000 cells/mL and an agitation speed of 27 rpm were used to promote cell aggregation. During the first days of differentiation, aggregates were maintained at an agitation speed of 25 rpm. Afterwards, to avoid the accumulation of bigger clumps, the agitation speed was increased to 30 rpm. Bright field photomicrographs showing iPSC-derived organoids during cerebellar differentiation from static and PBS MINI 0.1L conditions. Scale bar, 100 µm.

A larger number of iPSC-derived organoids can be generated with the PBS MINI 0.1L bioreactor without being excessively labor-intensive. Using the F002.1A.13 cell line, 24 hours after seeding, 431 ± 53.6 aggregates/mL were generated. This number decreased at day 2 for 114 ± 7.2 aggregates/mL but was maintained constant until the end of organoid culture (**Figure IV.3-A**). Probably, the merging of individual aggregates was promoted by the decrease in the agitation speed from 27 to 25 rpm, since the aggregate diameter increased 2-fold from day 1 to day 2 (**Figure IV.3-C**). Besides that, biomass analysis demonstrated that the total volume of biomass increased up to ~4-fold until day 21 (**Figure**

IV.3-B). At day 35, a slight decrease in the biomass volume was observed, consistent with a reduction in aggregate diameter observed at the same time-point (**Figure IV.3-B and C**).

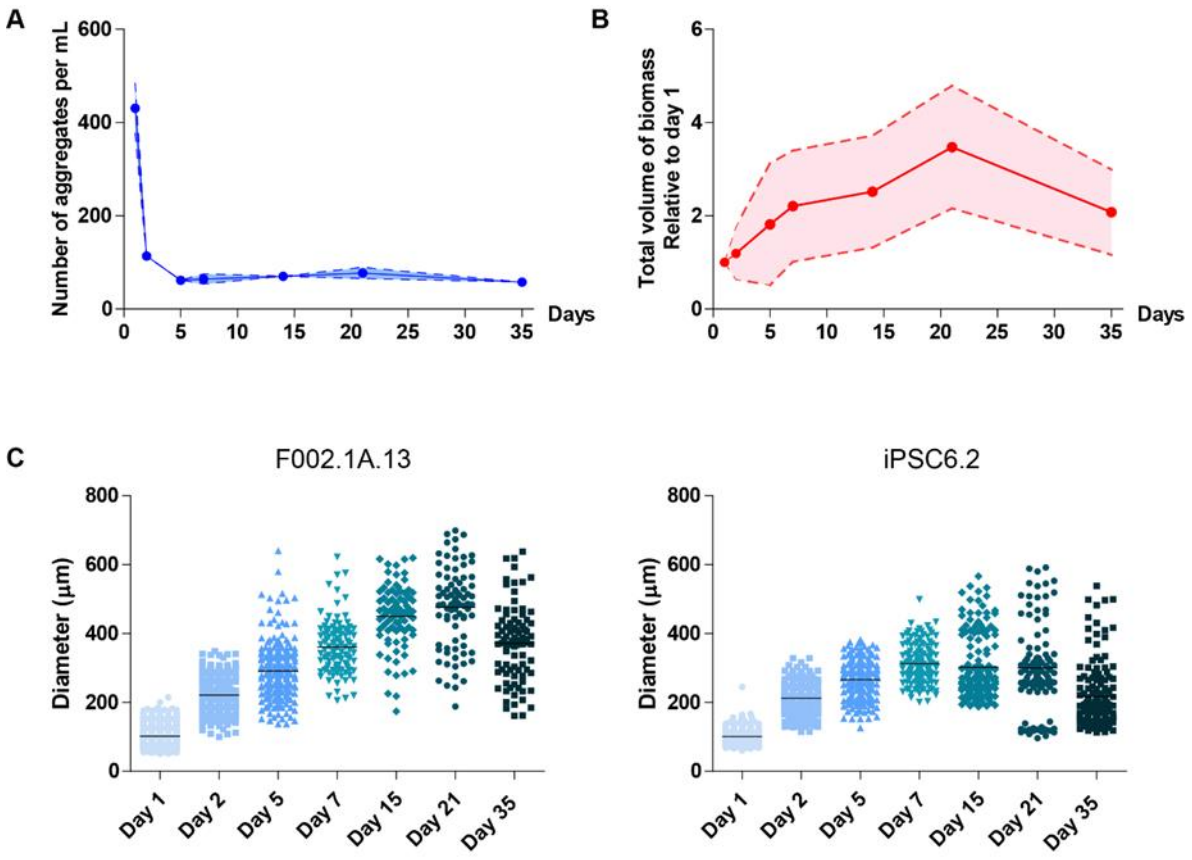

Figure IV.3. Expansion of iPSC-derived organoids. A) The number of aggregates decreases from day 1 to day 2 of differentiation, maintaining constant during the differentiation protocol. **B)** Volume of biomass increases until day 21 of differentiation. Data were obtained from 3 independent differentiation experiments using F002.1A.13 cells. Points show the mean and area fill represents SEM. **C)** Aggregate diameters during the differentiation protocol using different iPSC lines (data obtained from 3 independent experiments).

The analysis of aggregate diameters also revealed that organoids were able to grow until day 21 (**Figure IV.3-C**), which is important since the size of the system increases with the level of specialization in multicellular structures (Bell and Mooers, 1997). Besides that,

the diameters tend to be more widespread when the organoids are structurally more complex, from day 7 to day 35 (**Figure IV.3-C**).

In order to evaluate the population homogeneity in both static and PBS MINI 0.1L systems, we analyzed the coefficient of variation (CV), which measures the variability by correlating standard deviation with the mean of aggregate diameters. At day 7, CV was higher in the PBS MINI 0.1L in comparison with static condition for F002.1A.13 cell line, achieving about 14% and 10% of variation, respectively, explained by the fact that aggregates were maintained inside microwells until day 7 in static conditions controlling their size (**Figure IV.4**). In contract, for iPSC6.2 cell line the CV was similar in both conditions at day 7, demonstrating the ability to create controlled-size aggregates using the PBS MINI 0.1L bioreactor. From day 14, for F002.1A.13 cell line, the CV was retained constant in PBS MINI 0.1L, around 20%, but increasing until 30% in static conditions. The same tendency was observed in iPSC6.2 culture, about 10% of CV was maintained from day 7 until day 21 in PBS MINI 0.1L, much lower than static conditions that reached about 30% of variation. Therefore, PBS MINI 0.1L bioreactor maintained more homogeneous aggregate diameters during the differentiation protocol.

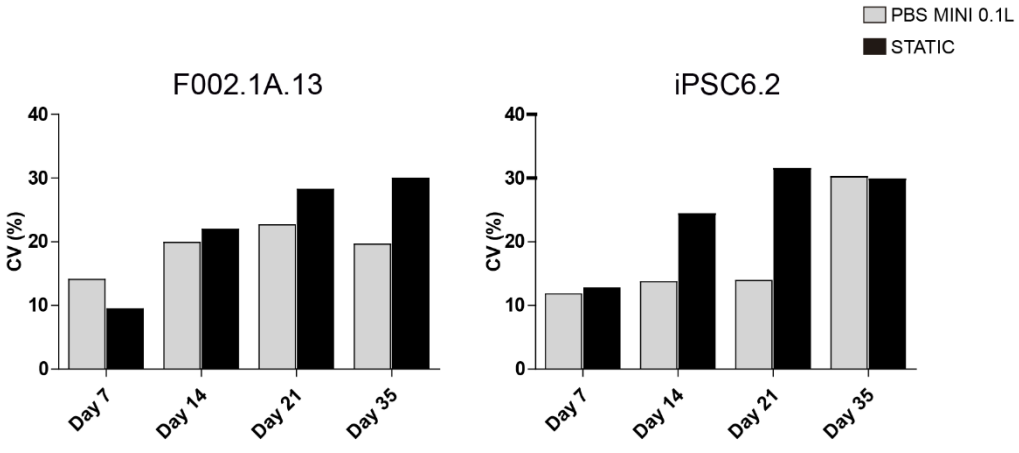

Figure IV.4. Coefficient of variation of iPSC-derived organoids at different time-points of differentiation (data obtained from 3 independent experiments).

Nevertheless, iPSC6.2 cell line presented similar diameter variation in both conditions at day 35, achieving about 30% (**Figure IV.4**). Indeed, when the agitation speed was changed to 30 rpm, iPSC6.2-derived aggregates tend to form smaller aggregates (**Figure IV.2**). Therefore, iPSC6.2 cell line seems to be more sensitive to agitation speed alterations and further optimizations should be performed in order to avoid the generation of smaller aggregates after the neural commitment.

In addition to CV analysis, when we evaluated the diameter distribution, the PBS MINI 0.1L condition exhibited more homogeneous distributions during the differentiation protocol when compared with static conditions (**Figure IV.5**). In addition, at the end of the organoid generation (day 35), much bigger aggregates were presented in static conditions, with some of them reaching 1 000 µm in both cell lines (**Figure IV.5**). In contrast, using PBS MINI 0.1L, organoids did not reach more than 800 µm.

Thus, a more homogeneous population of organoids with a limited size can be obtained using this dynamic culture system.

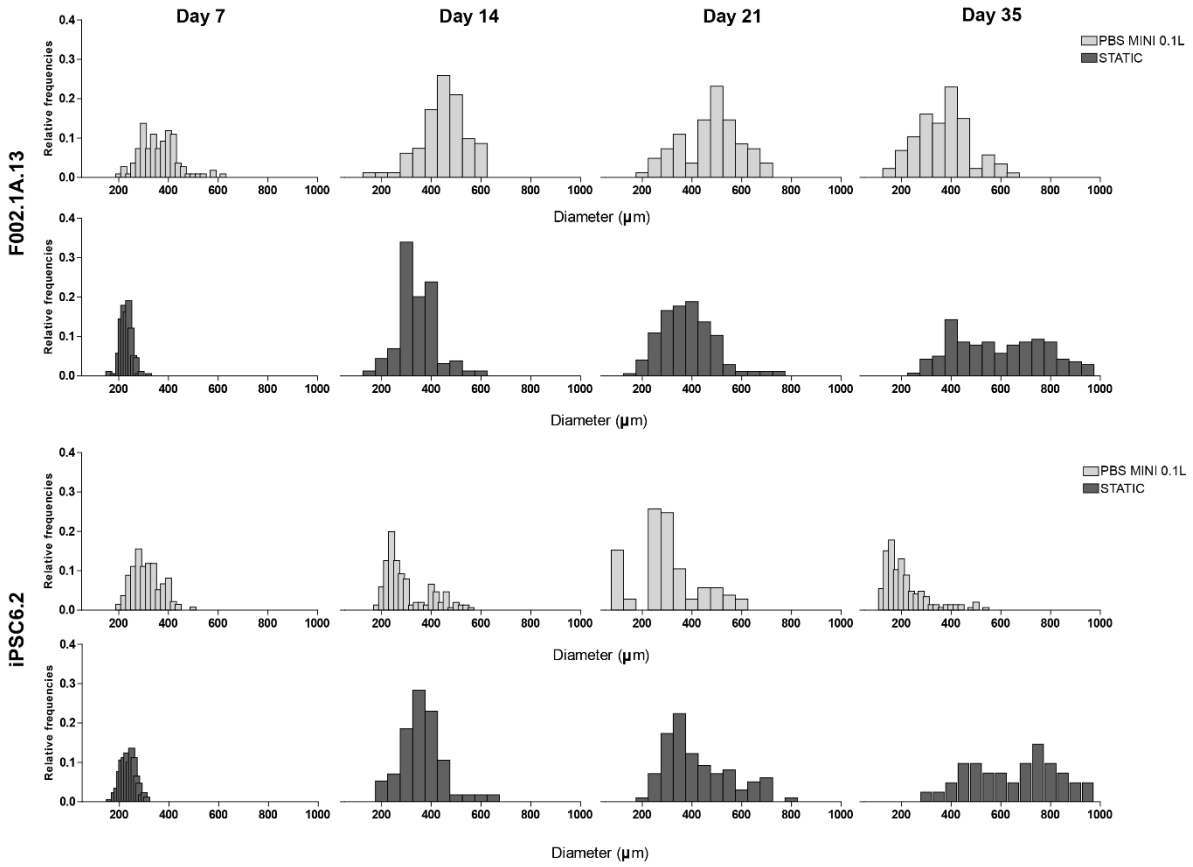

Figure IV.5. Diameter characterization of human iPSC-derived organoids. Distribution of organoid diameters demonstrates that culture becomes more heterogeneous in aggregate sizes along the differentiation protocol. At day 35, diameter distribution is more heterogeneous in static conditions when compared with PBS MINI 0.1 bioreactor. Data obtained from 3 independent differentiation experiments.

Efficient neural commitment in human iPSC-derived organoids

To induce the neural commitment, SB, FGF2 and insulin were used simultaneously, promoting neuroectodermal differentiation as well as a moderate caudalization necessary for mid-hindbrain patterning. Afterwards, FGF19 and SDF1 were introduced in the culture at days 14 and 28, respectively, to promote the generation of different cerebellar progenitors (**Figure IV.2**).

As expected, on day zero of differentiation, human iPSCs expressed pluripotency and self-renewal transcript *OCT4* (**Figure IV.6-A**). Subsequently to neural induction, a down-

regulation of *OCT4* mRNA levels was observed, being almost undetectable by day 7 of differentiation (**Figure IV.6-A**). Consistent with this significant down-regulation of the pluripotency gene expression, the mRNA levels of the neural marker *PAX6* increased, showing that neural commitment was reached after 7 days (**Figure IV.6-A**). Starting on day 7 and going onwards until day 35, organoids progressively expressed higher levels of *PAX6* (**Figure IV.6-A**), which is a transcription factor driving neurogenesis and important for neural stem cell proliferation (Sansom et al., 2009; Thakurela et al., 2016). During cerebellar development, PAX6 is also essential for the generation of all glutamatergic neurons (Yeung et al., 2016). Immunofluorescence analysis further supports that an efficient neural commitment of the iPSC-derived organoids is achieved already by day 7 of differentiation. The cryosections of organoids revealed many structures reminiscent to the neural tube, with most of cells expressing progenitor marker NESTIN at days 7 and 14 of differentiation (**Figure IV.6-B**). Furthermore, neuroepithelium-like structures showing apico-basal polarity are evident in these cultures, with $PAX6^{+}$ and $SOX2^{+}$ progenitors found at the luminal (apical) side marked by strong expression of apical marker N-cadherin (**Figure IV.6-B**). The expression of TUJ1, neuron-specific class III beta-tubulin, is detectable at day 14 of differentiation (**Figure IV.6-B**), suggesting an efficient generation of newborn neurons after the initial neural induction.

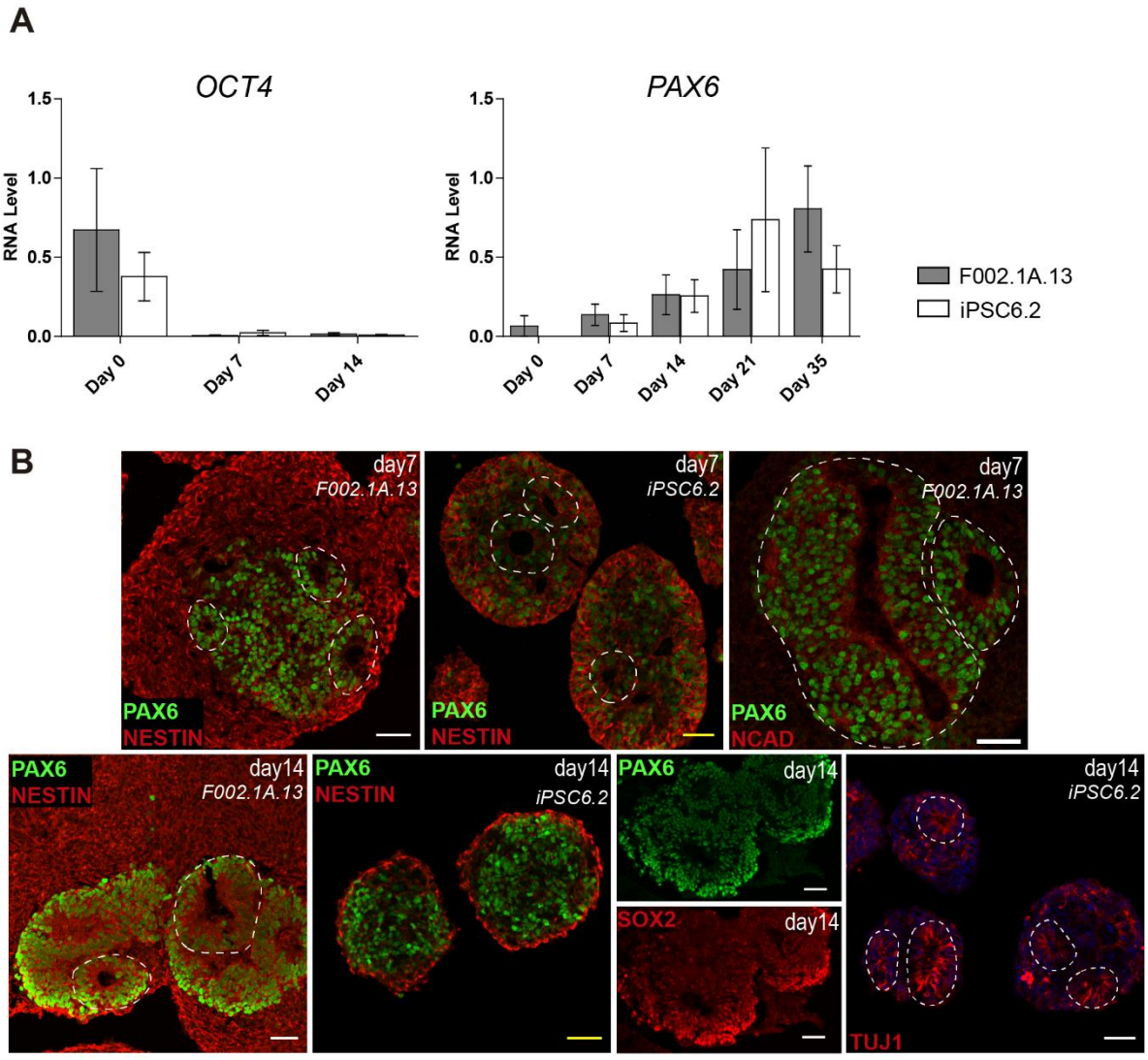

Figure IV.6. Efficient neural induction in human iPSC-derived organoids. A) qRT-PCR analysis of *OCT4* and *PAX6* mRNA levels relative to *GAPDH* levels at different time-points. For all graphics depicted, data were obtained from 5 and 3 independent differentiation experiments using F002.1A.13 and iPSC6.2 cell line, respectively. **B)** Immunofluorescence for NESTIN, PAX6, NCAD, SOX2 and TUJ1 on days 7 and 14 of differentiation. Scale bars, 50µm.

Generation of neuronal organoids that adopt cerebellar identity

During human neural development, the neural tube regionalization along anterior-posterior axis is characterized by differential expression of transcription factors that establishes a segmented pattern (Watson et al., 2015). From rostral to caudal direction,

different regions are observed, including forebrain, midbrain and hindbrain (**Figure IV.7-A**), which will originate the different neuronal types present in the cerebral cortex, cerebellum and spinal cord (Suzuki and Vanderhaeghen, 2015). In the dynamic conditions, generated neural tube-like structures appeared to express markers for both caudal and rostral regions (**Figure IV.7-B-D**). Under this differentiation environment, organoids exhibited a robust expression of *OTX2* gene (**Figure IV.7-B**), which is a forebrain-midbrain marker, important to delineate the rostral limit of early cerebellar territory (Broccoli et al., 1999) and required for cerebellum development (Frantz et al., 1994; Larsen et al., 2010). Its expression is maintained significantly high until day 35 of differentiation. In addition, an up-regulation of *GBX2* gene expression, an anterior hindbrain marker (Wassarman et al., 1997), was also observed at day 35 (**Figure IV.7-B**). A possible suppression of the *FGF8* and *EN2* expression promoted by increased mRNA levels for *OTX2* was not detected (Guo et al., 2007; Joyner et al., 2000). On the contrary, a significant increase in RNA levels of *FGF8* and *EN2*, which are crucial transcription factors involved in isthmic organizer (Chi et al., 2003; Martinez et al., 1999) and mid-hindbrain boundary maintenance (Joyner, 1996), were observed in the generated human iPSC-derived organoids, starting on day 21 and 7, respectively, and going onwards until day 35 (**Figure IV.7-C**). The expression of these two markers was reported to be important for the establishment of cerebellar territory (Chi et al., 2003; Zec et al., 1997), and in fact, enhanced expression of *EN2* and *FGF*8 was accompanied by an up-regulation of *KIRREL2* gene expression (**Figure IV.7-D**), which is the earliest marker of cerebellar territory, expressed in cerebellar GABAergic progenitors (Mizuhara et al., 2010). Thus, although the expression of markers for different neural tube regions has been observed, cerebellar commitment can be efficiently achieved in these conditions.

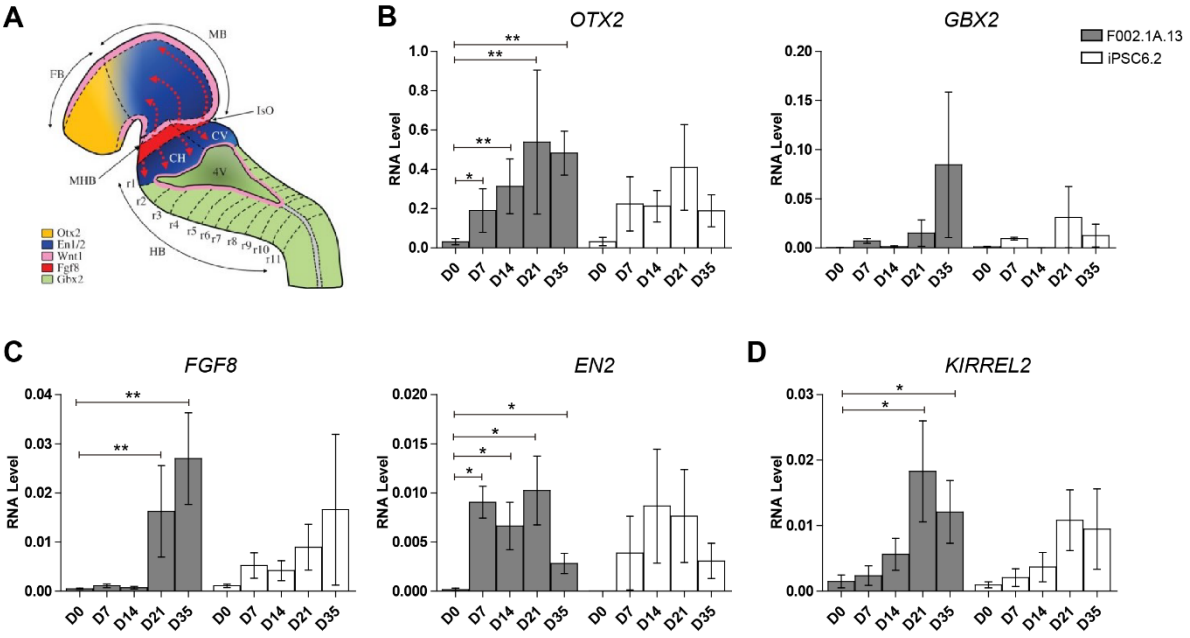

Figure IV.7. Regional patterning in human iPSC-derived organoids. A) Representative distribution of the gene expression gradients within the mouse neural tube at E11.5 (Watson et al., 2015). qRT-PCR analysis of *OTX2* (**B**), *GBX2* (**B**), *FGF8* (**C**), *EN2* (**C**) and *KIRREL2* (**D**) mRNA levels relative to *GAPDH* levels at different time-points. For all graphics depicted, data were obtained from 5 and 3 independent differentiation experiments using F002.1A.13 and iPSC6.2 cell line, respectively. Student´s t-test (two-tailed) statistics, * p<0.05, ** p<0.01; error bars represent SEM.

During days 21-35 of differentiation, a temporal self-formation of continuous neuroepithelium was observed (**Figure IV.8**). By day 21, human iPSC-derived organoids displayed neural tube-like structures (**Figure IV.8-A**) that reorganized into continuous neuroepithelium at later time-points. Afterwards, at day 28, an intense signal for TUJ1 was detected along these hollow structures, showing a radial orientation of newborn neurons (**Figure IV.8-A**). By day 35, $TUJ1^{+}$ newborn neurons appeared to migrate towards the organoid surface, reestablishing the radial alignment and revealing processes with end feet that terminated on the outer surface of the organoid (**Figure IV.8-A**). In addition, within iPSC-derived organoids, the observed flat-oval structures stained positively for the neural

progenitor markers NESTIN and PAX6 on day 21 of differentiation (**Figure IV.8-B**). Further neuronal differentiation was also confirmed by the presence of MAP2 expression on day 28 until day 35 (**Figure IV.8-B**), surrounding the continuous neuroepithelium that contains $PAX6^+$ neural progenitors.

After having established that iPSC-derived organoids were expressing critical genes required for early cerebellum morphogenesis, such as *FGF8*, *EN2* and *KIRREL2,* as well as an effective neuronal differentiation was being performed, we next focused on detecting specific cerebellar progenitors, including ventral and dorsal markers. An early detection of BARHL1 marker suggests the presence of dorsal cerebellar progenitors already at day 14 of differentiation (**Figure IV.8-C**). Along the differentiation protocol, we observed two different group of organoids that exhibited different cell organization. First, various flat-oval structures within the organoids were observed with apical side in the luminal region of these oval structures, containing $PAX6^+$ progenitors (**Figure IV.8-B**). Other organoids exhibited an inverted polarity with apical side on the outer surface (**Figure IV.8-C**). Muguruma et al. (Muguruma et al., 2015) demonstrated that this might have resulted from fusion of distinct neural tube-like structures promoted by SDF1 addition, by stimulating the generation of planar neuroepithelium. Thus, in this group of organoids, $BARHL1^+$ dorsal cerebellar progenitors were establishing a continuous and dense layer (**Figure IV.8-C**). $SOX2^+$ ventral progenitors were presented on the superficial side of the organoid (**Figure IV.8-C**). Although some $BARHL1^+$ and $SOX2^+$ cells seemed to co-localize (**Figure IV.8-C**), a fine layer of $SOX2^+$ progenitors was found spreading under the $BARHL1^+$ cellular layer (**Figure IV.8-C**). Consistent with positive expression of the ventral marker, SOX2, on the apical side, a strong signal of N-cadherin, an apical marker, was also detected on the organoid surface (**Figure IV.8-D**). Furthermore, $OLIG2^+$ progenitors, involved in Purkinje cell generation, were found dispersed on the deep side of the organoid (**Figure IV.8-E**).

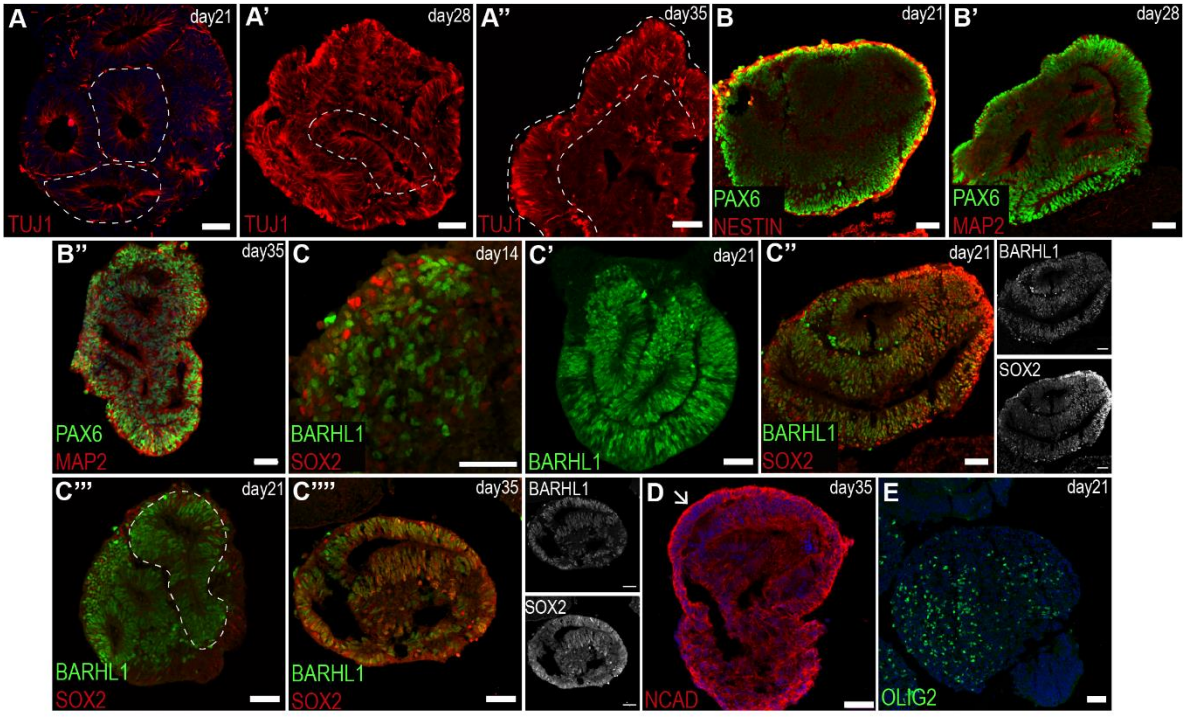

Figure IV.8. Human iPSC-derived organoids with cerebellar identity. Immunofluorescence for proteins (as indicated at the bottom of each image) on indicated time-points of differentiation (F002.1A.13 cells). Scale bars, 50µm.

An up-regulation of markers for different types of cerebellar progenitors was further detected by qRT-PCR analysis of iPSC-derived organoids along the differentiation protocol (**Figure IV.9**). These markers were: *PAX2* (expressed in cerebellar interneurons), *BARHL1* (required for the differentiation of cerebellar granule neurons), and *OLIG2* and *CORL2* (expressed in Purkinje cell progenitors). While the analysis of mRNA levels to *OLIG2* and *CORL2* demonstrated a continuous increase of gene expression with higher levels at day 35, *PAX2* and *BARHL1* peaked at different time-points of differentiation, which is consistent with their temporal expression during cerebellar development (Joyner, 1996; Li, 2004). The expression of *PAX2* gene is higher at day 7 and decreased thereafter, remaining significantly higher than day 0 (**Figure IV.9**). This is explained by its important role in cross-regulatory

interactions that stabilize the mid-hindbrain boundary at early stages of cerebellar embryonic development (Rowitch and McMahon, 1995), and its later expression in particular subsets of post-mitotic interneurons (Maricich and Herrup, 1999). *BARHL1* gene expression was observed to increase until day 21 (**Figure IV.9**), suggesting the presence of dorsal progenitors and dorsal-derived migratory neurons and, later, cerebellar granule cells (Li, 2004).

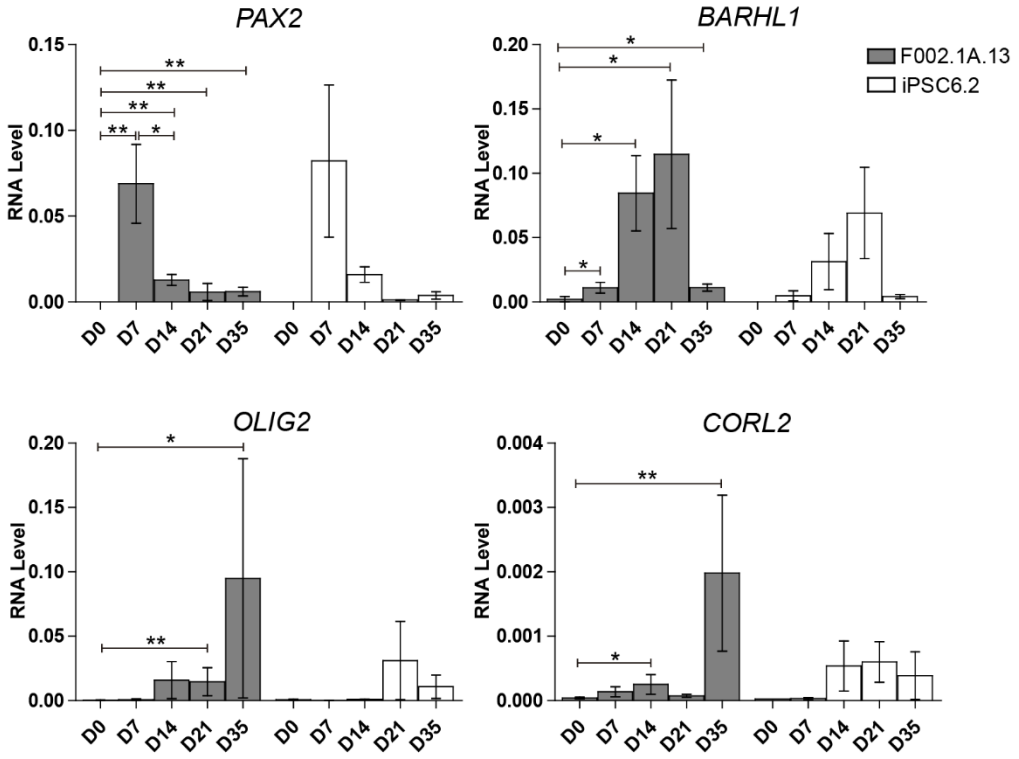

Figure IV.9. Differentiation of cerebellar progenitors in human iPSC-derived organoids. qRT-PCR analysis of *PAX2*, *BARHL1*, *OLIG2* and *CORL2* mRNA levels relative to *GAPDH* levels at the indicated time-points. For all graphics depicted, data were obtained from 5 and 3 independent differentiation experiments using F002.1A.13 and iPSC6.2 cells, respectively. Student´s t-test (two-tailed) statistics, * p<0.05, ** p<0.01; error bars represent SEM.

Production of cerebellar neurons from PBS MINI 0.1L bioreactor cultures

After the generation of cerebellar progenitors, further maturation was promoted by using BrainPhys™ medium (Bardy et al., 2015) supplemented with neurotrophic factors BDNF and GDNF. Organoids in this 3D dynamic culture system were maintained viable for up to 90 days, without requiring any additional maturation cues such as feeder layers. Immunostaining analysis of organoid cryosections revealed the presence of two major neuronal subtypes, inhibitory GABAergic and excitatory Glutamatergic neurons. On day 56, GABAergic neurons expressed both GAD67 and GAD65, which are two isoforms of the enzyme glutamic acid decarboxylase (GAD) that synthetizes inhibitory neurotransmitter GABA (Kanaani et al., 2010). Likewise, VGAT, a vesicular GABA transporter, was detected surrounding a dense cell layer located in the lumen on the surface of the organoids (**Figure IV.10-A**). In addition, V-GLUT1 expression was also detected on the outer surface, showing the presence of vesicular glutamate transporters in glutamatergic neurons (**Figure IV.10-A**). Accordingly, gene expression analysis also demonstrated an increase in levels of *GAD67*, *GAD65* and *VGLUT1* mRNAs until day 80 (**Figure IV.10-B**).

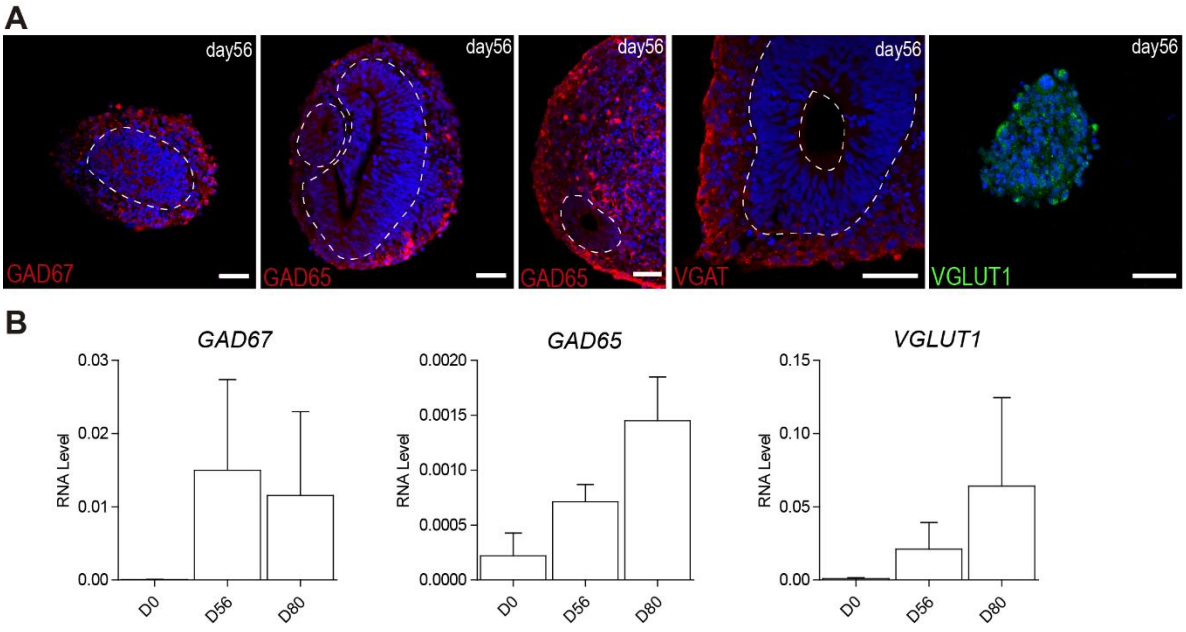

Figure IV.10. Generation of GABAergic and glutamatergic neurons. A) Immunostaining for GAD67, GAD65, V-GAT and V-GLUT1 and GAD65 in F002.1A.13-derived organoids on day 56 of differentiation. Scale bars, 50µm. **B)** qRT-PCR analysis of *GAD67*, *GAD65* and *V-GLUT* mRNA levels relative to *GAPDH* at the indicated time-points. Data were obtained from three independent differentiation experiments using F002.1A.13 cells.

Immunofluorescence staining was used to detect the major subtypes of cerebellar neurons. GABAergic neurons expressing a calcium-binding protein calbindin (CALB), that in cerebellum is restricted to Purkinje cells, were detected around the flat-oval structures (**Figure IV.11-A**). Thus, CALB staining demonstrated that compact meshwork of Purkinje cells was formed along the surface of the organoid (**Figure IV.11-A**). In smaller iPSC-derived 3D structures, a dense network of $CALB^{+}$ neurons was observed within the aggregate, where non-overlapping with CALB expression of parvalbumin (PVALB) indicates the presence of precursors of GABAergic interneurons (**Figure IV.11-B**). Another major cerebellar neuronal type, granule cells, was also identified as a subset of cells co-expressing PAX6 and MAP2 (**Figure IV.11-C**). Interestingly, immunofluorescence using antibodies to PAX6, expressed early in neural progenitors and later in cerebellar granule cells (Swanson et al., 2005), and to MAP2, neuron-specific microtubule protein, revealed a robust

organization within the iPSC-derived organoids. A dense layer of PAX6^{+} precursors was detected on the luminal side of the organoid, whereas MAP2^{+} fibers were distinguished basally to the progenitor's layer by day 56 of differentiation, and the co-localization of PAX6^{+} cells with MAP2^{+} neuronal network, during the maturation protocol, indicated the presence of granule cells (**Figure IV.11-C**). Along the maturation process, the initially large PAX6^{+} neuroepithelium was becoming smaller and simultaneously MAP2^{+} region was extended. Nevertheless, a niche of PAX6^{+}/MAP2^{-} progenitors remained until day 90. Other types of cerebellar neurons were detected, including Golgi cells expressing neurogranin (**Figure IV.11-D**, Singec et al., 2003) and deep cerebellar nuclei projection neurons expressing TBR1 (**Figure IV.11-E**, Fink et al., 2006).

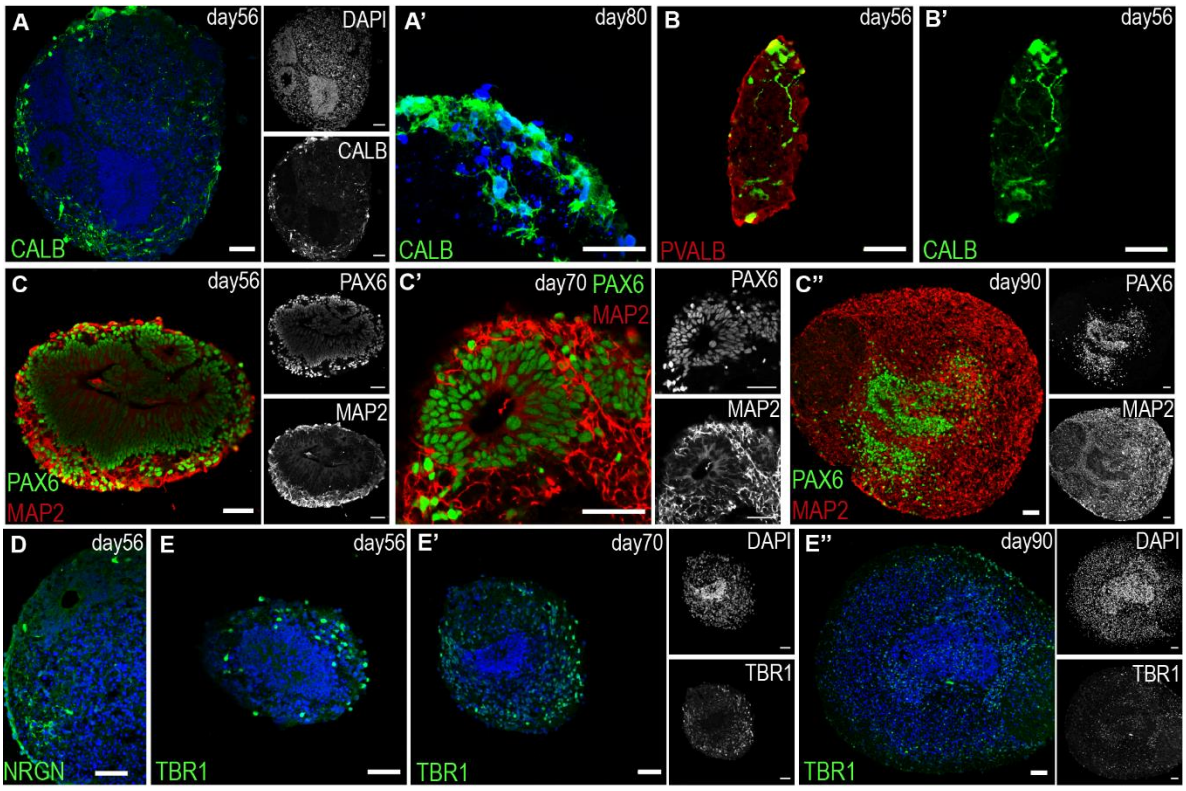

Figure IV.11. Generation of different types of cerebellar neurons. Immunofluorescence of distinct proteins (as indicated at the bottom of each image) on indicated time-points of differentiation (F002.1A.13 cells). Scale bars, 50µm.

In addition to immunofluorescence analysis, the quantification of mRNA levels of markers for distinct cerebellar neurons demonstrated their robust expression during the maturation protocol (**Figure IV.12**). For some transcription factors, like *PAX6* and *BARHL1*, their decreased expression after peaking at day 56 of differentiation (**Figure IV.12**), is in agreement to their broad early expression in glutamatergic progenitors and later restricted expression in granule neurons (Li, 2004; Swanson et al., 2005). In contrast, the expression of other genes associated with different types of cerebellar neurons were kept high until day 80 (**Figure IV.12**), including *TBR1*, the Purkinje cell-specific marker *L7*, Purkinje cell-specific glutamate receptor *GRID2*, the calcium-binding protein *PARVALBUMIN* and the calmodulin-binding protein *NEUROGRANIN* (**Figure IV.12**).

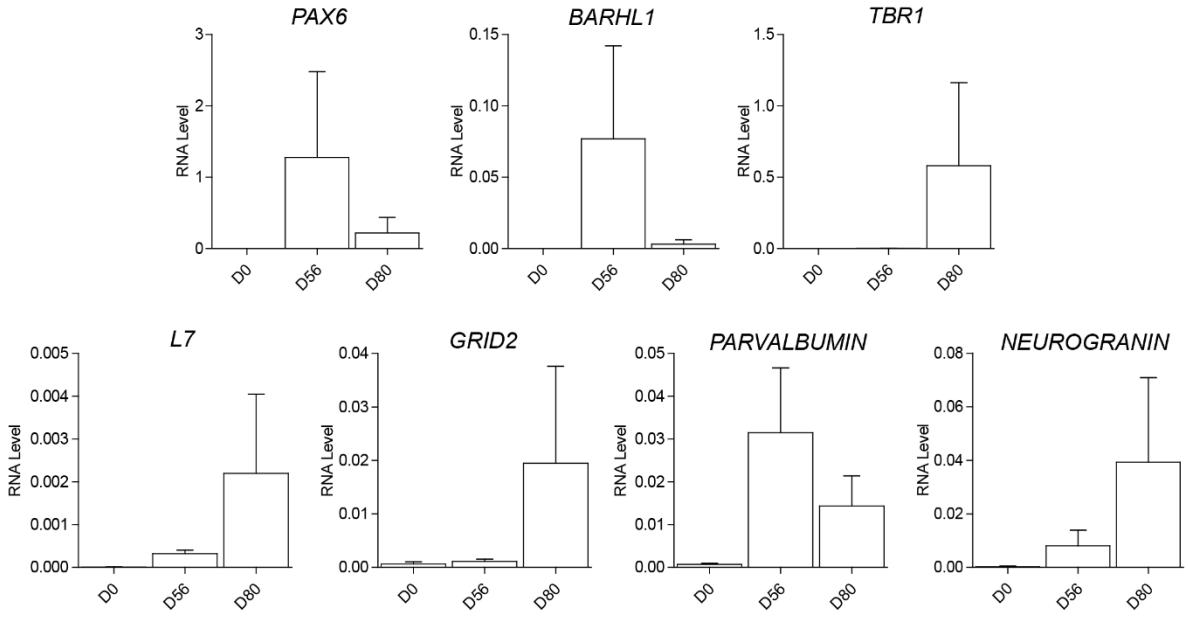

Figure IV.12. Distinct markers for cerebellar neurons. qRT-PCR analysis of *PAX6*, *BARHL1*, *TBR1*, *L7*, *GRID2*, *PARVALBUMIN*, and *NEUROGRANIN* mRNA levels relative to GAPDH at the indicated time-points. Data were obtained from three independent differentiation experiments using F002.1A.13 cells.

Functional maturation of generated neurons using PBS MINI 0.1L bioreactor

To evaluate physiological proprieties of neurons generated in organoids, single cell calcium imaging as well as electrophysiological patch clamp recordings were performed. As previously described, after organoid re-plating cells were incubated with a calcium indicator fluorescent dye Fura-2, and afterwards stimulated with KCl (50mM) and histamine (100µM). Since neural progenitors express histamine receptors, histamine stimulation leads to the increase of intracellular Ca^{2+} concentration in neural progenitors (Agasse et al., 2008; Molina-Hernández and Velasco, 2008; Rodríguez-Martínez et al., 2012). In contrast, neurons respond to KCl stimulation, increasing the influx of calcium in neurons by opening of voltage sensitive calcium channels (Ambrósio et al., 2000; Macías et al., 2001). Indeed, during the maturation process, organoid-derived cells showed a variation of intracellular Ca^{2+} in the presence of KCl, maintaining their baseline when stimulated with histamine, suggesting a highly efficient maturation (**Figure IV.13-A**). These results were further confirmed by calculating Histamine/KCl ratio, which allows to quantify immature cells and functional neurons, since neurons typically show ratios below 0.8 (Agasse et al., 2008; Rodrigues et al., 2017). Thus, the quantification of cells displaying a Histamine/KCl ratio below 0.8 indicated that about 75% of neurons were presented between days 40 and 55 of differentiation (**Figure IV.13-B**). This number was increasing during the maturation protocol, reaching about 83% of neurons in this dynamic culture system by day 90 (**Figure IV.13-B**).

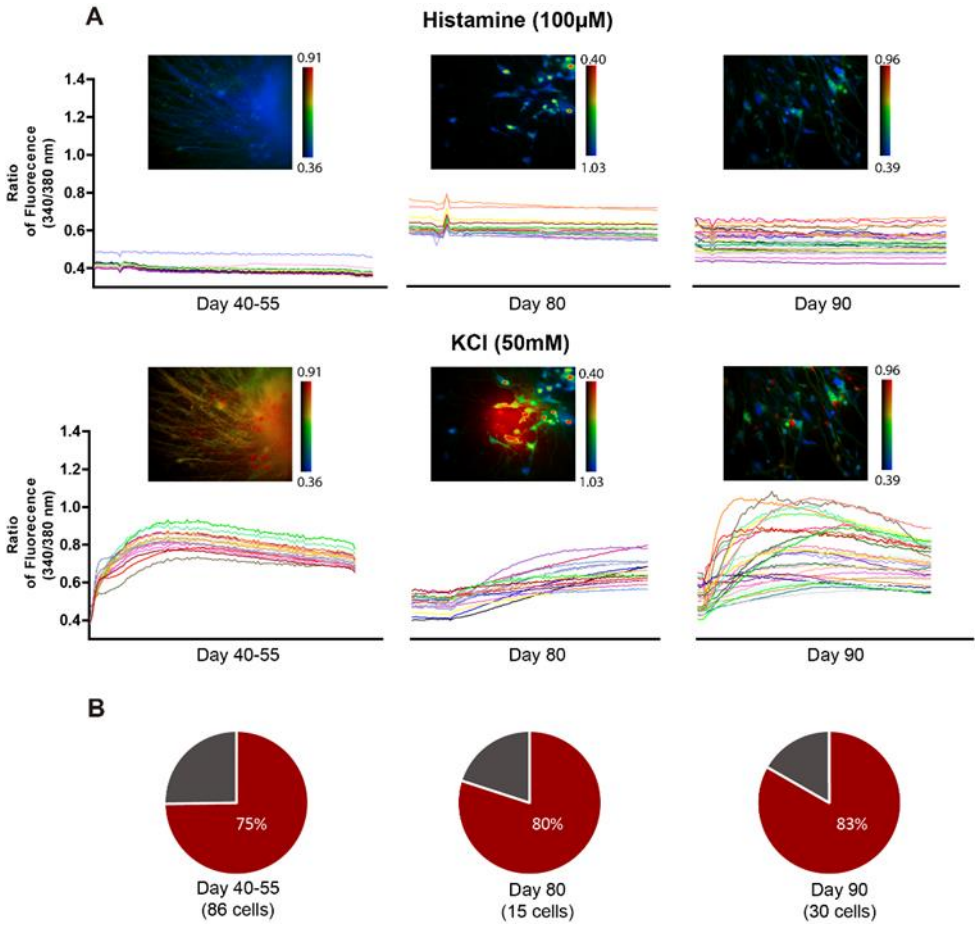

Figure IV.13. Single cell calcium imaging analysis. A) Representative ratio images and fluorescence ratio profiles of individual organoid-derived cells on indicated time-points of differentiation (F002.1A.13 cells). **B)** Percentage of cells displaying a Histamine/KCl ratio below 0.8 using F002.1A.13 cell line.

Lastly, we evaluated the electrophysiological properties of organoid-derived cells by using whole-cell patch clamp technique. On day 70 of differentiation, cells displayed a typical neuronal fire action potential upon a current injection (**Figure IV.14-A**). In addition, neurons demonstrated to be capable of rapidly recovering and responding to a second current injection (**Figure IV.14-A**). The immunostaining analysis of re-plated cells used in patch clamp recordings revealed that a dense neuronal network of $MAP2^{+}$ fibers was constructed (**Figure IV.14-B**). However, distinct pools of progenitors expressing PAX6, which did not stain for MAP2 were also found (**Figure IV.14-B**).

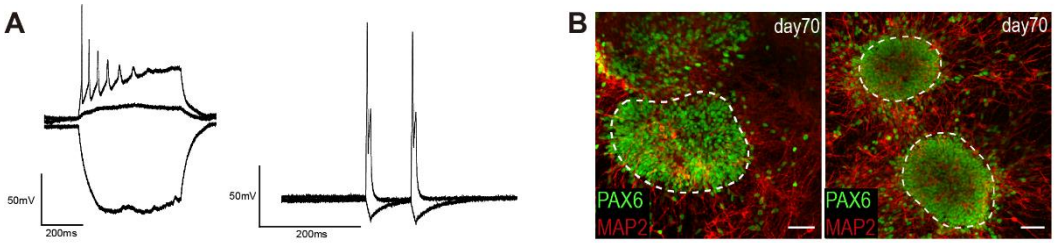

Figure IV.14. Analysis of physiological proprieties. A) Whole-cell patch clamp recordings. Representative traces of firing responses evoked under current-clamp mode by injection of a 500 ms current pulse and firing responses to two independent current injections (10 ms) separated by 80 ms. **B)** Immunofluorescence for PAX6 and MAP2 for re-plated organoid-derived cells on day 70 of differentiation (F002.1A.13 cells). Scale bars, 50µm.

Therefore, these results show that neurons generated from 3D dynamic culture conditions using PBS MINI 0.1L bioreactor are able to establish functional neuronal networks, while retaining their progenitor cell pool within these *in vitro* niches until later stages of differentiation.

IV.5 Discussion

For drug screening and regenerative medicine applications, the need of large cell numbers, as well as defined culture conditions to generate specific cell types, has been driving the development of scalable culture systems. In recent years, several groups have reported the scalable generation of neural progenitors as well as functional neurons (Bardy et al., 2013; Miranda et al., 2016; Rigamonti et al., 2016), providing significant advances for the development of new models for neurodegenerative disorders. Nonetheless, the recapitulation of some critical events as seen during embryonic development is still lacking and the maintenance of the generated functional neurons in suspension for long periods of time was not achieved (Rigamonti et al., 2016). Additionally, several groups reported the generation of neural organoids that are able to recapitulate major features of the human

central nervous system (CNS), offering the opportunity to study important aspects of neurodevelopment and mechanisms involved in neurodegeneration (Junghyun Jo et al., 2016; Lancaster et al., 2012; Muguruma et al., 2015; Qian et al., 2016). Still, the main limitation was the potential for the scaling up of these methodologies, since neural organoids were produced in static conditions, encapsulated individually in Matrigel and afterwards transferred to spinner flasks (Lancaster et al., 2012).

Here, we have developed a dynamic 3D culture system able to generate iPSC-derived neural organoids with cerebellar identity, and to further promote maturation into functional cerebellar neurons under chemically-defined and feeder-free conditions by using the novel PBS 0.1 (100 mL) Vertical-Wheel single-use bioreactor. These vertical-wheel bioreactors present a novel mixing mechanism generated by a large vertical wheel that rotates around a horizontal axis and allows a gentle and uniform fluid mixing (Croughan et al., 2016). Therefore, we ensured that a more uniform exposure of neural organoids to signaling molecules was reached. Moreover, the operation time and complexity, as well as the risk of contaminations, is reduced by using these single-use vessels, which facilitate the accomplishment of GMP conditions (Croughan et al., 2016).

With this dynamic culture system, we were able to address some critical issues. First, it is simple to generate a high number of organoids, which is important for high-throughput applications, achieving around 430 aggregates/mL on the first 24 hours after single cell inoculation. Beyond that, it is important to ensure that the seeding process leads to maximum cell survival and homogeneous aggregate production, since the aggregate size has a critical role to induce differentiation towards a specific cell lineage (Bauwens et al., 2008). Indeed, aggregation efficiencies of 54.1 ± 18.7% and 82 ± 14.1% were observed for two different human iPSC lines, showing a high percentage of cell survival. Moreover, aggregates formed in PBS 0.1 MINI bioreactor were uniform in size and shape, achieving the previously defined optimal diameter, about 200 µm (Miranda et al., 2015, 2016), to

initiate the neural induction at 48 hours after cell seeding. In comparison with static conditions, organoids retained a more homogeneous diameter in PBS 0.1 MINI bioreactor during the differentiation protocol, which can reduce variation between different experiments.

We started the neural induction by using FGF2 and insulin to caudalize the generated neural tissue and efficiently promote mid-hindbrain patterning (Muguruma et al., 2015). However, in addition to expression of *FGF8* and *EN2*, other transcription factors involved in forebrain/midbrain (*OTX2*), as well as hindbrain (*GBX2*) commitment were also enhanced in these cultures. Indeed, cellular diversity within neural organoids was already reported (Quadrato et al., 2017; Xiang et al., 2017). Even during forebrain differentiation protocols, single-cell RNA-sequencing revealed that a broad diversity of cells can be generated in PSC-derived neural organoids, including cerebral cortex, retina, astroglia and even mesodermal precursors (Quadrato et al., 2017; Xiang et al., 2017). In static conditions, the combination of FGF2 and insulin was shown to be very efficient for cerebellar induction due to their moderate caudalizing effect (Muguruma et al., 2010, 2015). Therefore, the FGF2 and insulin signaling are not specific for rostral hindbrain commitment inducing the mid-hindbrain domains in the PSC-derived aggregates (Muguruma et al., 2010, 2015). Yoshiki Sasai proposed that this combination can efficiently promote the self-formation of isthmic organizer tissue ($OTX2^+/EN2^+$) representing a small area within the organoid (Sasai, 2013). Afterwards, the self-production of signals from this organizer center, like FGF8, stimulate the generation of cerebellar territory (Sasai, 2013). In our dynamic culture, design features of vertical-wheel bioreactor offer gentle and uniform fluid mixing, efficient particle suspension, as well as higher mass transfer rates with minimum power input and low agitation speeds (Croughan et al., 2016). Therefore, mass transfer within the organoids is enhanced, promoting a uniform diffusion of signaling molecules, either exogenously provided morphogens or endogenous signals emanated by neighboring cells. One possible

explanation for *OTX2*, *FGF8*, E*N2* and *GBX2* enhanced expression could be that PSC-derived aggregates were exposed to an efficient and uniform diffusion of FGF signaling that could result in a larger area of the isthmic organizer tissue ($OTX2^+/EN2^+$). On the other hand, the maintenance of this organizer tissue is also dependent on the self-production of FGF and WNT signaling, as well as their suppression by inhibitors, in a reaction-diffusion model (Kondo and Miura, 2010; Turing, 1952). Thus, the more efficient fluid mixing can produce a more uniform exposure to signaling cues and enhance the feedback loops that operate in this self-organized system. Further studies to understand the effect of bioreactor design, as well as the uniform exposure to signaling molecules, on cerebellar commitment need to be performed to confirm the proposed mechanism.

Despite this limitation, an efficient cerebellar induction was achieved in our 3D dynamic system. Both dorsal (BARHL1) and ventral (PAX2, OLIG2 and CORL2) cerebellar progenitors were generated, which are required to produce glutamatergic and GABAergic cerebellar neurons, respectively. To date, the generation of functional cerebellar neurons was only achieved by co-culturing (Ishida et al., 2016; Muguruma et al., 2015; Wang et al., 2015). We first reported the maturation of cerebellar progenitors into functional cerebellar neurons by using a defined neuronal medium (Bardy et al., 2015) without co-culturing with feeder cells. Here, we successfully up-scaled cerebellar commitment of human iPSC and generation of different mature cerebellar neurons, including GABAergic and Glutamatergic neurons, as seen in distinct layers of human cerebellar cortex as well as in cerebellar nuclei. Specifically, the following cell types can be produced in our dynamic culture system: Purkinje cells ($Calbindin^+$), Golgi cells ($Neurogranin^+$), Granule cells ($Pax6^+/MAP2^+$) and DCN projection neurons ($TBR1^+$). Furthermore, calcium imaging and electrophysiological evaluation indicate that we have achieved an efficient maturation of cerebellar precursors in our cultures.

Most interestingly, in addition to the functional establishment of neuronal network connectivity, various pools of neural progenitors were maintained until 3 months in culture during the maturation process. The maintenance of a neural progenitor niche during CNS development is an important biological process achieved by the microenvironmental cues as well as cell-cell interactions, which are able to balance stem cell quiescence with proliferation and to direct neurogenesis versus gliogenesis (Conover and Notti, 2008). Also during cerebellar development, different niches of cerebellar progenitor cells are observed, the first in the ventricular zone and the second in the external granule layer (ten Donkelaar et al., 2003; Wingate, 2001). $SOX2^{+}$ progenitor niche is present in the ventricular zone, where this protein is highly expressed from the 20^{th} up to the 24^{th} week of gestation being down-regulated in developing human cerebellum, with undetectable expression at the 38^{th} week (Pibiri et al., 2016). On the other hand, external granular layer expressing PAX6 is observed by 20 to 38 weeks of gestation (Pibiri et al., 2016). Therefore, our 3D culture system recreated better the *in vivo* microenvironment when compared to re-plating cultures (as seen in the chapter II), and the temporal dynamic changes in the cerebellar progenitor niche appeared to be recapitulated using our approach, in which a pool of $PAX6^{+}$ progenitors was maintained. However, further studies are needed in order to characterize the generated stem/progenitor cell niche and to compare it with the embryo-fetal development of the human cerebellum.

Here, we describe for the first time the continuous and scalable generation of human iPSC-derived neural organoids that display cerebellar identity, as well as the generation of functional cerebellar neurons that were maintained in suspension for as long as 3 months. These culture conditions permit better monitoring of key culture parameters leading to increased reproducibility between experiments. Moreover, the possibility of large-scale production of neural organoids is reached, allowing their applicability in high-throughput processes, including drug screening and toxicological tests, as well as to study important

aspects of human cerebellar embryonic development and pathological pathways involved in cerebellar dysfunction.

IV.6 REFERENCES

Agasse, F., Bernardino, L., Silva, B., Ferreira, R., Grade, S., and Malva, J.O. (2008). Response to histamine allows the functional identification of neuronal progenitors, neurons, astrocytes, and immature cells in subventricular zone cell cultures. Rejuvenation Res. 11, 187–200.

Ambrósio, A.F., Silva, A.P., Malva, J.O., Mesquita, J.F., Carvalho, A.P., and Carvalho, C.M. (2000). Role of desensitization of AMPA receptors on the neuronal viability and an the [Ca2+](i) changes in cultured rat hippocampal neurons. Eur. J. Neurosci. 12, 2021–2031.

Amoroso, M.W., Croft, G.F., Williams, D.J., O'Keeffe, S., Carrasco, M.A., Davis, A.R., Roybon, L., Oakley, D.H., Maniatis, T., Henderson, C.E., et al. (2013). Accelerated High-Yield Generation of Limb-Innervating Motor Neurons from Human Stem Cells. J. Neurosci. 33, 574–586.

Arora, N., Imran Alsous, J., Guggenheim, J.W., Mak, M., Munera, J., Wells, J.M., Kamm, R.D., Asada, H.H., Shvartsman, S.Y., and Griffith, L.G. (2017). A process engineering approach to increase organoid yield. Development 144, 1128–1136.

Bardy, C., van den Hurk, M., Eames, T., Marchand, C., Hernandez, R. V, Kellogg, M., Gorris, M., Galet, B., Palomares, V., Brown, J., et al. (2015). Neuronal medium that supports basic synaptic functions and activity of human neurons in vitro. Proc. Natl. Acad. Sci. U. S. A. 112, E2725–E2734.

Bardy, J., Chen, A.K., Lim, Y.M., Wu, S., Wei, S., Weiping, H., Chan, K., Reuveny, S., and Oh, S.K.W. (2013). Microcarrier Suspension Cultures for High-Density Expansion and Differentiation of Human Pluripotent Stem Cells to Neural Progenitor Cells. Tissue Eng. Part C Methods 19, 166–180.

Bauwens, C.L., Peerani, R., Niebruegge, S., Woodhouse, K. a., Kumacheva, E., Husain, M., and Zandstra, P.W. (2008). Control of Human Embryonic Stem Cell Colony and Aggregate Size Heterogeneity Influences Differentiation Trajectories. Stem Cells 26, 2300–2310.

Bell, G., and Mooers, A.O. (1997). Size and complexity among multicellular organisms. Biol. J. Linn. Soc. 60, 345–363.

Boissart, C., Poulet, A., Georges, P., Darville, H., Julita, E., Delorme, R., Bourgeron, T., Peschanski, M., and Benchoua, A. (2013). Differentiation from human pluripotent stem cells of cortical neurons of the superficial layers amenable to psychiatric disease modeling and high-throughput drug screening. Transl. Psychiatry 3, e294.

Boulting, G.L., Kiskinis, E., Croft, G.F., Amoroso, M.W., Oakley, D.H., Wainger, B.J., Williams, D.J., Kahler, D.J., Yamaki, M., Davidow, L., et al. (2011). A functionally characterized test set of human induced pluripotent stem cells. Nat. Biotechnol. 29, 279–287.

Bratt-Leal, A.M., Carpenedo, R.L., and McDevitt, T.C. (2009). Engineering the embryoid body microenvironment to direct embryonic stem cell differentiation. Biotechnol. Prog. 25, 43–51.

Broccoli, V., Boncinelli, E., and Wurst, W. (1999). The caudal limit of Otx2 expression positions the isthmic organizer. Nature 401, 164–168.

Burridge, P.W., Thompson, S., Millrod, M.A., Weinberg, S., Yuan, X., Peters, A., Mahairaki, V., Koliatsos, V.E., Tung, L., and Zambidis, E.T. (2011). A universal system for highly efficient cardiac differentiation of human induced pluripotent stem cells that eliminates interline variability. PLoS One 6, e18293.

Chambers, S.M., Fasano, C.A., Papapetrou, E.P., Tomishima, M., Sadelain, M., and Studer, L. (2009). Highly efficient neural conversion of human ES and iPS cells by dual inhibition of SMAD signaling. Nat. Biotechnol. 27, 275–280.

Chi, C.L., Martinez, S., Wurst, W., and Martin, G.R. (2003). The isthmic organizer signal FGF8 is required for cell survival in the prospective midbrain and cerebellum. Development 130, 2633–2644.

Conover, J.C., and Notti, R.Q. (2008). The neural stem cell niche. Cell Tissue Res. 331, 211–224.

Croughan, M.S., Giroux, D., Fang, D., and Lee, B. (2016). Novel Single-Use Bioreactors for Scale-Up of Anchorage-Dependent Cell Manufacturing for Cell Therapies. In Stem Cell Manufacturing, pp. 105–139.

Ten Donkelaar, H.J., Lammens, M., Wesseling, P., Thijssen, H.O.M., and Renier, W.O. (2003). Development and developmental disorders of the human cerebellum. J. Neurol. 250, 1025–1036.

Eiraku, M., Watanabe, K., Matsuo-Takasaki, M., Kawada, M., Yonemura, S., Matsumura, M., Wataya, T., Nishiyama, A., Muguruma, K., and Sasai, Y. (2008). Self-Organized Formation of Polarized Cortical Tissues from ESCs and Its Active Manipulation by Extrinsic Signals. Cell Stem Cell 3, 519–532.

Felix-Oliveira, A., Dias, R.B., Colino-Oliveira, M., Rombo, D.M., and Sebastiao, A.M. (2014). Homeostatic plasticity induced by brief activity deprivation enhances long-term potentiation in the mature rat hippocampus. J. Neurophysiol. 112, 3012–3022.

Fink, A.J., Englund, C., Daza, R. a M., Pham, D., Lau, C., Nivison, M., Kowalczyk, T., and Hevner, R.F. (2006). Development of the deep cerebellar nuclei: transcription factors and cell migration from the rhombic lip. J. Neurosci. 26, 3066–3076.

Frantz, G.D., Weimann, J.M., Levin, M.E., and McConnell, S.K. (1994). Otx1 and Otx2 define layers and regions in developing cerebral cortex and cerebellum. J. Neurosci. 14, 5725–5740.

Guo, C., Qiu, H.-Y., Huang, Y., Chen, H., Yang, R.-Q., Chen, S.-D., Johnson, R.L., Chen, Z.-F., and Ding, Y.-Q. (2007). Lmx1b is essential for Fgf8 and Wnt1 expression in the isthmic organizer during tectum and cerebellum development in mice. Development 134, 317–325.

Hu, B.-Y., and Zhang, S.-C. (2009). Differentiation of spinal motor neurons from pluripotent human stem cells. Nat. Protoc. 4, 1295–1304.

Ishida, Y., Kawakami, H., Kitajima, H., Nishiyama, A., Sasai, Y., Inoue, H., and Muguruma, K. (2016). Vulnerability of Purkinje Cells Generated from Spinocerebellar Ataxia Type 6 Patient-Derived iPSCs. Cell Rep. 17, 1482–1490.

Joyner, A.L. (1996). Engrailed, Wnt and Pax genes regulate midbrain-hindbrain development. Trends Genet. 12, 15–20.

Joyner, A.L., Liu, A., and Millet, S. (2000). Otx2, Gbx2 and Fgf8 interact to position and maintain a mid-hindbrain organizer. Curr. Opin. Cell Biol. 12, 736–741.

Junghyun Jo, A., Xiao, Y., Xuyang Sun, A., King Tan, E., Shawn Je, H., and Ng, H.-H. (2016). Midbrain-like Organoids from Human Pluripotent Stem Cells Contain Functional Dopaminergic and Neuromelanin-Producing Neurons. 1–10.

Kanaani, J., Kolibachuk, J., Martinez, H., and Baekkeskov, S. (2010). Two distinct mechanisms target GAD67 to vesicular pathways and presynaptic clusters. J. Cell Biol. 190, 911–925.

Kondo, S., and Miura, T. (2010). Reaction-Diffusion Model as a Framework for Understanding Biological Pattern Formation. Science 329, 1616–1620.

Lancaster, M. a, Renner, M., Martin, C., Wenzel, D., Bicknell, L.S., Hurles, M.E., Homfray, T., Penninger, J.M., Jackson, A.P., Knoblich, J.A., et al. (2012). Cerebral organoids model human brain development and microcephaly. Nature 501, 373–379.

Larsen, K.B., Lutterodt, M.C., Møllgård, K., and Møller, M. (2010). Expression of the homeobox genes OTX2 and OTX1 in the early developing human brain. J. Histochem. Cytochem. 58, 669–678.

Li, S. (2004). Barhl1 Regulates Migration and Survival of Cerebellar Granule Cells by Controlling Expression of the Neurotrophin-3 Gene. J. Neurosci. 24, 3104–3114.

Liu, Y., and Zhang, S.C. (2010). Human stem cells as a model of motoneuron development and diseases. In Annals of the New York Academy of Sciences, pp. 192–200.

Macías, W., Carlson, R., Rajadhyaksha, A., Barczak, A., and Konradi, C. (2001). Potassium chloride depolarization mediates CREB phosphorylation in striatal neurons in an NMDA receptor-dependent manner. Brain Res. 890, 222–232.

Mariani, J., Coppola, G., Pelphrey, K.A., Howe, J.R., and Vaccarino Correspondence, F.M. (2015). FOXG1-Dependent Dysregulation of GABA/ Glutamate Neuron Differentiation in Autism Spectrum Disorders. Cell 162, 375–390.

Maricich, S.M., and Herrup, K. (1999). Pax-2 expression defines a subset of GABAergic interneurons and their precursors in the developing murine cerebellum. J. Neurobiol. 41, 281–294.

Martinez, S., Crossley, P.H., Cobos, I., Rubenstein, J.L., and Martin, G.R. (1999). FGF8 induces formation of an ectopic isthmic organizer and isthmocerebellar development via a repressive effect on Otx2 expression. Development 126, 1189–1200.

Miranda, C.C., Fernandes, T.G., Pascoal, J.F., Haupt, S., Brüstle, O., Cabral, J.M.S., and Diogo, M.M. (2015). Spatial and temporal control of cell aggregation efficiently directs human pluripotent stem cells towards neural commitment. Biotechnol. J. 10, 1612–1624.

Miranda, C.C., Fernandes, T.G., Diogo, M.M., and Cabral, J.M.S. (2016). Scaling up a chemically-defined aggregate-based suspension culture system for neural commitment of human pluripotent stem cells. Biotechnol. J. 11, 1628–1638.

Mizuhara, E., Minaki, Y., Nakatani, T., Kumai, M., Inoue, T., Muguruma, K., Sasai, Y., and Ono, Y. (2010). Purkinje cells originate from cerebellar ventricular zone progenitors positive for Neph3 and E-cadherin. Dev. Biol. 338, 202–214.

Molina-Hernández, A., and Velasco, I. (2008). Histamine induces neural stem cell proliferation and neuronal differentiation by activation of distinct histamine receptors. J. Neurochem. 106, 706–717.

Muguruma, K., Nishiyama, A., Ono, Y., Miyawaki, H., Mizuhara, E., Hori, S., Kakizuka, A., Obata, K., Yanagawa, Y., Hirano, T., et al. (2010). Ontogeny-recapitulating generation and tissue integration of ES cell-derived Purkinje cells. Nat. Neurosci. 13, 1171–1180.

Muguruma, K., Nishiyama, A., Kawakami, H., Hashimoto, K., and Sasai, Y. (2015). Self-Organization of Polarized Cerebellar Tissue in 3D Culture of Human Pluripotent Stem Cells. Cell Rep. 10, 537–550.

Peerani, R., Rao, B.M., Bauwens, C., Yin, T., Wood, G. a, Nagy, a, Kumacheva, E., and Zandstra, P.W. (2007). Niche-mediated control of human embryonic stem cell self-renewal and differentiation. EMBO J. 26, 4744–4755.

Pibiri, V., Ravarino, A., Gerosa, C., Pintus, M.C., Fanos, V., and Faa, G. (2016). Stem/progenitor cells in the developing human cerebellum: An immunohistochemical study. Eur. J. Histochem. 60, 2686.

Qian, X., Nguyen, H.N., Song, M.M., Hadiono, C., Ogden, S.C., Hammack, C., Yao, B., Hamersky, G.R., Jacob, F., Zhong, C., et al. (2016). Brain-Region-Specific Organoids Using Mini-bioreactors for Modeling ZIKV Exposure. Cell 1–17.

Qian, X., Jacob, F., Song, M.M., Nguyen, H.N., Song, H., and Ming, G. (2018). Generation of human brain region–specific organoids using a miniaturized spinning bioreactor. Nat. Protoc. 13, 565–580.

Qu, Q., Li, D., Louis, K.R., Li, X., Yang, H., Sun, Q., Crandall, S.R., Tsang, S., Zhou, J., Cox, C.L., et al. (2014). High-efficiency motor neuron differentiation from human pluripotent stem cells and the function of Islet-1. Nat. Commun. 5, 3449.

Quadrato, G., Nguyen, T., Macosko, E.Z., Sherwood, J.L., Yang, S.M., Berger, D.R., Maria, N., Scholvin, J., Goldman, M., Kinney, J.P., et al. (2017). Cell diversity and network dynamics in photosensitive human brain organoids. Nature 545, 48–53.

Rigamonti, A., Repetti, G.G., Sun, C., Price, F.D., Reny, D.C., Rapino, F., Weisinger, K., Benkler, C., Peterson, Q.P., Davidow, L.S., et al. (2016). Large-Scale Production of Mature Neurons from Human Pluripotent Stem Cells in a Three-Dimensional Suspension Culture System. Stem Cell Reports 6, 993–1008.

Rodrigues, C.A., Silva, T.P., Nogueira, D.E., Fernandes, T.G., Hashimura, Y., Wesselschmidt, R., Diogo, M.M., Lee, B., and Cabral, J.M. (2018). Scalable culture of human induced pluripotent cells on microcarriers under xeno-free conditions using single-use vertical-wheelTM bioreactors. J. Chem. Technol. Biotechnol.

Rodrigues, R.S., Ribeiro, F.F., Ferreira, F., Vaz, S.H., Sebastião, A.M., and Xapelli, S. (2017). Interaction between cannabinoid type 1 and type 2 receptors in the modulation of subventricular zone and dentate gyrus neurogenesis. Front. Pharmacol. 8, 516.

Rodríguez-Martínez, G., Velasco, I., García-López, G., Solís, K.H., Flores-Herrera, H., Díaz, N.F., and Molina-Hernández, A. (2012). Histamine is required during neural stem cell proliferation to increase neuron differentiation. Neuroscience 216, 10–17.

Rowitch, D.H., and McMahon, A.P. (1995). Pax-2 expression in the murine neural plate precedes and encompasses the expression domains of Wnt-1 and En-1. Mech. Dev. 52, 3–8.

Sansom, S.N., Griffiths, D.S., Faedo, A., Kleinjan, D.J., Ruan, Y., Smith, J., Van Heyningen, V., Rubenstein, J.L., and Livesey, F.J. (2009). The level of the transcription factor Pax6 is essential for controlling the balance between neural stem cell self-renewal and neurogenesis. PLoS Genet. 5, e1000511.

Sasai, Y. (2013). Next-generation regenerative medicine: Organogenesis from stem cells in 3D culture. Cell Stem Cell 12, 520–530.

Sasai, Y., Eiraku, M., and Suga, H. (2012). In vitro organogenesis in three dimensions: self-organising stem cells. Development 139, 4111–4121.

Singec, I., Knoth, R., Ditter, M., Frotscher, M., and Volk, B. (2003). Neurogranin expression by cerebellar neurons in rodents and non-human primates. J. Comp. Neurol. 459, 278–289.

Sousa, M.F.Q., Silva, M.M., Giroux, D., Hashimura, Y., Wesselschmidt, R., Lee, B., Roldão, A., Carrondo, M.J.T., Alves, P.M., and Serra, M. (2015). Production of oncolytic adenovirus and human mesenchymal stem cells in a single-use, Vertical-Wheel bioreactor system: Impact of bioreactor design on performance of microcarrier-based cell culture processes. Biotechnol. Prog. 31, 1600–1612.

Suzuki, I.K., and Vanderhaeghen, P. (2015). Is this a brain which I see before me? Modeling human neural development with pluripotent stem cells. Development 142, 3138–3150.

Swanson, D.J., Tong, Y., and Goldowitz, D. (2005). Disruption of cerebellar granule cell development in the Pax6 mutant, Sey mouse. Dev. Brain Res. 160, 176–193.

Takahashi, K., Tanabe, K., Ohnuki, M., Narita, M., Ichisaka, T., Tomoda, K., and Yamanaka, S. (2007). Induction of Pluripotent Stem Cells from Adult Human Fibroblasts by Defined Factors. Cell 131, 861–872.

Thakurela, S., Tiwari, N., Schick, S., Garding, A., Ivanek, R., Berninger, B., and Tiwari, V.K. (2016). Mapping gene regulatory circuitry of Pax6 during neurogenesis. Cell Discov. 2, 15045.

Thomson, J.A. (1998). Embryonic Stem Cell Lines Derived from Human Blastocysts. Science. 282, 1145–1147.

Turing, A.M. (1952). The Chemical Basis of Morphogenesis. Society 237, 37–72.

Wang, S., Wang, B., Pan, N., Fu, L., Wang, C., Song, G., An, J., Liu, Z., Zhu, W., Guan, Y., et al. (2015). Differentiation of human induced pluripotent stem cells to mature functional Purkinje neurons. Sci. Rep. 5, 9232.

Wassarman, K.M., Lewandoski, M., Campbell, K., Joyner, A.L., Rubenstein, J.L., Martinez, S., Martin, G.R., Abbott, L., Jacobowitz, D., Acampora, D., et al. (1997). Specification of the anterior hindbrain and establishment of a normal mid/hindbrain organizer is dependent on Gbx2 gene function. Development 124, 2923–2934.

Watson, L.M., Wong, M.M.K., and Becker, E.B.E. (2015). Induced pluripotent stem cell technology for modelling and therapy of cerebellar ataxia. Open Biol. 5, 150056.

Wingate, R.J.T. (2001). The rhombic lip and early cerebellar development. Curr. Opin. Neurobiol. 11, 82–88.

Xiang, Y., Tanaka, Y., Patterson, B., Kang, Y.J., Govindaiah, G., Roselaar, N., Cakir, B., Kim, K.Y., Lombroso, A.P., Hwang, S.M., et al. (2017). Fusion of Regionally Specified hPSC-Derived Organoids Models Human Brain Development and Interneuron Migration. Cell Stem Cell 21, 383–398.e7.

Xie, A.W., Binder, B.Y.K., Khalil, A.S., Schmitt, S.K., Johnson, H.J., Zacharias, N.A., and Murphy, W.L. (2017). Controlled Self-assembly of Stem Cell Aggregates Instructs Pluripotency and Lineage Bias. Sci. Rep. 7, 14070.

Yeung, J., Ha, T.J., Swanson, D.J., and Goldowitz, D. (2016). A Novel and Multivalent Role of Pax6 in Cerebellar Development. J. Neurosci. 36, 9057–9069.

Zec, N., Rowitch, D.H., Bitgood, M.J., and Kinney, H.C. (1997). Expression of the homeobox-containing genes EN1 and EN2 in human fetal midgestational medulla and cerebellum. J. Neuropathol. Exp. Neurol. 56, 236–242.

V. CONCLUDING REMARKS

V.1 GENERAL DISCUSSION

During this project, we aimed to generate new bioengineering tools to model cerebellar ataxias. Cerebellar ataxias represent a heterogeneous group of disorder for which no cure is available, with an urgent need to create an effective therapy (Anheim et al., 2012; Manto and Marmolino, 2009a). For that, efforts to uncover the pathological mechanisms involved in cerebellar degeneration have been made. However, most of the current knowledge has been based on human post mortem tissues, animal models and immortalized cell lines, which do not recapitulate the physiological and mechanistic characteristics of human organ (Manto and Marmolino, 2009b; Tiscornia et al., 2011). With advances in iPSC technology and their *in vitro* differentiation towards the neural lineage, the generation of cerebellar neurons as well as *in vitro* embryonic cerebellar neuroepithelium recapitulation has been demonstrated (Erceg et al., 2012; Muguruma et al., 2010, 2015; Tao et al., 2010; Wang et al., 2015).

However, excessive variability was reported during the generation of cerebellar neurons from PSCs, particularly associated with the use of feeder cells to promote the maturation. Therefore, we aimed to generate cerebellar neurons using chemically-defined conditions and without the need for co-culturing. We first controlled the size of 3D cell aggregates as previously described (Ungrin et al., 2008), leading to an efficient neural commitment (Bauwens et al., 2008; Miranda et al., 2015). Our organoids were able to form neural tube-like structures organized in layers with apico-basal polarity. Most interesting, compared to findings from a previous study (Muguruma et al., 2015), the organoids in our cultures exhibited an earlier neuronal maturation pattern, expressing the GAD65 protein present in presynaptic terminals already at the day 35 (Esclapez et al., 1994). Because the onset of GAD65 expression in the cerebellum occurs after synaptogenesis (Greif et al., 1991), we conclude that an interconnected neuronal network has been formed in organoids

by day 35. By using a defined basal medium optimized for neuronal cell culture (Bardy et al., 2015), re-plated cerebellar progenitors were able to mature into distinct cerebellar neurons without the need for co-culturing, including Purkinje cells with a characteristic long axon and highly arborized dendrites stained for CALB (Nag and Wadhwa, 1999; Whitney et al., 2008). Based on dendritic spine morphology analyses, calcium imaging, and electrophysiological evaluations, we demonstrated that an efficient maturation of cerebellar precursors was achieved in our cultures. Therefore, we showed for the first time that is possible to generate different types of electrophysiologically functional cerebellar neurons in feeder free long-term cultures.

Since reported protocols for Purkinje cell generation yielded low differentiation efficacies (Muguruma et al., 2015; Su et al., 2006; Tao et al., 2010; Wang et al., 2015), our next effort was focused on increasing the yield of cerebellar GABAergic neurons as well as efficient Purkinje cell differentiation and maturation. In an innovative study, we were able to generate large quantities of $OLIG2^{+}$ progenitors, which in cerebellar ventricular zone originate Purkinje cell progenitors (Ju et al., 2016; Seto et al., 2014). Also, a dense layer of GABAergic neurons was created by day 28 of differentiation. It was reported that SDF1 addition leads to a significant down-regulation of ventral markers, suggesting a moderate dorsalizing effect, in PSC-derived cerebellar organoids (Muguruma et al., 2015). Thus, we trust that combination of FGF19 and SAG used in our study is enough to create a larger amount of GABAergic progenitors preceded by the generation of continuous cerebellar neuroepithelium by day 28, without requiring SDF1 addition. During the maturation protocol, we observed that the addition of 5-HT, which was reported to be involved in dendritic growth and synapse formation in Purkinje cells (Kondoh et al., 2004; Oostland and van Hooft, 2013; Oostland et al., 2013), increased the Purkinje cell survival, probably by mimicking signals that are generated by granule cells during cerebellar development (Baptista et al., 1994; Miquel et al., 1994; Morrison and Mason, 1998). Furthermore, the addition of 5-HT to re-

plated cells, derived from cerebellar organoids, stimulated an enhanced expression of Purkinje cell-specific markers, L7 and GRID2, showing a relevant role of serotonin in Purkinje cell generation and maturation. Thus, a robust generation of cerebellar GABAergic progenitors can be reached by manipulation SHH signaling as well as differentiation and maturation of Purkinje cells by 5-HT-derived stimulation.

Since one of the major limitation of organoid production is the possibility for scaling up, because the neural-derived organoids have been produced in static conditions, encapsulated in Matrigel and then transferred to spinner flasks (Lancaster et al., 2012), we attempted to develop a novel dynamic 3D culture system to generate cerebellar organoids and promote their maturation in this 3D conditions. For that, cerebellar organoids were cultured in chemically-defined and feeder-free conditions in the novel PBS 0.1 (100 mL) Vertical-Wheel single-use bioreactor. With this dynamic culture system, we were able to generate a significant number of organoids with a high percentage of cell survival and uniform size and shape. The generated neural tissue using PBS MINI 0.1L promoted an efficient expression of *FGF8* and *EN2*, transcripts involved in mid-hindbrain specification as well as other transcription factors involved in forebrain/midbrain (*OTX2*) and hindbrain (*GBX2*) commitment. We suggest that exogenous stimulation by FGF2 as well as endogenous stimulus by FGF and WNT signaling were enhanced by a high mass transfer within the organoids promoted by the bioreactor design, leading to a uniform diffusion of signaling molecules (Croughan et al., 2016). Besides that, an effective cerebellar induction and an efficient maturation of cerebellar progenitors into functional cerebellar neurons by using a defined neuronal medium was achieved in our 3D dynamic system. In the maturation process a functional neuronal network connectivity was observed and distinct pools of neural progenitors were maintained until 3 months in culture during the maturation process. Therefore, this dynamic culture appeared to better recapitulate temporal changes in the cerebellar progenitor niche as seen during cerebellar development (Pibiri et al., 2016). Thus,

this work opened the possibility of large-scale production of neural organoids, which is necessary for high-throughput applications, including drug screening and toxicological tests.

V.2 CONCLUSIONS

This work represents an important contribution to the advancement of cerebellar ataxias disease modeling using iPSC technology. Here, we showed the optimization of a cerebellar differentiation protocol allowing to obtain reproducible long-term cerebellar differentiation using chemically-defined and feeder-free culture conditions. Besides that, important insights on increasing the efficiency of cerebellar GABAergic progenitor generation and further differentiation and maturation of Purkinje cells were made. Thus, a promising platform for studying the preferential degeneration of Purkinje cells in cerebellar dysfunction has been created. The scalable generation of cerebellar organoids was also accomplished in this work, representing a valuable tool for studying pathological pathways involved in cerebellum degeneration, starting from its embryonic development and going towards functional cerebellar neuronal generation. Furthermore, high throughput screening for identifying molecules that restore cerebellar function may be performed using cerebellar organoids obtained using this scalable system.

Thus, this project sets the foundation for the possibility of efficient generation of cerebellar neurons from patient-derived iPSCs, which can then be used to model neurogenerative diseases that are caused by cerebellar dysfunction.

V.3 FUTURES TRENDS

Modeling cerebellar ataxias by using iPSC technology has been a challenge due to the complexity of generation of specific cerebellar neurons, particularly Purkinje cells, as well as low efficiency of the differentiation protocols. Here, we demonstrated novel experimental systems and methodologies that offer the opportunity to model this group of cerebellar disorders. However, the proof-of-concept for the optimized protocols is lacking. Thus, the application of these novel methods for human iPSC-based cerebellar ataxia modeling will be the next step. Moreover, the effect of some pharmacological compounds that modulate signaling pathways involved in the cerebellar degeneration could be evaluated.

Specifically, for different group of results, additional studies could be addressed in order to clarify some relevant issues.

Chapter II: Generation of mature cerebellar neurons from human induced pluripotent stem cells under defined and feeder-free conditions

An important contribution of this thesis was the establishment of a defined and feeder-free differentiation protocol to generate cerebellar neurons from human iPSCs. To better characterize this novel approach, the quantification of distinct subtypes of cerebellar progenitors should be addressed. In addition, the quantification of each subtype of cerebellar neurons after the initial stage of maturation could unravel the proportion of progenitor proliferation and neuronal maturation. A main limitation of this study is the level of Purkinje cell maturation, which did not reach the maturation level as seen in the post-natal human cerebellum. Further studies to investigate signaling molecules that are involved in the

dendritic formation and synaptic development could promote a more complete maturation of Purkinje cells.

Chapter III: Controlling the regional identity of human pluripotent stem cell-derived cerebellar organoids

Although important steps were made in this chapter for increasing the efficiency of functional Purkinje cell generation, these results should be validated using different human PSC lines from those used in the study. Here, we demonstrated an effective mid-hindbrain patterning before adding SAG, but it would be important to investigate the presence of oligodendrocytes at later stages of organoids generation to prove that a robust cerebellar differentiation was in fact achieved. Besides that, we believe that SDF1 can alter the expression of ventral markers in our ventral cerebellar differentiation, thus further investigation should be done to understand its effects. In addition to Purkinje cell markers, the evaluation of other ventral as well as dorsal markers should be performed to confirm the robustness of the induced ventralization.

At day 28 of differentiation, we observed that a dense layer of $OLIG2^{+}$ progenitors was formed, however the expression of CORL2 was not evaluated, which could provide important information about the Purkinje cell progenitor generation at this time-point. We also proposed that the combination of FGF19 and SAG is sufficient to promote continuous cerebellar neuroepithelium generation, but more experiments should be made to quantify the proportion of distinct subtypes of cerebellar progenitors as well as a rigorous comparison between day 28 and day 35, using the protocol developed in chapter II.

During maturation, 5-HT appeared to have effect on Purkinje cell generation. A more detailed analysis of 5-HT effect should be done as well. Beyond quantification of Purkinje cell number in treated and non-treated culture, the maturation level of differentiated Purkinje

cells must be evaluated. For example, the expression of GRID2 and L7 protein should be quantified to validate data from gene expression analysis. Functional analysis of generated Purkinje cell is required to assess the effect of 5-HT on the generation of functional neurons.

Chapter IV: Scalable generation of mature cerebellar neurons from human pluripotent stem cells using Single-Use Vertical-Wheel™ bioreactors

In the last chapter, we proposed the scalable generation of mature cerebellar neurons. Here, we need to better understand the effect of bioreactor design on the initial mid-hindbrain commitment and further cerebellar specification. In addition, the maturation of cerebellar neurons using this novel dynamic system should be validated using different human PSC lines. For the functional analysis, we proceeded to cell dissociation and re-plating on laminin-coated plates. For this, a more robust technique could be applied, in which slices of organoids could be used to maintain the cell organization, allowing to investigate the functional proprieties of cells localized near luminal side or on the surface of the organoid. During the maturation process, we observed a conserved progenitor niche until day 90. It would be interesting to perform a more detailed characterization of these progenitors and try to compare their molecular profile with the different stages of human cerebellar development. Lastly, to better clarify the overall effect of this dynamic culture condition in the differentiation process a robust comparison between static and dynamic culture conditions could be made.

V.4 REFERENCES

Anheim, M., Tranchant, C., and Koenig, M. (2012). The Autosomal Recessive Cerebellar Ataxias. N. Engl. J. Med. 366, 636–646.

Baptista, C. a, Hatten, M.E., Blazeski, R., and Mason, C. a (1994). Cell-cell interactions influence survival and differentiation of purified Purkinje cells in vitro. Neuron 12, 243–260.

Bardy, C., van den Hurk, M., Eames, T., Marchand, C., Hernandez, R. V, Kellogg, M., Gorris, M., Galet, B., Palomares, V., Brown, J., et al. (2015). Neuronal medium that supports basic synaptic functions and activity of human neurons in vitro. Proc. Natl. Acad. Sci. U. S. A. 112, E2725–E2734.

Bauwens, C.L., Peerani, R., Niebruegge, S., Woodhouse, K. a., Kumacheva, E., Husain, M., and Zandstra, P.W. (2008). Control of Human Embryonic Stem Cell Colony and Aggregate Size Heterogeneity Influences Differentiation Trajectories. Stem Cells 26, 2300–2310.

Erceg, S., Lukovic, D., Moreno-Manzano, V., Stojkovic, M., and Bhattacharya, S.S. (2012). Derivation of Cerebellar Neurons from Human Pluripotent Stem Cells. In Current Protocols in Stem Cell Biology, (Hoboken, NJ, USA: John Wiley & Sons, Inc.), chapter 1.

Esclapez, M., Tillakaratne, N.J., Kaufman, D.L., Tobin, a J., and Houser, C.R. (1994). Comparative localization of two forms of glutamic acid decarboxylase and their mRNAs in rat brain supports the concept of functional differences between the forms. J. Neurosci. 14, 1834–1855.

Greif, K.F., Erlander, M.G., Tillakaratne, N.J.K., and Tobin, A.J. (1991). Postnatal expression of glutamate decarboxylases in developing rat cerebellum. Neurochem. Res. 16, 235–242.

Ju, J., Liu, Q., Zhang, Y., Liu, Y., Jiang, M., Zhang, L., He, X., Peng, C., Zheng, T., Lu, Q.R., et al. (2016). Olig2 regulates Purkinje cell generation in the early developing mouse cerebellum. Sci. Rep. 6, 30711.

Kondoh, M., Shiga, T., and Okado, N. (2004). Regulation of dendrite formation of Purkinje cells by serotonin through serotonin1A and serotonin2A receptors in culture. Neurosci. Res. 48, 101–109.

Lancaster, M. a, Renner, M., Martin, C., Wenzel, D., Bicknell, L.S., Hurles, M.E., Homfray, T., Penninger, J.M., Jackson, A.P., Knoblich, J.A., et al. (2012). Cerebral organoids model human brain development and microcephaly. Nature 501, 373–379.

Manto, M., and Marmolino, D. (2009a). Cerebellar ataxias. Curr. Opin. Neurol. 22, 419–429.

Manto, M., and Marmolino, D. (2009b). Animal models of human cerebellar ataxias: A cornerstone for the therapies of the twenty-first century. Cerebellum 8, 137–154.

Miquel, M.C., Kia, H.K., Boni, C., Doucet, E., Daval, G., Matthiessen, L., Hamon, M., and Verge, D. (1994). Postnatal development and localization of 5-HT1A receptor mRNA in rat forebrain and cerebellum. Brain Res Dev Brain Res 80, 149–157.

Miranda, C.C., Fernandes, T.G., Pascoal, J.F., Haupt, S., Brüstle, O., Cabral, J.M.S., and Diogo, M.M. (2015). Spatial and temporal control of cell aggregation efficiently directs human pluripotent stem cells towards neural commitment. Biotechnol. J. 10, 1612–1624.

Morrison, M.E., and Mason, C.A. (1998). Granule neuron regulation of Purkinje cell development: striking a balance between neurotrophin and glutamate signaling. J. Neurosci. 18, 3563–3573.

Muguruma, K., Nishiyama, A., Ono, Y., Miyawaki, H., Mizuhara, E., Hori, S., Kakizuka, A., Obata, K., Yanagawa, Y., Hirano, T., et al. (2010). Ontogeny-recapitulating generation and tissue integration of ES cell-derived Purkinje cells. Nat. Neurosci. 13, 1171–1180.

Muguruma, K., Nishiyama, A., Kawakami, H., Hashimoto, K., and Sasai, Y. (2015). Self-Organization of Polarized Cerebellar Tissue in 3D Culture of Human Pluripotent Stem Cells. Cell Rep. 10, 537–550.

Nag, T.C., and Wadhwa, S. (1999). Calbindin immunoreactivity in the developing and adult human cerebellum. J. Chem. Neuroanat. 17, 1–12.

Oostland, M., and van Hooft, J.A. (2013). The role of serotonin in cerebellar development. Neuroscience 248, 201–212.